Author:
Sarria Dulcey, Maryory J

Title:
The effect of climate change on Southern Ocean benthic calcifiers

The effect of climate change on Southern Ocean benthic calcifiers

By

MARYORY J. SARRIA DULCEY

Supervisors: D. N. Schmidt, E. J. Rayfield and Katrin Linse (BAS)

School of Earth Sciences
UNIVERSITY OF BRISTOL

A dissertation submitted to the University of Bristol in accordance with the requirements of the degree of DOCTOR OF PHILOSOPHY in the Faculty of Sciences.

JULY 2020

ABSTRACT

Southern Ocean (SO) warming has been increasing in the last decades and it is expected to continue, which will cause ice loss and changes in the food web. Similarly, short undersaturation events are projected from 2030 onwards. Antarctic organisms, and especially those with shells, are expected to be one of the most affected by climate change, and therefore there is an importance to assess if different environmental conditions lead to changes in the shell structure specifically in ontogeny, size, integrity, and geochemistry. The Southern Ocean has many different types of natural environmental, which makes it an ideal place to test the responses of species with different lifestyles (infaunal and epifaunal). In the Amundsen Sea, there are warmer waters with the carbonate undersaturated Circumpolar Deep Water upwelling onto the shelf. In contrast, the Weddell Sea is a region of colder down-welling water masses. North to the Weddell Sea, South Sandwich Islands present high productivity compared with the other two SO regions. Further north of the Polar Front, the Magellan region has high temperatures and aragonite saturation. The results show that *Dentalium majorinum*, *Limopsis marionensis* and *Cyclocardia astartoides* present different morphologies in the different regions. *D. majorinum* and *C. astartoides* specimens from the Weddell Sea are larger than those from Amundsen Sea. Likewise, larger specimens were found on South Sandwich Island for *L. marionensis* individuals, all of these in areas of higher productivity. The variability between the different regions of the studied species suggests a plastic morphology, which can help them compensate for environmental changes. Finite element analysis (FEA) revealed that the shape (curvature) and length increase the risk of breakage under hydrostatic pressure load whilst ornamentation (number of ribs) enhance the shell strength under drag flow. Age determination of *D. majorinum* (23 years) and *C. astartoides* (25 years) are in accordance with others although they need to be taken with caution. In the three species studied, the density of the shell and the geochemistry do not show great differences between regions, except for *L. marionensis*, which has a higher density at the north of the Polar Front. This suggests a high biomineralization control. All collected specimens show different levels of dissolution, suggesting that they are compensating for environmental pressures. All analysed specimens were collected alive, which suggest that they are currently coping with the environmental pressures. Nevertheless, as the Southern Ocean continues to become warmer and undersaturated, a continued assessment is necessary.

ACKNOWLEDGEMENTS

Firstly, I want to thank God for the opportunity to do my PhD in Bristol. It was a dream that became possible. To my supervisors Dani Schmidt, Katrin Linse, and Emily Rayfield, who were guiding and advising me.

I would also like to thank all the laboratory managers, but especially to Tom Davies and Stuart Kerns, who with their expertise and advice helped me with the data collection. To the "paleos", who often provided advice and practical help. Similarly, to all my colleagues in the G44 office with whom I shared good laughs, discussions, and outings. Hope to see you all again.

My friends Claudio and Eduardo, who gave me their unconditional support, and who helped me out of complex moments. To my in-law family, Anne and Oliver who were also present supporting and providing a home for me.

I thank to my husband Philipp who has been my unconditional support and believe in me, especially when I was writing. Du bist der beste!

My greatest thanks to my family, my mom, dad, Jonathan, and David, who have always encouraged me. I owe you everything, you are one of my greatest joys. Gracias por ayudarme a ser quien soy, y por brindarme las oportunidades para completar mi doctorado. Ustedes son mi ejemplo de vida. Los amo!

AUTHOR'S DECLARATION

I declare that the work in this dissertation was carried out in accordance with the requirements of the University's Regulations and Code of Practice for Research Degree Programmes and that it has not been submitted for any other academic award. Except where indicated by specific reference in the text, the work is the candidate's own research. Work done in collaboration with, or with the assistance of, others, is indicated as such. Any views expressed in the dissertation are those of the author.

MARYORY J. SARRIA DULCEY

TABLE OF CONTENTS

x

LIST OF FIGURES

FIGURE

LIST OF TABLES

TABLE

CHAPTER 1 : INTRODUCTION

1.1. *Context*

Anthropogenic climate change is rapidly impacting both land and ocean. The ocean has taken up to 93% of the heat from global warming (Gattuso et al. 2015), with the latter accelerating since the beginning of the 20th century, especially in the upper ocean (Hoegh-Guldberg et al. 2018). Ocean warming is already impacting ecosystems, resulting in changes in phenology, distribution, abundance, ecosystem services, and biodiversity (Pörtner et al 2014, Poloczanska et al. 2013, Hoegh-Guldberg et al. 2018). The Southern Ocean has on average been warming in the last decades (Swart et al. 2018). In South Georgia, the upper 150 m has been in average warmed in 2.3°C since 1925 (Whitehouse et al. 2008). In the West Antarctic Peninsula (WAP) since 1950s the increase is nearly 1.5°C (Meredith & King 2005). In medium (4.5) and high (8.5) IPCC emissions scenarios, a considerable warming is expected by 2100 (Chapman et al. 2020). Consequently, approximately 90% of the Antarctic Peninsula ice glaciers (Cook et al. 2014) and many west Antarctic ice glaciers are retreating (Cook et al. 2016, Jenkins et al. 2010). Trends are not linear, though, as the WAP ice decreased from the 1970s to 2000s by 40% but has extended since the last decade (Stammerjohn et al. 2012; Smith & Stammerjohn 2001, Turner et al. 2016; Schofield et al., 2017). Similarly, the South Orkney islands glaciers do not present a consistent trend (Murphy et al. 2014). Increased evaporation and ice melt are changing ocean salinity with projected impacts on ocean circulation (Pörtner et al. 2014, Meredith et al. 2018). Sea level is projected to rise due to deglaciation and glacial meltwater discharges.

Additionally, the absorption of anthropogenic carbon dioxide by the ocean increases the acidity of the ocean and decreases carbonate saturation (Caldeira & Wickett 2003). Most of the surface ocean is in equilibrium with the atmosphere, resulting in similar uptake of CO_2. pH has decreased by ~ 0.11 ± 0.03 units between 20°S and 20°N from 1770 to 2000 (Jiang et al. 2019), equivalent to a 30% increase in hydrogen ion concentration (Orr et al. 2005, Denman et al. 2007). The high CO_2 (aq) leads to undersaturation in calcite and aragonite (Watson et al. 2012), the main minerals for skeletal organisms. Polar oceans are more affected by ocean acidification (OA) than mid- to low latitude seas because CO_2 solubility increases with decreasing temperature, thereby impacting

carbonate saturation. The Southern Ocean (SO) is thought to have taken up about ~30% of anthropogenic CO_2 (Gruber et al. 2019a), but the uptake varies substantially on time scales (Gruber et al. 2019b). Consequently, the SO is projected to have seasonal undersaturation events that will be more common from 2030 onward, affecting >70% of the ocean by the end of 21st century (Hauri et al. 2016). As the entire Antarctic seafloor habitat is naturally undersaturated in carbonate (Gutt et al. 2015), an increase in acidification will expand the areas of undersaturation, potentially altering marine habitats and their structures. The largest increase in dissolved CO_2 is expected for water depths between 100 and 700 m, suggesting that undersaturation will affect most of the shelf of the Antarctic continent and of sub-Antarctic islands and their marine diversity (Peck 2018, Rintoul et al. 2018).

In this thesis, I use the natural environmental differences in the Southern Ocean as a natural laboratory to study the responses of two aragonitic molluscs to different environments in four regions: Weddell, South Sandwich Islands, Amundsen Sea and Magellan. I focus on using the shell as an archive of the environment, growth history and calcification using periodic growth structures in their skeletons, referred to as banding (Jones 1983). These bands are visible in marine organisms such as corals (Cobb et al. 2003), bivalves, and fish otoliths (Wanamaker et al. 2012, Yan et al. 2014). I also focus on the patterns of dissolution within the shell and if there are differences in density and geochemistry due to environmental differences. I determine the function of some of the plastic morphological characteristics to investigate the link between environment and biomechanical shell function.

1.2. *Using regional environmental differences as test cases for impacts of environmental change on benthic shelled Mollusca*

This thesis focuses on environmental change in the South Sandwich Islands, the Weddell Sea, the Amundsen Sea in the Southern Ocean, and the Magellan region (Figure 1.1).
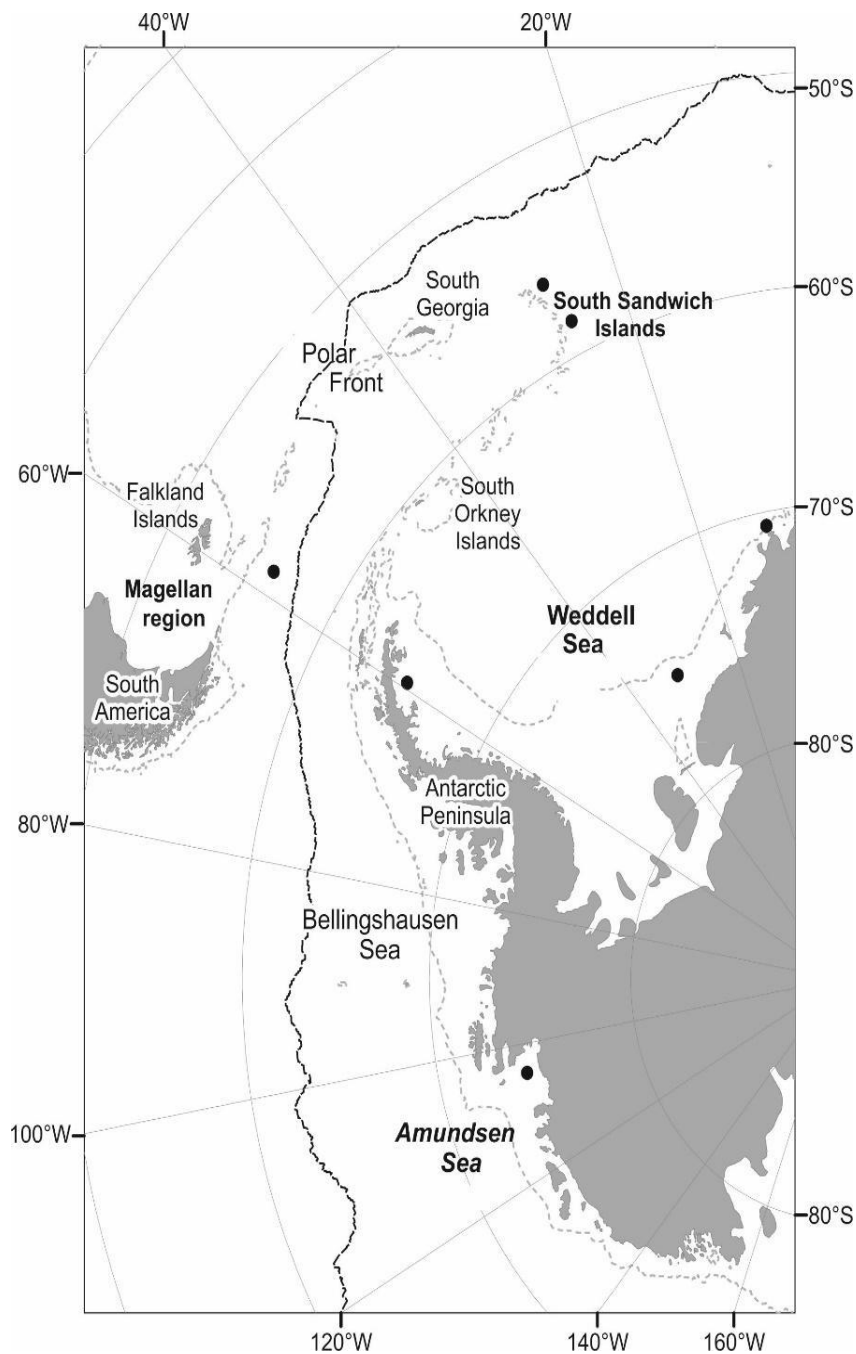
Figure 1.1. The four study regions: South Sandwich Islands, Weddell Sea, and Amundsen Sea in the Southern Ocean and the Magellan region north of the Polar Front. Black points represent sample areas, and the grey dotted line represents the 1000 m depth bathymetric contour line.

Although the Weddell Sea, Amundsen Sea, and South Sandwich Islands are part of the Southern Ocean, they differ significantly in their oceanography. The regions north and south of the Polar Front (which is located at 60° S, produces a natural barrier), are separated by the clockwise-flowing Antarctic Circumpolar Current (ACC, Figure 1.2). The ACC consists mainly of Circumpolar Deep Water (CDW), which is overlain by Antarctic Surface Water (AASW) (Nicholls et al. 2009). CDW

is derived from North Atlantic Deep Water (NADW) mixed with Antarctic Bottom Water (AABW) (Figure 1.3). The CDW has low saturation waters leading to dissolution of the underlying carbonates (Hauck et al. 2012). The AABW is freshening due to the breakup of Larsen ice shelves and the increased glacier discharge (Hellmer et al. 2011). The Weddell Sea is a region of down-welling of water masses formed on the shelf. This region is influenced by the clockwise flowing Weddell Gyre, in which Ice Shelf Water (ISW) interacts with Warm Deep Water (WDW) to create Weddell Sea Bottom Water (WSBW), which subsequently forms AABW.
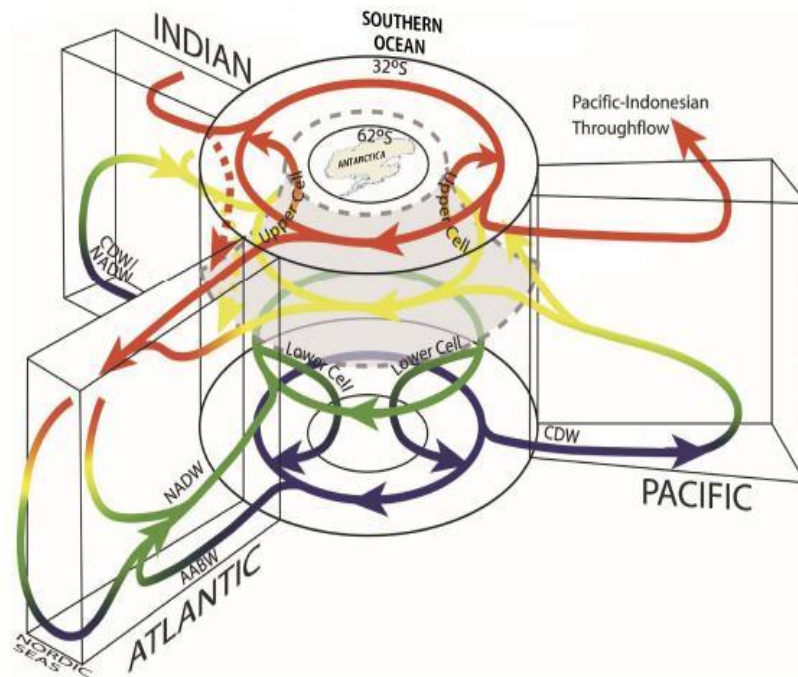
Figure 1.2. Circulation and dynamics of the main Southern Ocean water masses: Circumpolar Deep Water (CDW); North Atlantic Deep Water (NADW); and Antarctic Bottom Water (AABW). Image taken from NASEM (2015).

The potential water temperature of surface and near-surface water masses around Antarctica ranges between -2°C east of the Antarctic Peninsula in the Weddell Sea to just over 1.5°C west of the Antarctic Peninsula (Jenkins et al. 2016) (Figure 1.3). The surface and near-surface waters in the south-western Weddell Sea are colder, fresher, and much richer in oxygen than in the Amundsen Sea counterpart (Nicholls et al. 2009).

In the Amundsen Sea, the CDW is the dominant water mass (Jacobs et al. 2012). Old, relatively warm, and carbonate-undersaturated CDW is upwelling onto the shelf in the eastern part at depths of up to 300 m with salinities above 34.6 psu and temperatures higher than 3.5°C (Jacobs et al.

2011). The upper 300-500 m have the characteristics of winter water (fresher and colder), while below 500 m the water become saltier (34.72 up to 34.72 psu) and warmer (up to 1.2°C) due to advection of Circumpolar Deep Water (Arneborg et al. 2012). Together with the WAP shelf and the Bellingshausen Sea, the Amundsen Sea is the region with the most significant warming in the SO in the order of 0.1° to 0.3 °C decade^{-1} (Schmidtko et al. 2014).

In the WAP, the CDW intrude also into the shelf, and mixed with AASW and Winter Water, creating a modified form of CDW (Jones et al. 2017). Mixed waters are a source of warm water and nutrients that enhance primary production in the upper ocean (Prézelin et al. 2000), which can compensate the effects of freshwater inputs, such as dilution of carbonates ions, increasing carbonate mineral saturation (Meredith et al. 2010, Hauri et al. 2015). Whereas the CDW derived from the ACC contribute to the degradation of the glaciers (Martinson & McKee 2012).

Likewise, the oceanography of the South Sandwich Islands is dominated by the ACC (Atkinson et al. 2001, Murphy et al. 1998). Between the Islands, water depth can reach a maximum of 8100 m (Howe et al. 2004). Compared to the Amundsen Sea with a pH of 8.1 and Ω_{Ar} of 1.6 in summer, this region is between ~1 to 2 °C warmer and has a higher pH (up to 8.3) and saturation Ω_{Ar} (2.4). However, the salinity differences are minimal (Tynan et al. 2016).
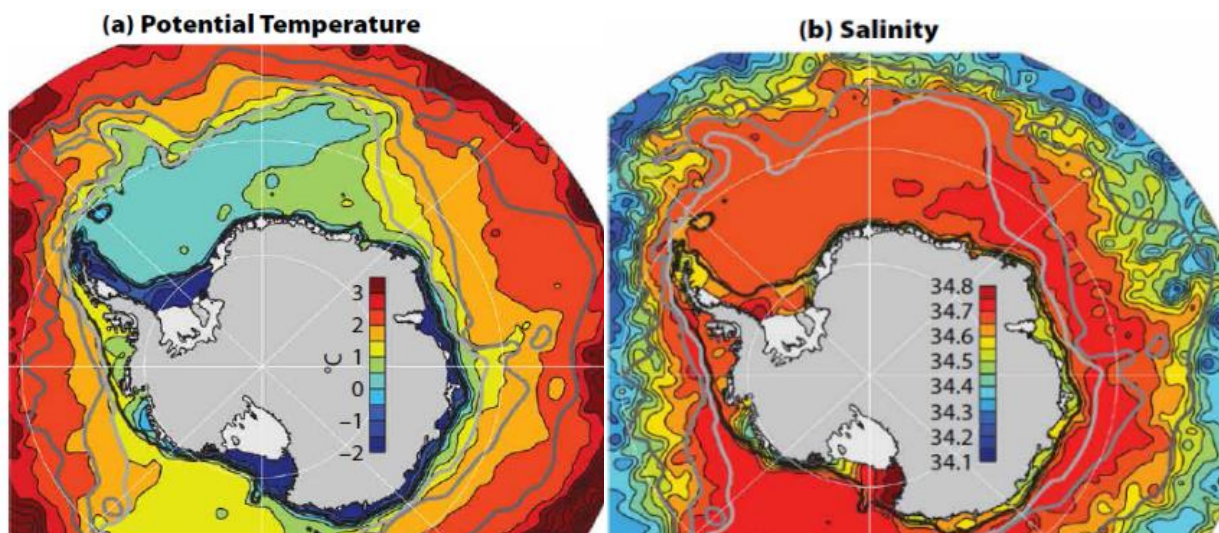
Figure 1.3. Potential temperature* (in °C, a), and salinity (in psu, b), south of 45°S averaged from 400 m depth to either 1.200 m depth or the seabed. Data are taken from the World Ocean Circulation Experiment Southern Ocean Atlas Database (Orsi & Whitworth 2005 in Jenkins et al. 2016).

*Potential temperature denotes the temperature of a parcel of water without changes in its salinity and with no exchanges of heat with its surroundings. It is a measure to compare ocean temperatures from different depths and therefore different pressures.

The Magellan region is north of the Polar Front. Consequently, temperature is higher, varying between 0°C to 12°C, with occasional ice scour (Barnes et al. 2005). This region is dominated by the Malvinas or Falkland Current, which is a branch of the ACC, forming at the east of the Drake passage (Peterson 1992).

The carbonate chemistry is this region is patchy. In areas adjacent to the Antarctic continent, the aragonite saturation horizon is about 1000 m (Jiang et al. 2015). However, at shallower depths it is possible to register aragonite undersaturation events, especially in locations where are exposed to the CDW, such as the WAP and Scotia Sea (Bednaršek et al. 2012a). The CDW is transported in the ACC around the Antarctic continent, but in other regions such as Ross, Weddell, and Kerguelen Gyres, the presence of gyres impedes to the ACC to intrude onto the shelf (Hauck et al. 2012). Nevertheless, the Ross Sea together with Bellingshausen Sea are experiencing short aragonite undersaturation events (Hauri et al. 2016).

The Rothera Time Series in the WAP, with an annual data since 2010, show an asymmetrical seasonal cycle (Jones et al. 2017) with an increase in pH and saturation state (Ω), and a decrease of dissolve inorganic carbon (DIC) and total alkalinity (TA) in spring/summer. By winter, the saturation state is low, and close to 1, while DIC increase in the upper ocean (Henley et al. 2019). Projections about surface aragonite saturation indicates that by the middle of the century the undersaturation events will increase and will be prolonged. Additionally, >70% of the SO will be undersaturated by the end of the century under the 8.5 IPCC scenario (Hauri et al. 2016).

Changes in carbonate chemistry impact phytoplankton productivity (Trimborn et al. 2013). The SO is characterised usually for low rates of net primary productivity (57g C m^{-2} yr^{-1} Arrigo et al. 2008), and by high seasonality in productivity, peaking during the austral summer during the phytoplankton bloom (Rogers et al. 2015). Primary production is affected by several regulators. Diatom-dominated phytoplankton are associated to an induced upper CDW upwelling site. This authors suggest that without this upwelling, the diatoms cannot increase their abundance or dominance due to a lack of growth requirements (Prézelin et al. 2000). Sea ice retreat has also linked to the increased of blooms in spring when the ice starts to melt. Melting ice make available micronutrients such as iron, which increase the proportion of phytoplankton bloom until its depletion at the end of the summer (Smith et al. 2008). Large parts of the Southern Ocean are

classified as High Nutrient Low Chlorophyll areas, where macronutrients such as nitrogen, phosphorus and silicate are high, with a deficiency in micronutrients leading to low productivity away from the ACC (Murphy et al. 2007). Low primary production might be due to low light levels and deep vertical mixing (Mitchell & Holm-Hansen 1991). Thus, light irradiance can be the limiting factor for the initiation and early development of phytoplankton blooms (Nelson & Smith 1991). In this case mixing plays an important role, since areas that have major depth mixing layers, will have a lower maximum chlorophyll concentration. In coastal areas, ice melt and shallow mix layers can lead to nutrient influx and higher productivity (Schofield et al. 2015).

Net primary productivity (NPP) is higher in the Weddell Sea (192 mg C m^{-2} d^{-1}) and lower in the Bellingshausen-Amundsen Sea (145 mg C m^{-2} d$^{-1)}$) due to ice cover (Arrigo et al. 2008). In the Weddell Sea, ice coverage decreases rapidly in the eastern sector during summer (Melles et al. 1995), whereas the west sector is characterised by perennial sea ice (Comiso & Gordon 1998). Primary production is higher around the South Sandwich Islands than in the other regions due to the upwelling of nutrient rich waters from the ACC (Whitehouse et al. 2008, Trathan et al. 2014), resulting in diatoms blooms. In the Magellan region, the primary productivity can reach values between 150-500 mg C m^{-2} d^{-1} (Longhurst 1995), which can be higher than the Amundsen Sea. Short bursts of the highest productivity can be found in the Southern Ocean polynyas. The Amundsen Sea Polynya is one of the most productive in the Southern Ocean (Arrigo & van Dijken 2003), due to long days of open water (120-130) and to high concentration of Fe (Gerringa et al. 2012). Intrusion of the warm CDW onto the shelf results in ice melt, which releases nutrients (Poulton & Raiswell 2005) and generates blooms. There are uncertainties in the primary production projections. However, most of the models predict an increase in Net Primary production by the end of the 21st century in the Southern Ocean due to warming, reduced ice cover, and increases in iron and light (Laufkötter et al. 2015).

There are not a significant trend in annual ice cover for satellite observations between 1979-2018 (Ludescher et al. 2019). However, there are regional trends: Summer and autumn ice coverage in the Amundsen Sea has been decreasing in the last decades (Parkinson & Cavalieri 2012). Decrease of winter sea ice season and stratification in summer result in a reduction of phytoplankton biomass at the north of the WAP (Rozema et al. 2017 in Schofield et al. 2017). In contrast, in the southern part of the WAP, during summer season, longer duration of ice-free conditions and larger area, causing an increase in phytoplankton biomass (Montes-Hugo et al. 2009). Consistent with this, a

shift in trophic structure is predicted (Smith et al. 2008). Trends in Antarctic ice sheets are more consistent, projecting to continuing lose mass along the 21st century (Meredith et al. 2019). This will keep causing changes in the salinity of the ocean and in the sea level (Meredith et al. 2019). However, salinity changes are not projected to be significant during the 21st century, with the exception of freshening around the Antarctic Peninsula (Barnes et al. 2009).

1.3. *Southern Ocean benthos and its response to environmental change*

The environmental change in the Antarctic over the last century, such as ice melting and glacier retreat (Rogers et al. 2020), has resulted in a change in benthic shelf communities (Gutt & Starmans 1998). These communities have an important role in generating and supporting biodiversity as well as exporting and removing carbon, with benefits for local diversity and nutrient enrichment of the seabed (Barnes et al. 2018). A shift in community composition in response to climate change is expected for the Southern Ocean (Molinos et al. 2016). Benthic macrospecies are the richest component of Antarctic biodiversity (Griffiths 2010). Calcifying benthos are sensitive to warming and ocean acidification because many are sessile and therefore unable to migrate (Henley et al. 2019). They also have slow development rates, long generation times, and fewer large eggs compared to low latitude counterparts, without an increase in mutation rate or population size, which reduces their capacity to adapt (Peck 2018).

As little is known about their response to climate change, information can be derived from species in other regions. There is considerable variability in the capability of benthic species to generate shells and their responses to changing environmental conditions (Pfister et al. 2016). pH and carbonate saturation impact physiological and behavioral processes in many marine organisms. Internal acid-base regulations impact the capability to build shells, and therefore skeletons can be affected (Orr et al. 2005; Melzner et al. 2009). After death, the decrease in carbonate saturation enhances the dissolution of carbonates on the seafloor. Studies on mussels in the Southern Ocean suggested shell dissolution (Michaelidis et al. 2005), and in benthic bivalves and echinoderms a decrease in calcification rate for the former and growth reduction for the latter has been reported (Gazeau et al. 2007, Shirayama & Thorton, 2005 in Fabry et al. 2008). Assessments of the capacity of Antarctic benthos to acclimate changing environmental conditions (pH, undersaturation, temperature) show species specific responses. For example, some organisms, such as *Liothyrella uva,* show little response to lowered pH (Cross et al. 2015) or respond to temperature instead of pH (i.e. *Mytilus edulis*, Mackenzie et al. 2014).

Yet, long term experiments in the SO with the possibility to acclimate are limited (Cross et al. 2018). For example, the 7 months study on the brachiopod *Liothyrella uva* (Cross et al. 2015, Cross et al. 2019), and the urchin *Sterechinus neumayeri* (cultured for 2 years in Suckling et al. 2015, incubated for 40 months in Morley et al. 2016) represent the few studies conducted showing the ability of this species to cope under changing environmental conditions.

Warming can impact organisms' survival since each species has a specific thermal tolerance window (Pörtner & Farrell 2008). Changes in temperature can impact physiology, modify life histories, alter interactions between species (Barnes & Peck 2008), and change distribution range (Griffiths et al. 2017). Response to thermal stress has shown less impact on development or growth, especially in ectotherms (Sheridan & Bickford 2011), while reduction in size due to oxygen depletion is more common (Pörtner & Knust 2007, Sheridan & Bickford 2011). Salinity influences stratification, and thus, potential light and oxygen availability for deep biological systems can be limited (Barnes et al. 2009). At least 50-60% of the species in the Southern Ocean are cold-adapted organisms, which are isolated by the Antarctic Circumpolar Current and the deep ocean (Barnes & Peck 2008). Warming may increase vulnerability of these cold-stenothermal species possessing a narrow thermal window (Peck 2004) many of which are endemic to the Southern Ocean. Griffiths et al. (2017) projected that from 963 analysed benthic species, 60% are expected to decrease their suitable habitat in response to warming. The largest habitat loss is expected for the region south of the Polar Front, with habitat reduction projected for 79% of the endemic species. The regions with the highest projected impact are the West Antarctic Peninsula, South Orkney Islands, and South Georgia, where warming impacts the survival of some species, and geographic isolation limits the colonization of species from northern waters. In contrast, the waters of the Weddell Sea, Ross Sea, and parts of the east Antarctic Peninsula are likely to increase in diversity, due to warming.

In the last years, more studies have assessed the importance of the synergistic or antagonistic interplay of environmental drivers for organisms' responses (Byrne & Przeslawski 2013). Short term experiments such as the study of Carey & Sigwart (2014) found that in chitons (Polyplacophora), smaller individuals are more sensitive to temperature increases, whereas larger individuals are more sensitive to temperature decreases and low pH. *Aplysia punctata* (Gastropoda) did not show any calcification change in response to low pH or high temperature

(Carey et al. 2016). Outside the polar areas, low pH leads to a shift away from calcifiers to non-calcifying species (Wootton et al. 2008).

There are many ways other than physiology in which species can respond to environmental stressors (Peck 2005). For example, they can alter their geographic range which may result in splitting populations in different habitats and ultimately lead to evolution of a new species. This option is limited for the Antarctic species because the Polar Front. At a given location, plasticity of a population can facilitate reallocation of energy to different processes.

Many of these responses of SO benthos are unknown though, and so are their different sensitivities to environmental change (Ingels et al. 2012). In recent years, effort has been made to document SO fauna, and the mechanisms they use to cope with changing environmental conditions (Griffiths et al. 2010). The efforts resulted in a data set with a report of about 8100 benthic species (De Broyer et al. 2011), and new records of their geographical and bathymetric distribution. This information is augmented by DNA sequencing, which provides a comprehensive genetic inventory in the Southern Ocean (Grant et al. 2011). Yet, there are still uncertainties about cryptic species and bipolar species, and little is known about their life history and the possible ecological importance.

Regionally and for specific groups our understanding is still very limited due to under-sampling in the east Antarctic, the Bellingshausen, and Amundsen Sea sector driven by their remoteness and poor accessibility (De Broyer et al. 2011). Plasticity might be a way by which an organism may cope or potentially adapt to rapid environmental change (Foo & Byrne 2016), and how it can provide resilience to environmental stressors over short time (Chevin et al. 2010).

Ideally longer datasets, covering decadal variability, would form the basis to elucidate the responses of communities and species to changing environmental conditions (Barnes et al. 2006). As these are rare in the dramatically under-sampled Southern Ocean, experiments could help to understand responses but cannot account for environmental change (Gutt et al. 2018) or are not long enough to show potential for acclimation as show by Ragazzola et al. (2013) in coralline algae.

1.4. *The importance of molluscs*

Globally, molluscs comprise of 50000 to 120000 species (Chapman 2009), of which 30000 are marine (Gosling 2003). Bivalves and gastropods are most studied due to their taxonomic richness (>80% of the total species, Gazeau et al. 2013) and ecological and economic value. The class Scaphopoda amongst the molluscs is poorly studied and comprises nearly 350 described species (Oehlmann & Schulte-Oehlmann 2003).

Molluscs are used as bioindicators (Markert et al. 1999) due to their wide distribution, their long-lifespan, and the direct contact of the shell with its habitat. 28 species in India are important for food and shell trade (Santhiya et al. 2013), and hence they are commercially bred (Ponis et al. 2003). Many molluscs species are used as medication in traditional cultures (Chakraborty et al. 2009, Ahmad et al. 2018). Metabolites isolated from nine bivalves species have been found to act against viral pathogens (Dang et al. 2011).

Molluscs are widely distributed and contribute a high biomass on different ecosystem levels (Oehlmann & Schulte-Oehlmann 2003), feeding echinoderms, fish, birds, and mammals (Purchon 1968). Bivalves occupy an important position in the trophic hierarchy, converting primary production and nutrients from the planktonic realm to benthic food webs (Gazeau et al. 2013). They are mainly suspension feeders (Winter 1978), thereby decreasing turbidity and increasing light penetration in the water column (Gazeau et al. 2013). Most organic particles are not ingested, but rather rejected as pseudofaeces (Bayne & Hawkins 1992). The molluscan metabolic cycle increases nutrients in the water such as ammonium, urea, and the biomineralization products, which may have a negative effect on habitat at large population densities, resulting in organic-rich sediments with low oxygen and reduced biodiversity (Castel et al. 1989). The shell also provides protection against predators, against the environmental conditions (Gutierrez et al. 2003), and it provides a habitat for some other organisms.

1.5. *Molluscs shells as records of environmental change*

Carbonate is an abundant mineral formed by organisms, predominantly in the form of aragonite, calcite and vaterite (Weiner & Dove 2003). Difference in morphology can be the results of plasticity within the species or genus, mutations, ontogenic development or adaptation (Zelditch et al. 2012). Several environmental factors can influence growth and calcification, such as food,

oxygen supply or temperature, resulting in changes in the chemical composition of the shell and the annual variation in growth (e.g., Schone et al. 2010, Schone & Gillikin 2012). However, biological organisms modify the update of elements from the environment, which is known as the vital effect (Urey 1951). Minerals often have specific characteristics such as crystal size, shape, and trace element concentrations (Weiner & Dove 2003) though shells often form composites of many minerals' crystal shapes. Molluscs exert control on biomineralization in which the cell creates an extracellular site called matrix composed of proteins, polysaccharides, and glycoproteins, in which biomineralization occurs (Crenshaw 1980). If the organism controls biomineralization too tightly, for example Echinodermata, they are not suitable for paleoenvironmental reconstructions (Weiner & Dove 2003). Kinetic effects can change chemical concentrations via calcium carbonate precipitation rates (Weber & Woodhead 1970; Ziveri et al. 2003). Crystal shape and crystal surfaces modify elemental uptake (Weiner & Dove 2003).

Next to elemental composition, I am using X-ray tomography to display internal dissolution and quantify relative density of the shell. It has been first used in carbonates to study progressive dissolution of the chambers in planktonic foraminifera (Johnstone et al. 2010), and it was utilized by Iwasaki et al. (2015) to determine relative density distribution in the test of *Globigerina bulloides* with X-microCT, and Prazares et al. (2016) in *Amphistegina lessonii* and *Marginopora vertebralis*. X-ray tomography was first applied to molluscs by Alma et al. (2020) to measure shell density for the scallop *Crassadoma gigantea*.

The focus of this project lies on aragonitic scaphopoda and bivalves since this composition shells are more susceptible to reach undersaturation levels in the SO by 2030 (McNeil & Matear 2008). They also have different lifestyles (living in, on and above the sediment) with circum-Antarctic distributions. The study draws on the comprehensive collections available at the British Antarctic Survey from SO locations. The chosen species are the scaphopod *Dentalium majorinum* and the bivalves *Cyclocardia astartoides* and *Limopsis marionensis.*

1.5.1. Scaphopoda

Scaphopods are the last clade of the Mollusca that appear in the fossil record (Steiner & Dreyer 2003). The oldest scaphopods are recorded from the Devonian at ca. 416 Ma (Ludbrook & Moore 1960). The group gradually diversified in late Palaeozoic and early Mesozoic times, although modern forms did not appear until the early Cretaceous (Ludbrook & Moore 1960).

There are few studies about the phylogenetics of Scaphopoda. The class is divided into two orders defined by the characteristics of their feet. The order Dentallida has a short foot, with a conical shape and an epipodial collar interrupted dorsally, resulting in a three- lobed appearance (Palmer 1979). Dentallida cannot retract their foot by extension, in contrast to the order Gadilida, which cannot retract their foot by inversion (Sigwart & Sumner-Rooney 2015). Within the Scaphopoda, Steiner (1992) suggested that the order Gadilida is a monophyletic group based on morphological characteristics, though Dentaliida remained unresolved. Reynolds (1997) incorporated the soft parts of the specimens into his analysis which led to the conclusion that both Gadilida and Dentaliida were monophyletic groups. This conclusion was corroborated by Reynolds & Osuku (1999) using morphological characteristics and cladistics parsimony methods. Using a 18S rDNA dataset, Steiner & Dreyer (2003) suggested a Scaphopoda-Cephalopoda clade. Scaphopoda share a lot of communality with gastropods: the univalve shell, the head with a radula, feeding habits, and the nervous system. At the same time, they share the digging foot, the bilateral symmetry, and the lack of eyes with the bivalves (Palmer 1979). Reynolds & Steiner (2008) suggested, based on the more recent morphological and molecular studies, that Gastropoda were closest to the Cephalopoda.

There are 816 extinct and 517 extant species of scaphopods. They are exclusively marine as they have a low tolerance to reduced salinity (Palmer 1979; Ludbrook & Moore 1960). In the ocean, Scaphopoda have a global distribution (Reynolds & Steiner 2008). Their diversity diminishes towards the poles (Reynolds 2006). Although they are known to live in the deep sea, their peak diversity is found on the deeper parts of the continental shelf and the upper continental slope in water depth between 200 and 1200m, with their maximum distribution ranging from 100m to 7000m depth (Reynolds 2006). The effect of environmental change has been reported for several taxa in the SO, though, few record has been generated for the class Scaphopoda.

The external calcified shell of Scaphopoda is tusk-like and has, after the protoconch is lost, one narrower, older apical aperture and a wider, younger anterior aperture (Sigwart & Sumner-Rooney 2015). In juveniles or specimens that have not lost the embryonal shell, the small end is not open. The head and the foot are located in the larger opening, while the narrow end is used for expelling detritus and water (Reynolds and Steiner 2008). Scaphopods burrow up to 30 cm into marine sediments with their short and eyeless head (Speer 2000), generally with the apical aperture

sticking out (Ludbrook & Moore 1960). They use octocyts to detect the environment and do not have gills, as they breathe through the mantle, taking water from the exterior and circulating it through cilia. When the O_2 content of the seawater is low, they expel the water.

There are eight species of scaphopods in the Southern Ocean, half of which are endemic (Brandt et al. 2012). *Dentalium majorinum* (Mabille & Rochebrune, 1889), an infaunal species, has a circum-Antarctic distribution (Steiner & Linse 2000). It has been found at a depth range from 24 m (Dell. 1990) to 2579 m (Melvill & Standen 1907). Specimens have a maximum length of 74 mm and are slender and with a moderately curved shell with numerous equally spaced ribs, (Mabille & Rochebrune, 1889).

Figure 1.4. Shown is the scaphopod *Dentalium majorinum* from different angles. The scale is display in the centre of the figure. Taken from Rochebrune & Mabille (1889) on the online Museum national d'Histoire naturelle.

Biominerals

Scaphopods have shown to have in general an aragonitic shell and a lower magnesium and strontium concentration (Smith & Spencer 2016). In scaphopods the anterior mantle margin is responsible for the shell growth (Lamprell & Healy 1998). The apical margin is responsible for a second mantle called "pipe", which forms the dorsal part, where the shell decollation occurs (Lamprell & Healy 1998). In this study, through Raman spectroscopy, it was possible to determine that *D. majorinum* have an aragonitic shell (Figure 1.5).
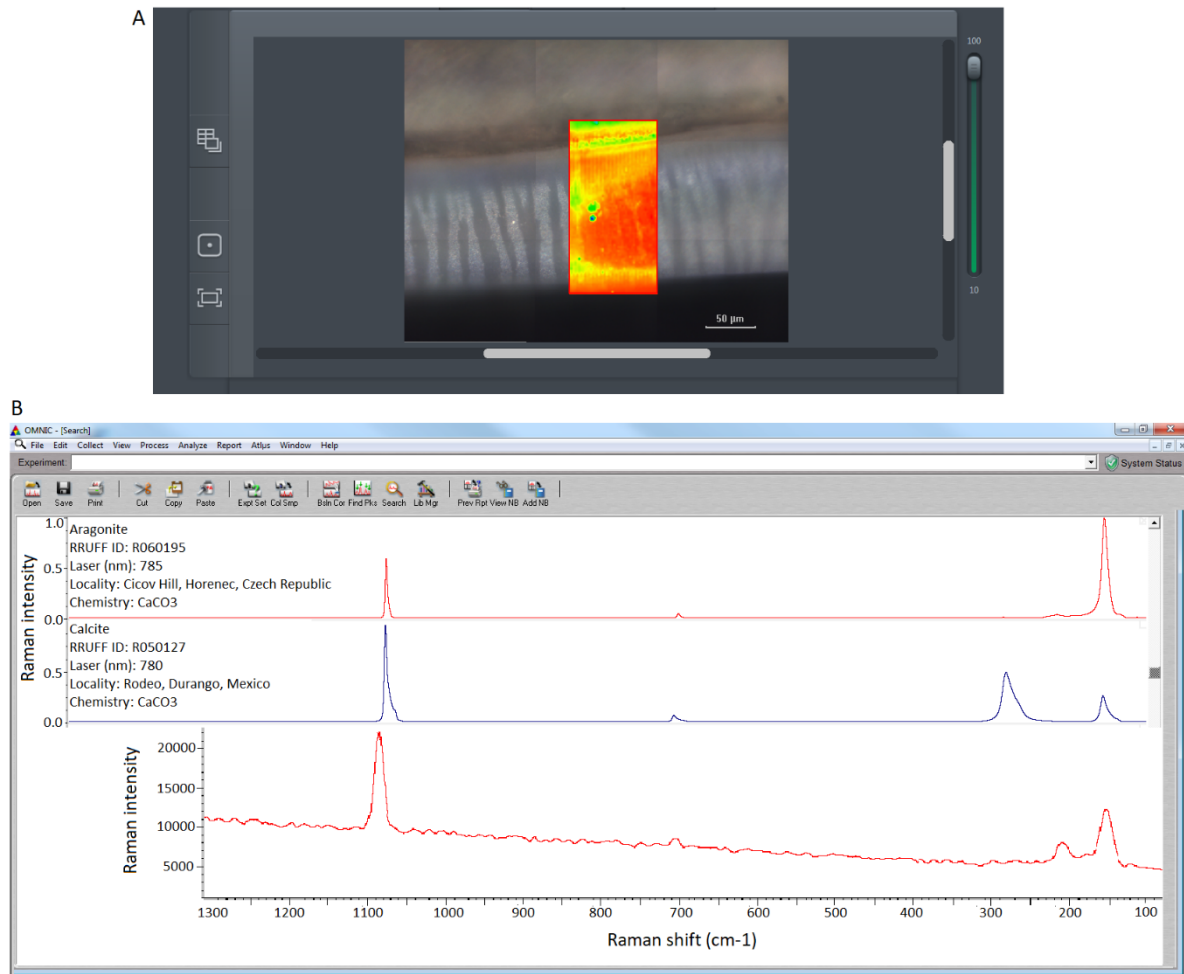
Figure 1.5. Raman spectroscopy analysis. A. Part of the specimen 1015.13 that was analysed in colour. B. Raman spectra plots of three different objects from up to down: aragonite stone from Czech Republic, Calcite from Mexico, and *D. majorinum* shell showing a wavelength frequency similar to the aragonite standard. In the y-axis the scattered light intensity and in the x-axis the frequency of light measured was number of waves per cm^{-1}.

1.5.2. Bivalvia

Bivalvia occur in both marine and freshwater environments. They are diverse, widespread, and abundant suspension feeders, which occupy coastal to deep-sea ecosystems from the northern to the southern high latitudes. Their survival is strongly linked to their shell integrity, since the shell provides protection against predators, and, in intertidal zones, from exposure to air (Stanley 1981, Andrade et al. 2019). Bivalve shells convert parts of the respiratory CO_2 into their shell minerals (Wheeler 1992). They buffer extracellular pH during periods of environmental exposure via in-vivo dissolution (Sokolova et al. 2000). As such, any change in shell production or strength could severely influence the survival of these organisms.

Bivalvia are found frequently in the Antarctic marine sediments. With 158 species (57% endemic for the SO, Brandt et al. 2012), bivalves are the second most diverse -in terms of number of species- molluscan group in the SO deep sea (Linse et al. 2006). Diversity is not changing with depth (Brandt et al. 2007).

Study species *Limopsis marionensis* (Smith, 1885)

Limopsis marionensis is one of the most common and wide-ranging Antarctic bivalves. It has an extensive circum-Antarctic and sub-Antarctic Island distribution and can be found in the Ross Sea, the Indian Ocean Subantarctic Islands, Chilean coast, and Falkland Islands from depths of 56- 1097m (Nicol 1966). The species is immobile and lies on the bottom surface associated with other organisms such as sponges (Pörtner et al. 1999). *L. marionensis* has a distinctive long hairy periostracum and is known to grow as large as 80mm (Engl 2012, Figure 1.6).

Figure 1.6. Shown is the bivalve *Limopsis marionensis*. The scale is display in the left side Taken from Rochebrune & Mabille (1889) on the online Museum national d'Histoire naturelle.

Study species *Cyclocardia astartoides* (Martens, 1878)

C. astartoides has a circum-Antarctic distribution (Nicol 1966). *Cyclocardia astartoides* lives in water depths shallower than 500 m (Buckeridge 1989, Troncoso et al. 2007), although Powell (1958, p. 177 in Nicol 1966) reported their occurrence at 640 m water depth. They live on hard ground, sandy bottom, and clay, stones, sand, and gravel. The shell is oval and radial approximately with 20 striates, valves are equal and not equilateral (Cruz 1990, Figure 1.7). The periostracum is well developed and irregular following the growth lines and has a concentric shape. No signals of sinus are visible, and the pallial line is not well marked (Nicol 1966). The anterior

adductor muscle is slightly longer than the posterior muscle (Cruz 1990). There is no evidence for incubation or young brood in breeding (Hain & Arnaud 1992).

Figure 1.7. Shown is the bivalve *Cyclocardia astartoides*. The scale is display in the left side.

Several bivalves species in the SO have been analysed for geochemistry such as *Laternula elliptica* (Nehrke et al. 2012), *Adamussium colbecki* (Lartaud et al. 2010), *Limatula pygmaea, Limatula ovalis, Limopsis marionensis, Limopsis knudseni, Lissarca miliaris, Lisssarca notorcadensis, Cyclocardia spurca and Aequiyoldia eightsii* Jennions unpub. thesis 2014), but no spatial comparison has been made along latitudinal gradients.

1.6. *An introduction to the chapters*

I will investigate the response of the *Dentalium majorinum* shell along depth gradients in the Amundsen- and Weddell seas. I will model the function of the skeletal variability quantified in chapter 2 and assess if plasticity in organisms improves function. I use methods developed in chapter 2 to assess the responses of two bivalves *Cyclocardia astartoides* and *Limopsis marionensis* to the environment following a latitudinal gradient. These chapters will summarize my projections on if future climate change will impact the ability of these species to provide their role in the ecosystems of the Southern Ocean.

1.6.1.   Regional responses in shell properties to natural environmental drivers in an Antarctic deep water scaphopod (Mollusca) (Chapter 2)

In this chapter, I characterise the shell of *D. majorinum* and quantify the impact of temperature and carbonate chemistry on growth, calcification, and skeletal structure with depth transects in the Amundsen Sea and Weddell Sea. Molecular genetics of specimens from the Amundsen and

Weddell seas show that the same species can be found in both regions. I assess if warmer waters and lower carbonate ion concentrations result in thinner shells and in-vivo dissolution invisible at the shell surface. I use morphometric measurements, CT scanning, growth increment analysis (GIA), Scanning Electron Microscopy (SEM) and electron microprobe analyses. I quantify shell density and geochemistry within water depth across the regions. Traditional morphometrics involved using a caliper to measure different distances and lengths on a specific organism as well as volumes or areas (Marcus et al. 1990). Growth lines have been assessed by eye via a light microscope, with a Scanning Electron Microscope and with acetate peels. Morphological plasticity is displayed in this species. This species shows different levels of dissolution but has strict biomineralization control.

1.6.2. Shell shape and ornamentation as a plasticity adaptation mechanism to environmental change (Chapter 3)

The environment might impact shelf formation and as such structural integrity. Finite element (FE) models are used to assess structural integrity of the scaphopod shell against hydrostatic water pressure and shear load. I use the morphological data generated in Chapter 2 to generate an FEA model of the scaphopod *D. majorinum*. I assess the role of ornamentations in improving strength of the shell and the impact of shell shape, which responds to the environment. The data provide insights about vulnerability of the species in response to environmental change, linking this to their biomechanical properties.

1.6.3. The response of Antarctic bivalves to environmental change in the Southern Ocean (Chapter 4)

Bivalve specimens from the Amundsen, Weddell Sea, Sandwich Islands and Magellan region were analysed for differences in density, mineralogy, and geochemistry as a result of different environments. Using morphology and density information based on the same methodologies as chapter 2, this chapter characterises and describes the shell in *Cyclocardia astartoides* and *Limopsis marionensis*. Additionally, I address if there are differences in shell dissolution within specimens and between regions. I address the question, if shell chemistry, specifically Sr and Mg, differs between the shells of the two seas. I use CT scanning for density measurements and electron microprobe for geochemistry measurements. As such, this chapter will contribute to our understanding of Southern Ocean bivalve responses to different environmental conditions.

1.7. *Methods used in this thesis.*

In the following I will briefly describe the methods which are applied.

1.7.1. Scanning Electron Microscopy Imaging (SEM)

The scanning electron microscopy (SEM) provides a non-destructive tool to analyse a specimen at micrometre scale (Gill 2014). SEM uses a beam of electrons to reveal the surface characteristics of a specimen and its three-dimensional structure (Holgate & Webb 2003). Samples examined in the SEM need to conduct electricity, which is often improved via coating by applying metallic layers (Boyde1972). Carbon is one of the most used materials, followed by gold. Samples were sectioned to provide a flat surface, while others were etched and then polished. Typical accelerating voltages are between 0.5 to 40 kV. Higher voltage decreases spot diameter and hence increases resolution but at the risk of damaging unstable materials such as carbonate (Holgate & Webb 2003). The interactions between the electron beam and the specimens are mapped as variations of brightness or deflections.

1.7.2. Electron Probe Micro-Analysis (EPMA)

Electron Microprobe Analysis (EPMA) shows the distribution of elements, in this case Ca, Sr, Mg, in a specimen and displays the concentrations via spot measurements, maps or transects. As only a small amount of material is ablated, it is possible to repeat the measurements as often as required. In a microprobe, two techniques are used: a wavelength disperser spectroscopy (WDS) and energy disperse spectroscopy (EDS). Both collect different emitted x-rays which reflect from a specimen that is exposed to a focused x-ray beam (Heath 2015). WDS is applied to trace elements while EDS is used to identify major elements. EPMA provides quantitative data at a sub-micrometer scale. Trace elements can be measured down to concentrations of 10ppm, although for most materials realistic concentrations are closer to 100 ppm (Heath 2015).

Carbonates are used to reconstruct past climates since the replacement of Ca (0.99 Å) with Mg (0.66 Å) is easy due to its similar size. Sr ion (1.12 Å) is isostructural with aragonite since the latter is orthorhombic. There are several studies that correlate those proxies with different drivers (Table 1.1).

Table 1.1. Sr and Mg proxies that are being use by different authors in bivalve shells and their relationship with environmental or kinetic controls.

Proxy	Species	Control or relationship with a driver	Author (s)
Sr/Ca	*Modiolus modiolus* *Mytilus edulis* *Mya arenaria*	(-) Growth	Swan (1956)
Mg and Sr	*Crassotrea virginica*	No correlation with temperature or salinity	Rucker & Valentine (1961)
Mg/Ca and Sr/Ca	*Mytilus edulis*	(-) Temperature	Dodd (1965)
Sr/Ca	*Mya arenaria*	(+) Age	Palacios et al. (1994)
Sr/Ca	*Calyptogena magnifica*	(+) Temperature	Hart & Blusztajn (1998)
Sr/Ca	*Saxidomus giganteus* and *Mercenaria mercenaria*	Control: Kinetic factors	Gillikin et al. (2005)
Sr/Ca	*Pinna nobilis*	No correlation with temperature	Freitas et al. (2005)
Mg/Ca		(+) Temperature at early growth phase	
Mg/Ca and Sr/Ca	*Ruditapes philippinarum*	Not under environmental control	Poulain et al. (2015)
Sr/Ca	*Tridacna gigas*	(-) Temperature	Yan et al. (2013)

1.7.3. X-ray microcomputed tomography

µ-CT scanning allowed the observation of internal structures of calcifiers without damaging or manipulating the shell before other analysis is made. In this technique, monochromatic X-rays are attenuated for an object. X-rays are reflected onto a panel detector transmitting an image, termed a projection. The number of projections depends on the size of the object and the resolution of the analysis. The projections are transcribed and used to generate a 3D reconstruction via an image stack. The sample is positioned in a material which allows X-rays to travel through without interference, like a foam. Scanning is performed with x-ray energy ranging for µCT from 20 to 100 kVp (Ritman 2004). The attenuation of the x-ray photons depends on the material which either

absorbs or scatters the energy. Filters can reduce artifacts created during scanning. The voxel size depends on the resolution that needs to be achieved and that allows good image segmentation and grey differentiation (next steps). Small element voxel sizes result in a higher resolution at the cost of higher scanning time resulting in large data sets. Large specimens can therefore be analysed with larger voxel size, whereas smaller structures will need higher resolution (Bouxsein et al. 2010). Beam hardening is a side effect of bench top setups (Schmidt et al. 2013). Beam hardening results from selective attenuation of a polychromatic x-ray beam passing through an object as the higher energy passes easily through the sample and the lower is preferentially absorbed. The effect is visible in the grey scale distribution, since an even homogenous sample will have different grey values (which can be used as density scale, in which brighter greys means denser material) (Bouxsein et al. 2010). After analysis, the images are segmented with AVIZO software using a preference threshold that can cover the target object. This software allows measurements in the images in a 2D or 3D form and like that be able to quantify morphological parameters and density.

1.7.4. Finite element analysis

Finite Element analysis (FEA) was developed originally to answer questions related with functionality and design in engineering but has since moved to medicine and biological areas as a tool to model different organism structures (Rayfield 2007, Figure 1.8). FEA is a numerical method where a structure is divided in smaller parts - so called finite elements (Zienkiewicz et al. 2005). The different finite elements are integrated in a mesh, where specific equations are solved. Firstly, a structure is generated to develop a 3D shape. Then a mesh is generated which consists of elements connected by nodes. Each element is assigned elastic properties to mimic the elasticity of the real structure. Boundary conditions are assigned to represent how the structure is fixed in space. To this digital model, loads and forces are applied and differential equations are solved. For each node, displacements are calculated, based on the applied loads, forces, structural geometry, and material properties (elasticities). A complete mechanical response to the applied loads is calculated. After the analysis, post-processing includes visualisation, representation, and interpretation of, for example, the stress-strain response of the model.

Step

Identifying structure of
interest and problem

Preprocessing

Model generation

Capturing digital
representation of
structure

FEEDBACK

Discretization

Dividing the continuum
structure into finite
element mesh and nodes

FEEDBACK

**Material property and
boundary condition assignment**

Mimicking elasticity of the
real structure

Recreating loading
conditions during function

Calculating nodal displace-
ments, strain and stress
during prescribed loading

Analysis

Representing and
interpreting results

Postprocessing

Stress   Strain   Deformation

Location

• CAD software
• Image analysis software
• FE preprocessing software

• Image analysis software
• FE preprocessing software

• FE preprocessing software

• FEA software

• FE postprocessing software

Figure 1.8. General steps of FEA analysis. In the pre-processing stage the shape of the modelled object is developed. In this step the object is discretised into elements and each element is assigned with an individual material property. The next step is the analysis, where the corresponding equations are solved on the computational grid. The last step is the post-processing, which involves investigating the results and possibly rerunning the analysis, based on the new results. Taken from Rayfield (2007).

CHAPTER 2 : REGIONAL RESPONSES IN SHELL PROPERTIES TO NATURAL ENVIRONMENTAL DRIVERS IN AN ANTARCTIC DEEP WATER SCAPHOPOD (MOLLUSCA)

Abstract

Regional differences in temperature, ocean acidification, carbonate chemistry and food availability can generate species-specific responses in molluscan shell shape and compositions with implication for vulnerability to climate change. Calcifying organisms additionally are at risk to diminishing their fitness due to changes in carbonate chemistry in waters with already low saturation. This is especially important in Antarctic, where species can be particularly vulnerable to environmental changes. The Weddell and Amundsen seas each display a distinctive oceanography which makes them ideal to assess biotic responses to different environmental conditions. Here, I assess shell morphology, dissolution, and geochemistry of the scaphopod *Dentalium majorinum* (Mabille & Rochebrune, 1889) from the Weddell and Amundsen seas using the environmental differences as a natural experiment. I combine morphometrics, μ-CT scanning, SEM, and electron microprobe analysis to evaluate phenotypic plasticity at intraspecific level, determine dissolution and elemental composition, and put the information into an ontogenetic framework to assess changes with age. Variability in shell morphometric parameters such as ventral and dorsal diameters, length, and arc are interpreted as morphological plasticity in response to different depths and regions which is driven by unequal oceanographic conditions that impact the temperature and food availability. Mg/Ca and Sr/Ca ratios differ between specimens with depth. Density is not dependent on size or age, suggesting a strong biomineralization control. Dissolution was evident in almost all the specimens, all of which were alive at time of collection, with some of them with >10% of the shell dissolved. This suggests a link with undersaturation events and/or low pH, but also a possible ameliorate food effect. I suggest that *D. majorinum* can cope with the stress environmental conditions if there is not extensive dissolution, and if there are available resources to counteract it.

2.1.   *Introduction*

Increasing atmospheric carbon dioxide is changing environmental factors such as pH, carbonate, and aragonite saturation (Ω_{Ar}), temperature, stratification, salinity, and primary production in the marine systems (Pörtner et al. 2014). Historical observations and climate model projections agree on a global warming of the ocean surface (0.87°C average compared with preindustrial time, Hoegh-Guldberg et al. 2018), an increase in surface ocean stratification, deoxygenation of the ocean interior, and regional changes in net primary production since the beginning of industrialisation, accelerating in the next decades (Keeling et al. 2010; Bopp et al. 2013). Warming and changes in carbonate chemistry are not globally equal, though (Roemmich et al. 2015). The Amundsen Sea (AS), to the southwest of the Antarctic Peninsula, is one of the regions with the largest warming in the Southern Ocean (SO) in the past decades (Schmidtko et al. 2014), while changes in surface water temperatures and sea-ice extent eastern Antarctic Peninsula, appear to be minor (Shadwick et al. 2013). In the AS, old, relatively warm, and carbonate-undersaturated Circumpolar Deep Water (CDW) upwells onto the shelf, making these water masses naturally low in carbonate saturation (Jacobs et al. 2011). In contrast, the Weddell Sea (WS) is a region of downwelling of cold and young water masses formed on the shelf, thereby exporting water with increasing CO_2 (Nicholls et al. 2009, Hoppema et al. 1999). Projections based on RCP 8.5 suggest that the SO will become undersaturated with regards to aragonite between 2035 and 2040, beginning in western sectors of the SO and quickly expanding towards the east (Hauri et al. 2016). Additionally, phytoplankton photosynthesis increases Ω_{Ar} in the surface waters by decreasing dissolved inorganic carbon (DIC) and increasing total alkalinity (TA) (DeJong et al. 2015). Some western SO areas such as the Bellingshausen and Ross seas are already experiencing short undersaturation in surface waters driven mainly by anthropogenic CO_2 emissions (Hauri et al. 2016).

Such environmental changes are suggested to impact the physiology of organisms differently, depending on their life history, genetic and phenotypic plasticity, and the rate of environmental change (Peck 2014). All these factors determine how much an organism is ecologically affected by environmental and climate change, and whether any of these factors could potentially cause local, global extinction or loss of ecosystem function.

In response to ocean acidification (OA) and warming, marine calcifiers globally are considered to be more sensitive than organisms without carbonate shells (Kroeker et al. 2013) as the change in

chemistry is projected to decrease the ability of marine calcifiers to generate skeletons and shells (Watson et al. 2012, Byrne & Przeslawski 2013). OA can affect calcification, acid-base regulation, immune response, and behaviour (Gazeau et al. 2013). Temperature also impacts the physiology of marine organisms and thereby limits their distribution (Pörtner 2008, Cole et al. 2016). Warming can also lead to loss of performance, changes in growth, and on an ecosystem level, impacts the food web (Pörtner et al. 2014).

An important group of calcifying organisms in the global marine ecosystems is the Mollusca, which has been affected by warming, one the most important drivers of biotic response to climate change in this group (Byrne & Przeslawski 2013). The responses of different species under thermal stress have been variable (Peck 2005). High temperature (25°C) decreased shell strength in the temperate *Crassadoma gigantea* (Alma et al. 2020). Similarly, under elevated temperature (20°C), the gastropod temperate *Litorina littorea* slows down the increase of weight and is shorter than those which grew under mean surface temperature (15°C, Melatunan et al. 2013). OA can also impact physiological processes in different ways. For example, adult clam, scallop, oyster, conch, and whelk species from temperate climates (e.g. *Mercenaria mercenaria, Mya arenaria Argopecten irradians*, *Crassostrea virginica,, Strombus alatus* and *Urosalpinx cinereal*) decrease their net calcification with increasing pCO_2 (Ries et al. 2009) while the temperate mussel *Mytilus edulis* exhibited no response. Similarly, in clams, conchs, periwinkles, and whelks, net dissolution of the shells was recorded only at 2856 ppm (Ries et al. 2009).

However, using data from individual drivers such as acidification or warming may be misleading as these can function as additive, synergistic, or antagonistic, and have the potential to exacerbate or ameliorate the impact of climate change (Hofmann et al. 2010, Byrne & Przeslawski 2013). Kroeker (2014a) showed that the impact of OA on the mussel *Mytilus galloprovincialis* was reduced under moderate warming. Similarly, the subtropical oyster C*rassostrea virginica* show a partial reduced effect of hypercapnia (pCO_2 800 ppm) by moderate warming (27°C), when both are combined (Matoo et al. 2013). Likewise, low pH and increased temperature caused dissolution and reduction in shell density with a high impact for the gastropods *Columbella rustica* and a lesser impact for *Nassarius nitidus* (Chatzinikolaou et al. 2017), whereas non synergistic effect of pCO_2 and temperature was found for shell strength and density in the bivalve *Crassadoma gigantea* (Alma et al. 2020). On other hand, it has been shown that food availability ameliorates the effect of OA (at 470, 1020 and 2110 µatm) in the growth and calcification in the juvenile of *Mytilus*

edulis (Thomsen et al. 2013). Similarly, high pCO$_2$ levels and low food concentrations decrease shell growth and cause shell internal dissolution, whereas with a high food availability there is a lower effect of the latter (Mezlner et al. 2011). Interestingly, the synergistic effect of pCO$_2$, temperature, salinity, and food on the larvae of the temperate Australian oyster *Ostrea angasi*, caused that the larvae were smaller under reduced salinity at both optimum and elevated temperatures (Cole et al. 2016). No effect of CO$_2$ was found on development in the absence of other stressors, but the CO$_2$ changes impacted growth under starvation.

Important groups of calcifying organisms in the SO marine ecosystems affected by OA are Mollusca and Brachiopoda. Physiological responses of Antarctic molluscs to one or several stressors have previously been explored in short laboratory culture experiments, yet field studies are limited. Gardner et al (2018) reported that the pelagic pteropod *Limacina helicina antarctica* showed shell malformation, dissolution, and a high larval mortality (up to 39%) in response to 5d exposure to OA (1.7°C and pH 7.6), 25% in acidified-warm (3.5°C and pH 7.6), and just 12% in warming (3.5°C at 8.1 pH). This was similar to what was found by Cross et al. (2019) in the brachiopods *Liothyrella uva* and *Calloria inconspicua* over 7 months and 3 months exposure, respectively, for a reduced pH in response to a business-as-usual scenario, but they did not find any effect on temperature on the shell. Likewise, Peck et al. (2004) reported an activity decline in response to warming of 2°C and 3°C, after 24h, in the Antarctic bivalve *Laternula elliptica* and Antarctic limpet *Nacella concinna*.

The effect of environmental drivers on Mollusca has been studied in the Bivalvia, Gastropoda, Polyplacophora and Cephalopoda (Gazeau et al. 2013, Parker et al. 2013), but little is known about the response of the Scaphopoda. In this study, I compare shells of the scaphopod *Dentalium majorinum* (Mabille & Rochebrune 1889) from two regions in the SO. Using the regional differences of the environments in the Amundsen and Weddell seas described above, I examine the morphological plasticity of *D. majorinum*. Combined with a novel approach of µ-CT scanning and electron microprobe analysis on specimens from both regions, from different water depth, and of different ages, I examine if 1) there are differences in shell morphology with depth and between regions, if 2) there are differences in shell thickness and density between populations from the two regions with depth, if 3) there is evidence of shell dissolution reflecting the differences in carbonate chemistry in the region, and 4) if Mg and Sr change with age of the specimen and in response to environmental conditions. I discuss these findings in the context of currently available

27

environmental information in the Amundsen and Weddell seas, phenotypic and aragonitic mineralogy plasticity, and how these findings can provide insights into future environmental changes in this region for molluscs.

2.2. *Materials and methods*

2.2.1. Study species and its biomineralization

In scaphopods, the anterior mantle margin is responsible for most of the shell growth, while the apical margin is responsible for a second mantle called "pipe", which forms the dorsal part, where the shell decollation occurs (Lamprell & Healy 1998). The shell is formed by an outer, organic, chitinous layer (the periostracum), and three biomineralized layers: a thick middle layer with a crossed-lamellar ultrastructure, an external prismatic layer, and finally an inner layer of concentric substructure (Palmer & Steiner 1998).

The scaphopod *Dentalium majorinum* (Mabille & Rochebrune 1889) has a circum-Antarctic distribution, infaunal lifestyle (Steiner & Linse 2000), and lives in a depth range from 24 m (Dell. 1990) to 2579 m (Melvill & Standen 1907). Shells are slender, with a moderate curve and adorned with numerous ribs placed evenly along it, separated by concave intervals. Maximum recorded shell length is 74 mm (Mabille & Rochebrune 1889).

A total of 452 scaphopod specimens were collected during expeditions of RRS James Clark Ross and RV Polarstern to the Amundsen and Weddell seas by Agassiz trawl (AGT), epibenthic sledge (EBS), Multi Grab (MG), in situ pump (ISP) and set gillnet (GSN). In the AS, 326 specimens (290 alive, 36 dead) were collected during JR179 in 2008, while 143 specimens were collected in the WS during RV Polarstern expeditions ANT-XXI/2 (8 alive; 2003; eastern WS), ANT-XXVII/3 (47 alive, 11 dead; 2011; western WS), and RRS James Clark Ross JR275 (57 alive, 3 dead; 2012; southern WS) (Figure 2.1, Appendix A, Table A1). All specimens were fixed 96% ethanol and samples are housed in the British Antarctic Survey Marine Specimen Store.

2.2.2. Environmental conditions in the study area

Temperature and salinity data were compiled from the RV Nathaniel B. Palmer (http://www.marine-geo.org/), RV Polarstern (https://www.pangaea.de) and RRS James Clark Ross (https://www.bodc.ac.uk) cruises from 2005 and 2014. The data was uploaded to the

Software Ocean Data View 5.1 for visualisation and analysis. I separate the depths according to the different water masses changes in the Amundsen Sea bundling specimens from a range of depths in accordance and follow the same pattern in the Weddell Sea. The average temperature and salinity in the AS shows coldest temperatures in shallowest depth (300-500 m= 0.566°C, 34.5 psu) and stable temperature and salinity below (501-800 m = 1.11 °C, 34.6 psu; 801-1200 m = 1.14°C, 34.7 psu; 1201-1600 m= 1.16 °C, 34.7 psu). While closer to the surface in the WS temperatures (300-500 m= -1.67°C, 34.4 psu) are colder, following by an increase of temperature with depth, although there are still colder than the AS waters. At depth 501-800 m = -1.04°C, 34.5 psu; 801-1200 m = 0.25°C, 34.6 psu; and 1201-1600 m = 0.0145°C, 34.7 psu, in the WS (Figure 2.1).
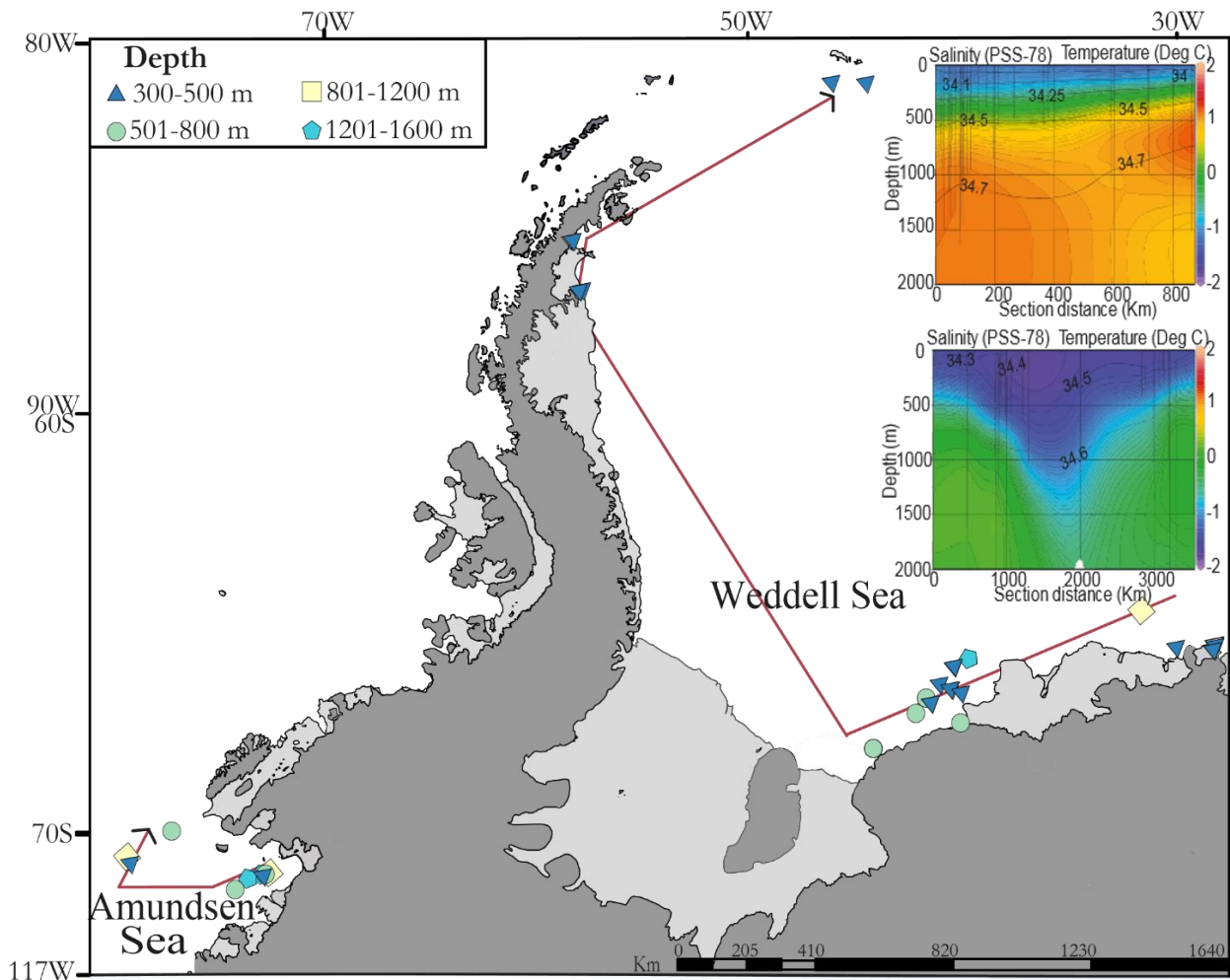
Figure 2.1. Map with sample locations and depth zones of *D. majorinum* in Amundsen and Weddell seas. Depth distributions of the samples are indicated with different colours and shapes in the left top legend generated with ArcMap 10. Dark blue triangle = 300-500 m, green circle = 501-800 m, yellow square = 801-1200 m, and blue light polygon = 1201-1600 m. The oceanographic water mass model of the regions in the top right generated with Ocean Data View. Profiles sections (indicated by red lines in the map) of the Amundsen Sea between 2005-2008 (top) and Weddell Sea between 2006-2014 (bottom) show the temperature (°C) colour coded, and salinities (PSS-78) at different depth ranges are displayed.

2.2.3. Molecular analysis

For molecular species validation, eight specimens of *Dentalium majorinum* and two specimens of *Dentalium megathyris* were analysed from the Weddell and Amundsen seas. DNA was extracted using standard protocol. Chiefly, 0.5 cm of tissue were dissolved in 180 µl of tissue lysis buffer ATL, 20 µl Proteinase K of the Qiagen DNeasy kit (DNeasy® plant mini kit Qiagen, Chatsworth, CA, USA) and incubated for 4h at 56°C. In a second step, 200 µl of AL buffer and 200 µl of ethanol were added and centrifuged for 15s. The extraction followed standard protocols. The DNA

was stored at -2°C degrees. Densitometric measurements of DNA were made with Thermo Scientific™ NanoDrop™ spectrophotometer to determine the relative quantity and purity of the samples for PCR.

The gene Cytochrome oxidase 1 (CO1) in the mtDNA region was amplified using the DNA primers LCO 1490 and HCO 2198 (Folmer et al. 1994). CO1 is a common barcoding gene that has the capability to differentiate species in molluscs. Each PCR run contained 1 µl NH4 RXN buffer, 1 µl MgCl2, 0.4 µl dNTPs stock, 0.2 µl Biotaq DNA polymerase (Biotaq DNA Polymerase kit, Bioline Ltd., UK), 4.6 µl PCR quality H2O, 0.4 µl of forward primer, 0.4 µl of reverse primer and 1–2 µl of DNA, totaling 10 µl of the PCR mix. Amplification was performed using the Techne Thermo cycler G-storm GS4 model (50 s at 98°C then 35 cycles of 10 s at 98°C, 10 s at 56°C and 90 s at 72°C, ramping to 72°C at 0.38°C/s). PCR products were separated by agarose gel electrophoresis and visualised by GelRed staining with UV light. PCR products of ten specimens were genetically sequenced by COMPANY, which provided CO1 sequences of eight specimens in good quality.

The resulting sequences were aligned using the NCBI Basic Local Alignment Search Tool (BLAST, http://blast.ncbi.nlm.nih.gov/Blast.cgi) and CodonCode Aligner, version 1.2.1, (CodonCode Corporation, Centerville, MA).

2.2.4. Morphology

All specimens were photographed using a digital Nikon Coulpix 995 camera. Shells were assessed for visual marks and holes that could indicate predation attacks. Shell length, dorsal and ventral aperture diameters were measured using digital Vernier calipers or an ocular micrometer under a Zeiss Semi SV6 stereomicroscope. The curvature of the shell, defined by its arc in the dorsal part, following the method of Steiner & Linse (2000), was measured with ImageJ (Figure 2.2).
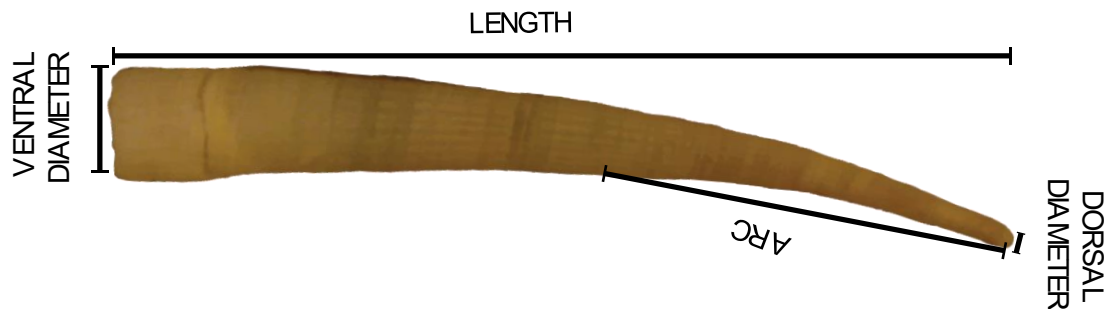
Figure 2.2. Definition of parameters for morphological measurements in *Dentalium majorinum* showing length, ventral diameter, dorsal diameter, and Arc curvature.

As fragmentation at the tips (dorsal diameter) is common, the assessment of completeness of the shell was made by correlating overall length with dorsal diameters. Any specimen which did not fall within the 95% confidence level of the regression was considered broken and removed from the analysis, reducing the dataset to 323 specimens. From these specimens, I chose specimens to analyse with the different techniques, which were representative from each water depth, different sizes and/or without visible signs of damage (Table 2.1). Individual specimens selected for different, further analyses are given in Table 2.2.

Table 2.1. Number of specimens used in each analysis for water depth in m. Performed analyses are Morphology, µCT-scanning, diet, EPMA and age determination.

Region	Depth (m)	Morphology	µCT scanning	Diet	EPMA	Age
Amundsen Sea	300-500	129	8	8	2	8
	501-800	36	4	4	2	
	801-1200	42	7	7	2	1
	1201-1600	17	2	2		1
Weddell Sea	300-500	74	10	10	3	8
	501-800	19	3	3	2	2
	801-1200	2	1	1		
	1201-1600	2	1	1		

Table 2.2. Details of specimens used for µ-CT scanning (density/shell integrity), diet, EPMA and age determination.

Region	Vial. Specimen No.	µ-CT scanning	Diet	EPMA	Age
Amundsen Sea	1015.3	x	x		
	1015.9	x	x		
	1015.71	x	x		
	1015.64	x	x	x	
	1015.83				x
	1015.76				x
	1015.1				x
	1015.13				x
	1015.44				x
	1151.12				x
	1151.4	x	x		
	1146.3	x	x		
	1096.16	x	x		
	1055.6	x	x	x	
	1116.3	x	x		
	1116.2	x	x	x	
	919.1	x	x		
	919.11	x	x		
	582.1	x	x		
	693.7	x	x		
	278.2	x	x	x	
	146.5	x	x	x	
	190	x	x	x	
	155.1	x	x		
	383.8	x	x		
	322.24	x	x		
	322.25	x	x		
Weddell Sea	114.29	x	x		
	114.27	x	x		
	114.23	x	x	x	
	114.21	x	x		
	114.9	x	x	x	
	114.22	x	x		
	114.4	x	x		
	1487.4				x
	1487.1	x	x		
	1487.3	x	x	x	
	684.2	x	x	x	
	1179	x	x		
	131.3	x	x	x	
	736.2	x	x		
	1220	x	x		
	259.4	x	x		
	199.2				x
	1385.8				x
	1487.1	x	x		
	447				x

2.2.5. Age determination

Lifespan in scaphopods is currently unknown (Davis 1987). As previous studies on other molluscs show changes in response to environmental drivers with age, I use growth lines to assess it. I am building on the assumption that these are annual like in SO bivalves (e.g. Roman-González et al. 2017). I used 20 specimens with no visual damage and coloration of different lengths to determine the age of *D. majorinum* (see Table 2.2) and establish a potential age-size relationship. Specimens were embedded in epoxy resin for 24 hours, and subsequently grinded to expose the shell with P800, P1200, P2400 and P4000 grinding paper, followed by a diamond-grade polish of 6µm, 3µm and 1µm. After every polish, the shell was sonicated to remove contaminant material for 3min. The shells were etched in 0.01M HCl for +/-60 minutes and one for 120 minutes. Finally, traces of acid were removed with water. Images were taken using a Hitachi S-3500N variable pressure scanning electron microscope (SEM). Between 30-70 images were obtained from each shell, depending on the size of the individual specimen. SEM Images were stitched together using the Fiji-ImageJ software (Rasband 2011), printed, and analysed. Clear annual growth increment determination was possible in ten of the 20 specimens.

2.2.6. µ-CT scanning

A total of 36 *s*pecimens were µ-CT scanned with the Nikon XTH225 ST at the University of Bristol. The scans were performed at 360° at 80 kV, 88 µA and 1.41s exposure with a 0.25 mm aluminium filter resulting in 3141 projections (voxel size = 5µm). For each scan, an aragonite crystal from Cumberland, UK with a density of ~2.93 g/cm^3 was used as a calibration standard to convert grey values into density of the aragonite scaphopod shells as shown by Chatzinikolaou et al. (2017) and Alma et al. (2020) for gastropods and bivalves. During the calibration procedure, centre of rotation, beam hardening correction, calibration factor and scaling factor setup were determined. The resulting scaling factor was applied to the corresponding scaphopod dataset with a grayscale value equivalent to the mean grayscale value for the complete aragonite standard dataset. This process minimizes variation in brightness in response to changes through time arising from within the µ-CT acquisition (e.g. changing efficacy of filament, warming up of the target, etc). The same settings were applied to the specimen scans.

The scans were reconstructed as 16bit Tiff files. Tiff stacks were exported using VG Studio Max 2.2 (Volume Graphics GmbH, Heidelberg, Germany) comprising up to 2000 cross-sectional slices. Only slices around the midpoint of the projections (slices 750–1250) were used in

the analysis (the shells have different length, but similar projections number). The carbonate of the aragonitic scaphopod shell was segmented in Avizo Lite (Version 9.7, Thermo Fisher Scientific, Merignac, France). The optimum grey value threshold 25000 at the base and 65535 at the top. Most of the shells were reconstructed manually on Avizo Lite V9.7 because the automatic threshold was including parts inside of the scaphopod (like food items and rocks), and a new relative density was generated (Appendix A, Figure A1).

Additional to density, shell thickness was measured, and shell dissolution was calculated in the same specimens and virtual slices through the specimen's shell. I categorised dissolution, i.e, volume loss, at five levels: no damage (1), holes in the ribs (2), holes in ribs and inside the main shell (3), holes in ribs, loss of ribs/loss outer shell and corrosion inside the shell (4) and more than 10% dissolved (5). Total shell volume was reconstructed by hand combining the holes, corrosion, and loss of shell (Appendix A, Figure A1). Shell dissolution was determined as:

  Shell dissolved (volume loss) = Total shell vol (reconstructed) – Vol of the shell without dissolution

Thickness was calculated in the slices 750, 900, 1050 and 1250 for consistency and all measurements were made in the same part of the specimen, avoiding the ribs. The average was calculated for each of the 36 investigated individuals.

The reconstructions of the µ-CT scans using Avizo lite V9.0 revealed the scaphopod soft parts as well as non-scaphopod content within the shells of the scaphopods. Images of the internal content, both before (interpreted as potential food before eating) and after the radula (interpreted as eaten food) were generated (Appendix, Figure A2). The content was predominantly Foraminifera which was taken as a proxy of diet. The taxonomy of the Foraminifera for identification followed Brady (1884) and Schmiedl et al. (1997). The Foraminifera in the images taken were frequently etched, dissolved, or damaged, making it difficult to see completely the ribs and chambers for identification. The lack of taxonomic detail made determination at species level nearly always impossible and hence often tentative genus assignment was performed.

2.2.7. Geochemistry

Trace elements can be found in the shell of the organisms and be controlled for different drivers, which can help to understand their ecology. The use of Mg or Sr as trace elements depends on the

composition of the shell. Calcite organisms can replace their Ca with Mg, due to their similar size, whereas aragonite organisms have an isostructural similarity with Sr. In aragonitic molluscs, Sr/Ca is inversely correlated with temperature, and with growth since this one is indirectly influenced by the former (Gillikin et al. 2005). Mg/Ca is being correlated in other groups such as corals and foraminifera with paleotemperatures (Eggins et al. 2003). There are other drivers that can influence the uptake of these impurities such as carbonate saturation, and kinetic effects.

Of the 36 scanned specimens, 11 which represent different depths, were embedded in epoxy resin in a longitudinal orientation for quantitative electron microprobe point analyses (EMPA) following the same procedure described in section 2.2.5. Samples were sonicated before carbon coating. The analyses were conducted using a Cameca SX100 electron microprobe. A 20kV accelerating voltage, 10 nA beam current, 12 μm spot size, and dwell time of 6 seconds were employed for all analyses. Calcium (Ca), Magnesium (Mg) and Strontium (Sr) were analysed in transects from the ventral to the dorsal areas of each specimen (500μm distance between points). The number of points per specimen differed due to differences in length of the investigated specimens. Points below the detection limit were removed. The Ca standard Wollastonite ($CaSiO_3$), the Mg standard Olivine ((Mg^{2+}, $Fe2^+$)$2SiO_4$) and the Sr standard $SrTiO_3$ were used in the analysis as it was used by Jennions (2014, unpublished thesis). The analytical precision of the trace elements measurements was expressed as two times standard deviation (2sd).

2.2.8. Statistical analysis

All statistical analyses were carried out using the R software package. All data was tested for normal distribution (Shapiro test; $p > 0.05$). For normally distributed data, ANOVA tests were carried out, followed by a Tukey post-hoc test. For non-normal distributions, a Mann-Whitney test was applied. Correlations were made between specimen thickness vs length, ventral diameter, dorsal diameter, depth, and volume loss. Correlations were also made between relative density vs length, thickness, depth/temperature, and volume loss, between age vs length, and between temperature vs length and Mg/Ca and Sr/Ca. A Pearson test was used for normal distributed data and a Kendall test when the data was not normally distributed.

2.3. *Results*

The molecular analyses showed that all specimens from the AS and WS morphologically assigned to *D. majorinum* belong to one Molecular Operational Taxonomic Unit (MOTU). I removed specimens which were morphologically similar to *D. megathyris* from further analysis (e.g. specimens 165 and 166), to eliminate different species as an explanation for any variability reducing the data set to 124 individuals.

2.3.1. Shell morphometrics

A total of 224 specimens from the AS and 97 specimens from the WS were measured for the morphometric differences in shell factors and volume (Figure 2.3). The average specimen length is 22.82 mm in the AS (8.57 min-43.39 max) and 28.04 mm in the WS (12.05 min-46.36 max). Shape is strongly constrained as length is highly correlated with ventral diameter (r= 0.872 p<0.001) and volume (p>0.05, Figure. 2.2). In the WS 10% and in the AS 8.92% of the specimens show marks or holes that could indicate predation.
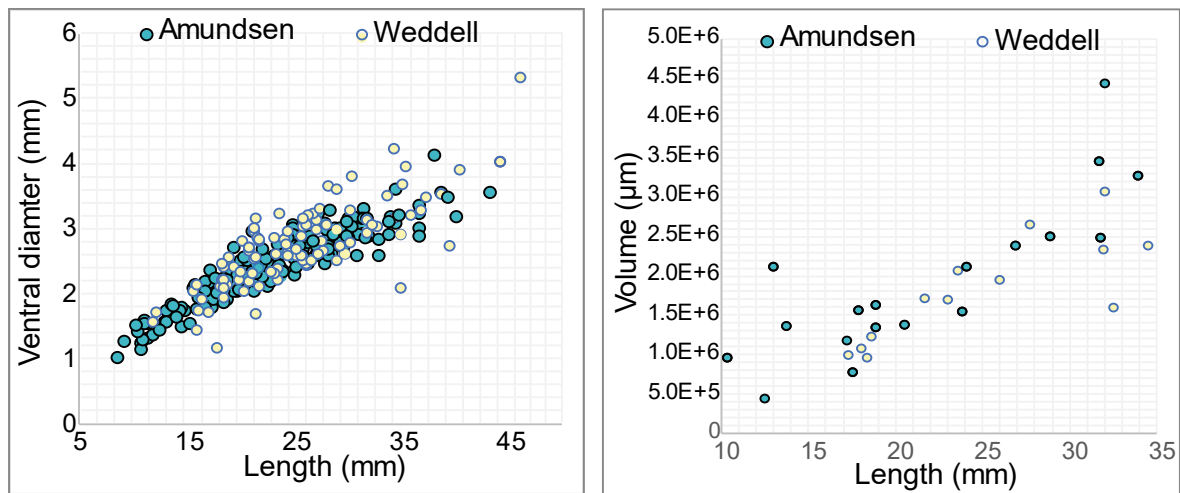
Figure 2.3. Correlation between shell length and ventral diameter (left) and shell volume (right) for the Amundsen Sea (AS, turquoise) and Weddell Sea (WS, yellow) regions.

In the AS, there is not much morphological variability with depth or temperature (Figure 2.3) except for the depth range between 501 and 800 meters (1.11°C). These specimens are longer than the other deeper/warmer sampling depth ($x^2 = 19.7$, df = 3, p-value < 0.005). Similarly, the arc of specimens between 300-500m and 501-800m are bigger than at other depth ($F_{3,220}$ p < 0.001). Dorsal diameter is smaller between 300-500 m ($x^2 = 21.6$, df = 3, p-value < 0.005) and no difference was found between the ventral diameters ($F_{3,220}$ p>0.05). Arc is decreasing with higher

37

temperatures and depth, and dorsal diameter increasing with higher temperatures (Pearson, p<0.0001, and Kendall, p<0.0001, respectively), (Figure 2.3.).
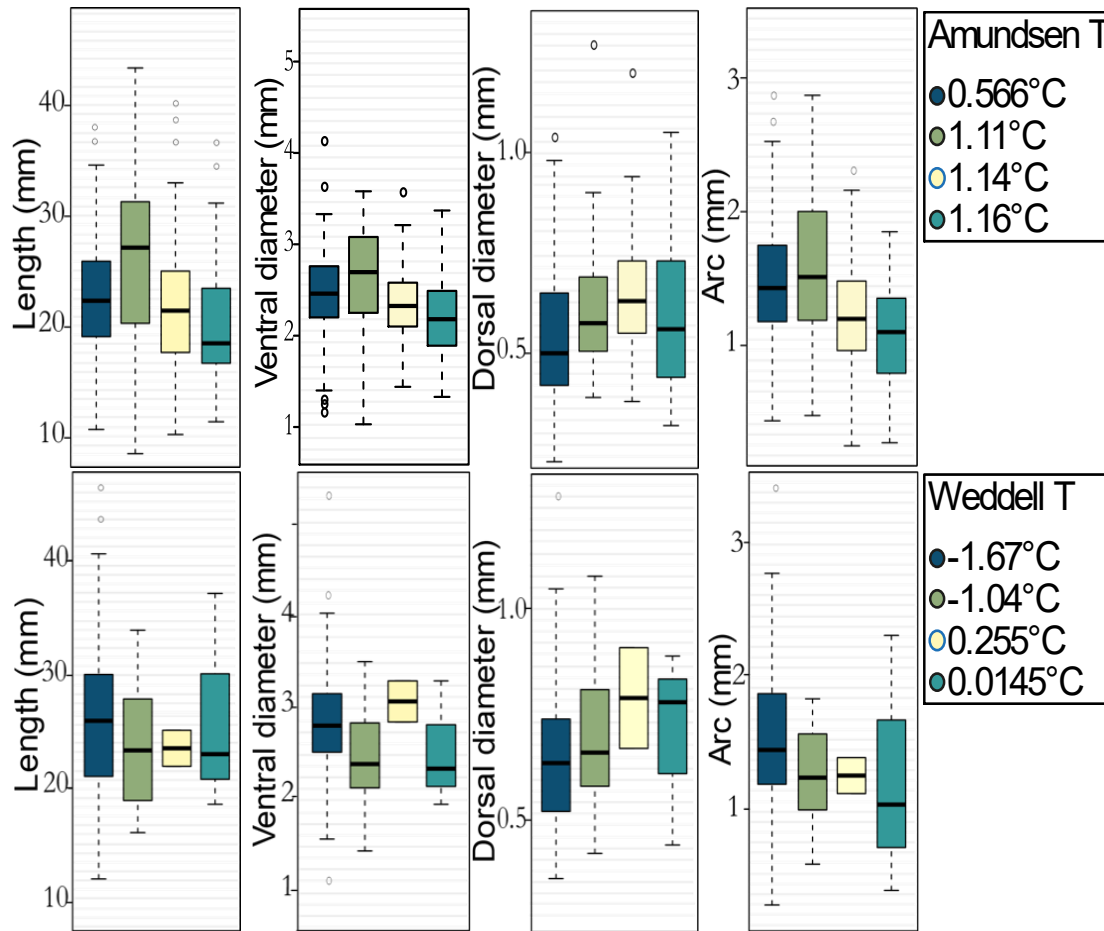
Figure 2.4. Box and whiskers plots of *D. majorinum* morphologies (length, ventral diameter, dorsal diameter, and arc). against water depths and temperature (°C) in the Amundsen (AS, top) and Weddell (WS, bottom) seas. Temperature is colour coded for each region. Amundsen Sea: Dark blue = 0.56°C, olive green = 1.11°C, yellow = 1.14°C, turquoise = 1.16°C. Weddell Sea: Dark blue = -1.67 °C, olive green = -1.04°C, yellow = 0.25°C, turquoise = 0.14°C.

In the WS, temperature and depth have no influence on length, and dorsal diameter (p<0.05), but ventral diameter is bigger for 300-500 m and 801-1200 m ($x^2 = 10.2$, df = 3, p-value < 0.05). Same is true for arc ($x^2 = 9.07$, df = 3, p-value < 0.05). Ventral diameter and arc decreasing with temperature and depth (p<0.05). When the two regions were compared, length ($x^2 = 9.40$, df = 1, p<0005), ventral diameter ($x^2 = 18.1$, df = 1, p<0.001) and dorsal diameter ($x^2 = 15.8$, df = 1, p<0.0001) are smaller in the AS while the arc ($x^2 = 0.449$, df = 1, p>0.05) is not significant different between them.

There is no significant difference in thickness between the regions (p>0.05) due to the high variability in thickness within the regions (average in AS is 123.4 µm, s.d 45.3; WS 102.1µm, s.d. 22.0). In the AS longer shells and with a bigger diameter are thicker (Table 3, Appendix A, Figure A3). In the WS, thickness is positively correlated with a wider ventral diameter and length. In the WS, thickness increases with depth (Table 2.3).

Table 2.3. Thickness statistics for Amundsen Sea (AS) and Weddell Sea (WS) specimens. *Pearson or Kendall correlation depending on the normality of the data (Shapiro-test). ***Significant values.

Shell characteristics	Region	*r	Factors	*t or T	p-value
Mean shell thickness	Amundsen Sea	0.355	Length	2.23	0.0251***
		0.427	Ventral	2.66	0.00761***
		0.137	Dorsal	0.850	0.394
		0.0492	Depth	0.304	0.760
		0.231	Volume loss (%)	1.33	0.183
	Weddell Sea	0.296	Length	59	0.1577
		55	Ventral	0.208	0.330
		-0.166	Dorsal	-0.823	0.410
		0.466	Depth	2.19	0.0293***
		0.179	Volume loss (%)	46	0.472
Thickness comparison between seas	Kruskal-Wallis		Thickness*seas		0.255

2.3.2. Age determination

Six specimens from the AS and four specimens from the WS of different shell length were successfully analysed for age determination with annual growth increments measured (Figure 2.4, right). The counted growths increments are an underestimation of the real age of the specimens as at the dorsal end their juvenile and younger age parts of the shell and therefore the annual growth increments for this section, are missing. The ventral diameter represents the largest diameter in a shell of *D. majorinum*. Length, ventral diameter, and age are correlated (r =0.773 p<0.05), although the correlation is less close for larger specimens. The oldest specimen from the Weddell Sea showed 23 years of growth increments at 22.8 mm shell length and 3.07 mm ventral shell diameter. The oldest measured specimen the Amundsen Sea showed 21 years of growth increments at 31.5 mm length and 3.19 mm ventral diameter. Although there are only six WS and four AS data points, they suggest that Amundsen Sea specimens grow faster per year (Figure 2.5).

A

B

C

Area	Specimens	Depth	Shell length	Age
AS	1015.1	480	31.51	21
AS	1015.13	480	25.18	14
AS	101544	480	18.29	14
AS	1015.76	480	24.99	14
AS	1015.83	480	11.47	10
AS	1151.12	488	13.62	11
WS	1385.8	439	18.43	14
WS	199.2	315	12.33	11
WS	1487.4	391	19.97	19
WS	447	607	28.17	23
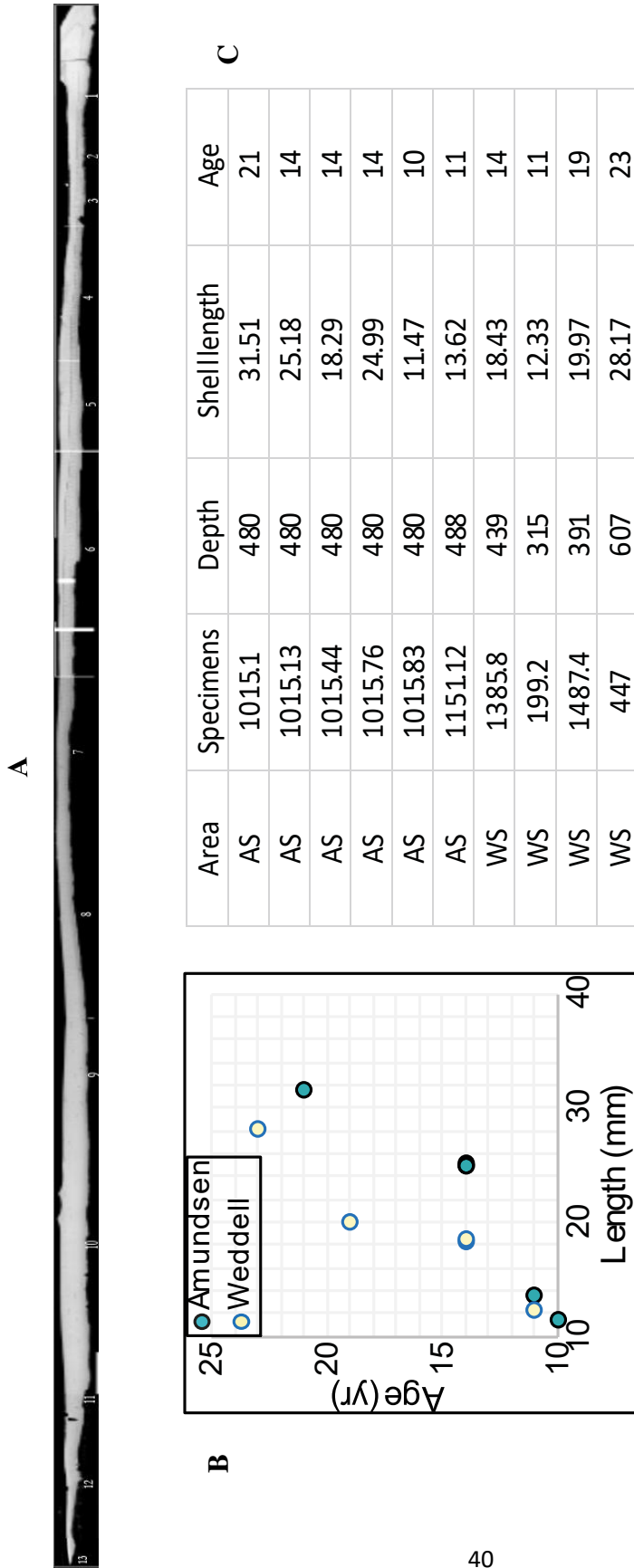
Figure 2.5. Age determination analysis. **A.** Shell showing the growth lines from the dorsal (oldest part) to the ventral part (where shell formation occurs). Stronger growth lines are being highlighted and are being interpreted as annual growth. The specimen size is 18.3 mm in length. **B.** Correlation between age and length in Amundsen Sea (AS, turquoise) and Weddell Sea (WS, yellow) specimens. **C.** Detailed information of the regions, specimens, depths, shell length and determined minimum ages.

2.3.3. Diet analysis

The μ-CT analysis of 21 scaphopods from the AS and 15 scaphopods from the WS (Table 2.4) visualised structures within their shells next to their soft parts, which were interpreted as mainly Foraminifera, a known scaphopod diet. Food content was found in 29 of the 36 analysed specimens while the other 7 were empty all from the AS. In total, I found 361 different specimens; 359 belong to Foraminifera, 1 to Radiolaria and 1 to Scaphopoda (Table 2.4). Due to preservation, it was not possible to identify 139 foraminifera specimens to species. (Table 2.4). All the foraminifer shells were found in the digestive system. Most of the foraminifera specimens which were intact enough for identification were in the proboscis before the radula, but it was possible to make some identification of crushed specimens after the radula (Appendix A, Figure A2). Of the Foraminifera it was possible to identify 14 species and 11 genera (Table 2.4). The genus *Bullimina* was most species diverse with four species present, while the other genera were represented by a single species.

Overall, within the 222 foraminiferans identified to species, 127 belong to the AS and 93 for the WS. The most common species were the planktonic foraminifer *Neogloboquadrina pachyderma* (88 specs, 22.68%) followed by benthic species *Bullimina sp*. (45 specs, 10.41%), *Trifarina angulosa* (35 specs, 8.10%) and *Bullimina aculeata* (34 specs, 7.87%). Other species were found in lower abundances such as *Globocassidulina subglobosa* with five specimens identified or *Melonis* sp. with three specimens (Table 2.4).

Table 2.4. Abundance of foraminifer species, in total and separate for the Amundsen Sea (AS) and Weddell Sea (WS).

Item	Amundsen Sea	Weddell Sea	Total
Analysed scaphopods	21	15	36
With food items			29
Without food items			7
Food items identified	127	95	222
Food items unidentifiable Foraminifera			139
Foraminifera, identifiable	127	93	220
Radiolaria		1	1
Scaphopoda		1	1
Total food items			361
No. of foraminifera specimens with food items			
Bullimina. sp.	16	29	45
B. aculeata	9	25	34
B. Mexicana		1	1
B. marginata	2		2
Cibicides sp.		1	1
Globocassidulina subglobosa		5	5
Gyroidinoides sp.	1		1
Melonis sp.	1	2	3
Neogloboquadrina pachyderma	68	20	88
Nuttallides umbonifer		1	1
Oolina sp.		2	2
Quinqueloculina sp.	2		2
Trifarina angulosa	27	8	35
Uvigerina peregrina	1	1	2

Unique foraminiferans for the Weddell Sea are, *Globocassidulina subglobosa, Oolina sp.*, *Nuttallides umbonifer*, *Cibicides sp.*, *Bullimina mexicana*, and for Amundsen Sea, *Bullimina marginata*, *Quinqueloculina sp.,* and *Gyroidinoides sp.* (Table 2.4). In the AS and WS similar number of foraminiferal species were identified as diet. In both seas, the same four species were the dominant food items. In the Weddell Sea the shell also contained a radiolarian and a scaphopod.

B. aculeata and *Bullimina sp.* are present from 300 m to 1600 m, *T. angulosa* from 300 m to 1200 m*, whereas Oolina sp., Melonis sp., N. umbonifer, U. peregrina* are present in over a wide range of depths. The other species were only found in one water depth range. The small number of specimen limits the interpretation of the data (Table 2.5).

Table 2.5. Foraminifera species present across the four investigated water depth ranges: 300-500 m, 501-800 m, 801-1200 m, 1201-1600 m.

	Depth range (m)			
	300-500	501-800	801-1200	1201-1600
Taxon	B. aculeata	B. aculeata	B. aculeata	B. aculeata
	Bullimina. sp.	Bullimina. sp.	Bullimina. sp.	Bullimina. sp.
	N pachyderma	N. pachyderma	N. pachyderma	N. pachyderma
	T. angulosa	T. angulosa	T. angulosa	
	Gyroidinoides sp.			
		U. peregrina		
	Oolina sp.		Oolina sp.	
	G. subglobosa		G. subglobosa	
		Cibicides sp.		
		B. mexicana		
			B. marginata	
	Melonis sp.			
	N. umbonifer			
		Quinqueloculina sp.		

2.3.4. Shell dissolution and density

Shell dissolution is externally visible in some specimens but not in all. Some of the externally intact specimens show holes internal to the ribs, indicating that dissolution starts in this area (Figure 2.6.2). The loss of the outer shell is a later step in the dissolution (Figure 2.6.4 and 2.6.5). Only two specimens had no damage (specimens 919.1 and 1015.64 from AS, Figure 2.6.1), nine showed holes in the ribs (Figure 2.6.2), 12 with holes in ribs and internal corrosion (Figure 2.6.3), and eight with holes in the ribs, loss of ribs/loss outer shell and corrosion inside the shell (Figure 2.5.4). Amundsen Sea specimens have a higher dissolution (0.79%) compared to the Weddell Sea specimens (0.36%). From the total, five were more than 10% dissolved (loss of ribs, corrosion inside, loss of outer shell, Figure 2.6.5 Appendix, Table A2). The specimens 1015.71 (300-500 m depth), 582.1 and 383.8 (both at 1200-1600 m depth) from the AS and the specimens 114.9 (300-500 m depth) and 1220 (1200-1600 m depth) from the WS could not be completely reconstructed due to severe dissolution and were removed from the analyses. All five have more than the 10% of the shell dissolved.
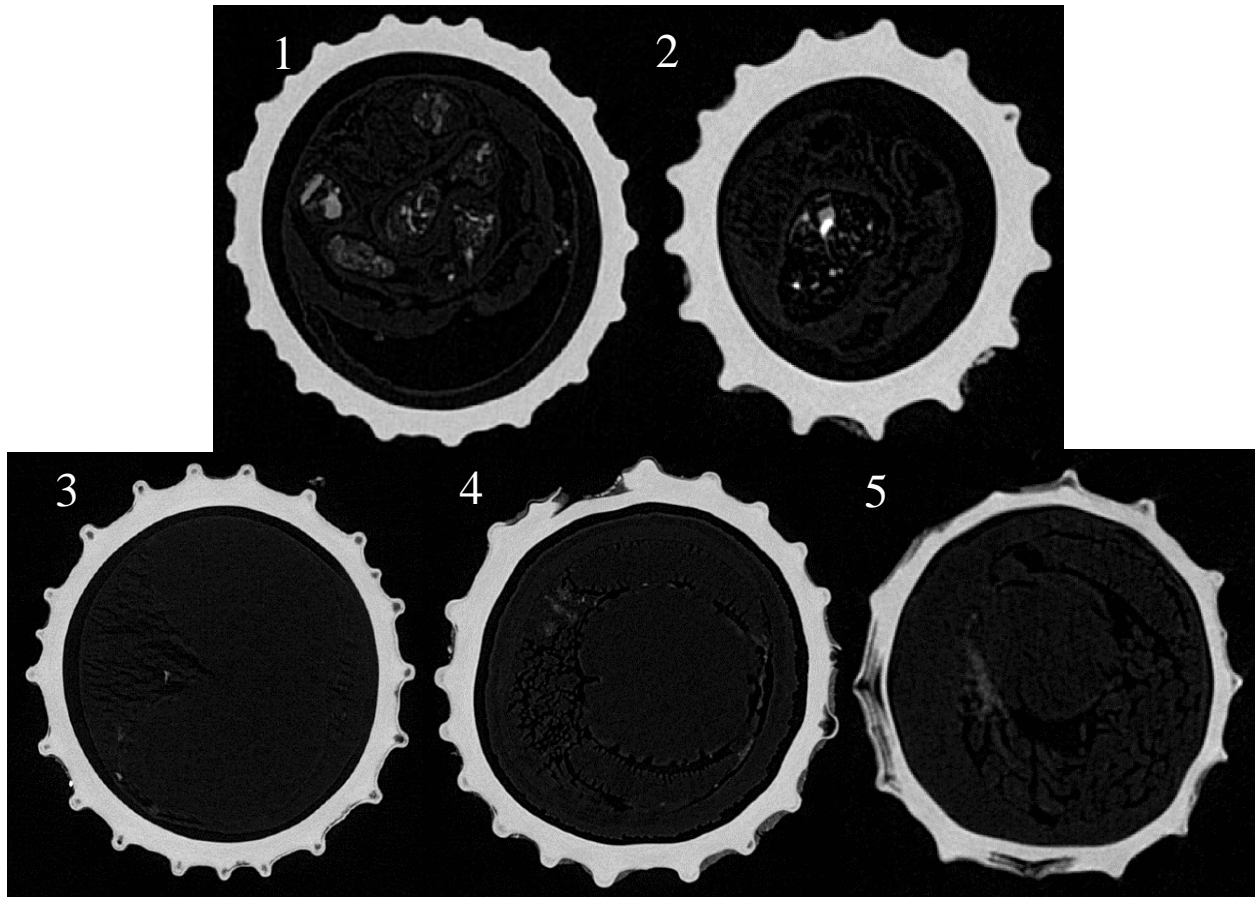
Figure 2.6. µ-CT images showing characterisation of dissolution levels. I place the specimens in the higher level of dissolution that they showed. 1 = no damage (specimen 919.1), 2 = holes in the ribs (specimen 684.2), 3 = holes in ribs and inside corrosion (specimen 736.2), 4 = holes in ribs, loss of ribs/loss outer shell and corrosion inside the shell (specimen 278.2), 5 = more than 10% dissolved (specimen 1015.71).

The relative shell loss is less frequent accounting for more than 10% of the total volume (five out of 36 analysed specimens). For most of them, relative shell loss is <5%, with an average of 0.66%. Average dissolution was higher in the AS (0.78%) than in the WS (0.35%).

The analysis of relative shell density on 21 specimens from the AS and 15 specimens from the WS showed no significant difference between the regions ($F=_{1,31}$ p=0.274). Average relative shell density in the AS is 2.61 ± 0.0397 g/cm^3 and in the WS 2.59 ± 0.0351g/cm^3. Shell density is not correlated to length or dissolution in either region (Figure 2.7). In the AS, dissolution is not correlated with thickness and depth (p<0.05) while WS specimens show a positive correlation of relative shell density with thickness (p>0.05, R=0.435) and depth (p>0.05, R=0.575; Figure 2.6).
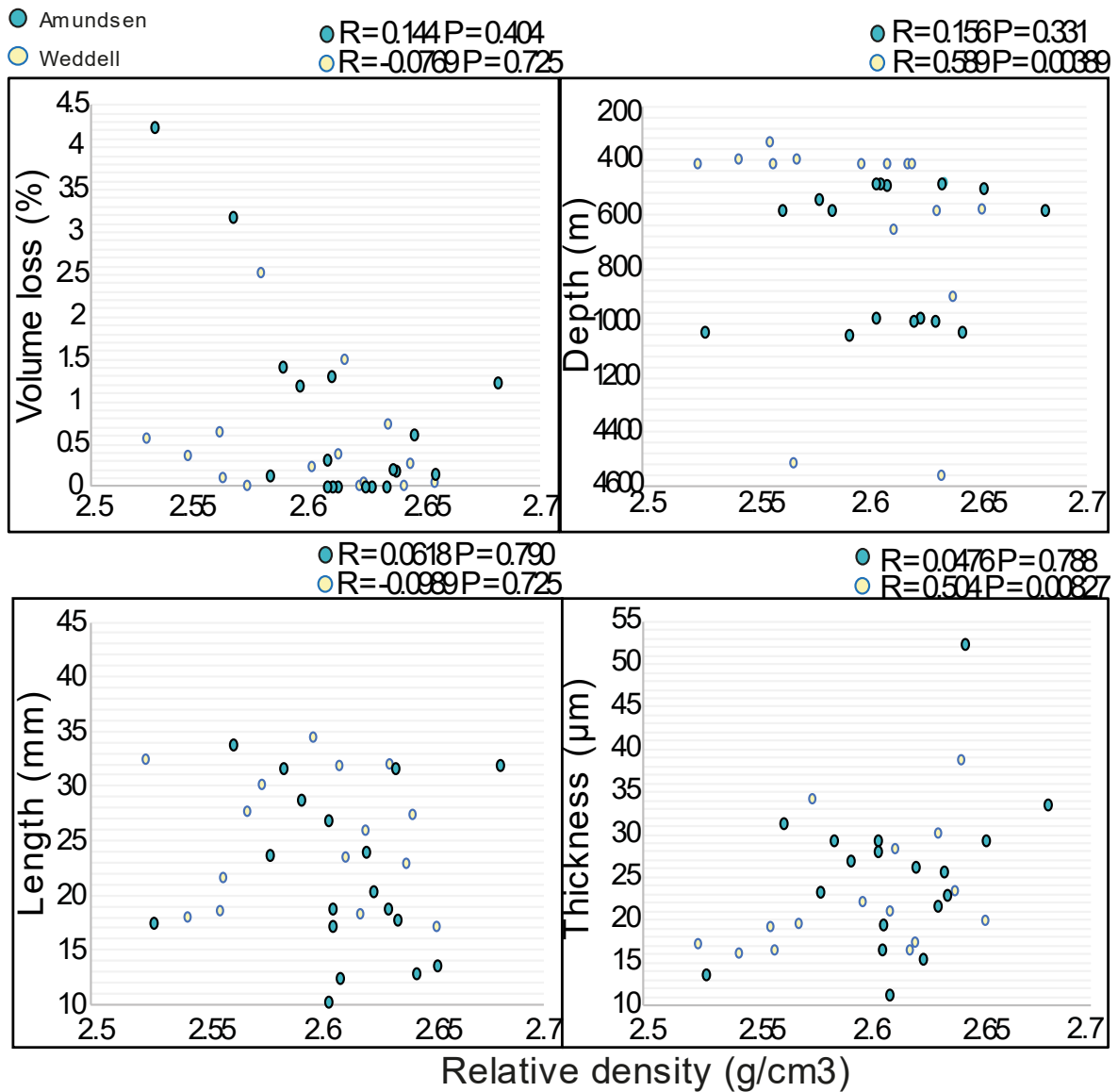
Figure 2.7. Relative density compared to volume loss, depth, length, and thickness. Colour coded turquoise for Amundsen Sea (AS) and yellow for Weddell Sea (WS).

2.3.5. Shell geochemistry

For the geochemical analysis, six specimens from the AS and five specimens from the WS were analysed (Table 2.1). Average Mg/Ca ratios in the AS are higher than in the WS (0.492 ± 0.120 mmol/mol vs 0.41 ± 0.0945 mmol/mol) as are Sr/Ca ratios (2.08 ± 0.312 mmol/mol vs 2.00 ± 0.306 mmol/mol). Variability in Mg/Ca is high in the specimens along the longitudinal shell transect but no trend with ontogeny in the Mg/Ca ratio in the AS ($W = 433.5$, p-value = 0.813), nor the WS specimens was found ($W = 495$, p-value = 0.513) (Appendix A, Figure A4). The same is true for Sr/Ca [Amundsen ($W = 484$, p-value = 0.622); Weddell ($W = 532$, p-value = 0.230)]

(Appendix A, Figure A5). The degree of dissolution does not influence the elemental composition (dissolution vs. Mg/Ca and Sr/Ca for the AS specimens, $p > 0.05$), which could be caused by the small sample set. Sr/Ca, which is often interpreted as growth rate in other species, does not vary with length ($p > 0.05$). In both regions, Mg/Ca ratios are lower in specimens from higher depth and temperature. There is no relation between Sr/Ca and water depth and temperature in either region (Figure 2.8).
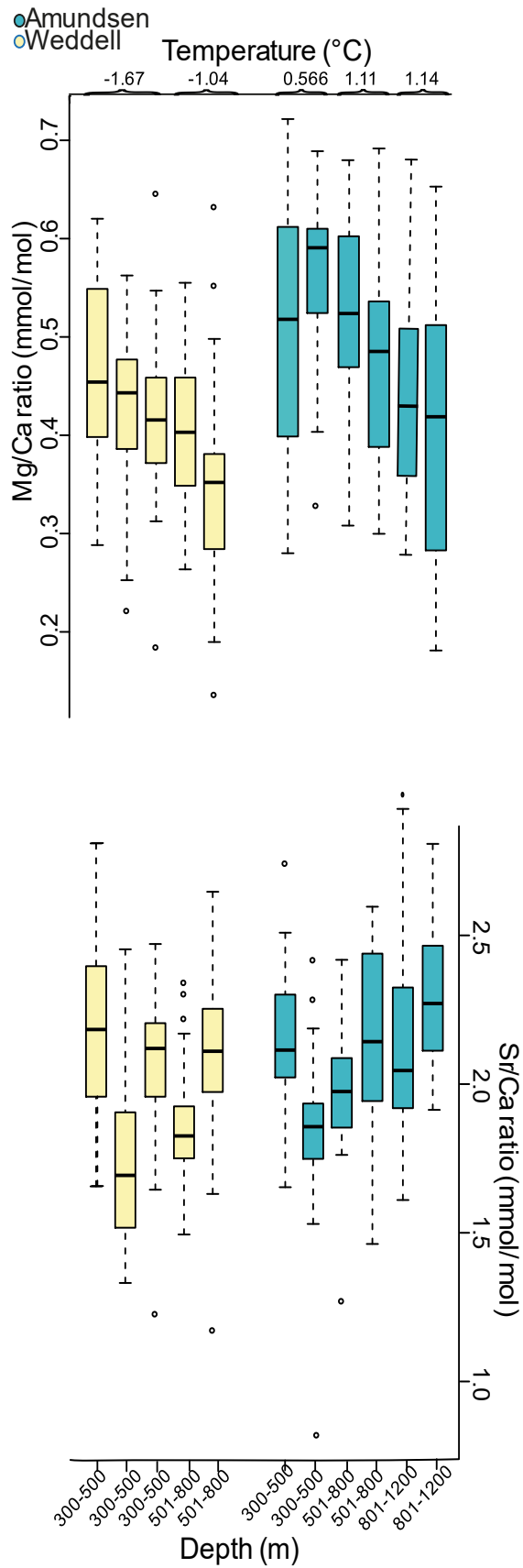
Figure 2.8. Boxplots showing the variation in Mg/Ca ratio and Sr/Ca ratio between specimens and between regions. Amundsen Sea (AS, turquoise) and Weddell Sea (WS, yellow).

2.4. *Discussion*

This study analysed plasticity in shell morphology and chemistry in the scaphopod *Dentalium majorinum* from the Amundsen Sea and Weddell Sea in the Southern Ocean. I provide an approximate estimate of this scaphopod species lifespan, for the first time done for a scaphopod. Regarding the shell integrity, shell dissolution has been observed in almost all the shells from either region. The results from the density and geochemistry analyses, showing no differences between specimens and/or regions, suggest that the biomineralization in this species is highly controlled.

Organisms have the ability to respond to environmental changes through altering their metabolism (Hendriks et al. 2015), prioritising one process over another (Gattuso & Hansson 2011) and reducing the energy demand (Dupont et al. 2010, Stumpp et al. 2011) all of which can result in changes to the organism's morphology. Adaptation to naturally variable environments (Pörtner & Farrell 2008) via metabolic changes or phenotypic plasticity are considered crucial to organisms survival under future environmental conditions (Chown et al. 2007, Kelly et al. 2012).

Morphological differences may reveal phenotypic plasticity
Our results show morphological changes that do not reflect genetic variability at species level, but instead a phenotypic plasticity in the species. Phenotypic plasticity may allow the population of a species to acclimatise or cope to environmental variability until adaptive evolution improves the fitness of the population (Chevin et al. 2010, Willi et al. 2006). A range of abiotic conditions such as temperature, (Peck 2011) and biotic drivers such as food supply (Arrigo & van Dijken 2003), predation pressure (Vermeij 1978), or cost of calcification (Coe 1993) are being proposed as reasons for morphological plasticity in species and their populations.

Our two study areas are dominated by different water masses. The WS is influenced by the clockwise flowing Weddell Gyre, and is a region of downwelling and bottom water formation (Vernet et al. 2019). The surface and near-surface WS are the source of the cold, fresh and oxygen rich waters in the SO (Nicholls et al. 2009). In contrast, the AS is dominated by circumpolar Deep Water (> 1°C) between 500-800m which can upwell onto the continental shelf (Jacobs 1996, Jenkins 2010). Our results show that AS specimens grow faster, yet they are smaller than WS specimens. The cost of calcification may be a plausible explanation for the morphological differences between regions. The warmer temperatures in AS could be accelerating their

metabolism, but lower carbonate ion concentration, and challenging calcification resulting in a smaller size. Cole & Fox (1942) and Sheridan & Bickford (2011) argue that an increase in temperature, increasing metabolic demands, without a sufficient food supply would result in decreasing organism size.

Next to abiotic impacts, biotic drivers such as predation pressure can impact size. The collected specimens of *D. majorinum* show some few obvious predation marks (such as drill holes), but there was no systematic difference between regions. Therefore, this observation would not support an interpretation on which morphological differences are due to predation pressure. In addition, the abundance of potential gastropod predators, such as naticids or muricids, was low or null in the trawl samples from which the scaphopods derived (K. Linse, personal observation). Finally, the infaunal lifestyle of the species may offer some protection from predators, as it is being suggested for the temperate bivalves, e.g. *Yoldia hyperborea* by burrowing into the sediment and *Mya truncata* and *Macoma calcarea* by living deeper in the sediment (>15 cm), (Fukuyama & Oliver 1985).

Carbonate saturation and food availability decrease with depth (Jiang et al. 2015, Bailey & Robinson 1986), which can explain the size decrease in AS individuals below 800 m. Changes in morphology with depth are often linked to habitat isolation and difference in energy resources (Rex & Etter 1998). Lack of food at depth larger organisms may result in difficulty to meet their metabolic requirements (Thiel 1975).

Lifespan and age determination
The width of the annual growth increments and the strength of their expression are often interpreted to be the result of abrupt environmental changes such as temperature (Purroy et al. 2015) or food availability (Nolan & Clarke 1993) and are often linked to seasonality in these parameters. Scaphopods are feeding on foraminiferans and are suggested to feed throughout the year in open ocean areas such as the Rockall Trough (Davies et al. 1987). In the Southern Ocean though, the surface ocean is seasonally covered by ice, potentially impacting the food sources for the foraminiferans (Mackensen & Douglas 1989). The Weddell Sea foraminiferans are dominated by *Trifarina angulosa* in areas with strong bottom currents such as the shelf break with high organic matter content of the sediment on the uppermost continental slope. The upper slope down to 2000 m water is dominated *Bullimina aculeata* assemblage in the warm (>0°C) Weddell Deep

Water often under higher productivity (Mackensen et al. 1990). In our set of data set, *B. aculeata* was found in both regions, as one of the most common species, like *T. angulosa*. Foraminiferans feed on phytoplankton or their detritus (Murray 1991) and therefore scaphopods could receive an annual signal through this.

Besides to have a seasonal growth, Antarctic and deep-water species tend to have long lifespans; for example, the bivalve *Aequiyoldia eightsii* (formerly known as *Yoldia*) has been found to live 52 years (Nolan & Clarke 1993), *Laternula elliptica* has recorded ages between 14 and 33 years, and *Aequiyoldia eightsii* between 22 and 58 years of age (Román-González et al. 2017). Here, I report an age for *D. majorinum* of more than 23 years. As there are no ages determinations for the taxon, I cannot compare our data to other studies. The ages have to be treated with caution as it is challenging to observe and count the growth lines. Secondary thickening in the dorsal part due to counterpart and apex reabsorption constantly dissolves the oldest part (Davis et al. 1987) and the larval and juveniles shell parts are not preserved in larger specimens through this process (Davis et al. 1987).

Constant density suggests strong biomineralization control

Biomineralization is a highly controlled process (Checa et al. 2006 and references herein), in which the organism uses cellular functions to direct the nucleation and deposition of minerals (Weiner & Dove 2003). A strong function of the shell and hence the biological need to control this process has been previous used to explain lack of change in density, thickness, and elemental composition of brachiopods over the last century (Cross et al. 2018). The energetic cost of calcification increases with decreasing pH and increasing temperature, which can diminish the fitness and survival of organisms in a population (Melzer 2011). To date, the biomineralization mechanisms in the Scaphopoda remain unexplored. It is also not clear whether the shell building mechanisms in molluscs is conserved, or it differs between groups (Arivalagon et al. 2016). Our density data suggest a strong biomineralization control, even under stress environment that could be in detriment of other biological processes.

In molluscs, the transport of Ca^{+2} ions can be costly due to the need to maintain a high concentration in the extrapallial fluid compared to seawater (Watson et al. 2012). The organism is required to move Ca^{+2} from the seawater to establish these concentrations against a concentration gradient (Carré et al. 2006). Watson et al. (2017) suggested that <10% of the total energy budget

in gastropods and <5% in bivalves was allocated to calcification. They also suggested that this cost would increase in response to acidification in the future by ~50 to 70% (Watson et al. 2017). Today surface Ω_{Ar} in the WS winter water are above the saturation level ~ 1.3 (Weeber et al. 2015), whereas the Bellingshausen regions which are surrounding the AS are already experiencing short undersaturation events (Jones et al. 2017). Due to the similarity in the oceanography, I speculate that the AS region is also experiencing undersaturation. Specimens in the AS are smaller than in the WS at same density. This could suggest that the energy in the AS is allocated to ensuring stable density at the detriment of shell growth.

Additional to the density of the aragonite, the elemental uptake must be controlled to ensure crystal growth. Thermodynamic predicts that in inorganic aragonitic, magnesium and strontium will decrease with increasing temperature (Dietzel et al. 2004), for which I see no evidence over the very small temperature difference in our dataset. The responses of molluscs related to Mg/Ca and Sr/ca proxies, has been variable. In aragonitic bivalves *Mesodesma donacium*, *Chione subrugosa*, *Mercenaria mercenaria*, Sr/Ca do not respond to salinity and temperature (Carré et al. 2006, Gillikin et al. 2005) or display a variability in Mg/Ca and Sr/Ca despite constant environmental conditions in *Ruditapes philippinarum*, (Poulain et al. 2015). Both trace elements have been linked as a proxy for growth rate in other species such as *Saxidomus giganteus* though there is not clear consensus how well the trace element data tracks growth rates (Klein et al. 1996, Gillikin et al. 2005). Here, Sr/Ca is no different between the two regions and at different depths. The non-correlation with final size, age or density suggests that in this group Sr is not indicative of organism's growth rates. Other biological factors that can influence Sr in aragonite include the macromolecules in the organic matrix (Roger et al. 2017), and the crystal size in the microstructure (Shirai et al. 2008) neither of which was analysed here.

The higher Mg/Ca ratio in the AS specimens is against expectations. If these specimens are under stronger biomineralizations stress, suggested due to the overall smaller sizes, maybe the selectivity to exclude Mg during crystallization is impacted. Higher than expected Mg/Ca have also been found in calcite specimens of planktic (Meland et al. 2006) and benthic foraminifers (Elderfield et al. 2006b, Yu & Elderfield 2008) in the Nordic Sea, and in coralline algae in the laboratory under OA conditions (Ragazzola et al. 2016). The elevated Mg has been interpreted as the response to very low carbonate ion concentration which are also prominent in the AS Sea. Marchitto et al. (2006) suggested a threshold around 30 µm/mol under which trace element uptake is impacted.

Additionally the prediction of increase of Mg/Ca with temperature support an increase between 8 to 11% in Mg/Ca for foraminifera per °C and 3% with inorganic calcite (Lea et al. 1999). However, the decrease with temperature in the sample is ~ 20% per °C. Therefore, I interpret the elevated Mg values (0.463 ± 0.129 mmol/mol in the AS vs 0.357 ± 0.294 mmol/mol in the WS) not to represent the environmental conditions but be the response to biomineralization being impacted by low carbonate ion.

Dissolution and mechanism to compensate it in a changing ocean

Shell integrity is important since protects the organism against predators and provide a mechanism to counteract other pressures such as water currents, sediment, and negative interactions with other animals such as epibionts (Kroeker et al. 2014b, Beuck et al. 2007). Despite investigating predominantly specimens which have been alive at time of collection, dissolution was found in most specimens. My finding agrees with experimental results in the temperate muricid gastropod *Nucella lamellosa*, where different CO_2 treatments resulted in shell dissolution and weight lost, despite constant calcification (Nienhuis et al. 2010). Similar to Bednaršek (2012b), I detect dissolution within the shell matrix in specimens that appeared fully intact from the outside. The organic matrix role is to This result suggest that the organic matrix is acting as an effective protection of the crystal structure for those specimens, which agrees with other molluscs. Corrosion and dissolution of the organic matrix was also observed, which can be weaken the shell. However, the fact of observed food content in most of them suggest that available food could be helping them to cope with the environmental stress conditions.

I propose that the scaphopod can partially dissolve the shell to generate a buffer against undersaturation. This process has been described in molluscs and crustaceans to regulate extracellular pH during hypercapnia (Henry et al. 1981, Michaelidis et al. 2005). The dominance of this process in the ribs might suggest that the aragonite in these regions is more susceptible to dissolution for example due to changes in organic to inorganic material or crystal size. It is yet unclear how much material can be dissolved before the function of the shell is lost. Specimens of *D. majorinum* with more than 20% of the shell dissolved had still soft parts present at the collection time suggesting a living organism and a functioning shell. Repair of the inner shell has been observed in pteropods (Lischka et al. 2011) and brachiopods (Cross et al. 2019), with a thickening of the shell at sites of previous shell dissolution, though the cost of repair has not been extensively studied. However, it was not possible to see any evidence for inner shell repair in *D. majorinum*.

Electron backscatter diffraction analysis of the crystal growth direction in the inner shell layer of *D. majorinum* would be able to shed further light on this question.

Ocean acidification is impacting carbonate chemistry resulting in shallowing of the aragonite saturation horizon specifically in areas with already low saturation such as the AS (Björk et al. 2013). Therefore, further investigations are needed to assess the impact on life histories and population performance.

2.5. *Conclusions*

This is the first approach to assess the responses of a scaphopod such as *D. majorinum* to different environmental conditions. The density of the shell of *D. majorinum* does not change considerable between regions and depth. This can be attributed to a strong biomineralization control. The internal dissolution of the shells suggests a need to buffer the internal carbonate chemistry at the calcification site. Thus, the impact of the low carbonate ion in the Southern Ocean, cause a possible detriment in the size of the shell. Amundsen Sea specimens show higher dissolution in living specimens and smaller shell length at comparable age than the Weddell ones, supporting this interpretation. Furthermore, the elevated Mg in the AS specimens, points towards pressures on biomineralization by analogy to other calcifiers. Specimens from the AS despite being smaller increase more rapidly in size through adult life than the Weddell ones, potentially in response to high calcification costs under low carbonate saturation and food supply. Size differences with water depth can be attributed to reduction in carbonate saturation and sources availability. *D. majorinum* shell dissolution suggest a weakened in the shell integrity but the fact of being alive suggest a way to cope with the stress conditions, especially if there is available food to take.

Chapter 3 : SHELL SHAPE AND ORNAMENTATION AS A PLASTICITY ADAPTATION MECHANISM TO ENVIRONMENTAL CHANGE

Abstract

Shells of organisms have multiple functions, though often the potential benefits of shell shape are not rigorously tested. Under climate change scenarios, shell formation is threatened, making paramount to assess the biomechanical relevance of the shell. This study investigates the biomechanical properties of the Southern Ocean scaphopod species *Dentalium majorinum*. The natural morphological plasticity of shell curvature, number of ribs and size in 322 specimens was measured. Finite Element Analysis was used to quantify the impact of the morphological plasticity to withstand hydrostatic pressure and drag flow at the sea floor. FE models were created with number of ribs varied between 0, 20 and 32, the length of the specimen varied from 9 mm, 23 mm to 40 mm and the curvature between 0 degrees, 7.3° and 14°. Generally, specimens under shear load experience more stress and strain than under hydrostatic pressure load. The results show that longer specimens and more curved specimens experience higher von Mises stress under hydrostatic pressure load. Under shear load, the curvature has less significance. In contrast, ribs which did not impact stress distribution due to hydrostatic stress reduce the stress in response to shear stress. Therefore, morphological changes in the scaphopod shell allow adaptation to variable environmental conditions.

3.1. *Introduction*

The shell of marine organisms has diverse functions such as support during movement, protection from predators, currents, and hydrodynamic forces (Gutierrez et al. 2003, Alyakrinskaya 2005). Often though the precise functions of plasticity in form and ornamentation is less clear. The force required to break shells varies between and within species, modulated by ornamentation, shape, shell thickness but also internal mineralogy such as microstructure and orientation of crystals (Lemanis & Zlotnikov 2018). Biomechanics is a tool to understand how shelled organisms perform

in the face of environmental change. These changes can alter morphological parameters in the organisms and the effects can be variable depending on the habitat, species, populations, and life story stages.

Environmental changes are commonly associated with changes in physiology, shifts in population dynamics, the ecosystem interactions and food webs (Gaylord et al. 2019). Ocean acidification (OA), the change in the oceans' carbonate system due to the uptake of anthropogenic CO_2, has been shown to impact calcification in several organisms (Kroeker et al. 2010) though our understanding of the impacts on shell function are still in their infancy. OA can evoke changes in mineralogy and geochemistry such as in the coralline algae *Lithothamnion glaciale* (Ragazzola et al. 2016) which may impact shell function as it increases the costs of physiological processes including calcification (Kroeker 2014b). Similarly, the marine gastropods *Tegula funebralis* reduced their shells strength by 50%, whereas *Nucella ostrina* experienced only a reduction of 10% (Barclay et al. 2019). OA can potentially as well generate an undersaturated carbonate chemistry making the shell weaker due to high dissolution as in the pteropod *Limacina helicina* (Bednaršek et al. 2012a). Likewise, warming affects shell strength, as has been evidenced for the bivalve *Mytilus edulis* at +4°C regarding the ambient temperature, with possible implications on surviving to predators (Mackenzie et al. 2014).

Mechanical properties such as hardness (the resistance to plastic deformation) and elasticity (the ability of a material to withstand tension or compression) are properties of the shell that can be affected as well. Li et al. (2016) found that the mechanical resistance of the shell of the tube worm *Hydroides elegans* decreases with decreasing pH. This paper also highlights the importance of multiple drivers as warmer temperature leads to higher shell resistance for those specimens. The increased shell fragility and reduced fracture toughness were also described for the blue mussel *Mytilus edulis* in response to pCO_2 increases from 550 to 750 µatm (Fitzer et al. 2015). In the juvenile oyster *Crassostrea virginica* (Dickinson et al. 2012, Ivanina et al. 2013) changes in the carbonate chemistry resulted in reduced fracture resistance and microhardness.

Shell morphology and shape plasticity also change with environment suggesting a link between morphology, shape plasticity and environmental change (Fitzer et al. 2015). This occurs both geographically and temporally in many species including marine bivalves (*Yoldiella valettei*, *Y. ecaudata*, and *Y. sabrina*) from the Southern Ocean (Reed et al. 2013) due to different geography

conditions (ecotypes), and freshwater gastropods *Anisus leucostoma* and *Biomphalaria glabrata* from Lake Bangong (China) due to habitat heterogeneity (Clewing 2015). Same is true for the bryozoan *Schizoporella errata*, from Italy, which showed growth size and colony development alteration due to environmental factors (Lombardi et al. 2011),

Organisms have different ways to cope, compensate or adapt to environmental changes, and those can differ between and within taxa (Byrne & Fitzer 2019). Phenotypic plasticity can act as a mechanism to compensate for changing environmental conditions and to increase the chance to reproduce and survive (Reed et al. 2013). Phenotypical plasticity is defined here, as the faculty of a genotype to express different phenotypes in response to different environmental changes (Fordyce 2006). This term was applied first to morphological traits and has evolved since then (Woltereck 1909, Whitman & Agrawal 2009). Phenotypic plasticity is linked to function in the mytilids *Crenomytilus grayanus, Mytilus coruscus*, and *Modiolus modiolus* as shape responds to water currents and geography (Vekhova 2013). Similarly, formation of rounder shells in response to ocean acidification has been linked to a possible protective mechanism against predators in the snail *Radix balthica* (Brönmark et al. 2011), that may be a way to compensate for a weaker shell.

Understanding the mechanical properties of the shell allows an interpretation of its function, which in turn can give insights into its ecology, and how the species will react to induced environmental change. While the function of the shell in bivalves and gastropods has been studied, the role of the shell in scaphopods is less understood. Scaphopods are benthic-infaunal deep sea organisms. As such, "in situ" studies assessing the impact of hydrostatic pressure and current speed are challenging. A complementary approach is the use of numerical models, such as Finite Element Analysis (FEA, Rayfield 2007). FEA does not attempt to reproduce the total complexity of a system, but instead tries to simplify it the structure to a testable model (Anderson et al. 2012).

My previous work (Chapter 2) documented the morphological plasticity of *Dentalium majorinum* in the Southern Ocean. Here I assess the importance of morphological features, specifically the degree of curvature of the shell or the amount of ribs, for mechanical stability against hydrostatic pressure and flow. I intend to answer the question about the function of shell plasticity between populations, and if morphological plasticity preserves shell function under environmental change. Specifically, I address whether 1) shell shape impacted the stress response of the shell, and whether 2) ornamentations increased the resistance of the shell to induce stress.

3.2. *Materials and methods*

3.2.1. Modelled specimens and collection

Dentalium majorinum is a scaphopod species with circum-Antarctic distribution that lives in up to > than 2000 m depth and has an infaunal lifestyle (Steiner & Linse 2000). In total 504 specimens of *D. majorinum* from multiple locations the Amundsen and Weddell seas were collected from different expeditions: ANDEEP II (2002), ANT-XXI/2(2003), ANDEEP III (2005), JR179 (2008), ANT-XXVII/3 (2011), JR275 (2012). From this, 322 were available for this study after assessment of completeness as refereed in Chapter 2. All samples were stored fixed in ethanol.

3.2.2. Environmental differences related to morphological plasticity

Temperature is ~1°C higher in Amundsen Sea than in the Weddell Sea. Aragonite carbonate saturation is higher in the Weddell Sea ~1.327 in 1000 m and the Sea Ice Concentration (SIC) is lower during summer in Amundsen Sea.

Sea	Mean ΩAr in 1000 m
Weddell	1.327
Amundsen	1.166
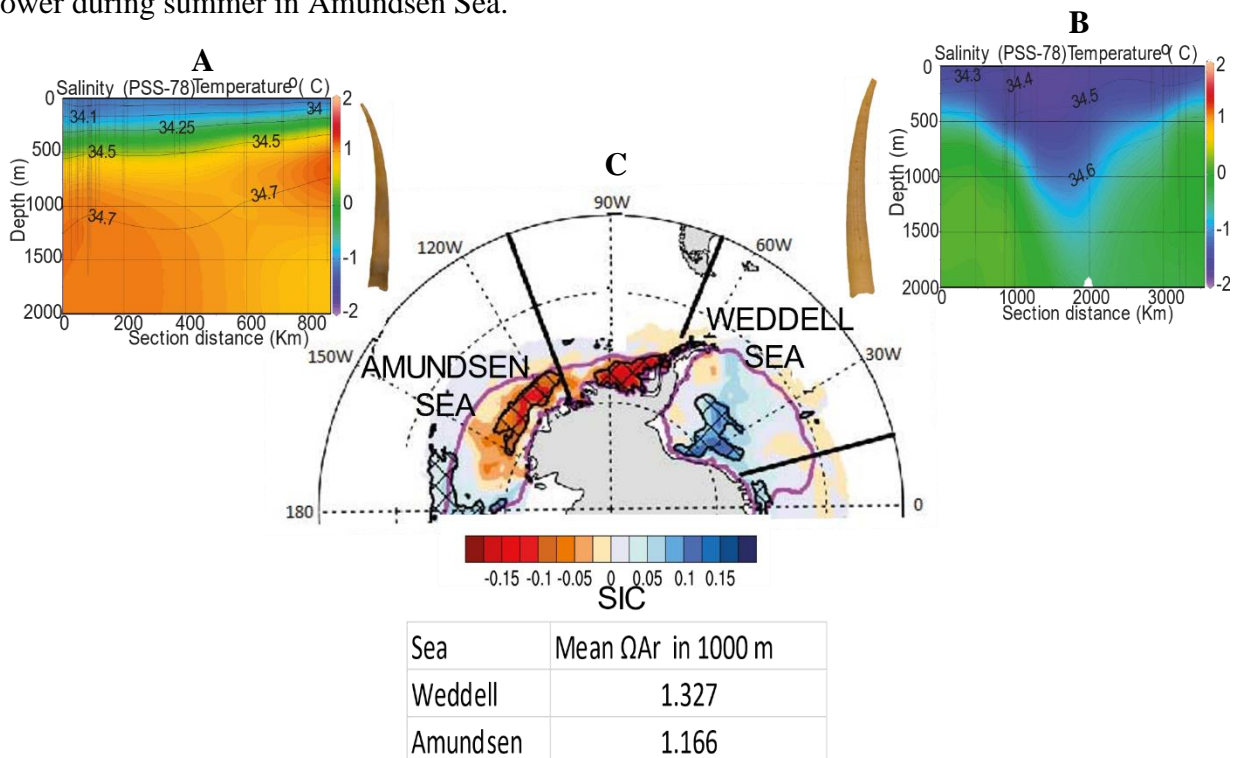
Figure 3.1. Environmental conditions in the Amundsen and Weddell seas. A. Oceanic mass model from the Amundsen Sea, showing the salinity (level lines) and temperature (colour coded) at different depths. At the right side, a representation of a *D. majorinum* specimen from that area. B. Oceanic mass model from the Weddell Sea, showing the salinity (level lines) and temperature (colour coded) at different depths. At the left side, a representation of a *D. majorinum* specimen from that area. C. The map shows the Sea Ice Concentration (SIC) during Southern Antarctic summer during between 1979–2014 taken from Hobbs et al. 2016.

To generate representative FEA models, curvature, size, and number of ribs were measured in 322 specimens. The length, arc (curvature) and number of ribs were used to constrain realistic input parameters for the modelling. Length of the specimens varied from ~ 8 mm to ~ 45 mm (rounding to the nearest 0.2 mm) and the number of ribs from 14 to 30. Amundsen Sea scaphopods are smaller than Weddell ones. In general, the longer the specimen, the higher its arc (Figure 3.2). There are not significant differences in arc between Amundsen and Weddell scaphopods, however arc is correlated with temperature and depth in Amundsen Sea specimens (tau=-0.1200252, p = 0.0192 and r=0.2976997, p=<0.0001, respectively). The number of ribs is independent of the length of the specimen (Figure 3.2). The specimens are derived from 300-1200 m water depth.
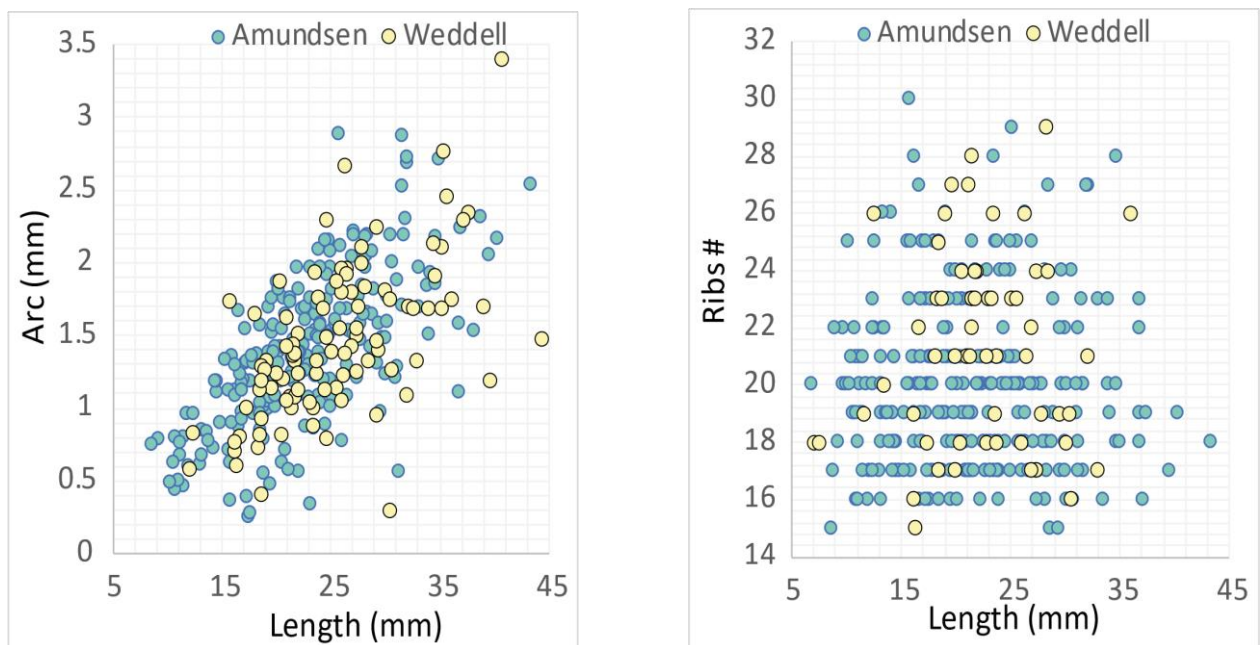
Figure 3.2. Arc (left) and number of ribs (right) against length of all measured specimen. Each yellow point represents one measured specimen from Amundsen (turquoise) and Weddell (yellow) seas

3.2.3. Finite Element Analysis

In the finite element method (Logan 2011) complex structures are divided into smaller parts, which are called finite elements (Zienkiewicz et al. 2005). Those finite elements are integrated in a mesh which is the modelling domain to solve the differential equations. This method permits the analysis of complicated surface topographies and complex mesh designs. In the biology realm, FEA was used in the biomedical research on bones primarily, followed by a broader use in palaeontology and zoology research. A FEA can be divided into three steps (Rayfield 2007), pre-processing,

analysis, and post-processing. Pre-processing includes model shape generation via a 3D digitally created shape or a CT scan. The 3D digital model is then transformed into a mesh (discretization) and the discreet elements are connected via nodal points to form the mesh. Each element is assigned with specific material properties, specifically Young's modulus and Poisson ratio. The Young's modulus describes the stiffness of a material, and it accounts for the resistance to deformation against a load. The Poisson ratio describes the compression of a material in one direction when is stretched in another one. Loads are forces that are acting on the model, which can be internal (joints), or external (hydrostatic pressure, currents, predators) and are typically added to nodal points. Constraints are points placed on the model where the displacement is known a priori, fixing the model, and preventing it from moving (Bright 2014). For each node, displacements are calculated, based on the applied loads, forces, structural geometry, and material properties. The mechanical response to the applied loads is calculated. After the analysis, the stresses are visualised. If the post-processing reveals that the mesh results have a poor quality, remeshing of parts of the model and a rerun of the analysis can be considered.

18 models representative for the smallest, average and largest values of length, curvature and number of ribs were built with the free, open-source software Blender 2.79. The models were constructed with 0, 20 and 32 ribs, 0° (no curvature), 7.3°- and 14°-degree curvature and 8 mm, 23 mm, and 40 mm length.

Models were imported as STL files to Geomagic Wrap 2017 (3D Systems, Korea, Inc., Seoul, Korea) to generate a mesh of each model. The size of the elements is based on the geometry and complexity of the model. Models were imported to Avizo 9.7 (VGS) to convert into HMASCII files. Imported models were re-meshed in Hypermesh (v. 11: part of the Hyperworks package from Altair, MI, USA) to create a better quality of the overall mesh. Element size, number of nodes and number of elements for each model size (9mm, 23 mm and 40 mm) are specified in Table 3.1 for each set of data (curvature and number of ribs).

Table 3.1. Specified element size, number of nodes and number of elements for each set of models (curvature left, and number of ribs right) for different model sizes of 9 mm, 23 mm, and 40 mm.

Curvature	Model size	Element size	# of Nodes	# of elements	# of Ribs	Model size	Element size	# of Nodes	# of elements
No curvature	**9mm**	0.055	128602	573591	0	**9mm**	0.055	39416	160347
7.3°		0.055	111424	483472	20		0.055	111424	483472
14°		0.055	114892	502973	32		0.055	140239	604174
No curvature	**23mm**	0.09	155904	639137	0	**23mm**	0.09	41422	148227
7.3°		0.09	145621	588619	20		0.09	145621	588619
14°		0.09	155636	643829	32		0.09	200627	819441
No curvature	**40mm**	0.08	355900	1493101	0	**40mm**	0.08	135147	492695
7.3°		0.08	314558	1294607	20		0.08	314558	1294607
14°		0.075	356399	1468187	32		0.075	398730	1623849

Fixed boundary conditions are applied at the bottom of the scaphopods representative of life position. All nodes at the ventral aperture side were constrained together mimicking the foot. Boundary conditions in all models were constrained to three degrees of freedom ($U_1 = U_2 = U_3 = 0$), where U represents the transitional movement in x, y, and z directions (1-3), with rotational movement permitted.

Each element is assigned an elastic, isotropic, homogeneous material with a Young's Modulus of $E = 78\ GPa$ and a Poisson ratio of n = 0.20 in Hypermesh. As material properties are not available for scaphopod shell, the average values of another aragonitic calcifiers were taken from Jennions (2014, unpublished thesis) for *Lissarca notorcadensis*, *L. miliaris*, and *Limatula spp*. To determine sensitivity to material properties, the Young's modulus, and Poisson ratio of the nautiloid *Michelinoceras unicamera* (45.8 GPa and 0.31 respectively) was also applied. The output for a model of 23 mm, 7.3° curvature, and 20 number of ribs with the nautiloid material properties, it has an increase of 3.23% in the von-Mises stress parameter, which is low. The stress distribution across the shell is similar also. Models were exported to the Finite Element software package Abaqus/CAE v.6.8-2 (Simula, USA, Dassault Systemes, //Simulia, Providence, RI, USA)

for analysis. The steps for building the scaphopod models until their analysis, can be consulted in the Appendix B, Protocol.

To assess the importance of the pressure load position on the stress distribution, two sets of models were created (shown in Figure 3.3A and 3.3B). In model A the unburied part (purple area) of the specimen has the same length at the top- and bottom part of the scaphopod, while in model B the bottom side of the unburied part (purple area) is slightly longer than along the top of the scaphopod. Both model geometries represent potential natural burial positions.
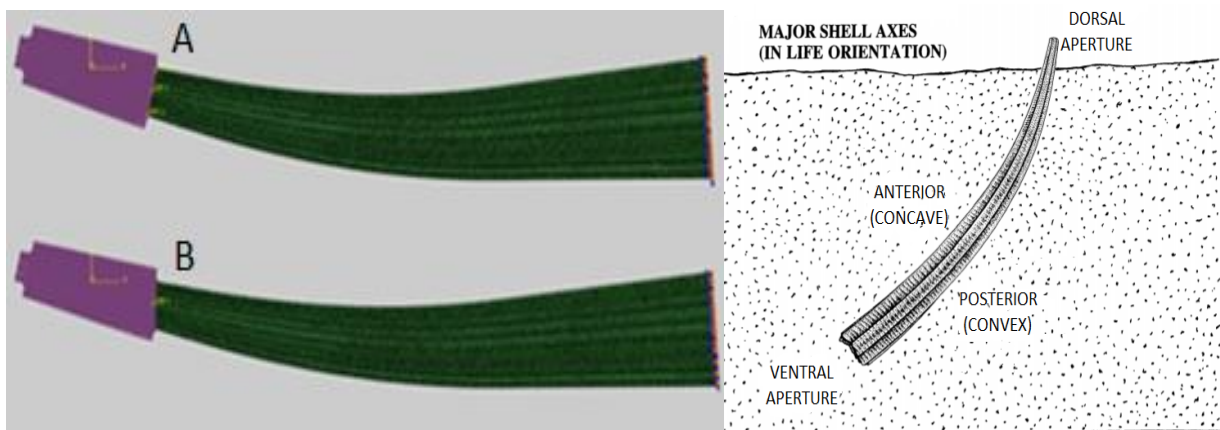
Figure 3.3. How the model was built. Left. Systematic overview of placement of pressure load of two sample models A and B. Model A was built with the same length from the tip to the cut of the purple area. Model B was built with the bottom side longer from the tip to the cut of the purple area. The fixed boundary conditions are shown at the right side of the shell (orange and blue markers). The purple area represents the surface where the force is applied at the dorsal aperture. This area is the unburied part of the shell which is exposed to all forces. The green part of the model represents the buried part of the scaphopod, where no forces are applied. Right. Schematic representation of a scaphopod position in the sediment in nature and the major shell axes orientation.

The von Mises values are scalar values, representing the distortion stress and strain tensors. Therefore, they give a value for the overall stress and strain. The Maximum principal stress or strain gives the magnitude of tension and the Minimum principal stress or strain the magnitude of compression.

The sensitivity of two different kinds of loading is explored: hydrostatic pressure load and shear load. Hydrostatic pressure is simulated by applying a uniform pressure equivalent to three different

water depths of 100, 500 and 850 m, which correspond to forces of about 1 N, 5.1 N and 8.7 N respectively.

Secondly, the impact of flow derived shear strength was assessed. A shear load was placed on the exposed part of the shell keeping the same constraints and boundary conditions as for the hydrostatic loading. A current speed of 1 ms^{-1} is used representing fast flow speed in the Southern Ocean at this depth. Drag force (the resistance of an object to a force) was calculated using the following equation:

$$F\,D = \frac{1}{2}\,C\,\rho\,A\,v^2\,,$$

where C is the drag coefficient (dimensionless) ρ is the seawater density (1025 Kgm^{-3}), A is the planar surface area exposed to the drag force, derived from $A = C \cdot l$ (C = circumference and l = length taken from a cylinder) for each scaphopod size model, and v the velocity of the current. The drag coefficient is dependent on various parameters, most importantly the shape and size of an object. As there are not experimentally measured drag coefficients for scaphopods available drag coefficients measured on a tubular frustum by Abrebekooh et al. (2011) were used as these have similar shapes to scaphopods. Resulting drag forces are 0.13 N for 9 mm, 0.47 N for the 23 mm and 0.95 N for the 40 mm model.

The results are structured to first show the results of the pressure load for both models, A and B (model geometries in Figure 3.3) followed by hydrostatic pressure and shear load. Stress values are represented with warm colours (orange/red) in case of high stress and cold colour (blue) for lower values. In each case (pressure load and shear load for model A and model B) influence of curvature (0°, 7.3° and 14°), number of ribs (0, 20 and 32) and length of the specimen (9 mm, 23 mm and 40 mm) is assessed for loads of 1N, 5.1 N and 8.7 N. For each model, von-Mises stress, Maximum-principal (tensile) and Minimum-principal (compressive) strains and the strain pattern for each model are shown. Principal strains are the eigenvalues of the strain tensor i.e. they are rotated in a coordinate system where no shear strain occurs. The Maximum-principal strain is the largest of the three eigenvalues (in 3D) and the minimum-principal strain is the smallest eigenvalue.

3.3. *Results*

3.3.1. Does the load position change the stress and strain output performance under the same load?

The pressure load placed evenly (model A) to the dorsal aperture of the scaphopod model shows similar results in comparison to pressure load that was applied unevenly (model B) (Figure 3.4) under the same pressure load (1N). For both, the von Mises stress (Figure 3.4a) generally increases with increasing curvature and increasing length. The same pattern is observed for the Maximum principal strain (Figure 3.4c). The Minimum principal shows consequently an opposite pattern: Small values for long specimen and large curvature and high values for short specimen and low curvature (Figure 3.4e). The differences of von Mises stress between Model A and Model B for all number of ribs is less than 11%. This shows that the way the load is placed does not have a large influence on those values. For that reason, just one model loading scenario, in this case Model A is analysed further.

The most important factors affecting von Mises stress, Maximum-principal and Minimum-principal strain under a hydrostatic pressure load are curvature and length of the specimen, while the number of ribs appears not to be so relevant (Figure 3.4 (a), (c) and (e)). Higher curvature leads to higher von Mises stress and tension. The difference in von Mises stress difference between 0° and 7.3° curvature models is small, but strongly increases in the scaphopod model with 14° curvature (Figure 3.4 a, c, e). The increase in stress and strain with curvature is more pronounced in the 23 mm and 40 mm length models (Figure 3.4 a, c, e). For the models with fixed curvature and varying ribs (Figure 3.4 b, d, f), stress and strain values are similar for all.
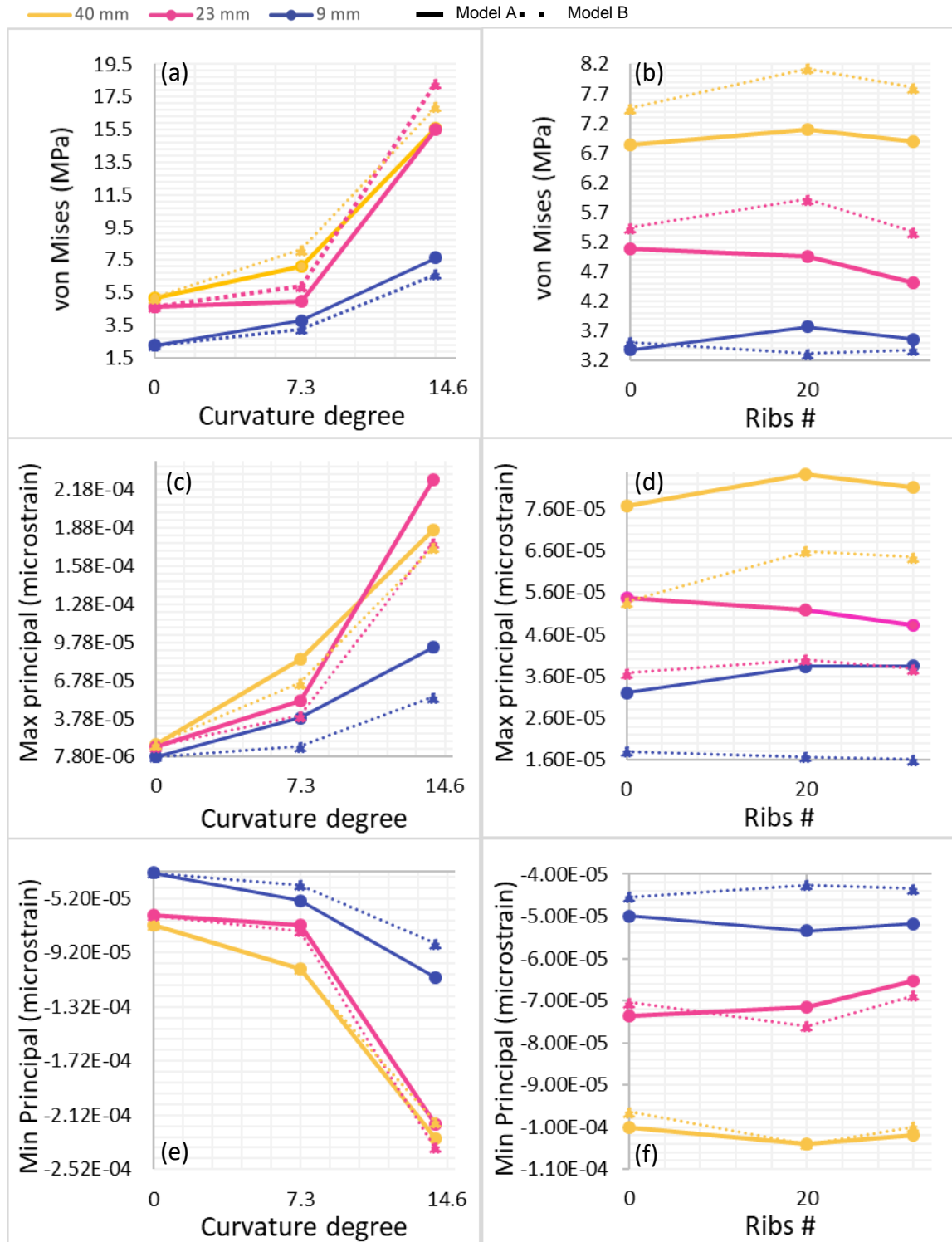
Figure 3.4. Stress response to 1N pressure load for Model A [solid line] and Model B [dashed line]. Left: von-Mises stress (a), Max principal (c)- and Min principal strain (e) for different curvatures and 20 ribs. The right figures ((b), (d) and (f)) shows the results for the same metrics with different number of ribs and a fixed curvature of 7.3°. In both cases the specimen lengths were 9 mm (blue), 23 mm (pink) and 40 mm (yellow) for Model A and Model B.

All models (varying curvature as well as varying number of ribs) display a similar pattern of stress distribution (Figure 3.5). Compression is mainly visible at the posterior ventral shell surface negative min principal strain) and tension at the anterior ventral surface shell (positive max principal strain). The central part of the specimen has low stress and strain and appears undeformed as would be expected in a bending shape. Number of ribs does not impact stress distribution, while for the uneven pressure load (Appendix B, Figure B1), the compression stress is higher at the anterior middle shell, and the tension is higher at the posterior middle shell.
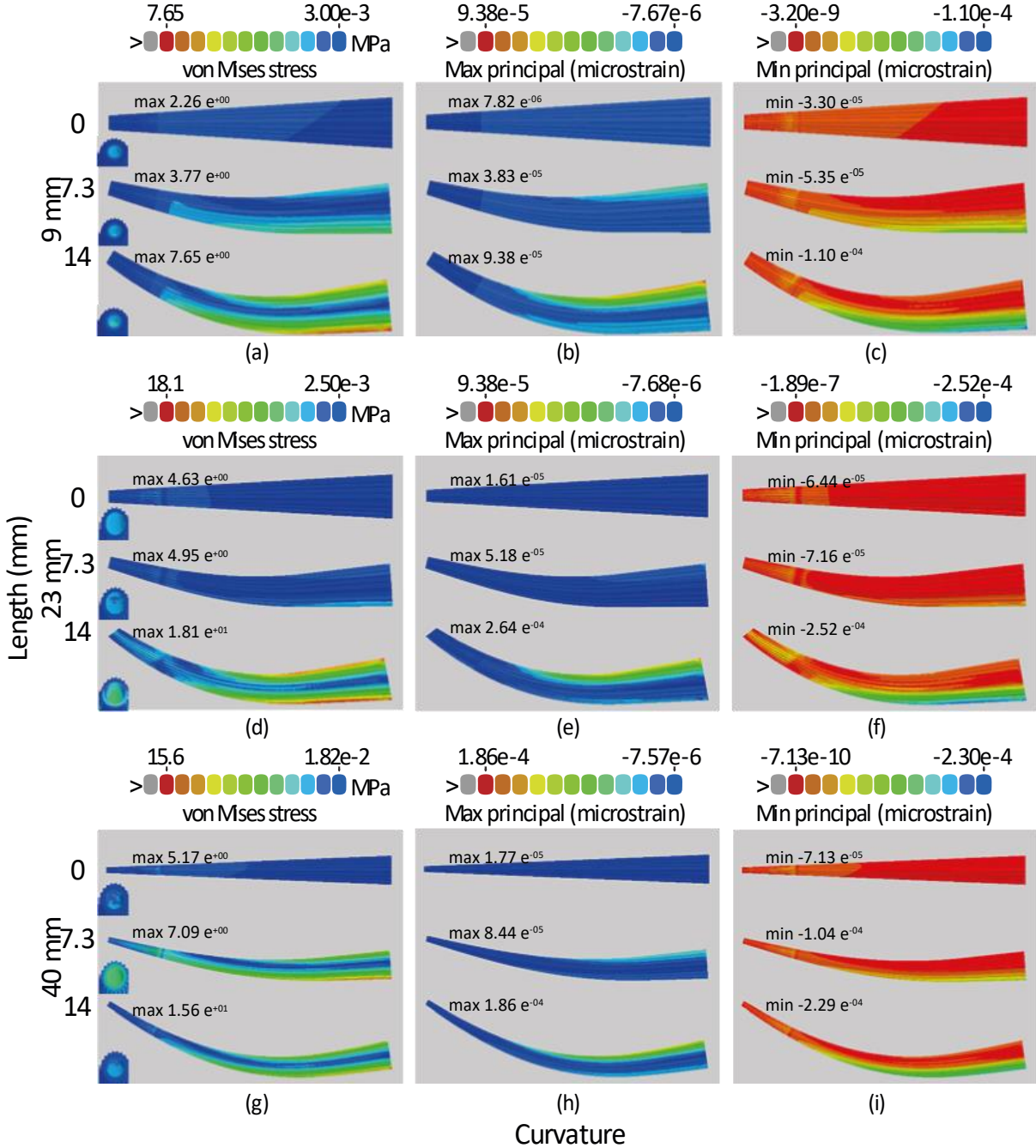
Figure 3.5. Figure caption on the next page.
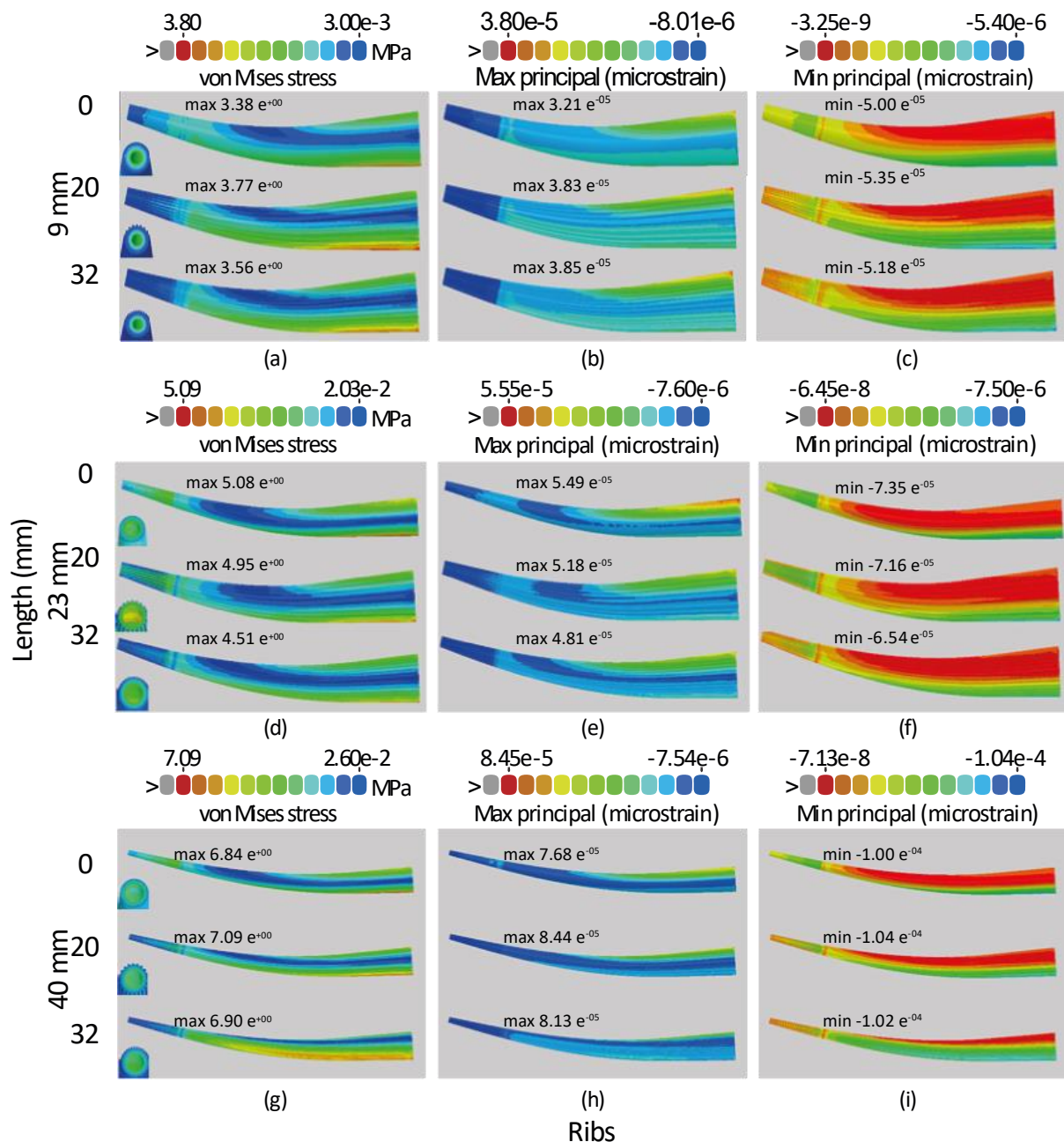
Figure 3.5. ongoing. Stress and strain distribution (von Mises, Minimum principal strain, and Maximum principal strain) of the 18 scaphopod FE models. Plots for the first set of data are organised into squares representing models with 0º to 14º curvature and starting on the top with 9 mm length ((a) to (c)), in the middle 23 mm length ((d) to (f)) and the bottom 40 mm length ((g) to (i)). For the ribs, the second set of data are organised into squares representing 0 to 32 ribs and starting on the top with 9 mm length ((a) to (c)), in the middle 23 mm length ((d) to (f)) and the bottom 40 mm length ((g) to (i)). Note, that the colour scale of the Minimum principal strain is reverted in comparison to the other figures (cool colours represents higher values). The force is applied as in Model A and for 1N pressure load.

3.3.2. Does the curvature and/or ribs increase the scaphopod performance under increasing hydrostatic pressure and shear load?

To assess the impact of the increasing hydrostatic pressure with water depth, forces representing depths of 100, 500 and 850 m (1N, 5.1N and 8.7N) were applied to model A with 20 ribs, to specimens of 9, 23- and 40 mm length. The higher the hydrostatic load, the greater the magnitude of stress and strain in the model. A model specimen of 9 mm length (top left figure) at a water depth of 100 m experiences 7 MPa maximum von Mises stress. At a water depth of 850 m, the same specimen model experiences 66 MPa.
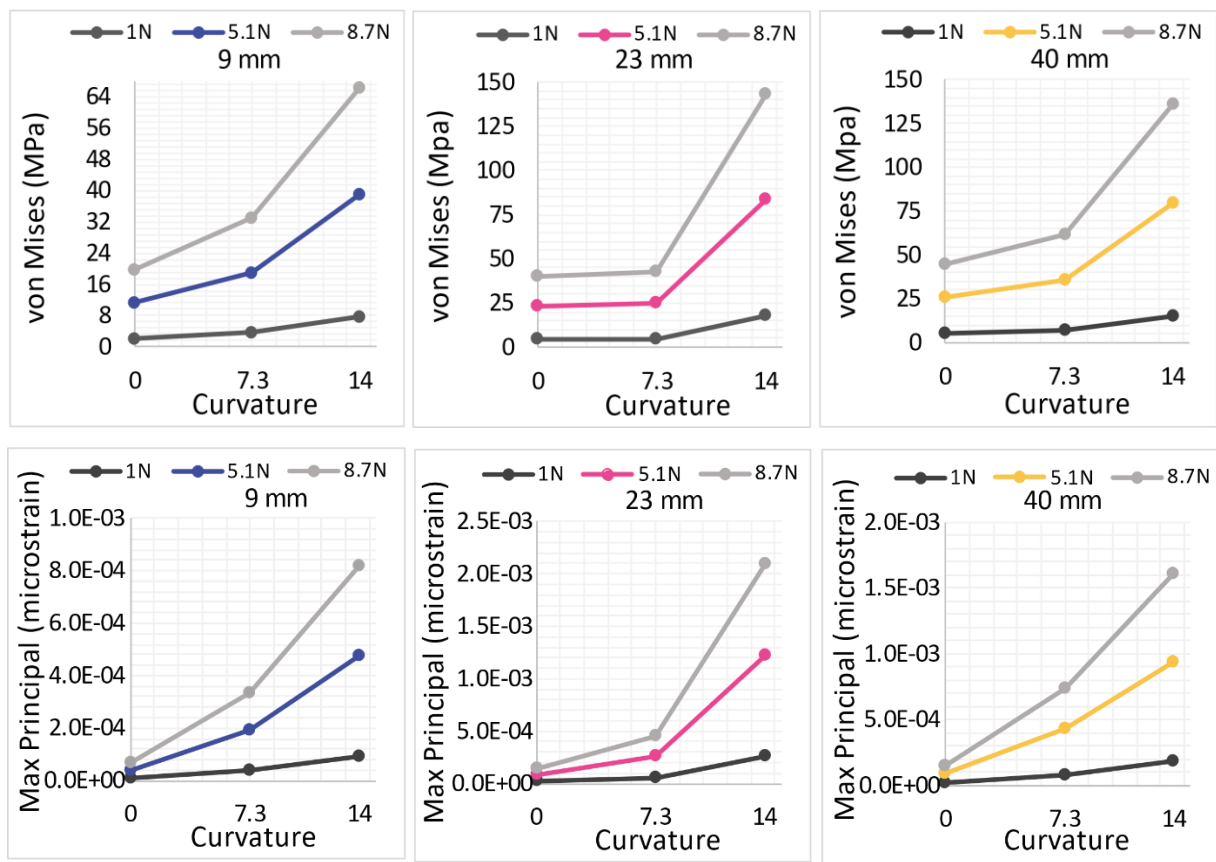
Figure 3.6. Response to different hydrostatic pressures in a scaphopod shell with 20 ribs. The pressure applied is 1N, 5.1 N and 8.7 N, representing different water depths. Von Mises stress and Max principal strain is shown for 0°, 7.3°, 14° curvature and a specimen lengths of 9mm, 23mm and 40mm. The higher the pressure, the higher the Von-Mises stress and Max principal strain.

Shear load were applied to the same models as the pressure load (Model A with 1 N shear force). Stress and strain magnitudes values vary greatly between the shear load and the hydrostatic pressure load models (Figure 3.7). Stresses are generally larger for shear in comparison to

hydrostatic pressure. Length of the specimen has a large impact when exposed to shear load with increasing stress with increasing size. On the contrary, curvature does not have a large impact compared to the response to pressure load. For the longest specimen, a decrease in stress is seen for increasing number of ribs but this is not visible for other lengths, however. A specimen with curvature of 7.3°, 23 mm length and 20 ribs experiences a von-Mises stress of 51.7 MPa in response to shear stress while for the same specimen hydrostatic pressure results in von-Mises stress of about 4.95 MPa. As such, flow dynamics is more important for structural integrity than water depth.

It is possible to see by eye that under shear load the scaphopods models are bending. Bending stress for some cross-lamellar aragonite bivalves are 95 MPa for *Mercenaria mercenaria* and 85 MPa for *Ensis siliqua* (Currey 1976). To my knowledge, the bending strength for scaphopods is unknown. The von Mises stress for the model size of 40 mm gives higher results, ranging from 286 MPa to 304 MPa from no curve to 14° curvature, which means that they are failing/fracturing (Figure 3.7). This can be explained for two factors: 1. In natural conditions the scaphopod planar area can be less exposed and hence have a lower drag force acting on it. 2. The estimate of current speed and hence the drag force equation assumes a drag coefficient and associated load that is greater than scaphopods experience in natural conditions.
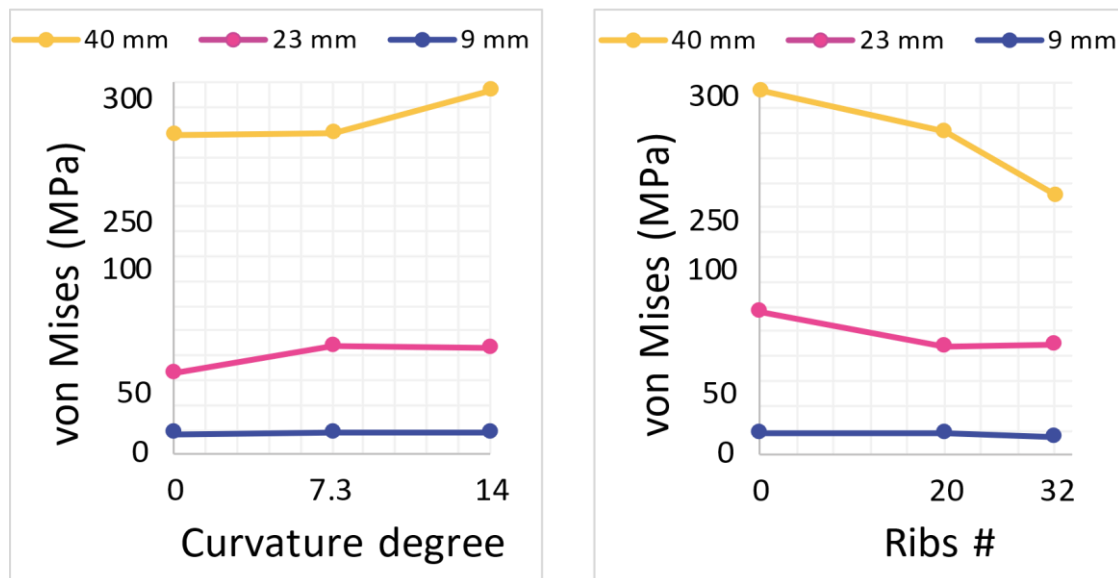
Figure 3.7. Von Mises stress for shear load models. Left: Stress in response to change in curvature and size. Right: changes in ribs and size. Note the y-axis is on a non-linear scale.

In comparison to pressure load, the shear load shows a different stress pattern with higher stresses in between the anterior and posterior sites and reduce loads at the anterior and posterior surfaces. The general pattern is best seen in the 3D-view in the bottom panel of Figure 3.8.
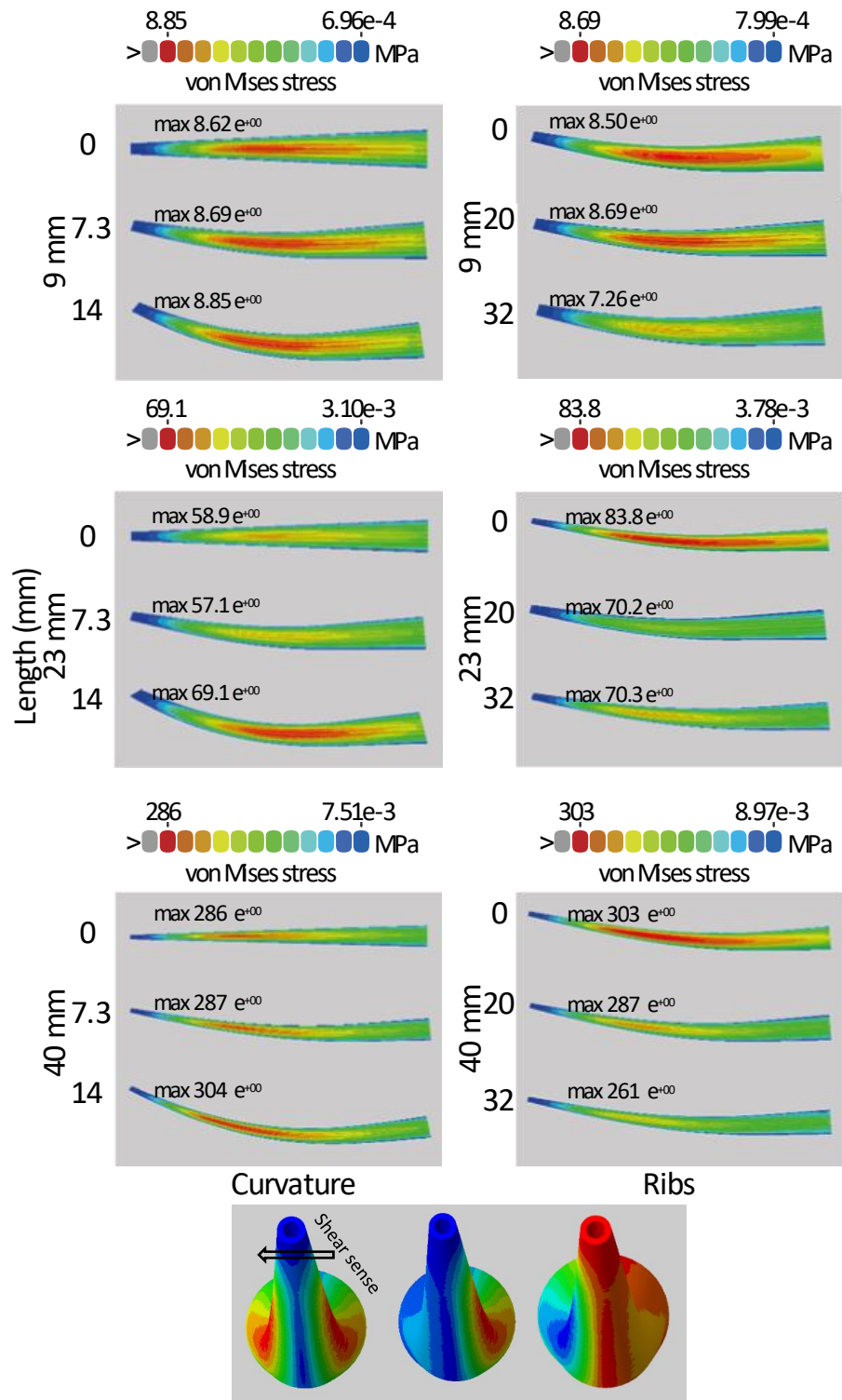
Figure 3.8. Finite-element stress distribution plots for all three modelled specimen lengths (9 mm, 23 mm, and 40 mm). The shear load is applied at the top and one side of the specimen (bottom panel). Left: varying curvature and fixed number of ribs; right varying number of ribs and fixed curvature. All the models bend slightly in response to the shear force. Maximum von Mises stress top of each plot. Highest stress is observed in the centre middle part of the scaphopods. The shear sense is schematically shown at the bottom of the figure (which shows the von Mises stress, Max principal strain and Minimum principal strain).

3.4. *Discussion*

Here, I used Finite Element Analysis to investigate the role of morphological variability in resistance to hydrostatic pressure and flow on the shell of *Dentalium majorinum* mimicking flows and pressures under natural conditions. Shell morphology is a characteristic to relate environment with ecosystem function, like as the ability of scaphopods to live in different hydrologic habitats and burrowing activity, as suggested by Vaughn & Spooner (2006) and Spooner & Vaughn (2006). The results show that curvature and length have the largest impact on the stress and strain values in response to hydrostatic pressure while the number of ribs does not influence stress distribution. The larger the specimen and the larger the curvature, the larger is the expected stress on the specimen, increasing by a factor of eight between the smallest and the largest specimen. My data supports suggestions that scaphopods are not impacted by hydrostatic pressure for their performance given the relatively lower loading and the more similar values. Scaphopods have two opening that reduce internal pressures which releasing body fluid (blood). This could be the reason why studies show that the internal pressures of scaphopods are low compared to bivalves (Trueman 1968).

On the other hand, the number of ribs is relevant for resistance against shear load. Increasing number of ribs reduces stress and strain. Comparing the impact of pressure load and shear load shows that the stress pattern varies. In response to the pressure load, highest stress is observed at the anterior and posterior edges of the scaphopod, while for the shear load the highest stress is observed between those sides. Von Mises stress is higher in response to stress representing flow, than those representing hydrostatic pressure by more than a factor of 10.

Waves and currents can induce phenotypical and adaptive modifications (Hornbach et al. 2010). Without accurate testing often links are made between form and flow without a clear assessment. For example, elongated shells of freshwater bivalves are found in slow flowing river habitats (Hornbach et al. 2010), but this shape has also been related to strong hydrodynamic action in lakes (Hinch & Bailey 1988). For scaphopods, a bigger organism may create a higher hydraulic disturbance, and hence increase the scour, whereas a smaller organism can reduce it. When water passes through the protruding portion of a burrowed shell, the vorticity of the water movement increases, which can lead to scouring (abrasion and/or erosion), if critical vorticity is reached (Stanley 1977). In contrast, in stable substrates some shelled organisms such as bivalves increase their obesity (the proportion between length and height). This has been shown for *Actinonais*

ligamentina, and *Quadrula pustulosa* downstream a river (Hornbach et al. 2010), and also in *Mytilus galloprovincialis*, which have smaller individuals in highly wave exposed sites, than those from sheltered sites (Steffani & Branch 2003).

Previous data show that *D. majorinum* from the Weddell Sea were bigger than Amundsen Sea specimens (Chapter 2). This could be interpreted due to other factors besides merely environmental ones: Trade-offs between carbonate saturation and size can be made, since decreasing size can be used as a mechanism to divert energy to other processes such as calcification and reproduction. Size has been demonstrated to be more frequently dependent on predation (Tyrrell & Hornbach, 1998, Zajac 2014) explained by food supply availability (Riccardi et al. 2016) or life history traits (Zajac et al. 2018). For example, in the Amundsen Sea specimens, those from shallower depths (<800 m) seemed to be bigger ($p < 0.05$), perhaps due to more available food and compensating the risks of a higher water scour, increasing their attaching structures.

Shell shape in the Scaphopoda group has been used for taxonomy (Reynolds 2002) suggesting limited plasticity within a species. The shape in recent Scaphopoda is suggested to be under strict control, as they do not display a wide range of curvature comparing with extinct ones, which exhibited both strong curvature or were essentially straight (Yochelson 2004). It appears then, that shell curvature in *D. majorinum* is more highly constrained with less free variation as it is possible to see in the results, with curvature varying tightly at the same time than length (Figure 3.2, left).

Many factors influence shell shape such as wave exposition, trophic level, increased of hydrostatic pressure due to water depth, predators, and population density (Akester & Martel 2000, Fox & Coe 1943, Eager 1978, Reimer et al. 1995, Seed 1968). In scallops, Pennington & Currey (1984) using FEA found that the curvature increased the stiffness of the shell. Likewise, Fitzer et al. (2015) reported that *Mytilus edulis* compensate the reduction of shell thickness becoming more curved to combated predation. However, in *D. majorinum*, a bigger curvature increased the stress to a pressure current. Interestingly the results in Chapter 2 showed that in Amundsen Sea specimens, the arc decreases with depth. As the hydrostatic pressure increases with depth, this could be one of the ways that *D. majorinum* decreases this force on the shell.

Regarding to ornamentation, the results of scaphopod ribs show that they increased the resistance of *D. majorinum* to a shear load. Ornamentations has been explained for different functions. Spikes and ridges in the *Laternula* and *Chione cancellata* respectively have been interpreted to increase stability to hold sediment (Stanley 1981), but they have other functions than stability of the shell. For example, different substrates might result in sinking in response to hydrostatic pressure which might be reduced in specimens with ribs. Prominent ribs were found to be related to soupy or silty clay sediments, whereas higher density ribs and less prominent ribs are linked to fine-sandy sediments in the bivalve *Arcomytilus* (Schneider et al. 2010). In scaphopods however, there is no clear link between sediment type and ornamentation (Lamprell & Healy 1998). On the contrary, Shimek (1989) suggested that in scaphopods a glossy shell can increase the ability to rapid burrow to escape from predation. Alternatively, is has been suggested that there is a relationship between burrowing and ornamentation. *Trachycardium egmontianum* for example, take fewer burrowing sequences in specimens with spines than without them (Stanley 1981). Likewise, ridges and spines can reduce scour in the bivalve *Trachycardium* (Stanley 1981) and by analogy scaphopod ribs may have a similar function. Interestingly, it has been observed that those individuals who have more ornamentation are more exposed above the substrate than those with smoother shells (Allen & Vaughn 2009) which is according with our results. *D. majornum* is one of the Scaphopoda species that does not burrow completely but instead leaves the dorsal aperture above the sediment; scour though, can be a constant threat. To address these questions a flow model assessment of the ornamentation would be useful (Rahman 2017).

Despite the advantage of ribs against bending under flow, not all scaphopods display ribs. Similarly, while scallops with ridges and furrows have a stronger shell (Pennington & Currey 1984) not all scallop shells are corrugate. This implies that despite the mechanical advantage of ribs, other constraints might be inhibiting rib growth, for example energy limitation in the deep-sea setting, and the characteristic life history traits of each species.

Importantly to note, most of the FE models do not break at different hydrostatic pressures and shear load, except the 40 mm ones. That could mean that the material properties of *D. majorinum* are resilient to water conditions and that their shell shape and ornamentations allow them to cope with the different environmental pressures that they are encounter. The study is the first of its kind and therefore uses some input parameters which are not directly verified and measured such as the drag coefficient, which depends on the shape and size of the object and could be the reason why

the 40 mm models break under these loads. The speed flow used in this study is higher than in natural conditions, where usual current speed varies between 1 cm/s^2 up to 45 cm/s^2 (Whitworth & Nowlin 1987), and this could explain the high stress in some models. However, the results are linear, which means that decreasing or increasing the loads will be giving the same results patterns. More importantly, in nature hydrostatic pressure and flow pressure both act on the same specimen. While individually stress pattern are similar, the amount of stress is very different, raising the question how these stresses interact when both applied.

3.5. *Conclusions*

This study used FEA to investigate how *Dentalium majorinum* behaves under flow and hydrostatic stress conditions. Large specimens with higher curvature experience more stress under hydrostatic pressure load suggesting that they might break easier. In nature, the curvature degree is correlated with the size of the specimen and hence is under more control. Under shear load, the curvature has less significance, but those specimens with higher number of ribs perform better, suggesting that ribs strengthen the shell. The comparative magnitude of stress suggest that hydrostatic pressure is less important in shell breakage than shear forces. Under different environmental pressures, the morphological plasticity of *D. majorinum* specimens can cope with them showing a resilient shell.

Chapter 4 : SHELL RESPONSES OF CYCLOCARDIA ASTARTOIDES AND LIMOPSIS MARIONENSIS TO ENVIRONMENTAL DIFFERENCES IN THE SOUTHERN OCEAN

Abstract

The Southern Ocean (SO) is considered to be highly vulnerable to climate change. The biotic response to warming and changes in carbonate chemistry in response to anthropogenic CO_2 emissions is, however, less well constraint. Using differences in the regional oceanography and resulting carbonate chemistry provides insights into a steady state response to lower saturation and warmer climates. Here, I assess the morphological-, geochemical-, and material differences in shells of Antarctic bivalves in response to their local environments. I will compare shells from different regions of the SO (Weddell Sea, Amundsen Sea, Magellan, and the South Sandwich Islands). Whilst the Magellan region is warmer than the other regions, the Amundsen Sea has the lowest aragonite saturation. The bivalve species *Cyclocardia astartoides* and *Limopsis marionensis* are bigger in regions with high productivity such as the Weddell Sea and South Sandwich Islands. Neither temperature and carbonate saturation impact Sr and Mg uptake in the shells. μ-CT scanning was used to quantify density differences and to reveal dissolution patterns of the shells. Shell density is higher in the Magellan region where aragonite saturation is high. All the shells show some level of internal dissolution and does not seem to impact the function. Our findings provide insights how bivalves response to different environmental conditions, which might shed lights into adaptation in response to future climate.

4.1. *Introduction*

Environmental change in the Southern Ocean (SO) is already detectable (Parkinson et al. 2001, Turner et al. 2005). Importantly, warming is not impacting the region equality and regional differences in climate change are evident. The Bellingshausen and Amundsen areas are one of the most affected zones by warming and ice retreat (Vaughan et al. 2003, Turner et al. 2014) with a

77

6.63% ice decline per decade^{-1} (Murphy et al. 2014). Mean sea surface temperature around South Georgia has increased by ~0.9°C in summertime and ~2.3°C in wintertime (Whitehouse et al. 2008). Importantly, warming is not impacting the region equally, and regional differences in climate change are evident. Whist glaciers in the South Orkney islands do not show a trend of decline over the last 50 years (Murphy et al. 2014), ice cover in the West Antarctic Peninsula (WAP) has reduced since the 1970s (Stammerjohn et al. 2012) although not unidirectionally (Turner et al. 2016). Comparing the temperature data from the first quarter of 20th century the 90s it has been shown that the upper depths of the SO (>1000 m) has been warming specially in the Antarctic Circumpolar Water (ACC, Liu & Curry 2010). By the end of the 21st century, under RCP 4.5 and 8.5 respectively further warming is projected (Chapman 2020).

The Southern Ocean, due to its cold temperature, is naturally taking up a vast amounts of CO_2 (DeJong et al. 2015) which leads to an undersaturation in calcite and aragonite in shallower depth than other ocean regions (Watson et al. 2012). The Bellingshausen and Ross Sea Antarctic regions, with their low total alkalinity, have already experienced short undersaturation events (Hauri et al. 2016). These events are projected to increase starting in western Antarctica and expanding to eastern Antarctica between 2035-2040 under a RCP8.5 CO_2 emission scenario. By the end of the century, >70% of SO surface water will be undersaturated with regards to aragonite (Hauri et al. 2016).

These environmental changes challenge the survival of individuals and species. Ocean acidification (OA) causes increases of metabolic requirements to continue physiological processes against a higher proton and a lower carbonate ion concentration (Stumpp et al. 2012). Undersaturation reduces the availability of carbonate ions to calcify and can cause a loss of shell density or, if exposed to such water, corrosion (Harvey et al. 2018). The maintenance of such skeletal structures is key for the organism making the balance between biomineralization and dissolution important for wellbeing of calcified organisms. Impacts of ocean acidification have been studied in many species across the world ocean. These showed that dissolution due to a decline in carbonate saturation has been identified in living pteropods of *Limacina helicina antarctica* (Bednaršek et al. 2012a), increasing the risk of reduced shell integrity. Responses to low pH vary as some species prioritise density over shell size, for example molluscs and echinoderms (Parker et al. 2013, Byrne et al. 2013), while others maintained their size but change their material properties like the deep-water coral *Balanophyllia europaea* (Fantazzini et al. 2015).

The impact of higher metabolic demands can be mediated by food uptake (Melzner et al. 2011, Comeau et al. 2013) and thus support the upkeep of growth and calcification.

Metabolic activity doubles every 10°C in cold blooded organisms. Therefore, warming increases metabolic demands, reducing the ability to allocate energy to other processes such as biomineralization (Ruddy et al. 1975). Warming can therefore weaken the shell as shown in the bivalve *Mytilus edulis*, and reduces surface area, shell thickness, and mechanical strength (Mackenzie et al. 2014). The gastropod *Viviparus viviparus* increases growth rate, alters shell structure specifically with a decrease in aragonite table width *(*Fullenbach et al. 2014). The impact is not only on the species but also multigeneration; for example, a decrease in offspring size has been reported in *Lissarca miliaris* (Reed et al. 2012). Ecologically, temperature impacts habitat range as species follow their temperature range (Griffiths et al. 2017). In the Southern Ocean, in response to RCPs 4.5 and 8.5 scenarios a redistribution in species, resulting in change in species richness and community composition are projected for the Southern Ocean (Molinos et al. 2016).

Based on the above understanding, calcifying species, and especially benthic species, are very sensitive to these environmental change because many are sessile and therefore unable to migrate to follow their ecological niche (Henley et al. 2019). Amongst and within taxa, available data suggest a considerable variation in the ability of species to respond to changing environmental conditions globally (Pfister et al. 2016) and specifically in the Antarctic benthos where some organisms show little effect at lowered pH (Cross et al. 2015) and other studies find greater effect of temperature compared to pH (Byrne et al. 2013).

Bivalves are a key piece of the Southern Ocean ecosystem and provide a habitat for many other organisms (Abele et al. 2009). The shell of bivalves is crucial for their survival, encasing the organism's soft tissues for protection from predation and, in intertidal zones, from exposure to air (Stanley 1981, Andrade et al. 2019). Their ontogeny can be recorded in their shells and geochemical changes to their shell composition record environmental changes (Jones 1983). Bivalve shells can be dissolved to buffer the extracellular pH during periods of environmental exposure (Sokolova et al. 2000). As such, any change in shell production or strength could severely influence the survival of these organisms.

Experimental studies of the impact of environmental changes on Southern Ocean species are logistically challenging. Often experiments are too short ranged to allow assessing the potential for adaptation to these changes. Therefore, I use the regional differences in the oceanography of the Southern Ocean as a test bed to assess potential changes to bivalve shells in response to climate change and adaptation potential. I present the results of natural populations from four different geographical areas in the broader Southern Ocean: Amundsen, Weddell, South Sandwich Islands and Magellan region. I compare the effects of carbonate saturation and temperature on size, morphology, and shell integrity of the bivalves *Cyclocardia astartoides* and *Limopsis marionensis*. To put the findings into a developmental context, growth rings were determined for *C. astartoides*. As environmental differences have the potential to lead to changes in the geochemical composition of the shell, Sr and Mg concentrations were determined. With this data, I would like to test: 1) if the environment, both with depth and geographically, affected the growth and density of the bivalves, 2) if the elemental composition changes across the regions in response to environmental factors, 3) if the size is correlated with age in this species living under extreme conditions and 4) if density and geochemistry change with age. This information will allow to assess how bivalves respond to a range of environmental conditions and therefore how much resilience to change they might have to environmental changes over time.

4.2. *Materials and methods*

4.2.1. Study species

Limopsis marionensis (Smith 1885) is a marine bivalve with an oblique, uneven, conical shell and with a russet-brown epidermis and hair-like bristles. Its shells have close radiating lines (Rochebrune & Mabille 1889). This species can be found between 73-2804 m depth with a circum-Antarctic and sub-Antarctic distribution (Griffiths et al. 2003, Engl 2012). It has an epifaunal mode of life (Cattaneo-Vietti et al. 2000), often associated with sponges (Pörtner et al. 1999) though can be found on other structures such as sand, rock, mud, and gravel (Nicol 1966). During reproduction, the embryos develop a free-swimming trocophore larvae, followed by a veliger which allows for dispersion (Melvill & Standen 1914).

Cyclocardia astartoides shell is oval and radial with approx. 20 striates. The valves are equal and not equilateral (Cruz 1990). The dorsal anterior is concave and the posterior convex. The periostracum is well developed, irregular, and concentric in its shape, following the growth line. They have radial ribs with interstitial spaces between them (Martens 1878). This species is one of

80

the most widely distributed Antarctic bivalves like the one above, with a circum-Antarctic and sub-Antarctic distribution (Linse 1999). *C. astartoides* can be found in water depths shallower than 500 m (Buckeridge 1989, Troncoso et al. 2007), although Powell (1958, p. 177 in Nicol 1966) reported their occurrence down to 640 m water depth. This species has an infaunal mode of life (Cattaneo-Vietti et al. 2000) in a wide range of substrates (Troncoso et al. 2007). During reproduction it develops a lecithotrophic larvae with no evidence for incubation or young brood in breeding (Hain & Arnaud 1992).

4.2.2. Sample collection

178 bivalve specimens of *L. marionensis* were collected alive during several research cruises (Figure 4.1). 114 specimens were collected from two stations in the Magellan region on the research cruise RV Nathaniel B Palmer (Robinson & Waller 2011) and RV Victor Hensen; 39 specimens from five stations in South Sandwich Islands during the research cruise RV Polarstern ANTARKTIS XIX/5 (LAMPOS) (Arntz & Brey 2003); 24 specimens at five stations in the east Weddell Sea during RV Polarstern ANTARKTIS XXI/2 (BENDEX) (Arntz & Brey 2005); one station during RV Polarstern ANTARKTIS XV/3 (EASIZ II) (Arntz & Gutt 1999). From the Amundsen Sea, one specimen was collected on the research cruise RSS James Clarke Ross (Enderlein & Larter 2008). Collection data are presented in table 4.1 and specify depths, collection gear, stations, and locations per region.

Table 4.1. Characterisation of specimens of *L. marionensis*. The specimens were collected on expeditions to the east Weddell region, Sandwich Islands, Amundsen Sea. and Magellan region. Collection gear, station, collection date, depth and location are specified for each vial number. Collection gears abbreviations are AGT = Agassiz Trawl, EBS= Epibenthic sledge.

Region	Vial	Number of specimens	Collection gear	Station	Collection date	Depth [m]	Latitude	Longitude
Eastern Weddell Sea	197	6	AGT	PS 65-090	09.12.03	288	-70.94222	-10.5436
	585	2	AGT	PS 65-276	28.12.03	268	-71.11778	-11.4577
	611	3	AGT	PS 65-121	11.12.03	274	-70.83528	-10.5872
	795	1	AGT	PS 65-324	03.01.04	694	-72.91444	-19.8038
	826	2	AGT	PS 65-326	03.01.04	606	-72.85917	-19.6455
	206	10	AGT	PS48/206	18.02.96	518	-71.00056	-11.7
South Sandwich Islands	663	2	AGT	PS61/207-1	16.04.02	514	57.68472	-26.4763
	655	8	AGT	PS61/194-1	15.04.02	278	-57.68611	-26.4358
	684	7	AGT	PS61/217-1	18.04.02	518	-59.92194	-32.4925
	849	10	AGT	PS61/217-1	18.04.02	518	-59.92194	-32.4925
	468	12	AGT	PS61/143-2	25.03.02	753	-58.44555	-25.1048
Amundsen Sea	421	1	EBS	BIO4-AGT-3A	2008	502	-74.4099	-104.655
Magellan Region	1279	2	EBS	1279	21.11.94	271	-54.29361	-70.8725
	7	112	Hein Dredge	7	12.05.11	300	-54.51194	-62.2347

62 specimens of *Cyclocardia astartoides* were collected from the Amundsen and the Weddell seas (Figure 4.1): Three specimens in three stations during RV Polarstern ANTARKTIS XV/3 (EASIZ II) (Arntz & Gutt 1999); 10 specimens at five stations during RV Polarstern ANTARKTIS XXI/2 (BENDEX); two specimens at two stations during RSS James Clarke Ross JR275 (Saucède et al. 2015); 47 specimens at 10 stations during RSS James Clarke Ross JR179 (Enderlein & Larter 2008). Table 4.2 provides information on sampling depths, collection gear, stations, and locations per region.

Table 4.2. Characterisation of specimens of *C. astartoides*. The specimens were collected on expeditions to the Weddell Sea (4 cruises) and the Amundsen Sea (1 cruise). Collection gear, station, collection date, depth and location are specified for each vial number. Collection gears abbreviations are AGT = Agassiz Trawl, BT = Bottom-trawl, RD = Rock dredge GSN = Set gillnet.

Region	Vial	# of specimens	Collection gear	Station	Collection date	Depth [m]	Latitude	Longitude
Eastern Weddell Sea	49	1	AGT	49	30.01.98	246	-70.87	-10.4833
	363	1	BT	PS 65-166	15.12.03	338	-70.9472	-10.5435
	812	1	RD	PS 65-325	03.01.04	458	-72.9127	-19.7247
	528	1	GSN	PS 65-259	24.12.03	300	-70.9428	-10.533
	187	4	AGT	PS 65-029	25.11.03	377	-54.5265	3.2175
	155	3	RD	PS 65-069	07.12.03	414	-70.4323	-8.6205
	266	1	AGT	29	20.02.02	576	-76.1990	-31.8602
	1570	1	AGT	15	04.03.02	413	-75.2389	-27.8486
	77	1	AGT	77	02.02.98	433	-71.1433	-12.4433
	62	1	AGT	62	30.01.98	248	-70.8766	-10.4767
Amundsen Sea	687	5	AGT	BIO5-AGT-3C	2008	539	-73.9864	-107.39
	1152	7	AGT	BIO4-AGT-3B	2008	488	-74.3989	-104.63
	1004	14	AGT	BIO6-AGT-3B	2008	480	-71.3416	-109.998
	1056	3	AGT	BIO6-AGT-3A	2008	480	-71.3482	-109.998
	731	4	AGT	BIO5-AGT-3D	2008	535	-73.9805	-107.408
	420	4	AGT	BIO4-AGT-3A	2008	502	-74.4099	-104.655
	802	1	AGT	BIO6-AGT-3A	2008	480	-71.3482	-109.998
	188	1	AGT	BIO3-AGT-1B	2008	578	-71.8012	-106.295
	537	3	AGT	BIO4-AGT-3B	2008	488	-74.3989	-104.63
	1074	5	AGT	BIO6-AGT-3C	2008	476	-71.3486	-110.006
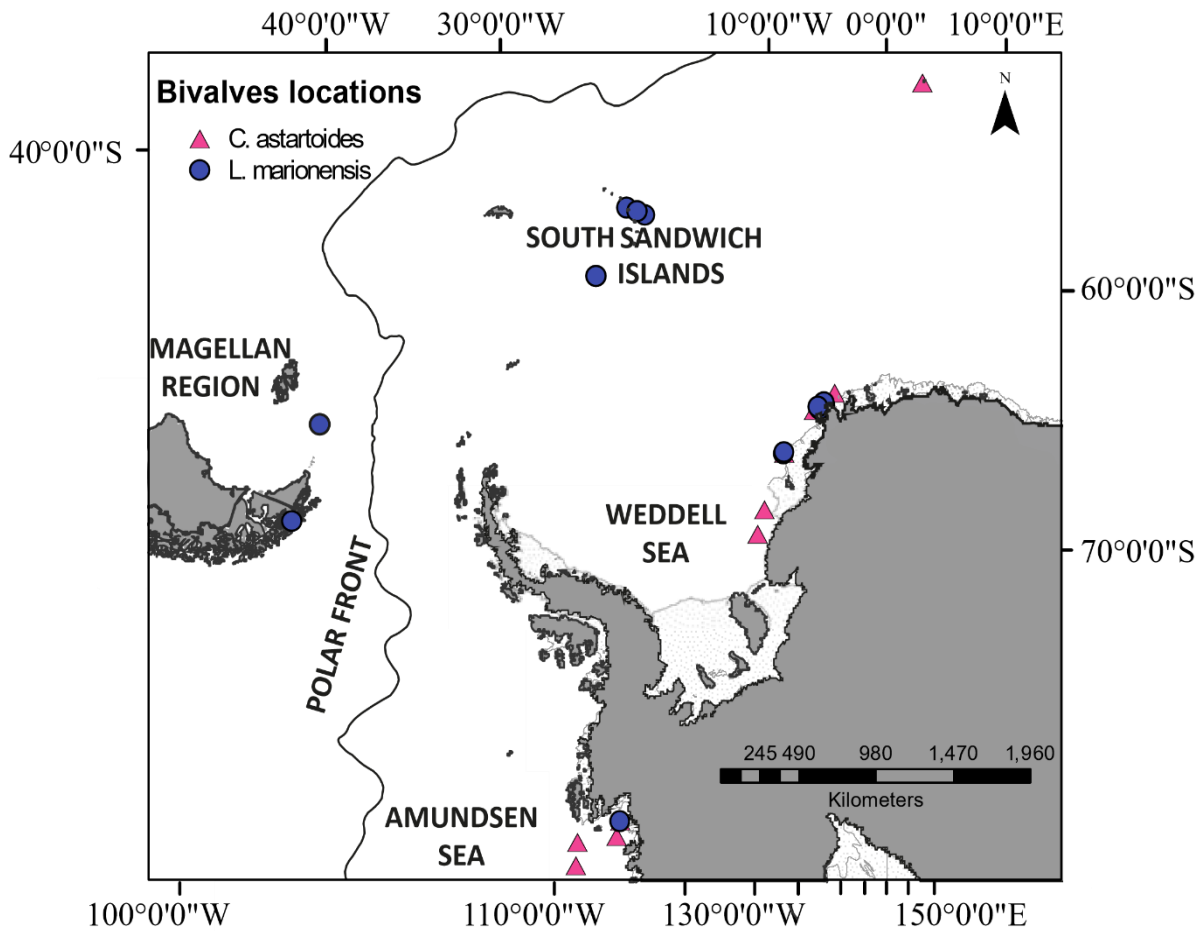
Figure 4.1. *Limopsis marionensis* and *Cyclocardia astartoides* collection from different SO regions. *L. marionensis* specimens (blue circles) were collected in the Magellan region, South Sandwich Islands, east Weddell Sea and Amundsen Sea. *C. astartoides* specimens (pink triangles) were collected from the Weddell and Amundsen seas (Cruise information in Table 4.1 and 4.2). The figure shows the Polar Front and the ice shelves in the Weddell and Amundsen seas.

4.2.1. Environmental background of the study sites

The environmental data was taken from GLODAPv2.2019 (Olsen et al. 2019) averaging the temperature for each region. While it would have been desirable to get local data for the collection sites, carbonate chemistry data for the Southern Ocean is rare. The Magellan region, located at the tip of South America, is north of the Polar Front. The temperature is higher than in the other regions of this study, with an average of 4.56°C over 1000 m depth, and the highest aragonite saturation (Ω_{Ar}) of 1.51. Both temperature and saturation are highest in the top 200 m. In the South Sandwich Islands, the Antarctic Surface water (AASW) in the top 250-meter has the lowest temperature and highest saturation, with an average of $\Omega_{Ar}= 1.22$ (Allen & Smellie 2008). Below the WDW

between 250 and 1000 m depth the average temperature increases to 0.8°C and the average $\Omega_{Ar}=$ 1.06 (van Caspel 2016, Table 4.3). The east Weddell Sea is the region with the lowest average SS temperature of -1.39°C and Ω_{Ar} of 1.33. The water masses in this region are winter water (WW) above 400 m depth or close to the shelf, with the lowest temperature and highest saturation (Table 4.3). Under this, the Modified Warm Deep Water (MWDW) can be detected between 400 to ~500-600 m depth and the Warm Deep Water (WDW) below ~500-600, with a higher temperature and lower saturation (Nichols et al. 2009). In the Amundsen Sea region, WW covers the top ~500m, and also is the water mass with low temperature and higher saturation ($\Omega_{Ar}=$ 1.166), while Circumpolar Deep Water (CDW), which can be find below, is warmer and less saturated (Arneborg et al. 2012). A more detailed description of the regions with the average temperature, salinity and Ω_{Ar} in 200 m depth intervals can be found in the table 4. 3.

Table 4.3. Environmental data taken from GLODAPv2.2019 (Olsen et al. 2019) from transects in the four regions: Magellan, South Sandwich Islands, Weddell, and Amundsen seas. Table specified for each 200 m depth range the depth, temperature salinity and aragonite saturation until 1000 m depth.

Region	Depth (m)	Mean Temperature (°C)	Mean Salinity (PSU)	Mean Ω_{Ar}
Magellan	0-200	5.77	34.0	1.83
	200-400	3.69	34.1	1.51
	400-600	3.41	34.3	1.42
	600-800	3.05	34.4	1.23
South Sandwich Islands	0-200	0.167	34.1	1.35
	200-400	0.715	34.6	1.10
	400-600	0.942	34.6	1.07
	600-800	0.749	34.7	1.03
Eastern Weddell Sea	0-200	-1.71	34.3	1.47
	200-400	-1.32	34.4	1.25
	400-600	-0.459	34.6	1.16
	600-800	-0.0833	34.6	1.10
Amundsen Sea	0-200	-1.65	33.7	1.34
	200-400	-0.767	34.2	1.04
	400-600	0.585	34.6	1.03
	600-800	0.968	34.7	1.02

4.2.2. Morphometric measurements

Three axes of the shell defined as height (maximum distance in the dorsal-ventral axis, through the middle axis of the shell), length (maximum distance on the anterior-posterior axis), and width (maximum distance in the lateral axis, between both valves of the closed shell) were measured for

178 *L. marionensis* specimens and 62 *C. astartoides* specimens (Figure 4.2 shown an sketchon how the morphometrics measurements were taken). Measurements were carried out with Vernier callipers with an uncertainty of 0.02 mm.
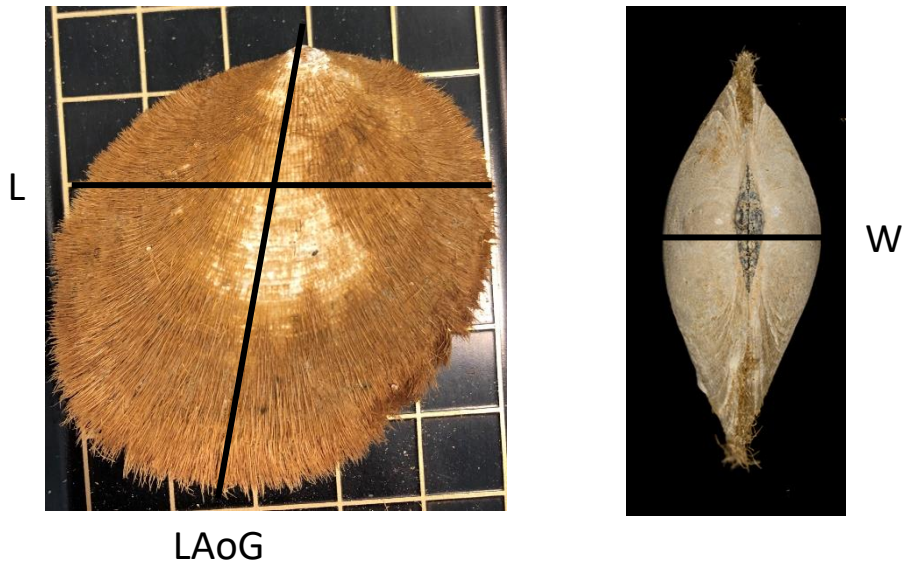
Figure 4.2. Bivalves transects for morphometric analysis: L= Length, LAoG = Maximum length of growth, W=width. In this images showing *L. marionensis*.

4.2.3. Sample selection

Specimens of *L. marionensis* were chosen from different regions, water depth and different body size (Table 4.4). Due to the coronavirus outbreak, some analysis such as age determination and geochemistry, could not be completed. Specimens of *C. astartoides* were chosen from different regions and sizes (Table 4.5).

Table 4.4. Description of the specimens of *L. marionensis* from the eastern Weddell, South Sandwich Islands, Amundsen, and Magellan region selected for density analysis. Vial No., long axis growth (width and length are reported in the Appendix C, Table C1) depth, temperature and aragonite saturation are reported for the selected specimens. Environmental conditions are from GLODAPv2.2019 (Olsen et al. 2019).

Region	Vial	Length (mm)	Depth (m)	Temperature (°C)	Ω_{Ar}	Analysis*
Eastern Weddell Sea	197.1	63	288	-1.319	1.25	Density
	585.1	19.2	268	-1.319	1.25	Density
	611.2	43.7	274	-1.319	1.25	Density
	611.3	16.4	274	-1.319	1.25	Density
	206.1	14.7	518	-0.459	1.159	Density
	206.2	13.3	518	-0.459	1.159	Density
	826.2	17	606	-0.459	1.159	Density
	795.1	46	694	-0.083	1.101	Density
South Sandwich Islands	655.1	54.4	278	0.715	1.098	Density
	655.2	33.4	278	0.715	1.098	Density
	655.3	26	278	0.715	1.098	Density
	684.7	25.2	518	0.942	1.068	Density
	849.1	42.1	518	0.942	1.068	Density
	849.2	33.1	518	0.942	1.068	Density
	849.3	26.2	518	0.942	1.068	Density
	468.2	30.1	753	0.942	1.068	Density
Amundsen Sea	421	17.9	502	0.585	1.034	Density
Magellan Region	Lm28	30.2	353	3.69	1.51	Density
	Lm33	30.3	353	3.69	1.51	Density
	Lm73	20.7	353	3.69	1.51	Density
	Lm74	37.1	353	3.69	1.51	Density
	Lm90	37.9	353	3.69	1.51	Density
	Lm211	20.0	353	3.69	1.51	Density
	Lm234	24.1	353	3.69	1.51	Density

*Due to the Coronavirus outbreak, age determination and geochemistry analysis were not completed.

Table 4.5. Description of specimens of *C. astartoides* from the Amundsen and Weddell Sea analysed for D = Density, Ds = Dissolution, G = Geochemistry, and A = Age. Vial No., length (width and height are reported in the Appendix C, Table C2), depth, temperature and aragonite saturation are reported for the selected specimens. Not all specimen showed clear growth rings; and specimen where age determination was possible are marked with two asterisks, and those which did not with one. Environmental conditions were taken from GLODAPv2.2019 (Olsen et al. 2019).

Region	Vial	Length (mm)	Depth (m)	Temperature (°C)	Ω_{Ar}	Analysis
Amundsen	1004.11	4.18	480	0.585	1.03	D/Ds
	1004_1.7	3.05	480	0.585	1.03	D/Ds/A*
	1004_1.8	4.89	480	0.585	1.03	D/Ds/G/A*
	1004_1.12	7.51	480	0.585	1.03	D/Ds/GA**
	1152_1.4	8.58	488	0.585	1.03	D/Ds/G/A*
	1152_1.1	14.3	488	0.585	1.03	D/Ds/G/A**
	1056_1.1	11.5	480	0.585	1.03	D/Ds/G/A**
	420.3	12.7	502	0.585	1.03	D/Ds/G/A*
	731_1.2	11.7	535	0.585	1.03	D/Ds
Eastern Weddell	49	10.8	246	-1.32	1.25	D/Ds/G/A*
	528	16.2	300	-1.32	1.25	D/Ds/A**
	363	11.12	338	-1.32	1.25	D/Ds
	187.4	3.26	377	0.162	1.11	D/Ds/G/A*
	187.2	15.0	377	0.162	1.11	D/Ds/G/Age*
	155.3	7.91	414	-0.459	1.16	D/Ds/G/A**
	812	18.5	458	-0.459	1.16	D/Ds/G/Age**

4.2.4. µ-Computed tomography

µ-Computed tomography using the Nikon XTH225 ST at the University of Bristol was used to determine the density of the shells. The measurement was standardised using aragonite phantoms from Cumberland, UK with a density of ~2.93 g/cm³. 23 specimens were scanned with a 100 KV voltage, 200 µA current, and 1.41 s exposure time resulting in a 20 µm voxel resolution for *L. marionensis*. Due to the smaller shell size, *C. astartoides* specimens were analysed with 80 KV, and a current of 375 µA resulting in a voxel size of 10 µm for the 16 scanned specimens. Each analysis consisted of 3141 projections. An 0.25 Aluminium filter was used to reduce artifacts and a beam hardening correction was applied. CT scaling is expressed as Hounsfield units (HU), and the conversion was performed with CT PRO 3D version 3.1.9 (Nikon, Tokyo, Japan). The HU for each pixel reflects the electron density of the imaged object, which is assigned to a gray scale

intensity (Lev & Gonzalez 2002). As the intensity drifts with time, a circular area was chosen from a middle slice of the aragonite standard for each scanned specimen to obtain a scaling factor.

TIFF files were digitally segmented with Avizo Software Fire 9.7 (Mercury Computer Systems Ltd, Chelmsford, MA, USA, www.tgs.com) to separate the shell from other objects. Under the selected conditions, the minimum grey value threshold was 20000 (where the majority of the shell is selected) and the maximum 65535, which is the maximum grayscale value of a 16-bit tiff image. Dissolution is indicated by difference in grey values as white carbonate is dissolved into grey areas. To quantify the areas of different densities, histograms were generated to discriminate areas of different grey value and hence density. Median filter were applied between 3-4 times to reduce noise and separated peaks to create a binomial distribution. This approach allowed to determine a reproducible threshold to separate partially dissolved from pristine material (Figure 4.3). Dissolution was assessed only for *C. astartoides* specimens characterising areas with holes interpreted as corrosion. Thickness measures were performed in three middle different parts of the shell, from the anterior to posterior.
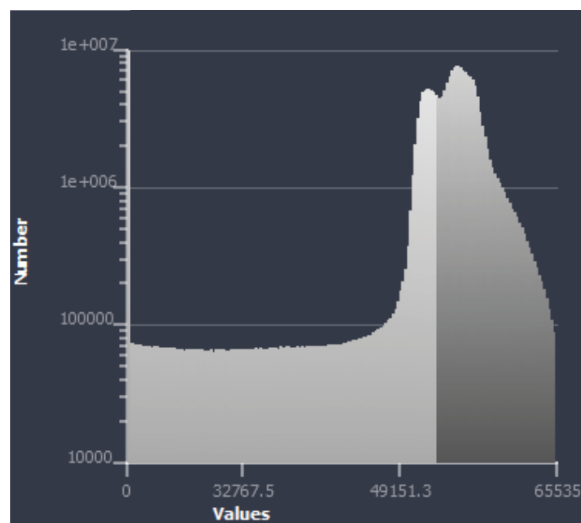
Figure 4.3. Histogram of grey density values showing a created differential through Median filter. This allow to separate between two thresholds the density values.
.

4.2.5. Sample preparation for geochemistry and age determination

13 right valves of *C. astartoides* were embedded in epoxy resin (Table 4.4). After 24h, each shell was cut along its maximum growth axis with a diamond wheel saw (Buehler Isomet). Silicon carbide grinding papers P800, P1200, P2400 and P4000 were used to expose the surfaces, followed

by diamond-grade polish of 9 μm, 3 μm, and 1 μm to generate the necessary smooth surface for analysis. After every polish, the shell was sonicated for ~3min to remove contaminant material.

4.2.6. Electron Probe Microanalysis (EPMA)

Polished specimens of *C. astartoides* were carbon coated by evaporative deposition on an Edwards Auto 306 coater. 11 specimens (six from the Amundsen and five from Weddell regions, Table 4.5) were chosen from the initial 16 that were scanned to represent the different geographic regions, sizes, and densities to assess for links between growth, environment, and density with chemical composition. Mg, Ca, and Sr concentrations were determined using a Cameca SX 100 microprobe in the School of Earth Science at the University of Bristol. Quantitative analyses were performed on the umbo as it records the ontogeny of the bivalve. Additionally, on specimens where the delineation between inner and outer layer was clear, cross sections of the outer and inner aragonitic layer were analysed. Measurements were performed with an accelerating voltage of 20 kV, a beam current of 10 nA, with a dwell time of 100ms resulting in a 12 μm beam diameter. The Ca standard Wollastonite ($CaSiO_3$), the Mg standard Olivine ((Mg^{2+}, $Fe2^+$)$2SiO_4$) and the Sr standard $SrTiO_3$ were used in the analysis as it was used by Jennions (2014, unpublished thesis). The analytical precision of the trace elements measurements was expressed as two times standard deviation (2sd).

As the temperature difference between Amundsen and Weddell regions is small (-0.18°C vs -0.89°C respectively) over the range from which the specimens were collected, we do not expect to be able to resolve temperature influences on trace elements. Growth can also influence trace element concentrations (Stecher et al. 1996, Takesue & van Geen 2004), and the impact was tested by correlation with long axis of growth (LAoG) measurements, and age.

4.2.7. Scanning Electron Microscope (SEM) and Light microscope

All the specimens were photograph in the SEM and light microscope for growth lines. To determine the age of specimens (Karney et al. 2011), images at a magnification between 80x-150x were taken with a Hitachi S-3500N variable pressure scanning electron microscope. The images were generated using a backscatter electron detector operating at a voltage of 20 KeV and a working distance of ca 14 mm. After analysis, the carbon coating was removed, and shells were polished with P4000 and diamond-grade pads of 9 μm, 3 μm, and 1 μm again. Images were taken with a stereomicroscope equipped with a Leica Camera. Between 6-20 images per specimen were

taken depending on the shell size. Individual image was stitched to determine bivalve age using the assumption that increments in the shell represent annual growth following Román-González et al. (2017). Clear annual growth increment determination was possible in six of the 13 specimens (Table 4.5) three from the Amundsen Sea and three from the Weddell Sea.

4.2.8. Statistical analysis

All statistical analyses were carried out using the R software package. All data were tested for normal distribution (Shapiro test). For normally distributed data, an ANOVA followed by a Tukey post-hoc test was used to interpret the geochemistry results. A T-test was used for Mg/Ca regions comparison. Simple correlations were made for all parameters. A Pearson test was used for normal distributed data and a Kendall test when the data was not normal distributed.

4.3. *Results*

Length, long axis of growth (LAoG), and width (p<0.05) of the bivalves *L. marionensis* (Figure 4.4) and *C. astartoides* (Figure 4.5) are highly correlated. The smallest and largest specimen of *L. marionensis* were found in in the eastern Weddell Sea (Table 4.6). Significant size differences between regions were only found between the small Magellan and larger South Sandwich Islands specimen (Kruskal-Wallis, p<0.05). Shell thickness is positively correlated with LAoG (Figure 4.6 left, Kendall, p<0.05).

Table 4.6. Morphometrics of *L. marionensis* and *C. astartoides* for individual regions. Maximum, minimum and mean for each morphological parameters Long Axis of Growth (LAoG, mm), length (mm) and width (mm) are reported.

Species	Region	LAoG (mm)			Length (mm)			Width (mm)		
		Min	Max	Mean	Min	Max	Mean	Min	Max	Mean
L. marionensis	Eastern Weddell	12.7	67.7	31.7	12.2	55.7	27.3	5.2	19.2	10.5
	S. Sandwich Islands	19.7	54.4	36.1	17.7	50.8	35.8	6	18.1	12.7
	Magellan	12.9	36.1	27.1	12.1	31.8	24.2	5.66	16.8	11.4
C. astartoides	Amundsen	3.05	15.3	9.07	2.85	13.5	8.32	2.07	8.51	5.22
	Eastern Weddell	2.98	21.84	12.4	1.99	18.2	10.5	1.58	13.8	6.66
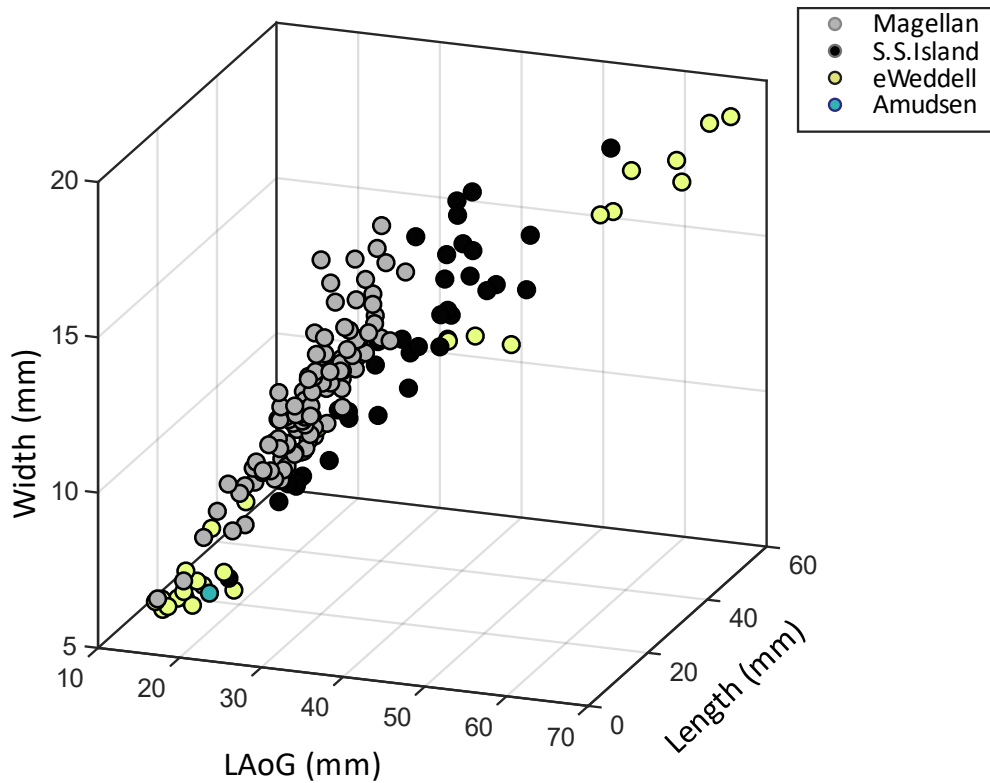
Figure 4.4. Length, long axis of growth (LAoG), and width in mm of 178 specimen of *L. marionensis*. Regions are colour coded with grey for Magellan, black for South Sandwich Islands (S.S. Islands), yellow for eastern Weddell Sea (eWeddell) and turquoise for Amundsen Sea.

Both the smallest and largest specimen of *C. astartoides* are from the eastern Weddell Sea. In general, Amundsen Sea specimens are smaller (LAoG) than the Weddell Sea ones (ANOVA, p<0.05). Shell thickness in this species is also positively correlated with LAoG (Figure 4.6 right, Pearson, p<0.01).
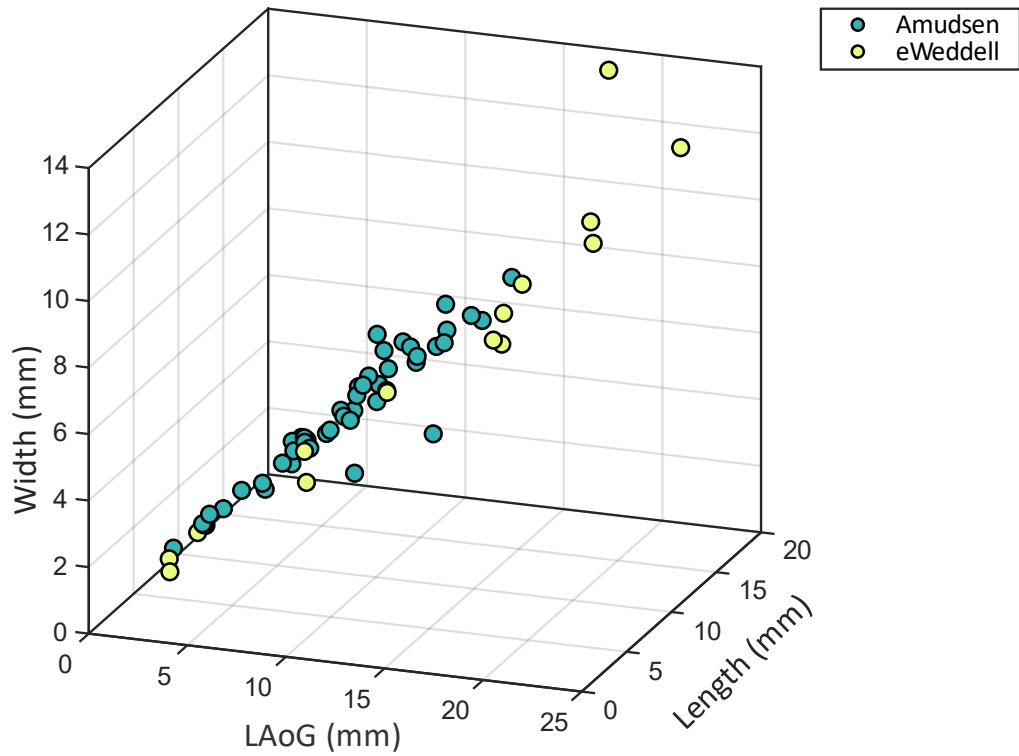
Figure 4.5. Relationships of length, long axis of growth (LAoG),, and width of 62 specimen of *C. astartoides*. Note the specimens are much smaller than *L. marionenisis* in Figure 4.3. Amundsen Sea (AS) specimen are turquoise and eastern Weddell Sea (eWeddell) specimens yellow.
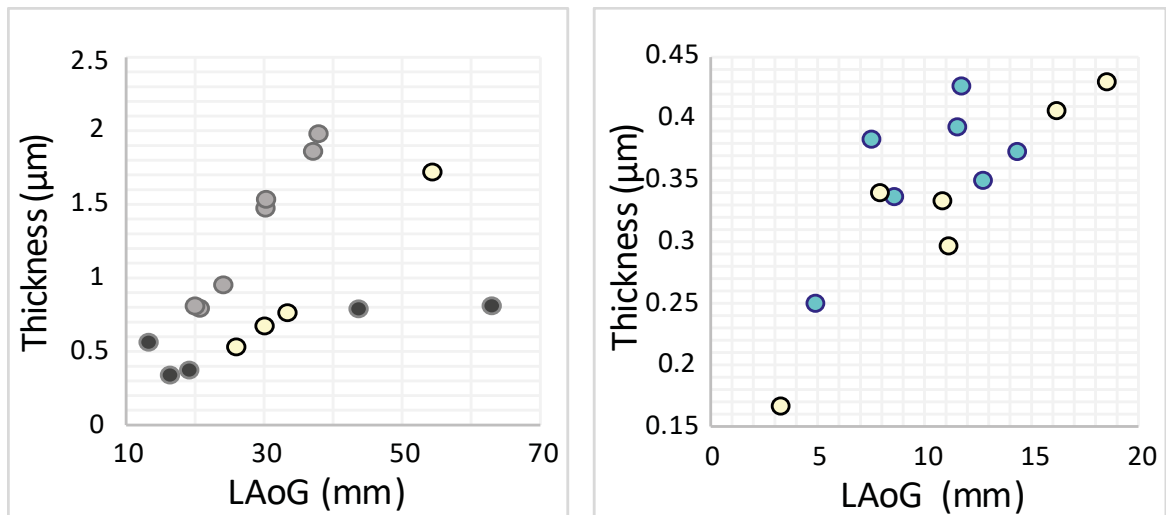
Figure 4.6. Correlation shell thickness of *L. marionensis* (left) and *C. astartoides* (right) with long axis of growth (LAoG) (mm) across regions: east Weddell Sea (WS) yellow, Amundsen Sea (AS) turquoise, Magellan grey and South Sandwich Islands black.

Density is highly variable within *L. marionensis* species and ranges from 2.5 g/cm^3 to 2.7 g/cm^3 (Figure 4.7). The Magellan region specimens which are from the same location have a similar density between 2.66 g/cm^3 and 2.7 g/cm^3 highlighting that the variability across the dataset is not within populations but externally driven. Only one specimen from the Amundsen Sea was analysed (Figure 4.7, turquoise dot).
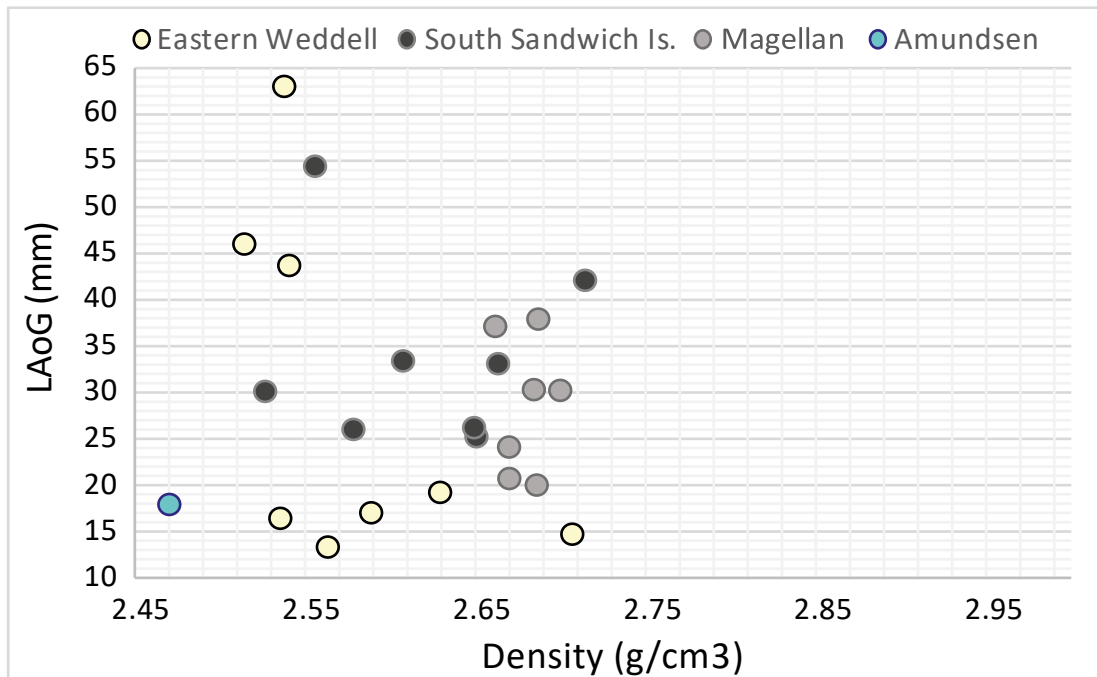
Figure 4.7. Density of *L. marionensis* specimens in g/cm^3 from four different regions vs. shell long axis of growth (LAoG). Eastern Weddell Sea (WS, yellow), South Sandwich Islands (black), Magellan Region (grey) and Amundsen Sea (AS, turquoise).

Density in *L. marionensis* does not correlate with LAoG, (Kendall's rank $p > 0.05$, Figure 4.7) nor thickness (Pearson, $p > 0.05$) (Figure 4.10 left). There is shell density is higher in specimens from the Magellan region compared with the other specimens (Kruskal-Wallis, $p > 0.05$, Figure 4.7). Shell density does not change with water depth over the range assessed (Table 4.4) (ANOVA, $p > 0.05$).
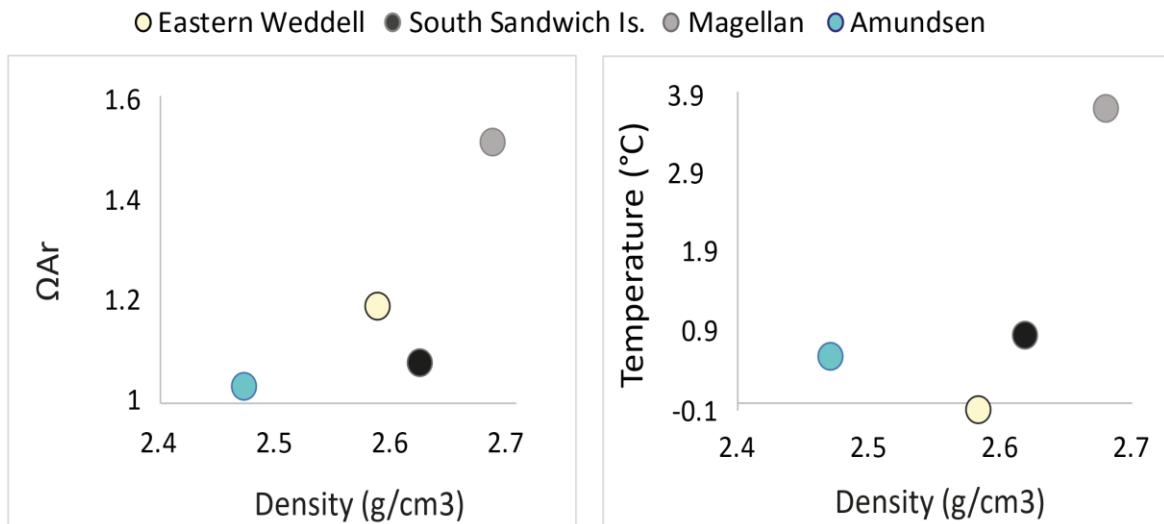
Figure 4.8. Density related with aragonite saturation (left) and temperature (right) for *L. marionensis.* The dots represent the mean value of the specimens density for each region (Amundsen is just one point). Eastern Weddell SD=0.063, South Sandwich Islands SD=0.062, Magellan region SD=0.013, (SD=Standard Deviation).

There is a trend of higher density at higher aragonite saturation in *L. marionensis* (figure 4.8 left) with specimens from South of the Polar Front having lower density than those from the Magellan Region (Kruskal-Wallis, $p<0.05$). As temperature and saturation are low in the Amundsen Sea and high in the Magellan regions, it is not possible to separate temperature from saturation.

In contrast in *C. astartoides* specimen shell density and LAoG are correlated in the Amundsen Sea and Weddell Sea (Figure 4.9, Pearson, $p<0.05$) with higher density in smaller individuals, and lower thickness in denser ones (Pearson, $p<0.05$, Figure 4.10 right). Similarly to *L. marionensis*, there is no impact of water depth on shell density for *C. astartoides* specimens in the Amundsen and Weddell seas (ANOVA, $p>0.05$).
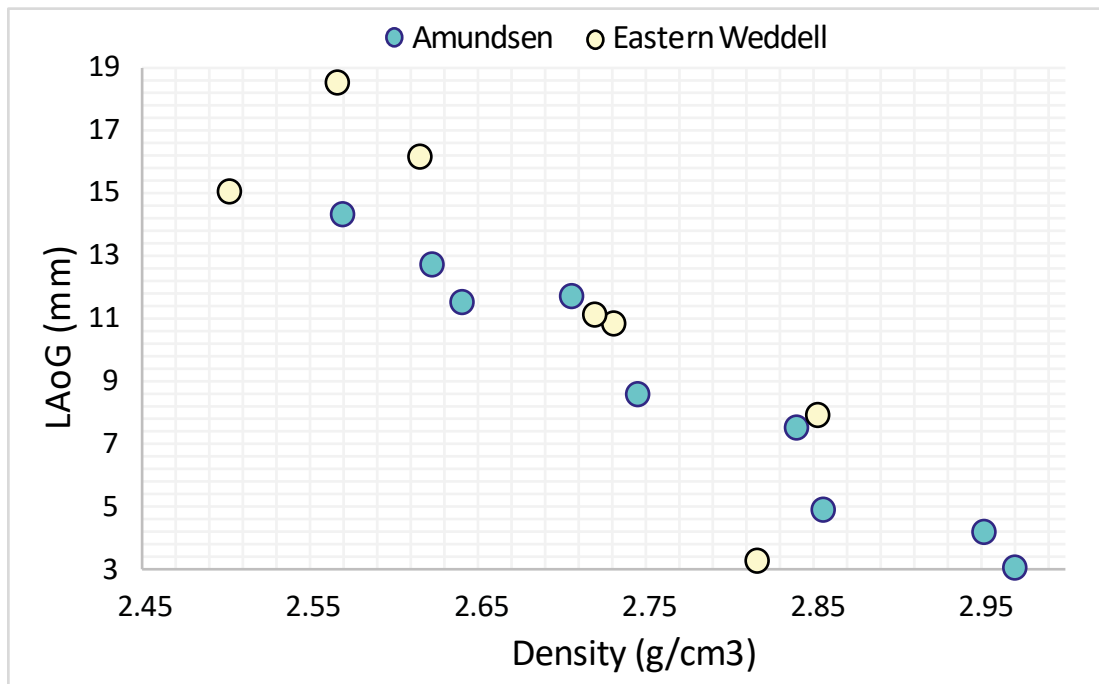
Figure 4.9. Correlation of density vs. long axis of growth (LAoG) of *C. astartoides* with specimen from the Weddell Sea (WS) in yellow and Amundsen Sea (AS) in turquoise.
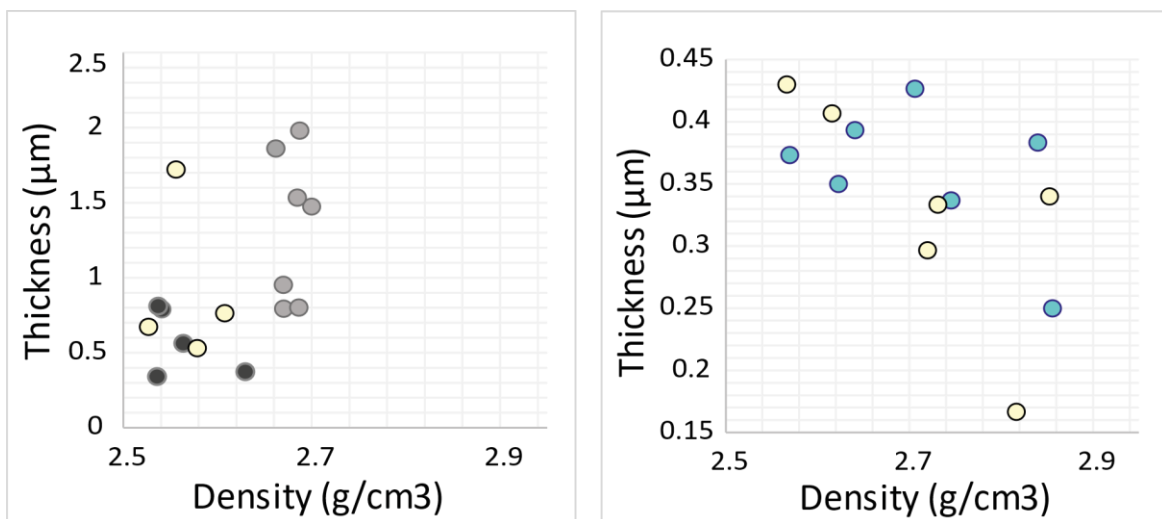
Figure 4.10. Correlation shell thickness of *L. marionensis* (left) and *C. astartoides* (right) with density (g/cm3) across regions: east Weddell Sea (WS) yellow, Amundsen Sea (AS) turquoise, Magellan grey and South Sandwich Islands black.

In general, low density parts of the shell were more prominent in the Weddell Sea specimens than the Amundsen Sea (Figure 4.11, Appendix C, Table C3). Dissolution markers appear to follow the growth line (Figure 4.11). Quantification of areas of high and low density shows that in the Weddell Sea, four out of seven specimens have low density in more than 50% of the volume (187.2

specimen 69%, 363 specimen 51%, 528 specimen 74% and 812 specimen 79%). Similarly, in the Amundsen Sea four out of seven specimens also have more than 50% of their volume within the low-density range (420.3 specimen, 57%, 731_1.2 specimen 50%, 1156_1.2 specimen 53%, 1152_1.1 specimen 65%). All individuals of *C. astartoides* showed dissolution resulting in holes in part of the shell (Figure 4.11). Little external damage was visible by eye or under a microscope, but internal dissolution was evident in the µ-CT analysis (Figure 4.12).
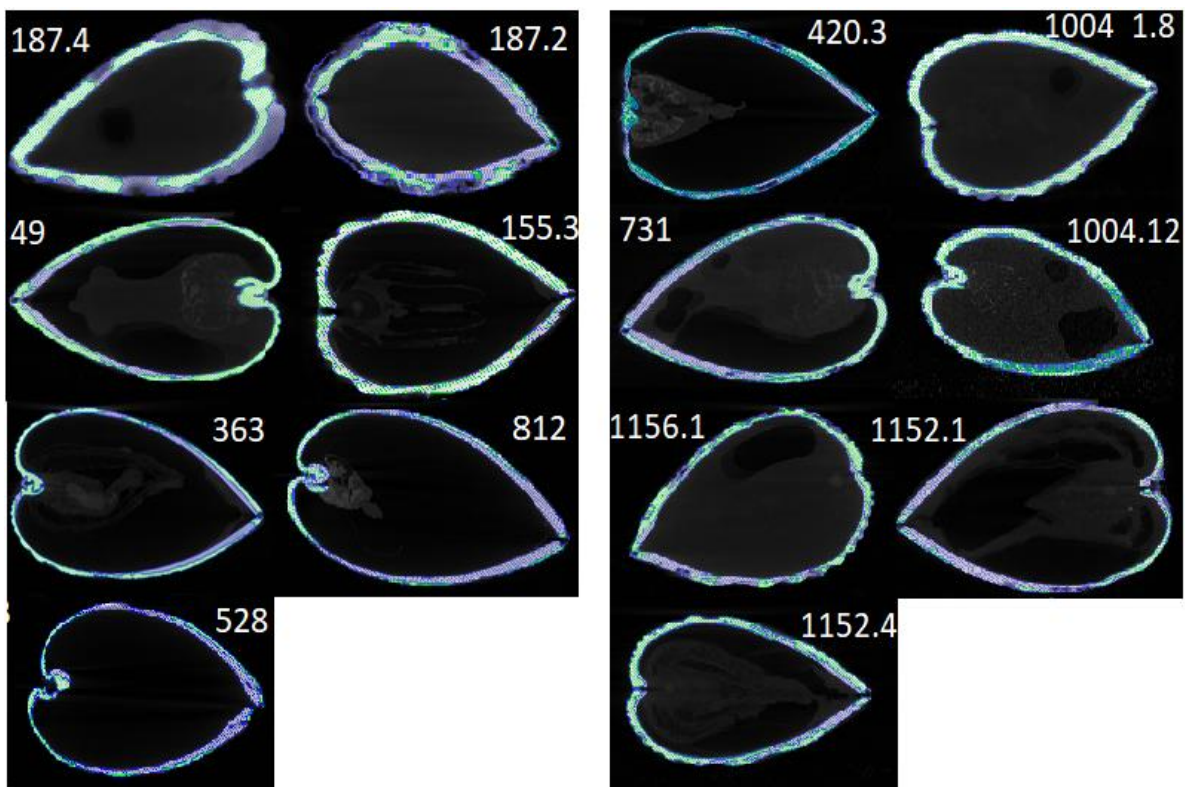
Figure 4.11. Characterisation of low- and high-density areas in *C. astartoides* individuals from the Weddell (left) and Amundsen (right) Sea. Blue colour denotes low density areas and turquoise high-density ones. All the shells are scaled to the same size for visualisation.

Figure 4.12. Selected slice to show examples of the dissolution ranking from density reduction in grey to holes in black. Shell shown is Amundsen Sea specimen 420.3.

.

For a preliminary analysis of the relationship between age and size in the different regions, one individual from each region from three different sizes was analysed. The banding pattern was faint (Figure 4.13) resulting in uncertainties, which increased in eroded shells such as Weddell Sea specimens 812. An inner crossed lamellar and the outer crossed lamellar layer (figure 4.12) can be separated. In general, smaller specimen displays fewer growth lines and hence size increases with age (Figure 4.14, Appendix C, Table C4).
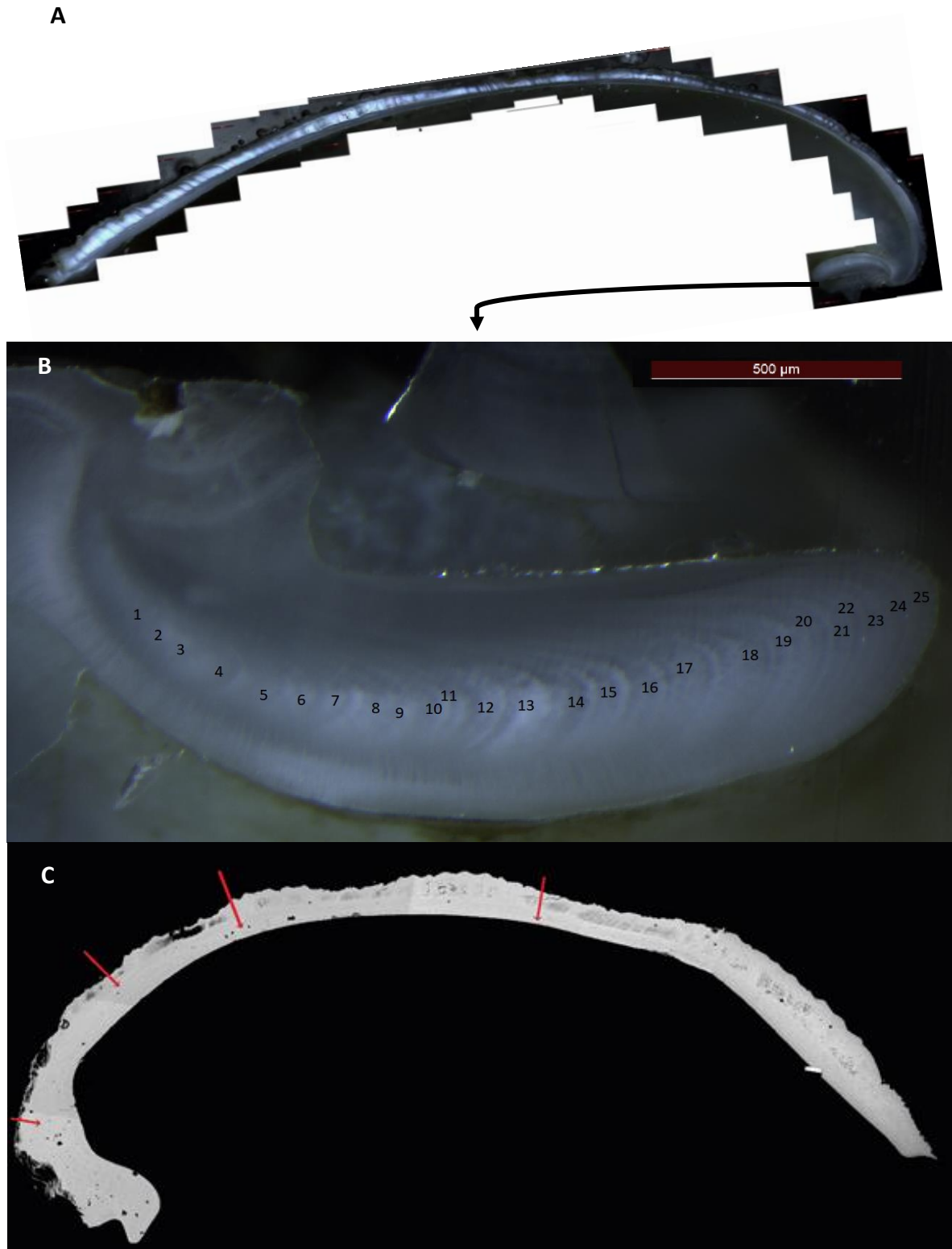
Figure 4.13. Age determination in *C. astartoides*. A. Internal annual growth bands in the shell section of the specimen 528. B. Internal annual growth bands from the umbo. Scale bar = 0.05cm. C. Layering of the shell into an outer and inner layer. Red arrows indicate the border between the layers in specimen 1004_1.12 with 7.51 mm of long axis of growth (LAoG).
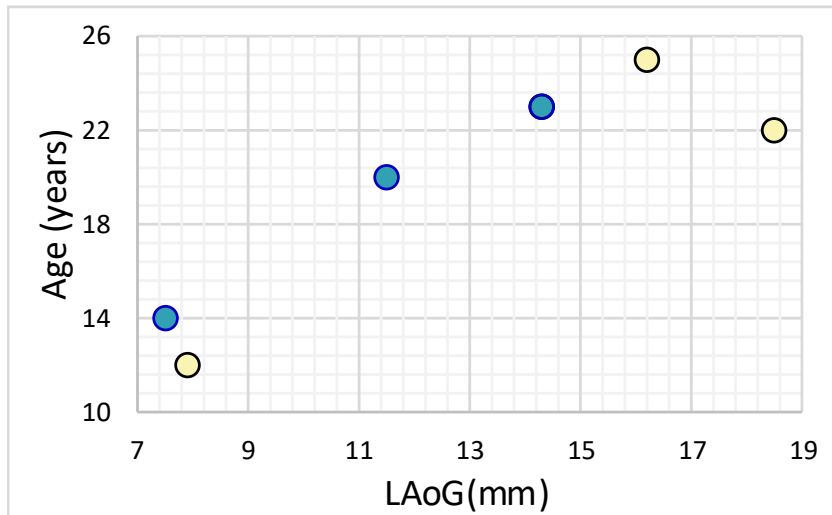
Figure 4.14. Relationship between estimated age and long axis of growth (LAoG), for three specimens from the Weddell (WS, yellow) and three specimens from the Amundsen (AS, turquoise) region.

The temperature between 200-600 m of the Amundsen Sea is on average -0.178°C and in the Weddell Sea -0.889°C. Mg/Ca ratios in the two regions are the no significant different (t-test, $p > 0.05$), except for the 187.2 specimen which has a lower density and strong dissolution (Kruskal-Wallis, $p < 0.005$) (Figure 4.15). In the Weddell Sea, Mg is not correlated with LAoG or density (Pearson test, $p > 0.05$). However, in the Amundsen Sea Mg/Ca ratio is decreasing with size and increasing with density though the results are not statistically significant (Pearson test, $p > 0.05$) and strongly influenced by sample 1152_1.1 (Figure 4.15, Appendix C, Table C3).
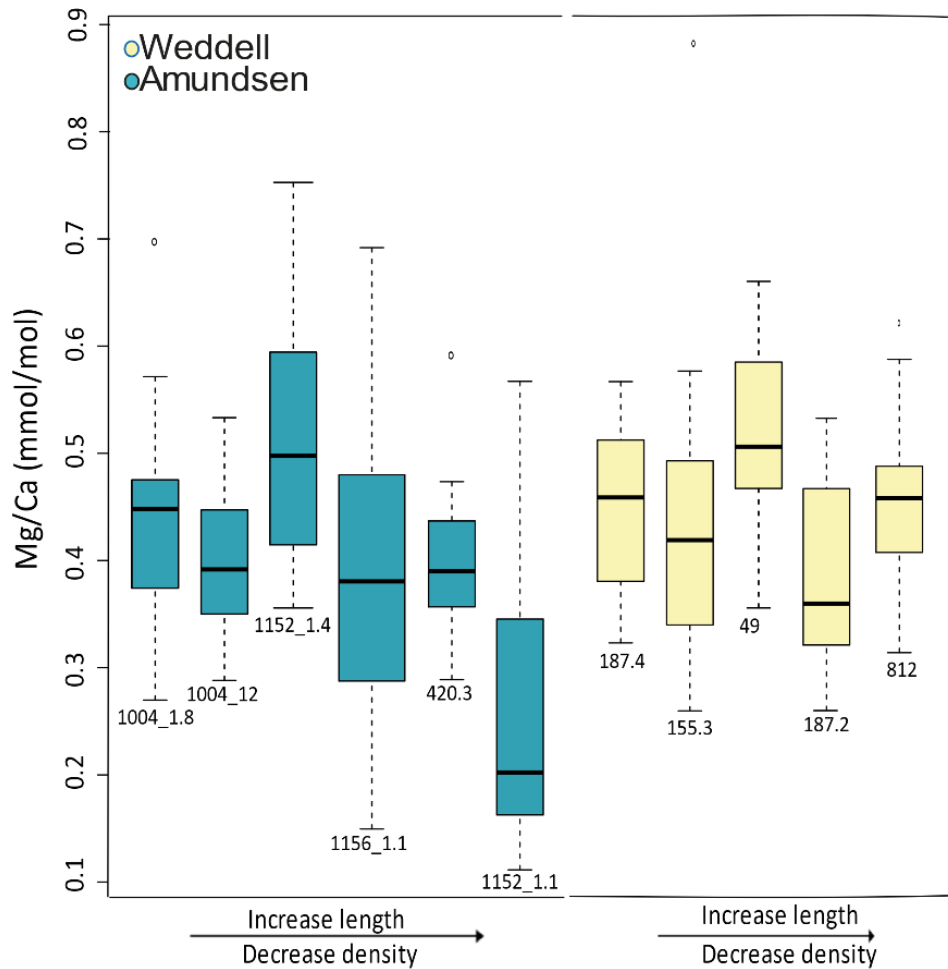
Figure 4.15. Mg/Ca ratio of *C. astartoides* from the Amundsen Sea (AS, turquoise) and Weddell Sea (WS, yellow). The specimens are ordered by increasing LAoG, while the density decreases from left to right. The black bar represents the median of all measurements and the size of the box the quartiles.

Sr/Ca ratios are not significantly different in the two regions, though the difference is approaching significance (t-test, p=0.051). No specific patterns was found for Sr/Ca concentration with LAoG or density for both regions (Figure 4.16, Pearson test p>0.05).
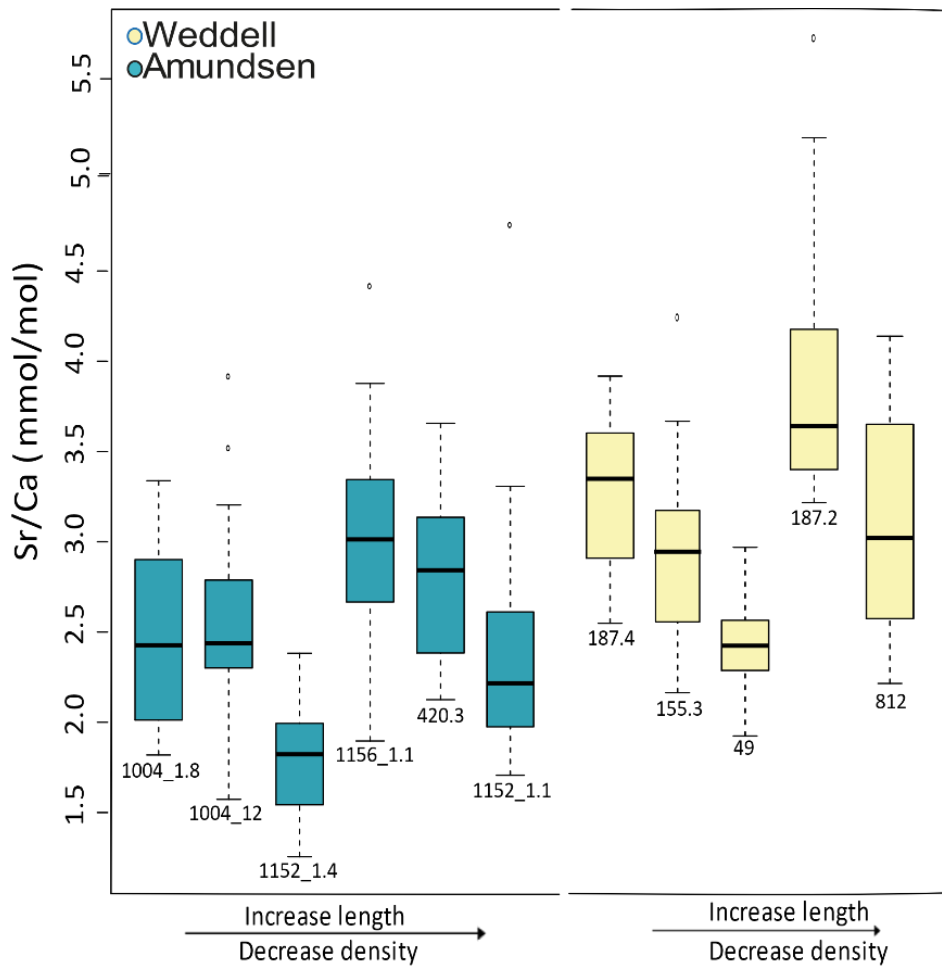
Figure 4.16. Sr/Ca ratio boxplots of *C. astartoides* from Amundsen and Weddell seas. Five Weddell Sea (yellow) specimens and six Amundsen Sea (turquoise) specimens are shown. The specimen LAoG increases, and the density decreases from left to right. The black bar represents the median of all measurements.

Mg/Ca and Sr/Ca ratios are not correlated with temperature nor with Ω_{Ar}, when all the specimens are considered (Figure 4.16, Person test p>0.05)). Sr/Ca concentrations for Weddell Sea appear to be close to correlations, but the number of specimens is too low for interpretation.
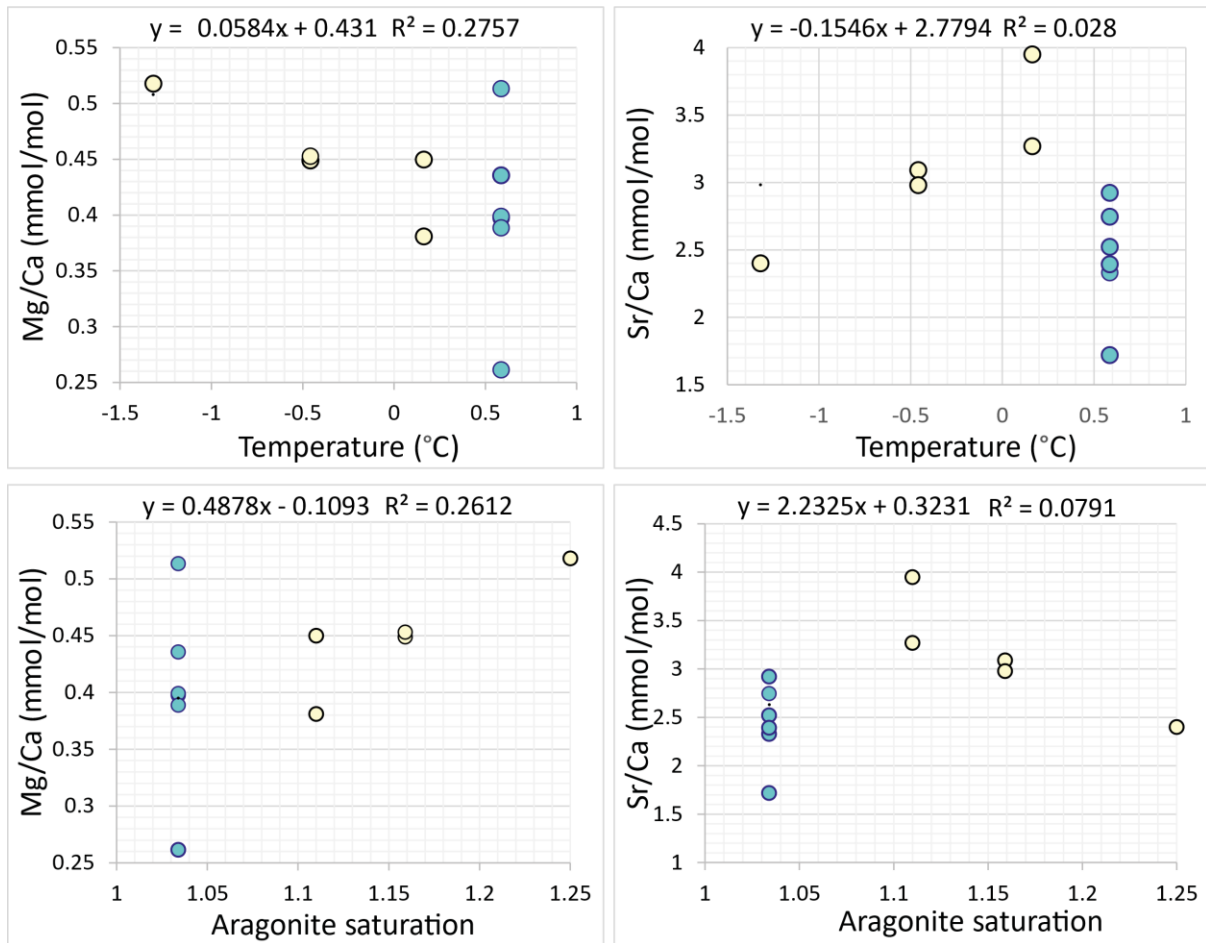
Figure 4.17. Correlation between temperature and aragonite saturation with Mg/Ca and Sr/Ca ratio in all analysed *C. astartoides* specimens. Turquoise dots represent Amundsen Sea (AS) and yellow for Weddell Sea (WS). For Weddell Sea specimens look close to correlation between Sr/Ca ratio and T/Ω_{Ar}.

The trace elements are not evenly distributed across the shell. The outer layer has a higher Mg/Ca and Sr/Ca ratios than the inner layer with an increase of 68% for Mg/Ca (0.85 vs 0.26 mmol/mol) and 44% for Sr/Ca (4.3 vs 2.4 mmol/mol) in the Amundsen Sea. The difference between the outer layer and the inner layer for Weddell Sea specimen is ~55.8% higher Mg/Ca (0.85 vs 0.35 mmol/mol) and 21.3%. higher Sr/Ca in the outer layer (3.5 vs 2.7 mmol/mol). Correlations between Mg/Ca and Sr/Ca ratio with temperature and aragonite saturation are not significant (Appendix C, Figure C3 $p<0.05$).

4.4. *Discussion*

This chapter focused on the impact of different environments on bivalve shells of two species from the Southern Ocean. Using the natural differences in temperature and saturation of samples from

the South Sandwich Islands, Amundsen Sea, Weddell Sea and the Magellan region, the shells were analysed for their size, density, geochemistry.

Age determination and size patterns

Analyses of growth lines were performed on the hinge section because this area contains a well-preserved growth record of the individual (Richardson et al. 1993). In contrast, the lower growth rate during the adult development makes it challenging to determine growth lines at the outer parts of the shell.

As expected, the data show that larger specimens are older supporting earlier work by Richardson et al. (1993). It was important to establish this overall link, as fluctuating environments have been suggested to increase growth rate and reduce lifespan (e.g. the *A. islandica* population from Iceland compared with the open Baltic Sea; Begum et al. 2010). Furthermore, after their fifth/seventh-year, growth in *Calista chione* has been shown to slow almost a half (Hall et al. 1974). As such I assessed changes in the growth age relationship. A similar growth reduction can be observed after the seven/eight years in *C. astartoides* (Figure 4.13).

Bivalve lifespans in the literature range between one year and 374 years. Shorter lifespans are associated with warm temperatures (Cardoso & Veloso 2003) while *Arctica islandica* is the longest-lived documented species thriving in cold waters (Schöne et al. 2005). Metabolic rates decreases with temperature (Peck 2000) and therefore the long lifespan of bivalve populations in high latitudes may be related to a low metabolic rate. Additionally, periods of fasting in response to seasonal food availability may cause a metabolic depression (Peck et al. 2005). There are few age determinations for Southern Ocean species. The brachiopod *Liothyrella uva* has a maximum age of 46-71 years (Peck et al. 1997) and the bivalve *Aequiyoldia eightsii* is between 19-41 years (Román-González et al. 2017). Both species are in a similar range as the 25-year lifespan of *C. astartoides.*

There are several factors that can influence the growth rate during the lifespan of these species, including salinity (Yan et al. 2014), and temperature (Purroy et al. 2018). Food availability has been shown to facilitate dealing with different, in parts challenging, environmental conditions including warming (Hoogenboom et al. 2012), and ocean acidification (Melzner et al. 2011). The South Sandwich Islands specimen of *L. marionensis* were larger than the Magellan region. Since

both regions have similar, high, primary productions (192 mg C m^{-2} d^{-1} Arrigo et al. 2008 vs 150-500 mg C m^{-2} d^{-1} (Longhurst 1995), it is possible that the Magellan specimens allocated their energy resources to build denser shells rather than to larger sizes.

Weddell Sea specimen of *C. astartoides* are larger than populations from the Amundsen Sea. Temperature cannot be the cause for this difference as the values are not more than ~2°C different (-1.32 to 0.585°C, Table 4.5). However, the Amundsen Sea, could be experiencing aragonite undersaturation events (Hauri et al. 2016) which may provide challenges to growth. Alternatively, Weddell Sea specimens derived from an upwelling area have one of the highest primary productivity in the SO and therefore might explain their ability to grow to a large size similar to *L. marionensis*.

Environmental influences on biomineralization

Our understanding of the calcification process in bivalves is still limited, as is our understanding of how the organisms alters the uptake of Mg and Sr in the extrapallial space (EPS, Wanamaker & Gillikin 2019). Consequently, unlike to planktic foraminifer and warm water corals, interpreting trace elements in bivalves is more challenging. The low trace element concentrations in bivalves compared to seawater show that they discriminate against the uptake of Sr and Mg (Elderfield, 2006a) indicating a strong biomineralization control. Sr/Ca ratio changes in bivalves have been linked to salinity, temperature, growth rate and age (Rucker & Valentine 1961, Freitas et al. 2005, Schöne et al. 2011). Species specific and geographically different responses have been documented. Swan (1956) proposed a negative relationship of Sr with growth rate for *Mytilus edulis*, *Mya arenaria* and *Modiolus modiolus* corroborated by Gillikin et al. (2005) in *Saxidomus giganteus*. However, no relationship was found for *Mercenaria mercenaria* (Stecher et al. 1996). Higher Sr/Ca ratios under warmer conditions were found for *M. merceraria* but the reverse was documented for *Spisula solidissima* (Stecher et al. 1996). In this sample set of *C. astartoides* no correlation was found with temperature, carbonate saturation or size (Figures 4.14, 4.15, and 4.16).

C. astartoides has higher Sr/Ca concentration than Mg/Ca which is typical for aragonite (Gillikin et al. 2005). There is no trend in Sr/Ca with growth. Since our sample set has only a small temperature difference, we would expect no environmentally driven Sr changes. While they are statistically not different, Sr/Ca in the Weddell Sea is higher while temperatures are lower.. The lack of correlation of Sr/Ca with carbonate saturation has been seen in the bivalve *Margaritifera*

margaritifera (Bailey & Lear 2006). Abiogenic aragonite and corals have a Sr partition coefficient of 1 (Dietzel 2004) while aragonitic bivalves have a much lower partition coefficient of 0.25, which means that it is far from the equilibrium (Gillikin et al. 2005) which is explained by kinetic and vital effects (Schöne et al. 2010).

Some studies suggest that Mg/Ca ratio in oysters is linked to age, growth rate (Durham et al. 2017) or temperature under high growth rate in juveniles in *A. islandica* (Mouchi et al. 2013). However, a controlled lab experiment with *Ruditapes philippinarum* found no relationship between salinity and temperature with Mg/Ca and Sr/Ca ratios *(*Poulain et al. 2015). Similarly, specimens of *C. astartoides* in this study do not show a significant difference over the very small gradient, though one sample is significantly lower than the others. This specimen shows strong signs of dissolution which is known to dissolve the higher Mg phase first.

Difference in Mg/Ca and Sr/Ca ratios in the outer and inner layers to the umbo could suggest biomineralization changing incorporation of these ions in the shell. Similar difference have been found in *A. islandica* between the outer and inner layer and hypothesized to be linked to changes in the amount of organics, crystallography, and changes in ion transport to the calcification site (Foster et al. 2009). Between 53-60%. higher Sr and Mg in the outer layer were also documented by Schöne et al. (2013) in *A. islandica*. The significantly higher value in the outer layer needs further investigation and speculatively might be related to changes in crystals structure in the cross lamellar wall with a high precipitation rate for the larger crystals. In the same way, Lebrato et al. (2020) have stated that there are not homogeneity in marine elemental ratios, and therefore should we be careful when different taxa or different ocean regions are compared.

Patterns of shell dissolution between species and regions
Specimens from north of the Polar Front in the Magellan region show a higher density than the ones from the east Weddell Sea. The Magellan region has high temperature and the highest saturation suggesting that the combined effect of result in high density in specimens of *L. marionensis.* Li et al. (2016) in the tubeworm *Hydroides elegans*, found that temperature can increase density and volume. As there is no relationship between density and long axis of growth (LAoG) in these species, density is not driven by population dynamics. In contrast, *C. astartoides* density is lowest in the largest specimen, suggesting that fast growth in this species might lead to lower densities thereby potentially impacting their structural integrity.

The hinge has the highest density in both species. The role of the hinge is resistance against shearing forces (Coen 1985) making it paramount that this part of the shell is hard and resistant. *C. astartoides* in this dataset have a higher shell density than *L. marionensis* specimens. Infaunal organisms, such as *C. astartoides*, live naturally in lower pH and carbonate saturation due to the decay of organic matter in the porewaters (view review on Widdicombe et al. 2011). Dissolution, shell lesions, and mortality has been observed in different infaunal species under low pH (*Mercenaria mercinaria* Turquoise et al. 2009, Talmage & Gobler 2009, *Ruditapes philippinarum* Rodriguez-Romero et al. 2014). Therefore, this result is unexpected. The shell in both species varies greatly, though, since *C. astartoides* are smaller and concave, whereas *L. marionensis* are bigger and flatter. Therefore, growing a much larger shell might impact density which might in turn impact structural integrity, something which would be tested in the future. *L. marionensis* also have hair that can stabilise the shell on the substratum, extend the range of tactile sensors, protect, and camouflage from predators, and minimize the settlements of epizoans (Bottjer & Carter 1980). This protection might facilitate that *L. marionensis* can build a less dense shell while preserving the function.

Undersaturated waters ($\Omega_{Ar}<1$) can lead to severe in-vivo dissolution such as pteropods resulting in mechanical weaken of the shells (Bednaršek et al. 2012a). *Nienhuis et al.* (2010) found that molluscs may be more susceptible to enhanced shell dissolution rather than decreased calcification under projected climate change. Bivalves though are able to cope with undersaturation, as some species in rocky foreshores experience a vast pH change during the tidal cycle (Campanati et al. 2018). Amundsen Sea waters are suggested to already experience undersaturation (Jones et al. 2017) and hence higher dissolution was postulated. However, no density differences were found in these life specimens of *C. astartoides* between Weddell and Amundsen region. Both regions have high productivity areas with the Amundsen Sea polynya (Arrigo et al. 2012) and the Weddell Sea upwelling which might provide energy in this species, to allocate to calcification.

It is important to remember that the specimens analysed here were alive at time of collections. Therefore, their outer shell had protection against dissolution. Bednaršek et al. (2014) reported less dissolution in pteropods compared to abiogenic aragonite, highlighting the protection by organic matter. An extreme example of such protection is the periostracum of *Bathymodiolus brevior* which allows the species to live in hydrothermal vents (Tunnicliffe et al. 2009). However, if

dissolution is resulting in holes or even pervasive corrosion its function would be compromised as in those species here which show dissolution in the periostracum and outer layer which is directly exposed to the water.

Dissolution is heterogeneously distributed in the shell. Dissolution appears to follow the growth line with more dissolution in the younger parts of the shell. Differences in biomineralization during development have previously been suggested based on geochemical differentiation (Wanamaker & Gillikin 2019, Mouchi et al. 2013). The inner shell layer is known to dissolve during anaerobic respiration to buffer the internal pH (Crenshaw 1980). While repair is not obvious in these specimens, the differential dissolution of younger parts compared to older could hint towards elemental composition which facilitates dissolution or an easier repair of the youngest part of the shell compared to the oldest ones. Li et al. (2016) demonstrated that the calcareous tubes with corrosion have reduced mechanical performance. Therefore, we anticipate that *C. astartoides* and *L. marionensis* with higher dissolution in the hinge have compromised shell integrity. In the future, measurement of material properties would allow to quantitatively test this in FEA models (see chapter 3).

4.5. *Conclusions*

Limopsis marionensis and *Cyclocardia astartoides* can grow to larger size in regions with a high primary productivity. *C. astartoides* Weddell Sea specimens analysed in this work are bigger than those collected in the Amundsen Sea. Temperature and carbonate saturation over the range in this study do not impact Mg/Ca and Sr/Ca ratios. Density is highest in the warmest region with high aragonite saturation. In the future, while the region will warm, saturation will drop suggesting that density and shell function might be compromised. Most of the shells show internal dissolution, yet as the specimens were collected alive, they can cope with the environmental stressors that they are currently encountering. To date, bivalves species cope with environmental change. However, as these changes increase, their capacity to buffer and counteract those pressures may decrease. Overall, a long-term monitoring for key species will help to quantity the possible detrimental results that appear.

Chapter 5 : CONCLUSIONS

The ocean has experienced severe environmental changes from the preindustrial era. A decrease in carbonate saturation, warming and ice loss has been seen in the Southern Ocean, changing the habitat of organisms, communities, and ecosystems.

This thesis investigates the response of scaphopods and bivalves to regional differences in environmental conditions. I combine laboratory techniques with modelling work to link the results to performance and function. The thesis gives insights to how species cope with potential future climate induced, increasing environmental stresses.

5.1. *Main conclusions and findings*

In chapter 2 and 4, I analysed plasticity in morphology, material properties and chemistry in shells of the scaphopod *Dentalium majorinum*, and the bivalves *Cyclocardia astartoides* and *Limopsis marionensis* in response to a range of natural environmental conditions in the Southern Ocean. I combined morphometrics, µ-CT scanning, SEM, and electron microbe analysis to evaluate phenotypic plasticity at intraspecific level, determine lifespan, and quantify density, dissolution, and trace elemental composition. In *L. marionensis*, age determination and trace element analysis could not be performed due to the Coronavirus outbreak. Hence, I will focus mainly on *D. majorinum* and *C. astartoides* for the comparisons between taxa.

Lifespans for SO species are often unknown and here a lifespan of over 23 years for the scaphopod *D. majorinum* and 25 years for the bivalve *C. astartoides* are determined. For the first time, a lifespan of a scaphopod has been determined. These lifespans of Antarctic shelled molluscs are long compared with species from tropical or even temperate regions, (e.g 9 year for the temperate cockle *Cerastoderma edule* vs 19-41 years for *Aequiyoldia eightsii*) and likely linked to low metabolism due to cold temperatures and lower predator pressures. The growth analysis showed that specimens of *D. majorinum* from the Amundsen Sea grew faster than those from the Weddell Sea.

D. majorinum specimens from the Amundsen Sea are smaller than the Weddell Sea specimens, possibly linked to the lower aragonite saturation and higher temperatures (0.585 in the Amundsen Sea vs -1.7 in this region. This regional difference is also observed for *C. astartoides* specimens, which are smaller in the Amundsen Sea compared tothe Weddell Sea. As only one (421 vial number) specimen of *L. marionensis* was available from the Amundsen Sea, a regional size comparison was hindered.

D. majorinum has a curved, tube-shape shell with multiple longitudinal ribs along the shell. Based on the scaphopod *D. majorinum* morphological data, I investigated the impact of size, shape, and ornamentation on shell protection against stress and strain using biomechanically modelling, specifically Finite element analysis. Large specimens with higher curvature will break more easily in response to hydrostatic pressure. Specimens with a higher number of ribs perform better when they are exposed to a shear load, suggesting that ribs strengthen the shell. Shear forces are generally higher and pressure forces showing that species are not hindered by shelf function to exploit deeper waters.

I found that neither temperature nor aragonite saturation impact Sr/Ca and Mg/Ca concentrations in *D. majorinum* or C. *astartoides* shells, which can be related to either strong biomineralization control or small environmental differences or a combination of both. *D. majorinum* specimens have higher Mg/Ca concentrations in the Amundsen Sea than in the Weddell Sea. Water temperatures between the two regions differ by only ~2°C and therefore no elemental differences should be small or none. *C. astartoides* in the Weddell Sea show an increase in Sr/Ca concentration with temperature, though the small number of specimen studied make this a tentative result.

The shell density of *D. majorinum* and *C. astartoides* does not change in response to water depth or regional differences in environmental variables of the regional waters within the Southern Ocean. However, a difference in shell density and size is seen between Magellan region specimens and eastern Weddell Sea specimens of *L. marionensis.* The latter showing increasing density, since is a region with higher aragonite saturation. At the same time the Magellan region specimens have a smaller size which can be related with a referential allocation of energy to build denser shells.

Though live-collected specimens were analysed, shell dissolution is observed in *D. majorinum* and *C. astartoides* specimens, predominantly within the shell structure, and less frequently impacting

the periostracum and outermost carbonate layer. I interpreted this as dissolution to buffer the pH in the calcifying fluid. In a few specimens dissolution reaching the outside of the shell could be a possible threat and if becoming more frequent impact the survival of shelled animals in response to warming. As specimens were collected alive the documented degree of internal dissolution does not impact the function outside the envelope the species can deal with. The future will show how scaphopods and bivalves will cope with increasing warming and undersaturation.

While the work only investigates one scaphopod species, it might be an example how similar species can respond to the environment. The next step should be to assess how these species will adapt in the future and if they can survive climate change.

5.2. *Future directions*

Having laid the foundations, future species of combating climate change impacts are discussed below.

5.2.1. Ecology of scaphopods and bivalves

The ecology of scaphopods and of many Southern Ocean bivalves is still poorly understood due to the challenges to monitor them closely in their natural habitats. A better understanding of their life history traits will generate a holistic understanding of the pressures that they are encounter. Data about their reproduction, diet, predator-prey interactions combined with local environmental monitoring of carbonate chemistry could give us a more comprehensive perspective of future diversity for shelled invertebrates in Southern Ocean benthic habitats.

5.2.2. Long term monitoring

This study approached regional environmental differences to substitute for temporal changes. The results suggested that phenotypic plasticity can play an important role in organismal survival. However, phenotypic plasticity can negatively impact the fitness of a population and hence long-term ability to deal with environmental change. Long term studies and long-term monitor is needed for key species.

5.2.3. Biomechanical modelling

This study used biomechanical models of scaphopods to assess function of the shells and shed lights on potential future changes in its function. Future model advances should consider the elastic properties of the sand/sediment of the habitat and the stress/strain interaction between the sediment and scaphopods. Ideally the same modelling approaches should also be used for the bivalves to investigate the role of their morphological plasticity on shell function. Ideally such a model would also consider the internal dissolution, a change in shell thickness due to ocean acidification and measure material properties in specimens and species.

5.2.4. Geochemistry

Since intraspecific variability in geochemistry is high in several species, any further interpretation of responses to relatively small environmental differences need to be based on a higher number of specimens ideally linked to in-situ environmental measurements.

The presented study, together with the given future directions and implications, give insights on how scaphopods and bivalves cope in response to their environment. This work is expected to provide the foundations of predicting biotic response to environmental change on shelled benthos in polar regions.

APPENDIX A

Table A1. Collection records of *D. majorinum* specimens and their allocated vial numbers. The specimens were collected on expeditions from the Amundsen Sea (1 cruise –JR179: 22 stations). Weddell Sea (5 cruises; 37 stations). Expeditions order by date, listing most recent one first.

Vial No.	No. of sp. p/sample vial	Expedition	Station	Date	Gear	Water depth (m)	Latitude	Longitude
131	6	JR275	21	19/02/2012	AGT	648	-77.3548	-35.3513
289	1	JR275	29	20/02/2012	AGT	575	-76.1990	-31.8601
447	1	JR275	35	21/02/2012	AGT	607	-76.0160	-26.960
561	4	JR275	42	22/02/2012	AGT	429	-75.7611	-30.4372
614	3	JR275	43	22/02/2012	AGT	428	-75.7645	-30.4529
684	3	JR275	47	22/02/2012	AGT	579	-75.7406	-31.2380
719	4	JR275	48	22/02/2012	AGT	585	-75.7450	-31.2506
736	4	JR275	49	22/02/2012	AGT	583	-75.7496	-31.2636
777	2	JR275	52	22/02/2012	AGT	419	-75.2434	-30.2453
1066	2	JR275	75	23/02/2012	AGT	2052	-74.3699	-28.1079
1179	1	JR275	81	26/02/2012	AGT	1558	-74.5083	-28.7452
1220	1	JR275	82	28/02/2012	AGT	1580	-74.4962	-28.7372
1362	6	JR275	92	28/02/2012	AGT	427	-74.7013	-29.5009
1385	9	JR275	93	29/02/2012	AGT	440	-74.6981	-29.4965
1487	10	JR275	101	29/02/2012	AGT	392	-75.2427	-29.0035
1549	2	JR275	103	04/03/2012	AGT	390	-75.2495	-29.0270
1578	1	JR275	106	04/03/2012	AGT	414	-75.2389	-27.8485
114	37	ANT-XXVII/3	PS77/217-5	19/02/2011	AGT	408	-61.1561	-43.9961
199	5	ANTXXVII-3	PS77/228-4	27/02/2011	AGT	316	-65.9372	-60.5755
245	5	ANTXXVII-3	PS77/248-3	07/03/2011	AGT	433	-65.9291	-60.3425
259	6	ANTXXVII-3	PS77/252-7	10/03/2011	AGT	327	-64.7063	-60.5255
282	2	ANTXXVII-3	PS77/265-2	22/03/2011	AGT	-	-70.8005	-10.6725
233	3	ANTXXVII-3	PS77/293-3	31/03/2011	MG	298	-70.9491	-10.5419
190	1	JR179	BIO3-AGT-1B	04/03/2008	AGT	579	-71.8011	-106.294

191	8	JR179	BIO3-AGT-1B	04/03/2008	AGT	579	-71.8011	-106.294
155	1	JR179	BIO3-AGT-1A	04/03/2008	AGT	577	-71.8103	-106.329
146	15	JR179	BIO3-AGT-1A	04/03/2008	AGT	577	-71.8103	-106.329
366	1	JR179	BIO4-AGT-1A	04/03/2008	AGT	1404	-74.3592	-104.730
321	1	JR179	BIO4-AGT-2C	05/03/2008	AGT	1026	-74.4774	-104.257
322	26	JR179	BIO4-AGT-2C	05/03/2008	AGT	1026	-74.4774	-104.257
247	1	JR179	BIO4-AGT-2A	05/03/2008	AGT	1203	-74.4789	-104.236
248	8	JR179	BIO4-AGT-2A	05/03/2008	AGT	1203	-74.4789	-104.236
279	1	JR179	BIO4-AGT-2B	05/03/2008	AGT	1037	-74.4800	-104.255
278	8	JR179	BIO4-AGT-2B	05/03/2008	AGT	1037	-74.4800	-104.255
383	12	JR179	BIO4-AGT-1B	06/03/2008	AGT	1404	-74.3579	-104.730
423	1	JR179	BIO4-AGT-3A	06/03/2008	AGT	502	-74.4098	-104.654
539	3	JR179	BIO4-AGT-3B	07/03/2008	AGT	488	-74.3988	-104.629
1146	6	JR179	BIO4-AGT-3C	07/03/2008	AGT	499	-74.4045	-104.611
1151	11	JR179	BIO4-AGT-3B	07/03/2008	AGT	488	-74.3988	-104.629
585	1	JR179	BIO5-AGT-1B	08/03/2008	AGT	1495	-74.1187	-105.823
582	4	JR179	BIO5-AGT-1A	08/03/2008	AGT	1505	-74.1266	-105.777
617	1	JR179	BIO5-AGT-2C	09/03/2008	AGT	1070	-73.8656	-106.298
681	2	JR179	BIO5-AGT-3A	10/03/2008	AGT	553	-73.9748	-107.422
693	15	JR179	BIO5-AGT-3C	10/03/2008	AGT	539	-73.9863	-107.390
753	27	JR179	BIO5-AGT-3D	10/03/2008	AGT	536	-73.9804	-107.408
888	1	JR179	BIO6-AGT-2A	12/03/2008	AGT	1006	-71.1751	-109.863
819	5	JR179	BIO6-AGT-3A	11/03/2008	AGT	481	-71.3481	-109.998

1055	13	JR179	BIO6-AGT-3A	11/03/2008	AGT	481	-71.3481	-109.998
1015	87	JR179	BIO6-AGT-3B	11/03/2008	AGT	480	-71.3415	-109.998
1096	33	JR179	BIO6-AGT-3C	11/03/2008	AGT	476	-71.3486	-110.006
1116	10	JR179	BIO6-AGT-2C	12/03/2008	AGT	975	-71.1821	-109.926
919	15	JR179	BIO6-AGT-2B	12/03/2008	AGT	989	-71.179	-109.894
468	1	ANT-XXI/2	PS65/232	01/12/2003	EBS	899	-71.3169	-16.9366
330	1	ANT-XXI/2	PS65/161	15/12/2003	AGT	280	-70.9452	-10.5297
588	1	ANT-XXI/2	PS65/276	28/12/2003	AGT	277	-71.1122	-11.4711
246	2	ANT-XXI/2	PS65/131	12/12/2003	ISP	450	-70.8241	-10.7527
617	1	ANT-XXI/2	PS65/161	15/12/2003	AGT	280	-70.9452	-10.5297
563	1	ANT-XXI/2	PS65/274	28/12/2003	GSN	291	-70.8711	-10.7358

Table A2. Dissolution characterization for each segmented specimen, specifying their region and vial number.

Region	Specimen vial No.	Description	Level of dissolution
Weddell	114.4	Reconstructed. Holes in ribs and corrosion inside the shell.	3
	114.9	95% Reconstructed. Holes in ribs and corrosion inside the shell. loss of ribs and outer shell.	4
	114.21	Reconstructed. Holes in ribs	2
	114.22	Reconstructed. Holes in ribs and corrosion inside the shell.	3
	114.23	Reconstructed. Holes in ribs	2
	114.27	Reconstructed. Holes in ribs and corrosion inside the shell.	3
	114.29	Reconstructed. Holes in ribs and corrosion inside the shell	3
	1179	Reconstructed. Holes in ribs and corrosion inside the shell	3
	155.1	Reconstructed. It is missing the outer layer in some areas. Holes in ribs and corrosion inside the shell.	4
	259.4	Reconstructed. Holes in ribs and corrosion inside the shell.	3
	131.3	Reconstructed. Holes in ribs and corrosion inside the shell. loss of ribs and loss of outer shell	4
	736.2	Reconstructed. Holes in ribs and corrosion inside the shell	3
	684.2	Reconstructed. Holes in ribs	2
	1487.1	Reconstructed. Holes in ribs and corrosion inside the shell.	3
	1487.3	Reconstructed. Holes in ribs and corrosion inside the shell. loss of ribs.	4
	1220	No reconstructed. It is missing the 25% of the shell	5
	278.2	Reconstructed. Holes in ribs and corrosion inside the shell. loss of ribs and loss of outer shell.	4
	1151.4	Reconstructed. Few and small holes in ribs.	2
	1116.2	Reconstructed. Holes in ribs and small corrosion inside the shell	3
	1116.3	Reconstructed. Holes in ribs and loss of ribs.	4

	190	Reconstructed. Holes in ribs and corrosion inside the shell. loss of the outer shell in some parts.	4
	383.8	85% Reconstructed. Holes in ribs and corrosion inside the shell. loss of ribs and loss of outer shell	4
Amundsen	582.1	85% Reconstructed. Holes in ribs and corrosion inside the shell. loss of ribs and loss of outer shell.	5
	146.5	Reconstructed. Holes in ribs and corrosion inside the shell. loss of ribs	4
	1096.16	Reconstructed. Holes in ribs	2
	322.24	Reconstructed. Holes in ribs	2
	322.25	Reconstructed. Holes in ribs and corrosion inside the shell. Loss of ribs and loss of outer shell.	4
	693.7	Reconstructed. Holes in ribs and corrosion inside the shell	3
	919.1	No visual holes or damage.	1
	919.11	Reconstructed. Holes in ribs and corrosion inside the shell.	3
	1015.9	Reconstructed. Holes in ribs	2
	1015.3	Reconstructed. Few and small holes in ribs	2
	1015.64	No visual holes or damage.	1
	1015.71	85% Reconstructed. Holes in ribs and in shell close to outer. loss of ribs and loss of outer shell.	5
	1146.3	Reconstructed. Holes in ribs	2
	1055.6	Reconstructed. Holes in ribs and corrosion inside the shell	3

Figure A1. Process of segmentation and reconstruction. Left, scanned specimen. Centre, segmented specimen. Right, reconstructed specimen with holes and dissolve parts cover.
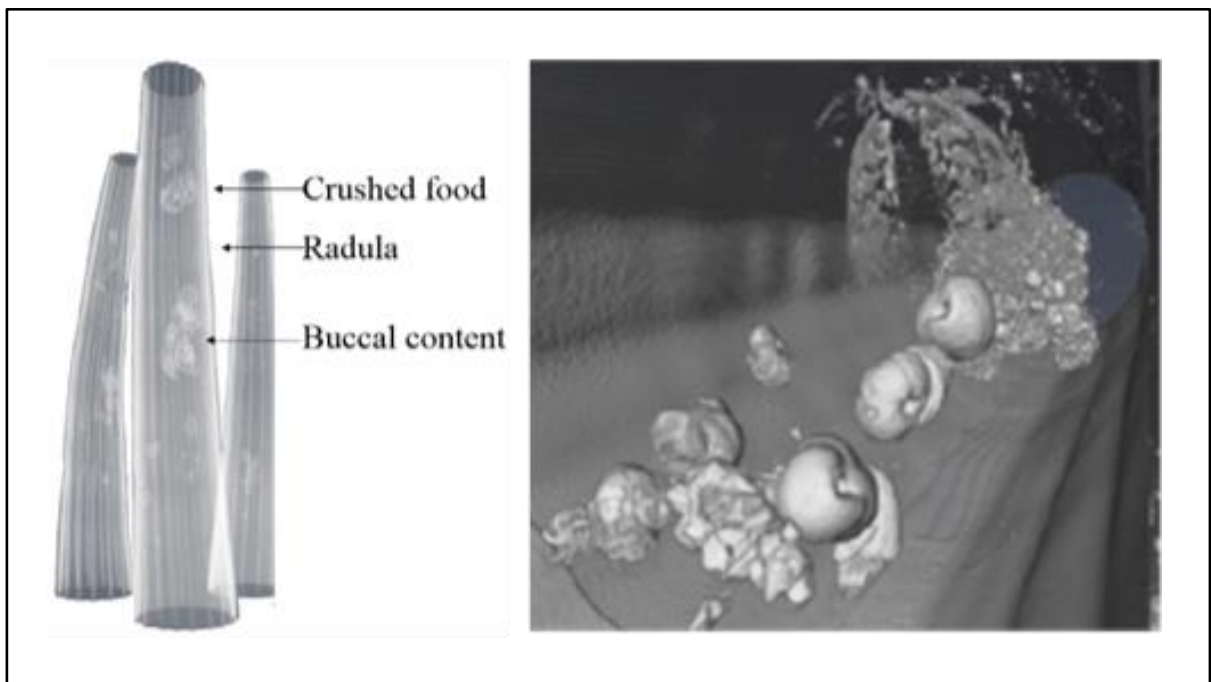
Figure A2. Food items inside of the scaphopod. Left side show the food item in the scaphopod. It is possible to see food item before and after the radula. Right side show in detailed the food item before the radula (almost complete) and after the radula (as crushed food).
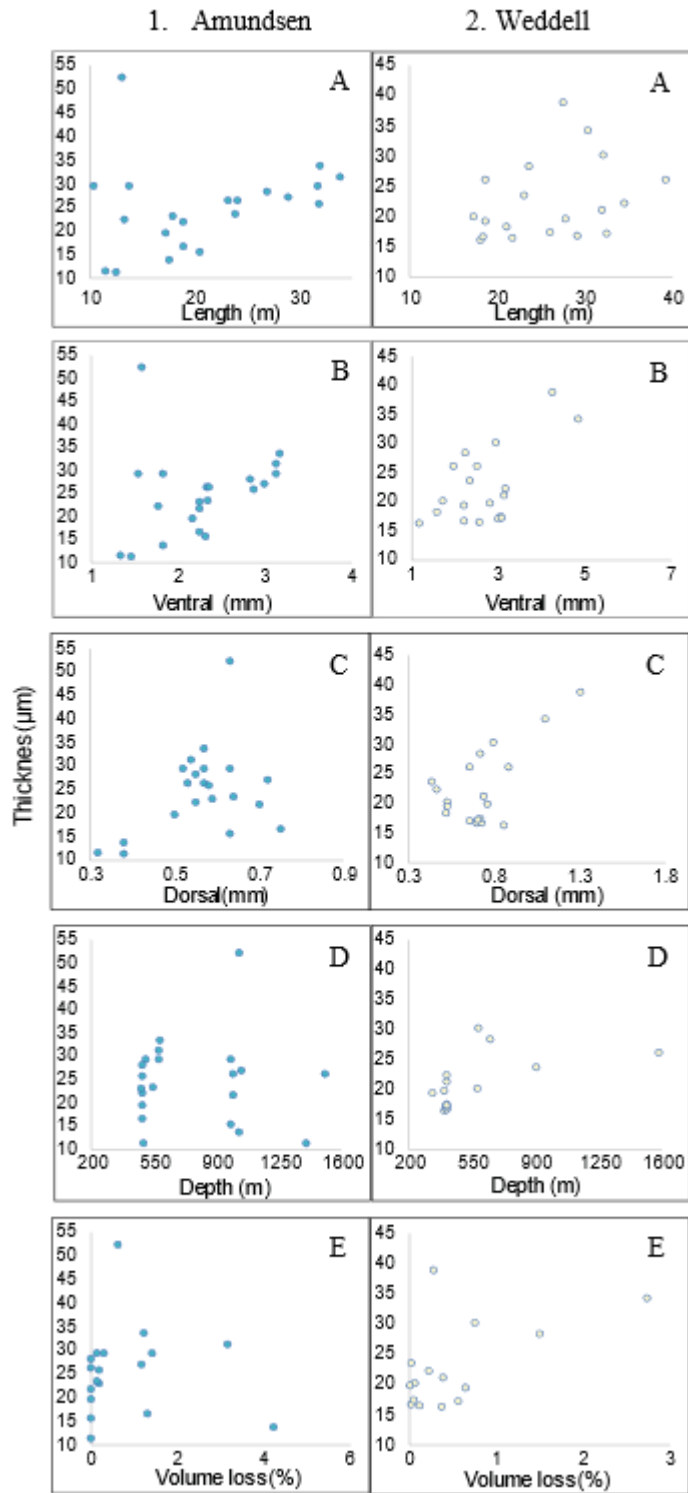
Figure A3. Correlations between shell thickness against morphometric and environmental parameters in 1) the Amundsen Sea and 2) the Weddell Sea. Tested parameters are A) length, B) ventral diameter, C) dorsal diameter, D) water depth, and E) volume loss.
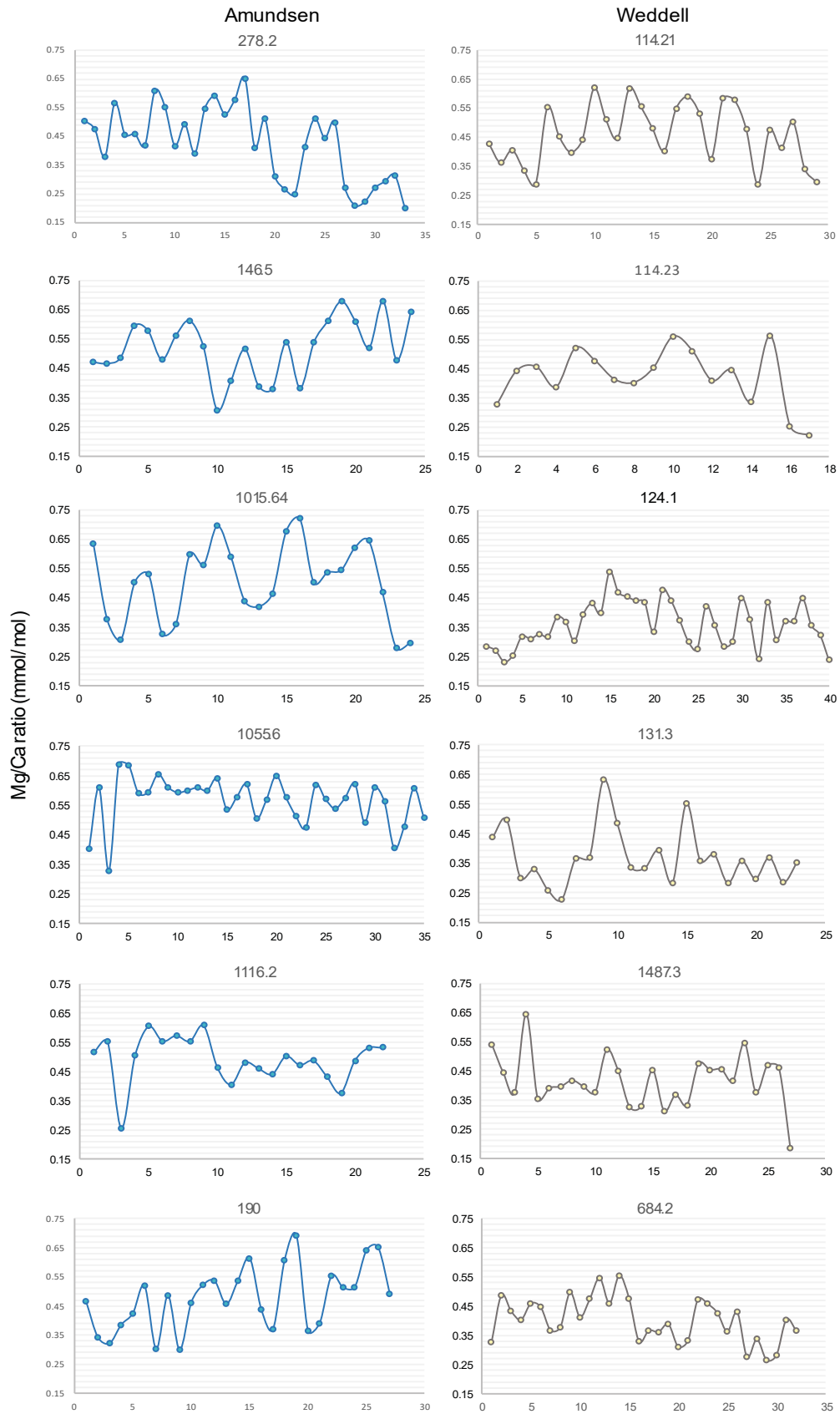
Figure A4. Mg/Ca ratio for Amundsen Sea (AS, turquoise) and Weddell Sea (WS, yellow) specimens taken longitudinally.
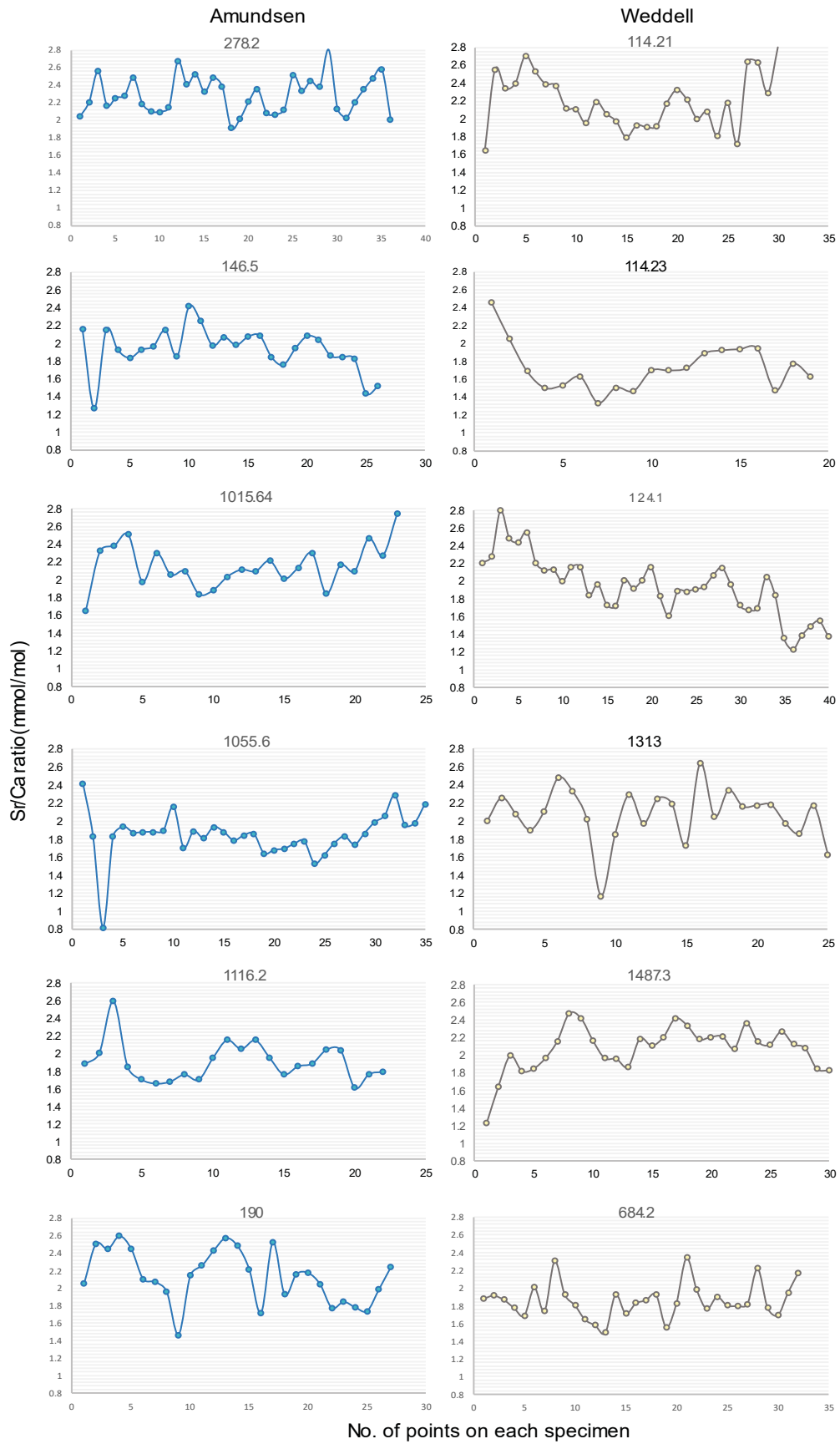
Figure A5. Sr/Ca ratio for Amundsen Sea (AS, turquoise) and Weddell Sea (WS, yellow) specimens taken longitudinally.

APPENDIX B

Protocol B1. Protocol modelling B1.

This protocol shows how to build the models from a 3D software until it can be analysed on Abaqus software. It includes a first part on how to create the 3D model in Blender and mesh it on Geomagic. Further, it explains how to assign material properties on Hypermesh and Abaqus. Additionally it describes the steps to analyse the model in the latter, adapting this part from a previous protocol made by Jen Bright (Hypermesh) and N.M. Gonzalez-Garcia (Abaqus).

1. Build the model in Blender

    a. Choose cylinder. In the bottom left part assign the dimensions.
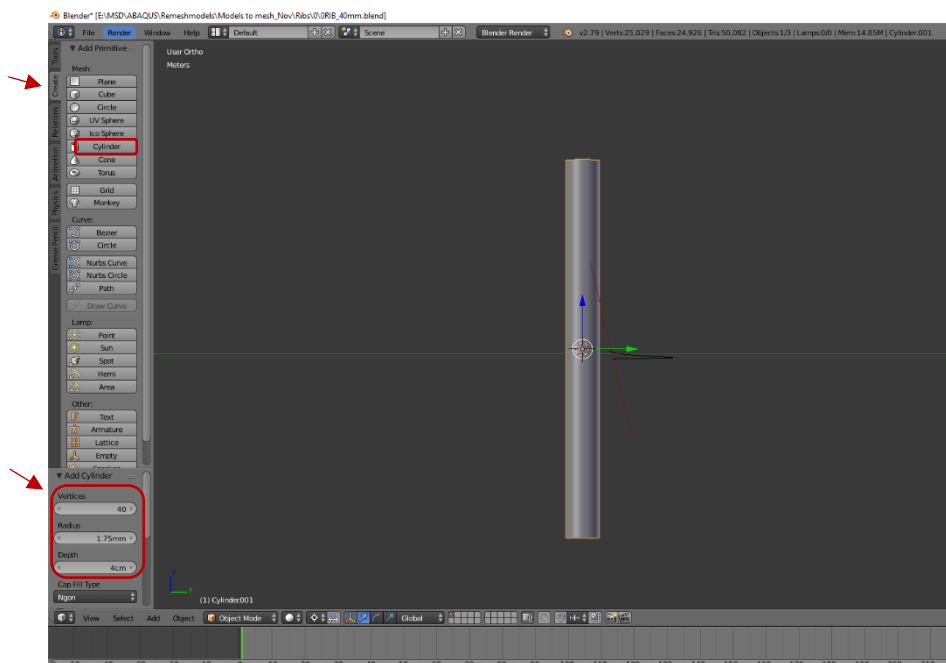
b. Go to dimensions icon and choose the millimetres.
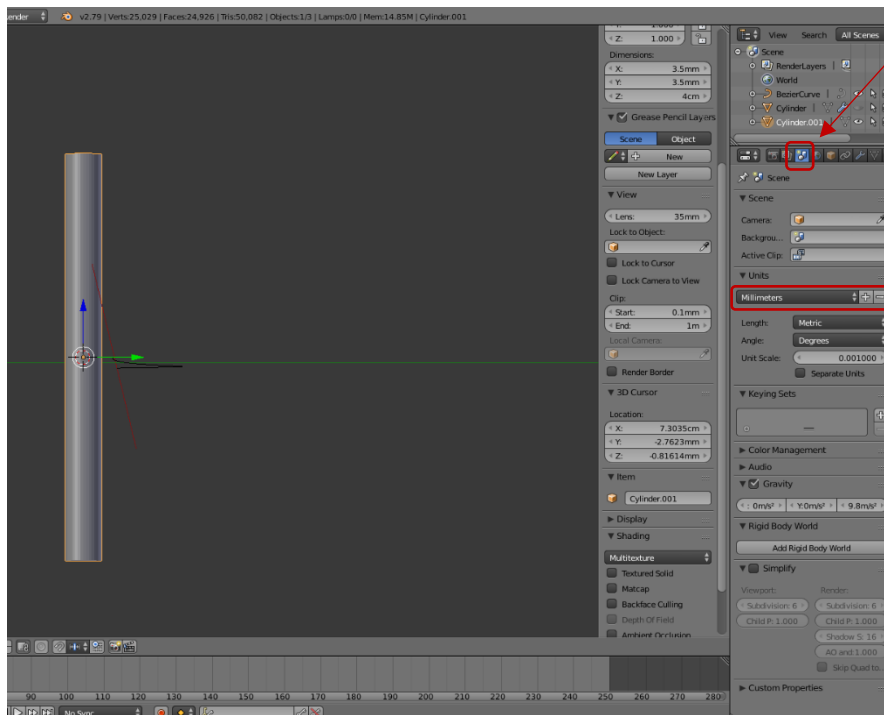
c. Change the object to "edit mode". Tick the area box. Click the top of the cylinder and tick the "S" key for scale. Move the cursor in the way that the top diameter decrease until the desire measurement (in this case 0.342mm^2). Right click on the face and select delete > only faces. Do this for the bottom and top faces.
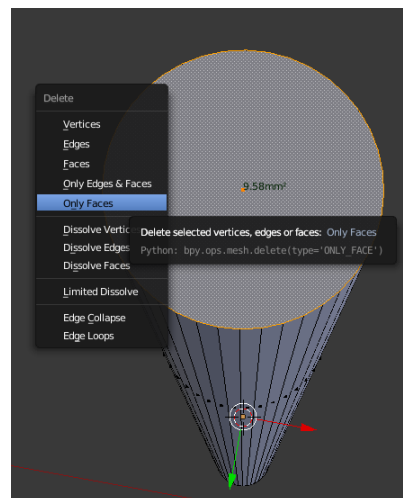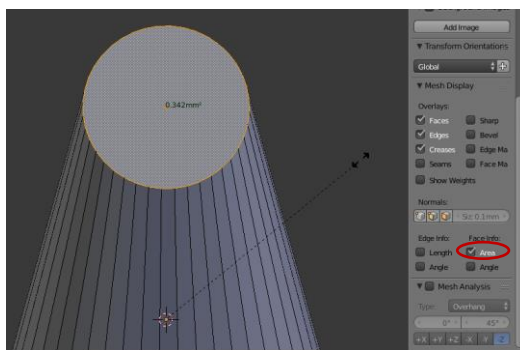
d. Tick the Length box. Select all the top of the cylinder (scaphopod) and press E (extrude) + S (scale) + move the cursor towards the centre until the desire thickness can be reach (0.117). Do the same for the bottom (0.114).
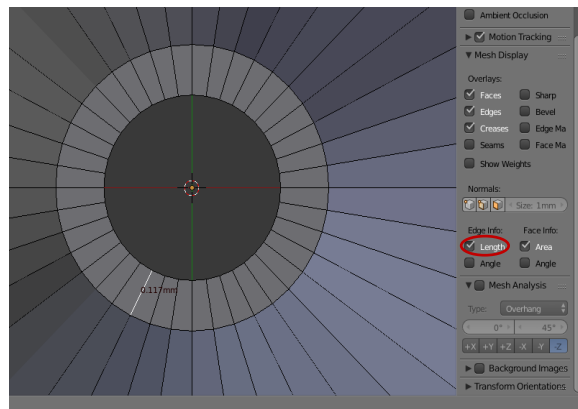
e. Select both circular edges from the bottom and top and ctrl + E and click Bridge edge loops
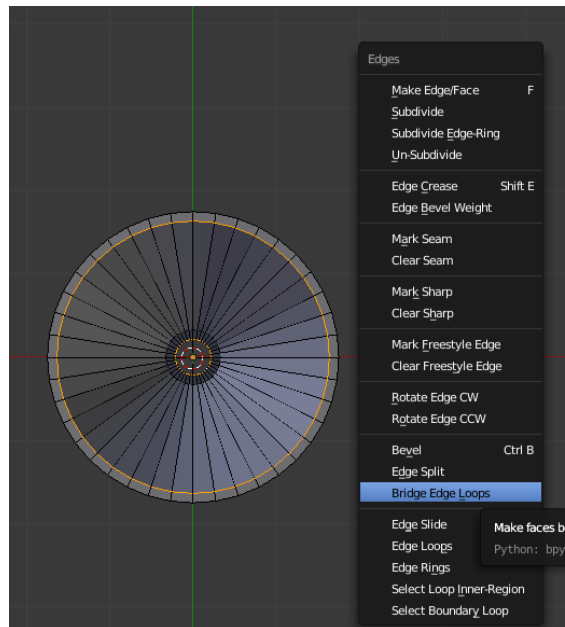
f. Create loops to be able to have the curvature. Loops gives to the model a smoother shape. Go to "Extrude" and choose "Create loops and Slides". The number of the loops depends on the shape that is aiming to create.
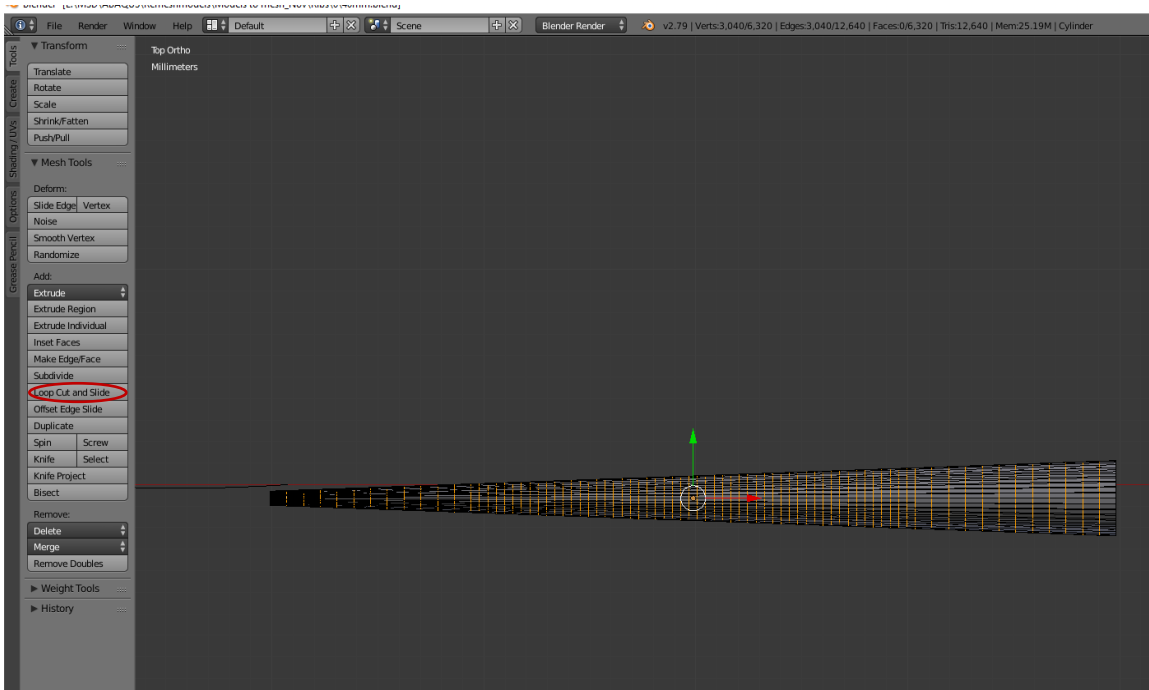
g. Made the curvature with "Bezier". Go to "Curve" in the left side and choose it. A curve shape will appear. It is possible to move the curve and fit it to the shape that is needed.
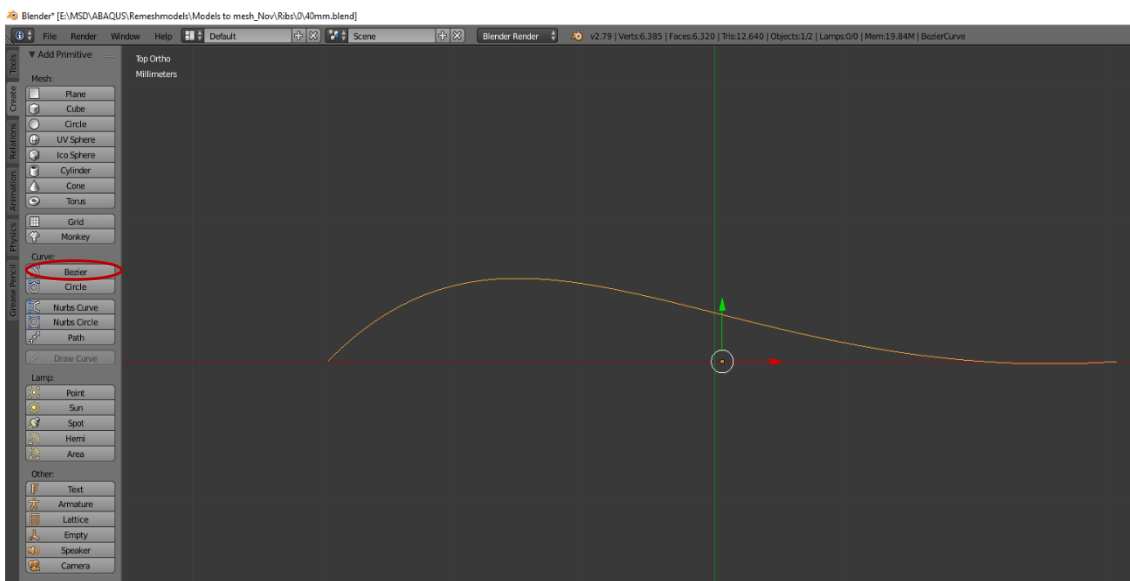
Once the model is ready, save it as a STL format.

2. Mesh the model in Geomagic Wrap. This is a software that allows easy and good quality mesh.

a. Import the STL file to Geomagic Wrap.
b. Go to the "Remesh" icon. Choose the element size and the different parameters. You can change this depending on what you need. Click ok. Sometime is necessary "remesh" several times. Repeat steps b and c, much ever is needed.
c. Go to Fie and click "Save as". Click the arrow and go down to choose "stl binary". Click save.

3. Import the STL model on Avizo and save it on HSMASCII format.

4. Repair and assign properties on Hypermesh

    a. Import the HMASCII file on Hypermesh. File > Import > Solver Deck.
    In the file selection select file type: HSCMASCII and find the file in the file option. Click
    import and when it is done (you can see the model on Hypermesh), click close.
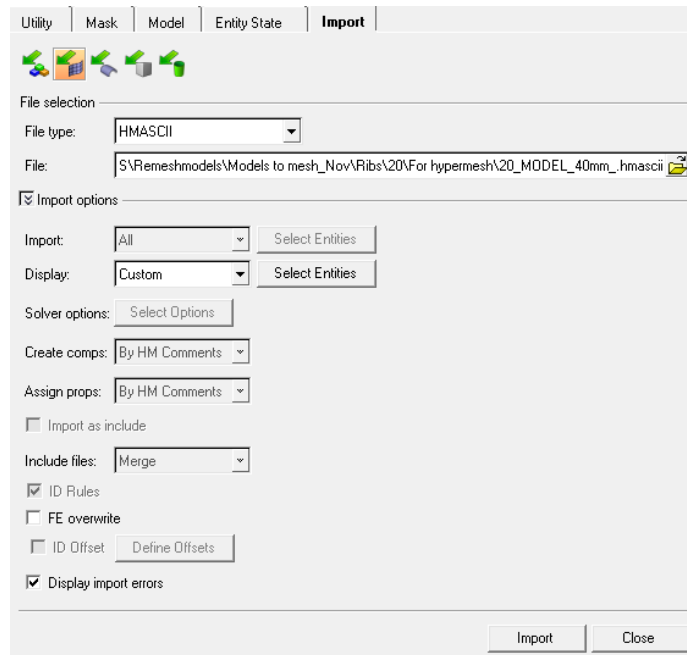
    b. Mesh quality. Go to the tools > check element panel, make sure the option on the left is set
    to 3D. Jacobian, free edges, but specially for Vol. Skew >0.98, Tet Collapse <0.2, Cell
    squish <0.5 and aspect ratio >10.
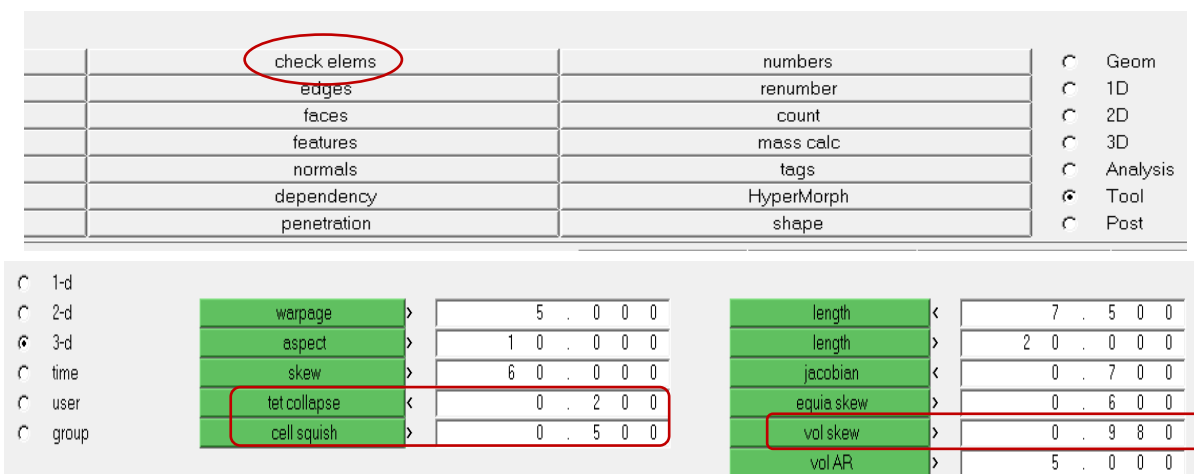
It is likely for find fail elements and there are several ways to repair them such as deleting, masking, and splitting and/or replace elements. In my case, I remesh several times, choosing the element quality target that it was needed.

Go to 3D>tetramesh>tetramesh parameters. Select optimize mesh quality and mesh speed as gradual. Hypermesh allows you to choose between Tet collapse, Cell squish and Vol skew. and repeting the remesh with the different parameter target until you don't get any fail. This guarantee no distorted elements in Abaqus.
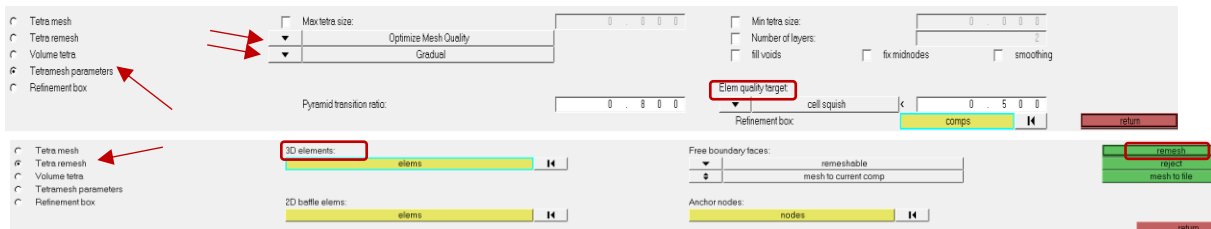
Then go to Tetra remesh and toggle element under 3D elements panel. Highlight the 3D elements toggling in 3D elements and click remesh. Do this much ever times you need it.

    c.   Assign material properties to the model

Click on "Materials" at the top panel

Select the menu Materials > create.
Material name = "x_mat"
Type = MATERIAL
Card image = ABAQUS_MATERIAL
Click "create/edit" and scroll down to select "elastic" > "isotropic" and ELASTIC
DATA CARDS = 1.
E(1) = Young's Modulus (in MPa); Nu(1) = Poisson's Ratio
Click "return" to accept changes.

Click on "Properties" at the top panel

Select the menu Properties > create.
Property name = "x_prop"
Type = SOLID_SECTION
Card image = SOLID_SECTON
Material = x_mat
Click "create", then "return".

Assign properties

Select the menu Collectors > edit > components

Select the "assign" sub-panel, the click the "comps" button and select the component you want to assign the property to from the list. Toggle to "Property =", double-click on it and select x_prop from the list of solid sections. Click apply and then ok.
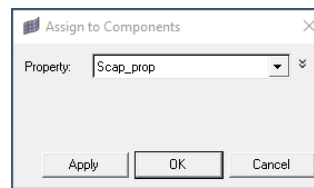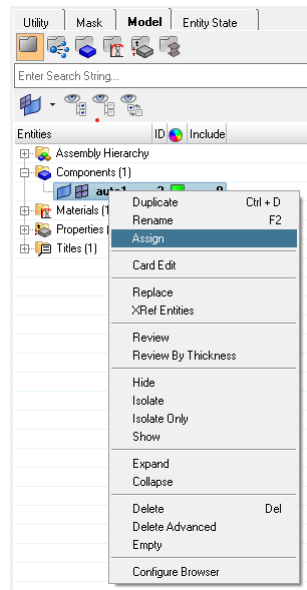
d. Export the model in inp format. Go to File > export > model and select Abaqus and standard3D as the export types. You need to specify the file path name in full, ending with. inp. Set the select entities to export dropdown to "custom" and choose which entities to export from the Entity State tab.
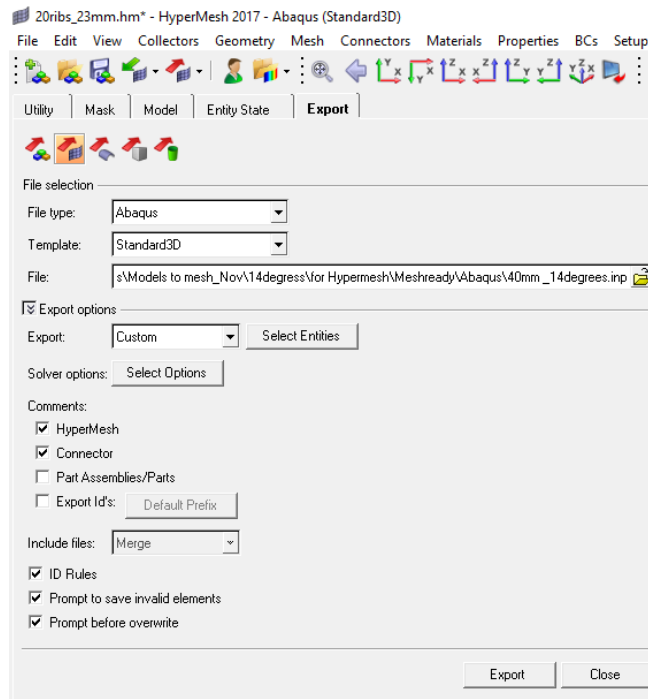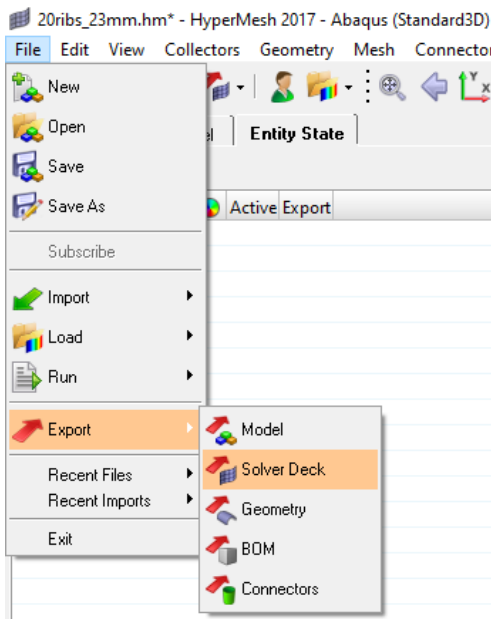
5. Import to Abaqus, create steps, constraints, boundary conditions and loads.

a. Create step. Click on "Create Step" A window called "Create Step" will appear. Indicate your "Step Name". Make sure "Initial" is selected under "Insert new step after" and "Static, General" is selected under "Procedure type". Click continue when you are finished.

A new window called "Edit Step" will appear. Default options should be okay in this case, so just click OK.

Click on "Create field output"

A window called "Create Field" will pop up. Select your step name from the drop-down menu and click continue.

A window called "Edit Field Output Request" will appear. Under "Output variables", select von Misses stress and max strain. Select those from the drop-down lists. Click on OK when finished.

a. Create constraints of the Scaphopod. Go to Tools>Set>Create. A window called "Create set" will appear. Name your set, choose "Node" under "Type", and click continue.
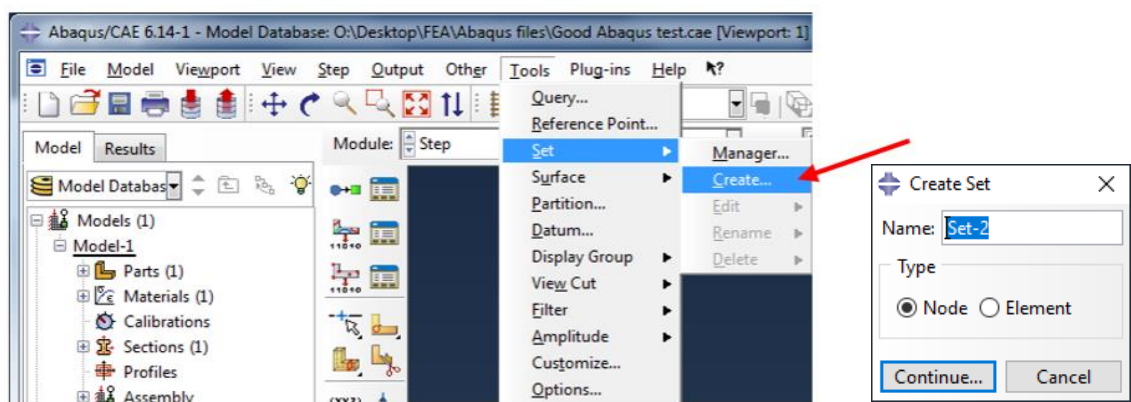
b. Select nodes by angle. Selected nodes are highlighted in red. Click done when you are finished.
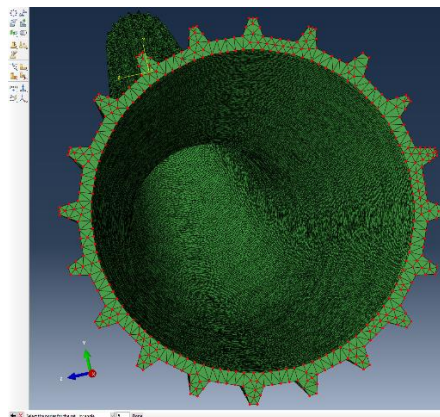
c. Create boundary conditions. Right click on BCs and select "Create". Name your boundary condition, choose the desired step from the drop-down list (choose Initial), select Category>Mechanical and Types for Selected Step>Displacement/Rotation, and click Continue.
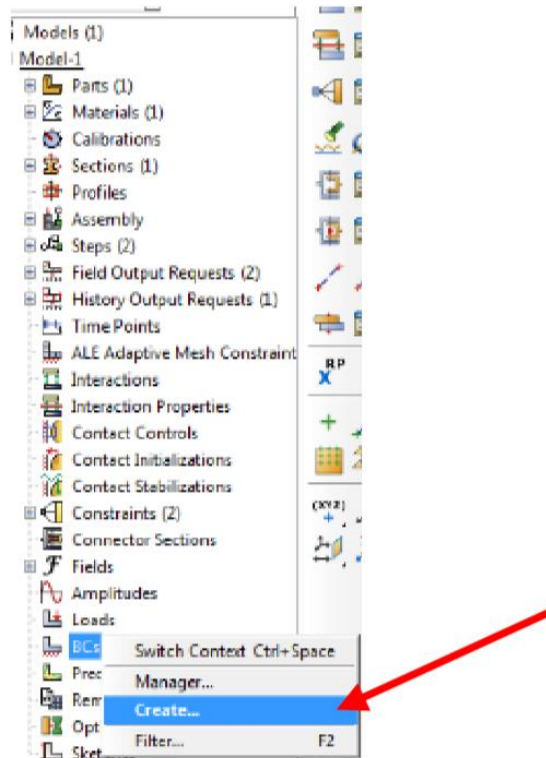
d. In the window called "Edit Boundary Condition" tick the desired degrees of freedom and click OK. Repeat the same steps for more boundary conditions if needed.

e. Mark a reference point (RP). Go to tools > Query > Distance. Measure the distance in which the RP will be place. Then change the module to "Interaction" and mark the point.
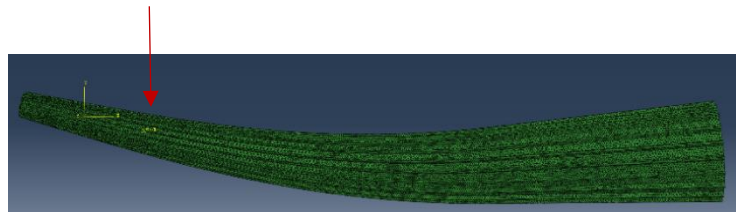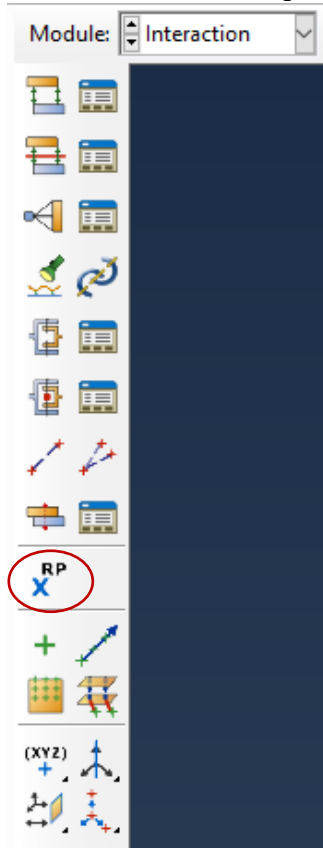
f. Create a load. Change the module to Load. Click on "Create Load". A window called "Create Load" will appear. Choose a name for the load and select the step you defined earlier from the drop-down list (do not choose Initial).
A set of options will now appear in the window. Make sure Category>Mechanical and Type of Selected Step>Pressure are selected. Click continue. Choose the element set of interest and click continue. A window called "Edit Load" will pop up. Put the force input (in Newtons) and click ok.

g. Run the model
Under the Analysis tree right click on "Jobs" and select "Create", In the "Create Job" window name your job, make sure the correct model is selected under "Source" and click on Continue.
Click OK on the next window

Under the Analysis tree, expand "Jobs" using the plus sign at the left, then right-click on your job's name and select "Submit"

At first it will say "Submitted" right next to your job's name, then it will say "Running", wait until it says "Completed", right click on it and select "Results". It will be possible to see the Results. Play with the different settings to analyse the model.
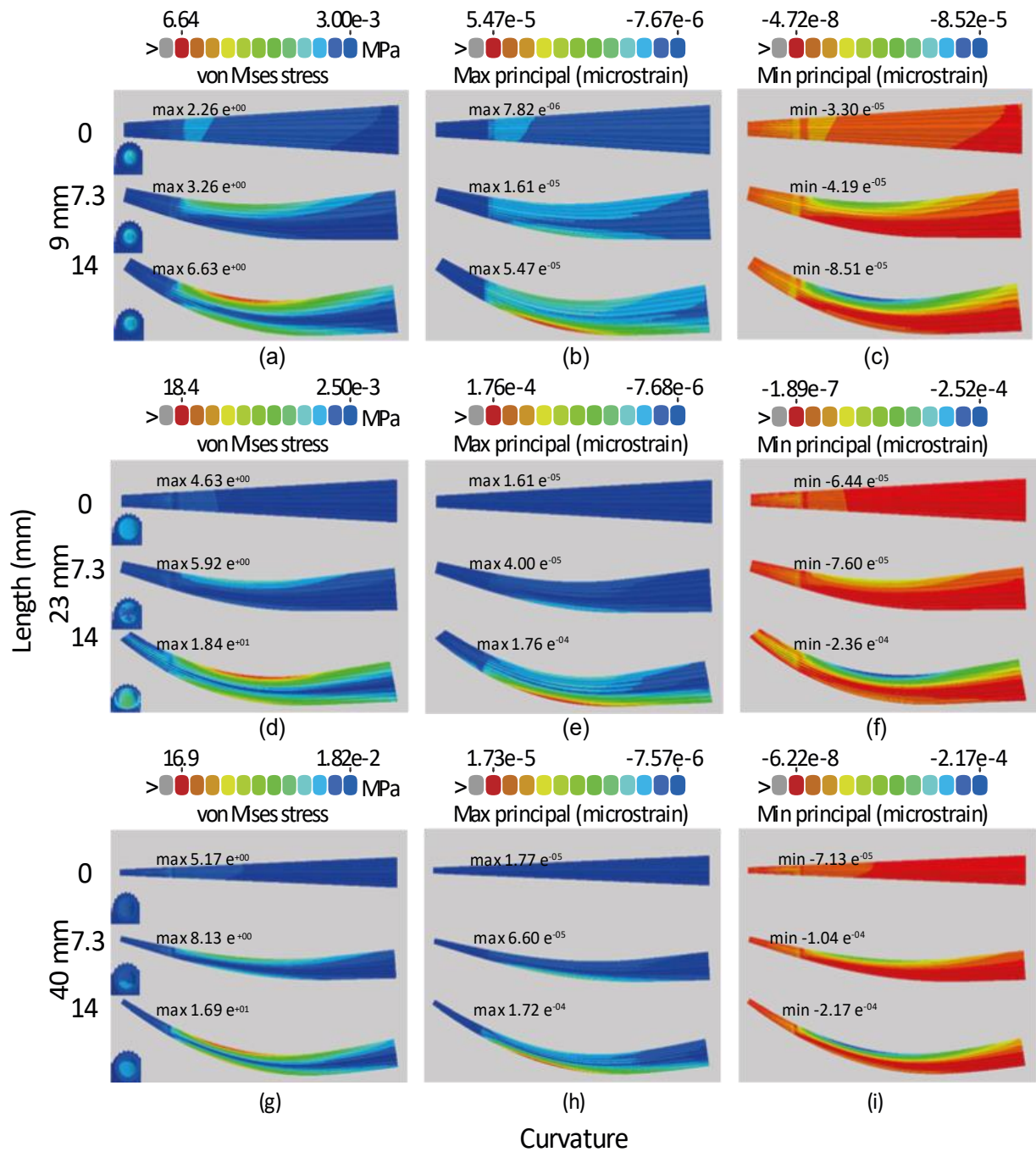
Figure B1. Caption explained on next page.
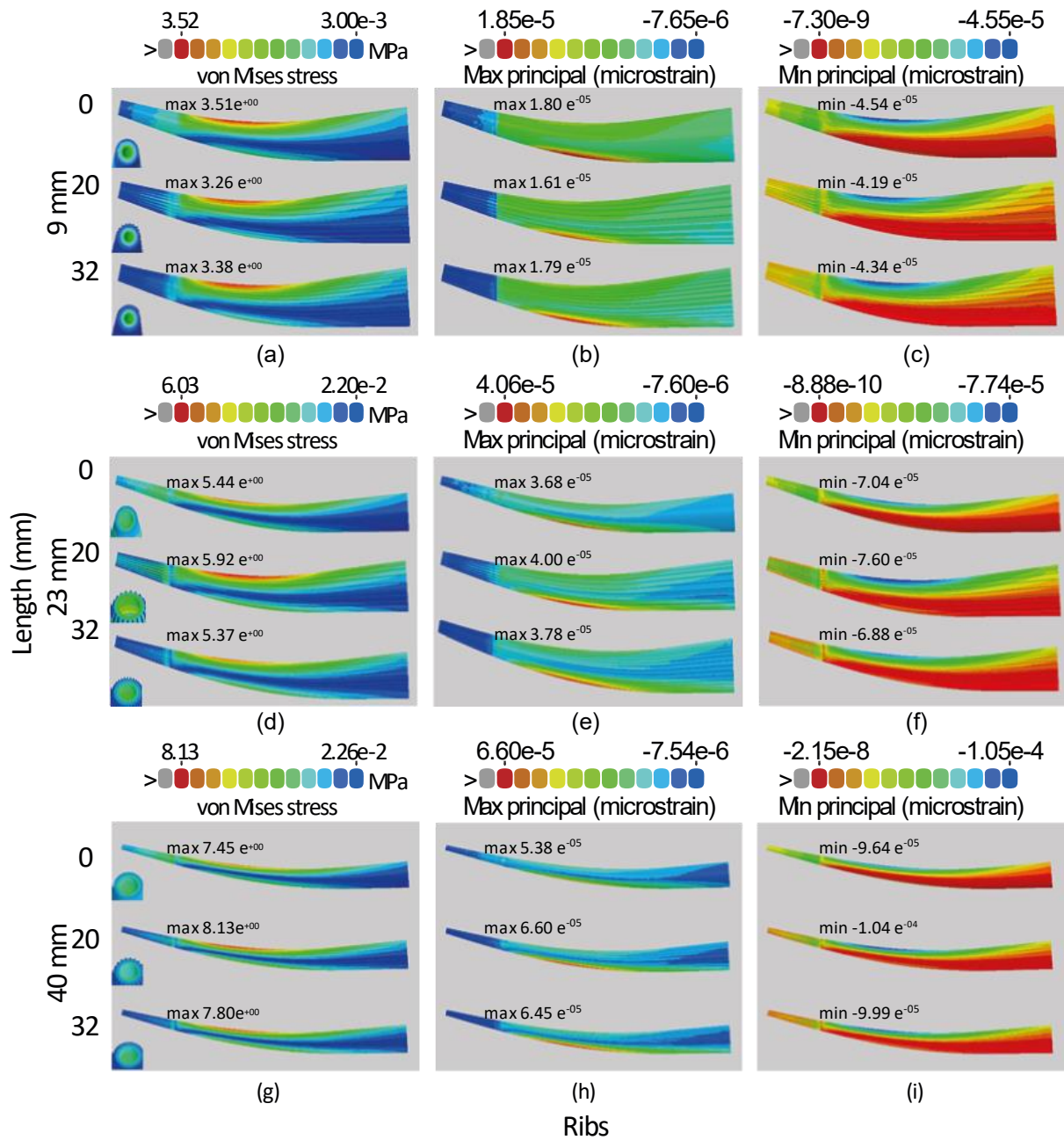
Figure B1. ongoing. Stress and strain distribution (von-Mises, Minimum principal strain, and Maximum principal strain) of the 18 scaphopods model for Model B (uneven load). Two sets of data are shown: the first page shows models where the curvature is varied (and ribs are fixed), the second page shows models where the number of ribs is varied (and curvature is fixed). Plots for the first set of data are organised into squares from 0° to 14° and starting on the top with 9mm ((a) to (c)), in the middle 23mm ((d) to (f)) and the bottom 40mm ((g) to (i)). For the ribs, the second set of data are organised into squares from 0 to 32 ribs and starting on the top with 9mm ((a) to (c)), in the middle 23mm ((d) to (f)) and the bottom 40mm ((g) to (i)). The force is applied as in the Model A and for 1N pressure load.

APPENDIX C

Table C1. Morphometric measurements for the specimens of *L marionensis* use in the different analysis in the different regions. Reported are the Vial number, length, height, and width.

Region	Vial	Length (mm)	Height (mm)	Width (mm)
Eastern Weddell Sea	197.1	63	49.3	18.1
	585.1	19.2	17.4	6.2
	611.2	43.7	34.6	13.1
	611.3	16.4	14.5	5.3
	206.1	14.7	14.2	5.5
	206.2	13.3	13	5.2
	826.2	17	16.4	5.8
	795.1	46	40.4	12.4
South Sandwich Islands	655.1	54.4	50.8	18.1
	655.2	33.4	30.2	10.6
	655.3	26	23.4	8.8
	684.7	25.2	22.5	8.8
	849.1	42.1	38	17.4
	849.2	33.1	31	12.9
	849.3	26.2	24.6	8.9
	468.2	30.1	29.3	10.7
Amundsen Sea	421	17.9	16.1	5.6
Magellan Region	Lm28	30.2	28.2	12.7
	Lm33	30.3	26.9	12.9
	Lm73	20.7	20.5	8.3
	Lm74	37.1	34.7	13.1
	Lm90	37.9	33.9	15.8
	Lm211	20.0	18.1	7.5
	Lm234	24.1	23.4	9.5

Table C2. Morphometric measurements for the specimens of *C. astartoides* use in the different analysis in the different regions. Reported are the Vial number, length, height, and width.

Region	Vial	Length (mm)	Height (mm)	Width (mm)
Amundsen	1004.11	4.18	3.61	2.7
	1004_1.7	3.05	2.85	2.07
	1004_1.8	4.89	4.37	3.02
	1004_1.12	7.51	7.32	4.64
	1152_1.4	8.58	7.75	4.73
	1152_1.1	14.3	12.5	7.39
	1056_1.1	11.5	10.6	6.84
	420.3	12.7	12.0	7.09
	731_1.2	11.7	10.8	6.34
Eastern Weddell	49	10.8	9.51	5.76
	528	16.2	12.9	8.51
	363	11.1	8.93	5.86
	187.4	3.26	1.99	1.58
	187.2	15.0	12.13	6.94
	155.3	7.91	6.77	4.38
	812	18.5	15.64	9.25

Table C3. Sr/Ca ratio, Mg/Ca measured in *C. astartoides*, measured temperature and Ω_{Ar} saturation taken from GLODAPv22019 (Olsen et al. 2019) for the Weddell Sea and the Amundsen Sea for the analysed specimens. The volume impacted by dissolution is separated as low- and high-density values determined by grey values thresholds of the CT images with a low threshold between 20000-53000 (first number) and high-density threshold between 53000-65535 (right number). Values are presented as volume and percentage. The Amundsen Sea specimen are all from the same location.

Region	Vial	Sr/Ca (mmol/mol)	Mg/Ca (mmol/mol)	Temperature (°C)	Ω_{Ar}	Volume (μm^3) at low/high threshold	Perc shell volume low/high %
Weddell Sea	187.4	3.27	0.452	0.16	1.10	0.78/1.31	37.1/62.9
	187.2	3.95	0.381	0.16	1.10	71.7/32.3	68.9/31.1
	363	Not use for this analysis		-0.46	1.16	28.8/28.2	50.5/49.5
	528	Not use for this analysis		-0.46	1.16	137/49.4	78.6/26.4
	812_	3.09	0.449	-0.46	1.16	196.8/53.4	78.6/21.3
	155.3	2.98	0.453	-0.46	1.16	5.63/16.5	25.5/74.5
	49	2.4	0.518	-1.32	1.25	29.6/30.8	49.0/51.0
Amundsen Sea	1004_1.12	2.52	0.40	0.58	1.03	11.7/23.7	32.9/67.1
	1004_1.8	2.39	0.44	0.58	1.03	2.82/7.22	29.1/71.9
	420.3	2.75	0.40	0.58	1.03	59.7/44.3	57.4/42.6
	1156_1.1	2.92	0.39	0.58	1.03	46.3/43.6	52.8/47.3
	731_1.2	Not use for this analysis		0.58	1.03	51.451.1	50.1/49.9
	1152_1.4	1.72	0.51	0.58	1.03	16.2/23.6	49.6/59.4
	1152_1.1	2.33	0.26	0.58	1.03	83.2/44.2	65.3/34.7

Table C4.. Age and length of *C. astartoides* from the Weddel Sea (WS) and the Amundsen Sea (AS) specimens.

Bivalve vial	Age (yr)	Length (mm)
155.3 (WS)	12	7.91
528 (WS)	25	16.2
812 (WS)	22	18.5
1004_1.12 (AS)	14	7.51
1152_1.1 (AS)	23	14.3
1156_1.1 (AS)	20	11.5

REFERENCES

Abele, D., Brey, T., & Philipp, E. (2009). Bivalve models of aging and the determination of molluscan lifespans. *Experimental gerontology*, *44*(5), 307-315.

Abrebekooh, Y. N., & Rad, M. (2011). Experimental and numerical investigation of drag force over tubular frustum. *Scientia Iranica*, *18*(5), 1133-1137.

Ahmad, T. B., Liu, L., Kotiw, M., & Benkendorff, K. (2018). Review of anti-inflammatory, immune-modulatory and wound healing properties of molluscs. *Journal of ethnopharmacology*, *210*, 156-178.

Akester, RJ, & Martel, AL (2000). Shell shape, dysodont tooth morphology, and hinge-ligament thickness in the bay mussel Mytilus trossulus correlate with wave exposure. *Canadian Journal of Zoology*, *78* (2), 240-253.

Allen, C. S., & Smellie, J. L. (2008). Volcanic features and the hydrological setting of Southern Thule, South Sandwich Islands. *Antarctic Science*, *20*(3), 301-308.

Allen, D. C., & Vaughn, C. C. (2009). Burrowing behavior of freshwater mussels in experimentally manipulated communities. *Journal of the North American Benthological Society*, *28*(1), 93-100.

Alma, L., Kram, K. E., Holtgrieve, G. W., Barbarino, A., Fiamengo, C. J., & Padilla-Gamiño, J. L. (2020). Ocean acidification and warming effects on the physiology, skeletal properties, and microbiome of the purple-hinge rock scallop. *Comparative Biochemistry and Physiology Part A: Molecular & Integrative Physiology*, *240*, 110579.

Alyakrinskaya, I. O. (2005). Functional significance and weight properties of the shell in some mollusks. *Biology Bulletin*, *32*(4), 397-418.

Anderson, P. S., Bright, J. A., Gill, P. G., Palmer, C., & Rayfield, E. J. (2012). Models in palaeontological functional analysis. *Biology letters*, 8(1), 119-122.

Andrade, M., De Marchi, L., Soares, A. M., Rocha, R. J., Figueira, E., & Freitas, R. (2019). Are the effects induced by increased temperature enhanced in Mytilus galloprovincialis submitted to air exposure?. *Science of the total environment*, *647*, 431-440.

Arneborg, L., Wåhlin, A. K., Björk, G., Liljebladh, B., & Orsi, A. H. (2012). Persistent inflow of warm water onto the central Amundsen shelf. *Nature Geoscience*, *5*(12), 876-880.

Arntz, W., & Gutt, J. (1999). The expedition ANTARKTIS XV/3 (EASIZ II) of RV" Polarstern" in 1998. *Berichte zur Polarforschung (Reports on Polar Research)*, *301*.

Arntz, W., & Brey, T. (2003). The Expedition ANTARKTIS XIX/5 (LAMPOS) of RV" Polarstern" in 2002. *Berichte zur Polar-und Meeresforschung (Reports on Polar and Marine Research)*, *462*.

Arntz, W., & Brey, T. (2005). The expedition ANTARKTIS XXI/2 (BENDEX) of RV" Polarstern" in 2003/2004. *Berichte zur Polar-und Meeresforschung (Reports on Polar and Marine Research)*, *503*.

Arrigo, K. R., & Van Dijken, G. L. (2003). Phytoplankton dynamics within 37 Antarctic coastal polynya systems. *Journal of Geophysical Research: Oceans*, *108*(C8).

Arrigo, K. R., van Dijken, G. L., & Bushinsky, S. (2008). Primary production in the Southern Ocean, 1997–2006. *Journal of Geophysical Research: Oceans*, *113*(C8).

Arrigo, K. R., Lowry, K. E., & van Dijken, G. L. (2012). Annual changes in sea ice and phytoplankton in polynyas of the Amundsen Sea, Antarctica. *Deep Sea Research Part II: Topical Studies in Oceanography*, *71*, 5-15.

Atkinson, A., Whitehouse, M. J., Priddle, J., Cripps, G. C., Ward, P., & Brandon, M. A. (2001). South Georgia, Antarctica: a productive, cold water, pelagic ecosystem. *Marine Ecology Progress Series*, *216*, 279-308.

Bailey, T. R., & Lear, C. H. (2006). Testing the effect of carbonate saturation on the Sr/Ca of biogenic aragonite: a case study from the River Ehen, Cumbria, UK. *Geochemistry, Geophysics, Geosystems*, *7*(3).

Bednaršek, N., Tarling, G. A., Bakker, D. C. E., Fielding, S., Jones, E. M., Venables, H. J., ... & Murphy, E. J. (2012a). Extensive dissolution of live pteropods in the Southern Ocean. *Nature Geoscience*, *5*(12), 881-885.

Bednaršek, N., Tarling, G. A., Bakker, D. C., Fielding, S., Cohen, A., Kuzirian, A., McCorkle, D., Lézé, B., & Montagna, R. (2012b). Description and quantification of pteropod shell dissolution: a sensitive bioindicator of ocean acidification. *Global Change Biology,* 18(7), 2378–2388.

Bednaršek, N., Tarling, G. A., Bakker, D. C., Fielding, S., & Feely, R. A. (2014). Dissolution dominating calcification process in polar pteropods close to the point of aragonite undersaturation. *PLoS One*, *9*(10).

Barclay, K. M., Gaylord, B., Jellison, B. M., Shukla, P., Sanford, E., & Leighton, L. R. (2019). Variation in the effects of ocean acidification on shell growth and strength in two intertidal gastropods. *Marine Ecology Progress Series*, *626*, 109-121.

Barnes, D. K., & Peck, L. S. (2008). Vulnerability of Antarctic shelf biodiversity to predicted regional warming. *Climate Research*, *37*(2-3), 149-163.

Barnes, D., Bergstrom, D., Bindschadler, R., Bockheim, J., Bopp, L., Bracegirdle, T., ... & Forcada, J. (2009). The next 100 years. Pp. 299–387 in J. Turner, R. Bindschadler, P. Convey, G. di Prisco, E. Fahrbach, J. Gutt, D. Hodgson, P. Mayewski, & C. Summerhayes, eds. Antarctic climate change and the environment – a contribution to the international polar year 2007–2008. SCAR, Cambridge, U.K.

Barnes, D. K., Fleming, A., Sands, C. J., Quartino, M. L., & Deregibus, D. (2018). Icebergs, sea ice, blue carbon and Antarctic climate feedbacks. *Philosophical Transactions of the Royal Society A: Mathematical, Physical and Engineering Sciences*, *376*(2122), 20170176.

Bayne, B. L., & Hawkins, A. J. S. (1992). Ecological and physiological aspects of herbivory in benthic suspension-feeding molluscs. *Plant-animal interactions in the marine benthos. Systematics Association Special Volume*, *46*, 265-288.

Begum, S., Basova, L., Heilmayer, O., Philipp, E. E., Abele, D., & Brey, T. (2010). Growth and energy budget models of the bivalve Arctica islandica at six different sites in the Northeast Atlantic realm. *Journal of shellfish research*, *29*(1), 107-115.

Beuck, L., Vertino, A., Stepina, E., Karolczak, M., & Pfannkuche, O. (2007). Skeletal response of Lophelia pertusa (Scleractinia) to bioeroding sponge infestation visualised with micro-computed tomography. *Facies*, *53*(2), 157-176.

Björk M, Fransson A, Torstenson A, Chierici (2014) Ocean acidification state in western Antarctic surface waters: controls and interannual variability. Biogeosciences, 11, 57–73 doi:10.5194/bg-11-57-2014

Bopp, L., Resplandy, L., Orr, J. C., Doney, S. C., Dunne, J. P., Gehlen, M., Halloran, P., Heinze, C., Ilyina, T., Seferian, R., et al. (2013). Multiple stressors of ocean ecosystems in the 21st century: projections with CMIP5 models. *Biogeosciences,* 10:6225–6245.

Bottjer, D. J., & Carter, J. G. (1980). Functional and phylogenetic significance of projecting periostracal structures in the Bivalvia (Mollusca). *Journal of Paleontology*, 200-216.

Bouxsein, M. L., Boyd, S. K., Christiansen, B. A., Guldberg, R. E., Jepsen, K. J., & Müller, R. (2010). Guidelines for assessment of bone microstructure in rodents using micro–computed tomography. *Journal of bone and mineral research*, *25*(7), 1468-1486.

Boyde, A. (1972). Scanning electron microscope studies of bone. *The biochemistry and physiology of bone*, *1*, 259-310.

Brady, H. B. (1884). Report on the foraminifera dredged by HMS Challenger during the years 1873-1876. *Report on the scientific results of the voyage of the HMS Challenger during the years 1873-1876, Zoology*, *9*, 1-814.

Brandt, A., Gooday, A. J., Brandao, S. N., Brix, S., Brökeland, W., Cedhagen, T., ... & Diaz, R. J. (2007). First insights into the biodiversity and biogeography of the Southern Ocean deep sea. *nature*, *447*(7142), 307-311.

Brandt, A., De Broyer, C., Ebbe, B., Ellingsen, K. E., Gooday, A. J., Janussen, D., ... & Tyler, P. A. (2012). Southern Ocean deep benthic biodiversity.

Bright, J. A. (2014). A review of paleontological finite element models and their validity. *Journal of Paleontology*, *88*(4), 760-769.

Brönmark, C., Lakowitz, T., & Hollander, J. (2011). Predator-induced morphological plasticity across local populations of a freshwater snail. *Plos one*, *6*(7).

Buckeridge, J. S. (1989). Marine invertebrates from late Cainozoic deposits in the McMurdo Sound region, Antarctica. *Journal of the Royal Society of New Zealand*, *19*(3), 333-342.

Byrne, M., & Przeslawski, R. (2013). Multistressor impacts of warming and acidification of the ocean on marine invertebrates' life histories. *Integrative and comparative biology*, *53*(4), 582-596.

Byrne, M., Foo, S., Soars, N. A., Wolfe, K. D., Nguyen, H. D., Hardy, N., & Dworjanyn, S. A. (2013). Ocean warming will mitigate the effects of acidification on calcifying sea urchin larvae (Heliocidaris tuberculata) from the Australian global warming hot spot. *Journal of experimental marine biology and ecology*, *448*, 250-257.

Byrne, M., & Fitzer, S. (2019). The impact of environmental acidification on the microstructure and mechanical integrity of marine invertebrate skeletons. *Conservation physiology*, *7*(1), coz062.

Caldeira, K., & Wickett, M. E. (2003). Anthropogenic carbon and ocean pH. *Nature*, *425*(6956), 365-365.

Campanati, C., Dupont, S., Williams, G. A., & Thiyagarajan, V. (2018). Differential sensitivity of larvae to ocean acidification in two interacting mollusc species. *Marine environmental research*, *141*, 66-74.

Cardoso, R., & Veloso, V. (2003). Population dynamics and secondary production of the wedge clam Donaxhanleyanus (Bivalvia: Donacidae) on a high-energy, subtropical beach of Brazil. *Marine Biology*, *142*(1), 153-162.

Carey, N., & Sigwart, J. D. (2014). Size matters: plasticity in metabolic scaling shows body-size may modulate responses to climate change. *Biology Letters*, *10*(8), 20140408.

Carey, N., Dupont, S., & Sigwart, J. D. (2016). Sea hare Aplysia punctata (Mollusca: Gastropoda) can maintain shell calcification under extreme ocean acidification. *The Biological Bulletin*, *231*(2), 142-151.

Carré, M., Bentaleb, I., Bruguier, O., Ordinola, E., Barrett, N. T., and Fontugne, M. (2006). Calcification rate influence on trace element concentrations in aragonitic bivalve shells: evidences and mechanisms. *Geochimica et Cosmochimica Acta*, 70(19):4906–4920.

Castel, J., Labourg, P. J., Escaravage, V., Auby, I., & Garcia, M. E. (1989). Influence of seagrass beds and oyster parks on the abundance and biomass patterns of meio-and macrobenthos in tidal flats. *Estuarine, coastal and shelf science*, 28(1), 71-85.

Cattaneo-Vietti, R., Chiantore, M., Schiaparelli, S., & Albertelli, G. (2000). Shallow-and deep-water mollusc distribution at Terra Nova Bay (Ross Sea, Antarctica). *Polar Biology*, 23(3), 173-182.

Chakraborty, C., Hsu, C. H., Wen, Z. H., Lin, C. S., & Agoramoorthy, G. (2009). Zebrafish: a complete animal model for in vivo drug discovery and development. *Current drug metabolism*, 10(2), 116-124.

Chapman, A. D. (2009). Numbers of living species in Australia and the world.

Chapman, C. C., Lea, M. A., Meyer, A., Sallée, J. B., & Hindell, M. (2020). Defining Southern Ocean fronts and their influence on biological and physical processes in a changing climate. *Nature Climate Change*, 1-11.

Clewing, C., Riedel, F., Wilke, T., & Albrecht, C. (2015). Ecophenotypic plasticity leads to extraordinary gastropod shells found on the "Roof of the World". *Ecology and evolution*, 5(14), 2966-2979.

Checa, A. G., Okamoto, T., and Ramírez, J. (2006). Organization pattern of nacre in Pteriidae (Bivalvia: Mollusca) explained by crystal competition. *Proceedings of the Royal Society B: Biological Sciences*, 273(1592): 1329–1337.

Chevin, L.-M., Lande, R., and Mace, G. M. (2010). Adaptation, plasticity, and extinction in a changing environment: towards a predictive theory. *PLoS biology*, 8(4):e1000357.

Chown, S. L., Slabber, S., McGeoch, M. A., Janion, C., & Leinaas, H. P. (2007). Phenotypic plasticity mediates climate change responses among invasive and indigenous arthropods. *Proceedings of the Royal Society B: Biological Sciences*, 274(1625), 2531-2537.
Clarke A (1993) Temperature and extinction in the sea: a physiologist's view. *Paleobiology*, 19, 499–518.

Clewing, C., Riedel, F., Wilke, T., & Albrecht, C. (2015). Ecophenotypic plasticity leads to extraordinary gastropod shells found on the "Roof of the World". *Ecology and Evolution*, 5(14), 2966-2979.

Cobb, K. M., Charles, C. D., Cheng, H., Kastner, M., & Edwards, R. L. (2003). U/Th-dating living and young fossil corals from the central tropical Pacific. *Earth and Planetary Science Letters*, 210(1-2), 91-103.

Coen, L. D. (1985). Shear resistance in two bivalve molluscs: role of hinges and interdigitating margins. *Journal of Zoology*, 205(4), 479-487.

Cole, W. R. & Fox, D. L. (1942). Biology of the California sea-mussel (Mytilus californianus). influence of temperature, food supply, sex and age on the rate of growth. *Journal of Experimental Zoology,* 90(1):1–30.

Cole, V. J., Parker, L. M., O'Connor, S. J., O'Connor, W. A., Scanes, E., Byrne, M., and Ross, P. M. (2016). Effects of multiple climate change stressors: ocean acidification interacts with warming, hyposalinity, and low food supply on the larvae of the brooding flat oyster Ostrea angasi. *Marine biology,* 163(5):125.

Comeau, S., Edmunds, P. J., Spindel, N. B., & Carpenter, R. C. (2013). The responses of eight coral reef calcifiers to increasing partial pressure of CO2 do not exhibit a tipping point. *Limnology and Oceanography*, 58(1), 388-398.

Comiso, J. C., & Gordon, A. L. (1998). Interannual variability in summer sea ice minimum, coastal. *Antarctic Research Series*, 74, 293-315.

Cook, A. J., Vaughan, D. G., Luckman, A. J., & Murray, T. (2014). A new Antarctic Peninsula glacier basin inventory and observed area changes since the 1940s. *Antarctic Science*, 26(6), 614-624.

Cook, A. J., Holland, P. R., Meredith, M. P., Murray, T., Luckman, A., & Vaughan, D. G. (2016). Ocean forcing of glacier retreat in the western Antarctic Peninsula. *Science*, *353*(6296), 283-286.

Crenshaw, M. A. (1980). Mechanisms of shell formation and dissolution. *Skeletal growth of aquatic organisms: biological records of environmental change/edited by Donald C. Rhoads and Richard A. Lutz.*

Cross, E. L., Peck, L. S., & Harper, E. M. (2015). Ocean acidification does not impact shell growth or repair of the Antarctic brachiopod Liothyrella uva (Broderip, 1833). *Journal of Experimental Marine Biology and Ecology*, *462*, 29-35.

Cross, E. L., Harper, E. M., and Peck, L. S. (2018). A 120-year record of resilience to environmental change in brachiopods. *Global change biology*, 24(6):2262–2271.

Cross, E.L., Harper, E. M., and Peck, L. S. (2019). Thicker shells compensate extensive dissolution in brachiopods under future ocean acidification. *Environmental Science & Technology*, 53. 5016-5026.

Cruz, M. (1990). Estudio del bentos marino Antártico en Bahía Chile o Discovery, Isla Greenwich (islas Shetland del Sur), Antártida. *Acta Antártica Ecuatoriana*, PROANTEC, *Ecuador*, 2(1): 33-45.

Dang, V. T., Speck, P., Doroudi, M., Smith, B., & Benkendorff, K. (2011). Variation in the antiviral and antibacterial activity of abalone Haliotis laevigata, H. rubra and their hybrid in South Australia. *Aquaculture*, *315*(3-4), 242-249.

Davies, G. J. (1987). Aspects of the biology and ecology of deep-sea Scaphopoda (Mollusca). PhD thesis, Heriot-Watt University.

De Broyer, C., & Danis, B. (2011). How many species in the Southern Ocean? Towards a dynamic inventory of the Antarctic marine species. *Deep sea research Part II: Topical studies in oceanography*, *58*(1-2), 5-17.

DeJong, H. B., Dunbar, R. B., Mucciarone, D., & Koweek, D. A. (2015). Carbonate saturation state of surface waters in the Ross Sea and Southern Ocean: controls and implications for the onset of aragonite undersaturation. *Biogeosciences*, *12*(23), 6881-6896.

Dell, R. K. (1990). Antarctic Mollusca with special reference to the fauna of the Ross Sea. *Royal. Soc. New Zealand, Bull*, (27), 1-311.

Denman, K. L., Brasseur, G., Chidthaisong, A., Ciais, P., Cox, P. M., Dickinson, R. E., Hauglustaine, D., Heinze, C., Holland, E., Jacob, D., Lohmann, U., Ramachandran, S., Leite da Silva Dias, P., Wofsy, S. C., and Zhang, X.: Couplings Between Changes in the Climate System and Biogeochemistry. In: Climate Change 2007: The Physical Science Basis. Contribution of Working Group I to the Fourth Assessment Report of the Intergovernmental Panel on Climate Change, edited by: Solomon, S., Qin, D., Manning, M., Marquis, M., Averyt, K., Tignor, M. M. B., Miller, H. L., and Chen, Z. L., Cambridge University Press, Cambridge, UK and New York, USA, 2007.

Dickinson, G. H., Ivanina, A. V., Matoo, O. B., Pörtner, H. O., Lannig, G., Bock, C., Beniash E., & Sokolova, I. M. (2012). Interactive effects of salinity and elevated CO_2 levels on juvenile eastern oysters, Crassostrea virginica. *Journal of Experimental Biology*, 215(1), 29-43.

Dietzel, M., Gussone, N., & Eisenhauer, A. (2004). Co-precipitation of Sr2+ and Ba2+ with aragonite by membrane diffusion of CO2 between 10 and 50 C. *Chemical Geology*, *203*(1-2), 139-151.

Dodd, J. R. (1965). Environmental control of strontium and magnesium in Mytilus. *Geochimica et Cosmochimica Acta*, *29*(5), 385-398.

Dupont, S., Dorey, N., & Thorndyke, M. (2010). What meta-analysis can tell us about vulnerability of marine biodiversity to ocean acidification?. *Estuarine, Coastal and Shelf Science*, *89*(2), 182-185.

Durham, S. R., Gillikin, D. P., Goodwin, D. H., & Dietl, G. P. (2017). Rapid determination of oyster lifespans and growth rates using LA-ICP-MS line scans of shell Mg/Ca ratios. *Palaeogeography, palaeoclimatology, palaeoecology*, *485*, 201-209.

Eager, R. M. C. (1978). Shape and function of the shell: a comparison of some living and fossil bivalve molluscs. *Biological Reviews*, *53*(2), 169-210.

Elderfield, H., Holland, H. D., Elderfield, H., & Turekian, K. K. (Eds.). (2006a). *The oceans and marine*

Elderfield, H., Yu, J., Anand, P., Kiefer, T., & Nyland, B. (2006b). Calibrations for benthic foraminiferal Mg/Ca paleothermometry and the carbonate ion hypothesis. *Earth and Planetary Science Letters*, *250*(3-4), 633-649.

Enderlein, P., & Larter, R. D. (2008). Cruise Report JR 179-RRS James Clark Ross-February to April 2008-Marine biological and marine geological and geophysical studies in the Amundsen and Bellingshausen Seas. *British Antarctic Survey.*

Engl, W. (2012). *Shells of Antarctica*. ConchBooks.

Fabry, V. J., Seibel, B. A., Feely, R. A., & Orr, J. C. (2008). Impacts of ocean acidification on marine fauna and ecosystem processes. *ICES Journal of Marine Science*, *65*(3), 414-432.

Fantazzini, P., Mengoli, S., Pasquini, L., Bortolotti, V., Brizi, L., Mariani, M., ... & Prada, F. (2015). Gains and losses of coral skeletal porosity changes with ocean acidification acclimation. *Nature Communications*, *6*(1), 1-7.

Fitzer, S. C., Vittert, L., Bowman, A., Kamenos, N. A., Phoenix, V. R., & Cusack, M. (2015). Ocean acidification and temperature increase impact mussel shell shape and thickness: problematic for protection? *Ecology and evolution*, *5*(21), 4875-4884.

Fitzer, S. C., Bin San Chan, V., Meng, Y., Chandra Rajan, K., Suzuki, M., Not, C., Toyofuku, T., & Fal, L. (2019). H2 Established and Emerging Techniques for Characterising the Formation, Structure and Performance of Calcified Structures under Ocean Acidification. In *Oceanography and Marine Biology*. Taylor & Francis.

Folmer, O., Hoeh, W., Black, M., and Vrijenhoek, R. (1994). Conserved primers for PCR amplification of mitochondrial DNA from different invertebrate phyla. *Molecular Marine Biology and Biotechnology*, 3:294–299.

Foo, S. A., & Byrne, M. (2016). Acclimatization and adaptive capacity of marine species in a changing ocean. In *Advances in marine biology* (Vol. 74, pp. 69-116). Academic Press.

Fordyce, J. A. (2006). The evolutionary consequences of ecological interactions mediated through phenotypic plasticity. *Journal of Experimental Biology*, *209*(12), 2377-2383.

Foster, L. C., Allison, N., Finch, A. A., & Andersson, C. (2009). Strontium distribution in the shell of the aragonite bivalve Arctica islandica. *Geochemistry, Geophysics, Geosystems*, *10*(3).

Fox, D. L., & Coe, W. R. (1943). Biology of the California sea-mussel (Mytilus californianus). II. Nutrition, metabolism, growth and calcium deposition. *Journal of Experimental Zoology*, *93*(2), 205-249.

Freitas, P., Clarke, L. J., Kennedy, H., Richardson, C., & Abrantes, F. (2005). Mg/Ca, Sr/Ca, and stable-isotope ($\delta 18O$ and $\delta 13C$) ratio profiles from the fan mussel Pinna nobilis: Seasonal records and temperature relationships. *Geochemistry, Geophysics, Geosystems*, *6*(4).

Fukuyama, A. K., & Oliver, J. S. (1985). Sea star and walrus predation on bivalves in Norton Sound, Bering Sea, Alaska. *Ophelia*, *24*(1), 17-36.

Füllenbach, C. S., Schöne, B. R., & Branscheid, R. (2014). Microstructures in shells of the freshwater gastropod Viviparus viviparus: a potential sensor for temperature change?. *Acta biomaterialia*, *10*(9), 3911-3921.

Garabato, A. C. N., McDonagh, E. L., Stevens, D. P., Heywood, K. J., & Sanders, R. J. (2002). On the export of Antarctic bottom water from the Weddell Sea. *Deep Sea Research Part II: Topical Studies in Oceanography*, *49*(21), 4715-4742.

Gardner, J., Manno, C., Bakker, D. C., Peck, V. L., and Tarling, G. A. (2018). Southern Ocean pteropods at risk from ocean warming and acidification. *Marine biology*, 165(1):8.

Gattuso, J.-P. & Hansson, L. (2011). Ocean acidification: background and history. Ocean acidification, pages 1–20.

Gattuso, J. P., Magnan, A., Billé, R., Cheung, W. W., Howes, E. L., Joos, F., ... & Hoegh-Guldberg, O. (2015). Contrasting futures for ocean and society from different anthropogenic CO2 emissions scenarios. *Science*, *349*(6243).

Gaylord, B., Barclay, K. M., Jellison, B. M., Jurgens, L. J., Ninokawa, A. T., Rivest, E. B., & Leighton, L. R. (2019). Ocean change within shoreline communities: from biomechanics to behaviour and beyond. *Conservation physiology*, *7*(1), coz077.

Gazeau, F., Quiblier, C., Jansen, J. M., Gattuso, J. P., Middelburg, J. J., & Heip, C. H. (2007). Impact of elevated CO2 on shellfish calcification. *Geophysical research letters*, *34*(7).

Gazeau, F., Parker, L. M., Comeau, S., Gattuso, J.-P., O'Connor, W. A., Martin, S., Pörtner, H.-O., & Ross, P. M. (2013). Impacts of ocean acidification on marine shelled molluscs. *Marine biology*, 160(8):2207–2245

Gerringa, L. J., Alderkamp, A. C., Laan, P., Thuroczy, C. E., De Baar, H. J., Mills, M. M., ... & Arrigo, K. R. (2012). Iron from melting glaciers fuels the phytoplankton blooms in Amundsen Sea (Southern Ocean): Iron biogeochemistry. *Deep Sea Research Part II: Topical Studies in Oceanography*, *71*, 16-31.

Gill, R. (2014). *Modern Analytical Geochemistry: an introduction to quantitative chemical analysis techniques for Earth, environmental and materials scientists*. Routledge.

Gillikin, D. P., Lorrain, A., Navez, J., Taylor, J. W., André, L., Keppens, E., Baeyens, W., and Dehairs, F. (2005). Strong biological controls on Sr/Ca ratios in aragonitic marine bivalve shells. *Geochemistry, Geophysics, Geosystems,* 6(5).

Gosling, E. M. (2003). *Bivalve molluscs*. Blackwell Pub.

Grant, R. A., Griffiths, H. J., Steinke, D., Wadley, V., & Linse, K. (2011). Antarctic DNA barcoding; a drop in the ocean?. *Polar Biology*, *34*(5), 775-780.

Green, M. A., Waldbusser, G. G., Reilly, S. L., Emerson, K., & O'Donnell, S. (2009). Death by dissolution: sediment saturation state as a mortality factor for juvenile bivalves. *Limnology and Oceanography*, *54*(4), 1037-1047.

Griffiths, H. J., Linse, K., & Crame, J. A. (2003). SOMBASE–Southern Ocean Mollusc Database: a tool for biogeographic analysis in diversity and ecology. *Organisms Diversity & Evolution,* 3(3), 207-213.

Griffiths, H. J., Barnes, D. K., & Linse, K. (2009). Towards a generalized biogeography of the Southern Ocean benthos. *Journal of Biogeography*, *36*(1), 162-177.

Griffiths, H. J. (2010). Antarctic marine biodiversity–what do we know about the distribution of life in the Southern Ocean? talmage*PloS one*, *5*(8).

Griffiths, H. J., Meijers, A. J., & Bracegirdle, T. J. (2017). More losers than winners in a century of future Southern Ocean seafloor warming. *Nature Climate Change*, *7*(10), 749-754.

Gruber, N., Clement, D., Carter, B. R., Feely, R. A., Van Heuven, S., Hoppema, M., ... & Monaco, C. L. (2019a). The oceanic sink for anthropogenic CO2 from 1994 to 2007. *Science*, *363*(6432), 1193-1199.

Gruber, N., Landschützer, P., & Lovenduski, N. S. (2019b). The variable Southern Ocean carbon sink. *Annual review of marine science*, *11*, 159-186.

Gutiérrez, J. L., Jones, C. G., Strayer, D. L., & Iribarne, O. O. (2003). Mollusks as ecosystem engineers: the role of shell production in aquatic habitats. *Oikos*, *101*(1), 79-90.

Gutt, J., & Starmans, A. (1998). Structure and biodiversity of megabenthos in the Weddell and Lazarev Seas (Antarctica): ecological role of physical parameters and biological interactions. *Polar Biology*, *20*(4), 229-247.

Gutt, J., Bertler, N., Bracegirdle, T. J., Buschmann, A., Comiso, J., Hosie, G., ... & Xavier, J. C. (2015). The Southern Ocean ecosystem under multiple climate change stresses-an integrated circumpolar assessment. *Global Change Biology*, *21*(4), 1434-1453.

Gutt, J., Isla, E., Bertler, A. N., Bodeker, G. E., Bracegirdle, T. J., Cavanagh, R. D., ... & De Master, D. (2018). Cross-disciplinarity in the advance of Antarctic ecosystem research. *Marine genomics*, *37*, 1-17.

Hain, S., & Arnaud, P. M. (1992). Notes on the reproduction of high-Antarctic molluscs from the Weddell Sea. In *Weddell Sea Ecology* (pp. 303-312). Springer, Berlin, Heidelberg.

Hall Jr, C. A., Dollase, W. A., & Corbató, C. E. (1974). Shell growth in Tivela stultorum (Mawe, 1823) and Callista chione (Linnaeus, 1758) (Bivalvia): annual periodicity, latitudinal differences, and diminution with age. *Palaeogeography, Palaeoclimatology, Palaeoecology*, *15*(1), 33-61.

Hart, S. R., & Blusztajn, J. (1998). Clams as recorders of ocean ridge volcanism and hydrothermal vent field activity. *Science*, *280*(5365), 883-886.

Harvey, B. P., Agostini, S., Wada, S., Inaba, K., & Hall-Spencer, J. M. (2018). Dissolution: the Achilles' heel of the triton shell in an acidifying ocean. *Frontiers in Marine Science*, *5*, 371.

Hauck, J., Gerdes, D., Hillenbrand, C. D., Hoppema, M., Kuhn, G., Nehrke, G., ... & Wolf-Gladrow, D. A. (2012). Distribution and mineralogy of carbonate sediments on Antarctic shelves. *Journal of Marine Systems*, *90*(1), 77-87.

Hauri, C., Friedrich, T., & Timmermann, A. (2016). Abrupt onset and prolongation of aragonite undersaturation events in the Southern Ocean. *Nature Climate Change*, *6*(2), 172-176.

Heath, J., & Taylor, N. (2015). Electron probe microanalysis.

Hellmer, H. H., Huhn, O., Gomis, D., & Timmermann, R. (2011). On the freshening of the northwestern Weddell Sea continental shelf.

Hendriks, I. E., Duarte, C. M., Olsen, Y. S., Steckbauer, A., Ramajo, L., Moore, T. S., Trotter, J. A., & McCulloch, M. (2015). Biological mechanisms supporting adaptation to ocean acidification in coastal ecosystems. *Estuarine, Coastal and Shelf Science,* 152: A1–A8.

Henley, S. F., Schofield, O. M., Hendry, K. R., Schloss, I. R., Steinberg, D. K., Moffat, C., Peck, L.S., Costa, D.P., Bakker, D.C., Hughes C. & Rozema, P. D. (2019). Variability and change in the west Antarctic Peninsula marine system: Research priorities and opportunities. *Progress in oceanography*, *173*, 208-237.

Henry, R. P., Kormanik, G. A., Smatresk, N. J., & Cameron, J. N. (1981). The role of $CaCO_3$ dissolution as a source of HCO_3-for the buffering of hypercapnic acidosis in aquatic and terrestrial decapod crustaceans. *Journal of Experimental Biology*, *94*(1), 269-274.

Hinch, S. G., & Bailey, R. C. (1988). Within-and among-lake variation in shell morphology of the freshwater clam Elliptio complanata (Bivalvia: Unionidae) from south-central Ontario lakes. *Hydrobiologia*, *157*(1), 27-32.

Hoegh-Guldberg, O., Jacob, D., Bindi, M., Brown, S., Camilloni, I., Diedhiou, A., ... & Hijioka, Y. (2018). Impacts of 1.5 C global warming on natural and human systems. *Global warming of 1.5° C. An IPCC Special Report*.

Hofmann, G. E., Barry, J. P., Edmunds, P. J., Gates, R. D., Hutchins, D. A., Klinger, T., & Sewell, M. A. (2010). The effect of ocean acidification on calcifying organisms in marine ecosystems: an organism-to-ecosystem perspective. *Annual review of ecology, evolution, and systematics*, *41*, 127-147.

Hogg, O. T., Barnes, D. K., & Griffiths, H. J. (2011). Highly diverse, poorly studied and uniquely threatened by climate change: an assessment of marine biodiversity on South Georgia's continental shelf. *PloS one*, *6*(5).

Holgate, J. H., & Webb, J. (2003). MICROSCOPY| Transmission Electron Microscopy.

Hoogenboom, M. O., Campbell, D. A., Beraud, E., DeZeeuw, K., & Ferrier-Pages, C. (2012). Effects of light, food availability and temperature stress on the function of photosystem II and photosystem I of coral symbionts. *PLoS one*, *7*(1).

Hoppema, M., Fahrbach, E., Stoll, M. H., & de Baar, H. J. (1999). Annual uptake of atmospheric CO2 by the Weddell Sea derived from a surface layer balance, including estimations of entrainment and new production. *Journal of Marine Systems*, *19*(4), 219-233.

Hornbach, D. J., Kurth, V. J., & Hove, M. C. (2010). Variation in freshwater mussel shell sculpture and shape along a river gradient. *The American Midland Naturalist*, *164*(1), 22-36.

Howe, J. A., Shimmield, T. M., & Diaz, R. (2004). Deep-water sedimentary environments of the northwestern Weddell Sea and South Sandwich Islands, Antarctica. *Deep Sea Research Part II: Topical Studies in Oceanography*, *51*(14-16), 1489-1514.

Ingels, J., Vanreusel, A., Brandt, A., Catarino, A. I., David, B., De Ridder, C., Dubois P, Gooday A.J., Martin P., Pasotti F. & Robert, H. (2012). Possible effects of global environmental changes on Antarctic benthos: a synthesis across five major taxa. *Ecology and evolution*, *2*(2), 453-485.

Ivanina, A. V., Dickinson, G. H., Matoo, O. B., Bagwe, R., Dickinson, A., Beniash, E., & Sokolova, I. M. (2013). Interactive effects of elevated temperature and CO2 levels on energy metabolism and biomineralization of marine bivalves Crassostrea virginica and Mercenaria mercenaria. *Comparative Biochemistry and Physiology Part A: Molecular & Integrative Physiology*, *166*(1), 101-111

Iwasaki, S., Kimoto, K., Sasaki, O., Kano, H., Honda, M. C., & Okazaki, Y. (2015). Observation of the dissolution process of Globigerina bulloides tests (planktic foraminifera) by X-ray microcomputed tomography. *Paleoceanography*, *30*(4), 317-331.

Jacobs, S. S., Hellmer, H. H., and Jenkins, A. (1996). Antarctic ice sheet melting in the southeast pacific. *Geophysical Research Letters,* 23(9):957–960.

Jacobs, S. S., Jenkins, A., Giulivi, C. F., & Dutrieux, P. (2011). Stronger ocean circulation and increased melting under Pine Island Glacier ice shelf. *Nature Geoscience*, *4*(8), 519.

Jacobs, S., Jenkins, A., Hellmer, H., Giulivi, C., Nitsche, F., Huber, B., & Guerrero, R. (2012). The Amundsen Sea and the Antarctic ice sheet. *Oceanography*, *25*(3), 154-163.

Jenkins, A., Dutrieux, P., Jacobs, S. S., McPhail, S. D., Perrett, J. R., Webb, A. T., & White, D. (2010). Observations beneath Pine Island Glacier in West Antarctica and implications for its retreat. *Nature Geoscience*, *3*(7), 468-472.

Jenkins, A., Dutrieux, P., Jacobs, S., Steig, E. J., Gudmundsson, G. H., Smith, J., & Heywood, K. J. (2016). Decadal ocean forcing and Antarctic ice sheet response: Lessons from the Amundsen Sea. *Oceanography*, *29*(4), 106-117.

Jennions, S. M. (2014). *The effect of environmental change on bivalve mollusc biomineralisation* (Doctoral dissertation, University of Bristol).

Jiang, L. Q., Feely, R. A., Carter, B. R., Greeley, D. J., Gledhill, D. K., & Arzayus, K. M. (2015). Climatological distribution of aragonite saturation state in the global oceans. *Global Biogeochemical Cycles*, *29*(10), 1656-1673.

Jiang, L. Q., Carter, B. R., Feely, R. A., Lauvset, S. K., & Olsen, A. (2019). Surface ocean pH and buffer capacity: past, present and future. *Scientific Reports*, *9*(1), 1-11.

Jones, D. S. (1983). Sclerochronology: reading the record of the molluscan shell: annual growth increments in the shells of bivalve molluscs record marine climatic changes and reveal surprising longevity. *American Scientist*, *71*(4), 384-391.

Jones, E. M., Fenton, M., Meredith, M. P., Clargo, N. M., Ossebaar, S., Ducklow, H. W., ... & de Baar, H. J. (2017). Ocean acidification and calcium carbonate saturation states in the coastal zone of the West Antarctic Peninsula. *Deep Sea Research Part II: Topical Studies in Oceanography*, *139*, 181-194.

Johnstone, H. J., Schulz, M., Barker, S., & Elderfield, H. (2010). Inside story: An X-ray computed tomography method for assessing dissolution in the tests of planktonic foraminifera. *Marine Micropaleontology*, *77*(1-2), 58-70.

Karney, G.B., Butler, P.G., Scourse, J.D., Richardson, C.A., Lau, K.H., Czernuszka, J.T., Grovenor, C.R.M., 2011. Identification of growth increments in the shell of the bivalve mollusc Arctica islandica using backscattered electron imaging. J. Microsc. 241, 29–36.

Keeling, R. F., Körtzinger, A., & Gruber, N. (2010). Ocean deoxygenation in a warming world.

Kelly, M. W., Sanford, E., & Grosberg, R. K. (2012). Limited potential for adaptation to climate change in a broadly distributed marine crustacean. *Proceedings of the Royal Society B: Biological Sciences*, *279*(1727), 349-356.

Klein, R. T., Lohmann, K. C., & Thayer, C. W. (1996). SrCa and 13C12C ratios in skeletal calcite of Mytilus trossulus: Covariation with metabolic rate, salinity, and carbon isotopic composition of seawater. *Geochimica et Cosmochimica Acta*, *60*(21), 4207-4221.

Kroeker, K.J., Kordas, R.L., Crim, R.N., Singh, G.G., (2010). Meta-analysis reveals negative yet variable effects of ocean acidification on marine organisms. *Ecology Letters* 13, 1419–1434.

Kroeker, K. J., Kordas, R. L., Crim, R., Hendriks, I. E., Ramajo, L., Singh, G. S., ... & Gattuso, J. P. (2013). Impacts of ocean acidification on marine organisms: quantifying sensitivities and interaction with warming. *Global change biology*, *19*(6), 1884-1896

Kroeker, K. J., Gaylord, B., Hill, T. M., Hosfelt, J. D., Miller, S. H., & Sanford, E. (2014a). The role of temperature in determining species' vulnerability to ocean acidification: a case study using Mytilus galloprovincialis. *PloS one*, *9*(7), e100353.

Kroeker, K. J., Sanford, E., Jellison, B. M., & Gaylord, B. (2014b). Predicting the effects of ocean acidification on predator-prey interactions: a conceptual framework based on coastal molluscs. *The Biological Bulletin*, *226*(3), 211-222.

Lamprell, K. L., & Healy, J. M. (1998). A revision of the Scaphopoda from Australian waters (Mollusca). *RECORDS-AUSTRALIAN MUSEUM-SUPPLEMENT-*.

Lartaud, F., Chauvaud, L., Richard, J., Toulot, A., Bollinger, C., Testut, L., & Paulet, Y. M. (2010). Experimental growth pattern calibration of Antarctic scallop shells (Adamussium colbecki, Smith 1902) to provide a biogenic archive of high-resolution records of environmental and climatic changes. *Journal of Experimental Marine Biology and Ecology*, *393*(1-2), 158-167.

Laufkötter, C., Vogt, M., Gruber, N., Aita-Noguchi, M., Aumont, O., Bopp, L., ... & Hauck, J. (2015). Drivers and uncertainties of future global marine primary production in marine ecosystem models. *Biogeosciences*, *12*(23), 6955-6984.

Lebrato, M., Garbe-Schönberg, D., Müller, M. N., Blanco-Ameijeiras, S., Feely, R. A., Lorenzoni, L., ... & Oschlies, A. (2020). Global variability in seawater Mg: Ca and Sr: Ca ratios in the modern ocean. *Proceedings of the National Academy of Sciences*, *117*(36), 22281-22292.

Lemanis, R., & Zlotnikov, I. (2018). Finite element analysis as a method to study molluscan shell mechanics. *Advanced Engineering Materials*, *20*(3), 1700939.

Lev, M. H., & Gonzalez, R. G. (2002). CT angiography and CT perfusion imaging. In *Brain mapping: the methods* (pp. 427-484). Academic Press.

Li, C., Meng, Y., He, C., Chan, V. B., Yao, H., & Thiyagarajan, V. (2016). Mechanical robustness of the calcareous tubeworm Hydroides elegans: warming mitigates the adverse effects of ocean acidification. *Biofouling*, *32*(2), 191-204.

Linse, K. (1999). Mollusca of the Magellan region. A checklist of the species and their distribution. *Scientia Marina*, *63*(S1), 399-407.

Linse, K., Griffiths, H. J., Barnes, D. K., & Clarke, A. (2006). Biodiversity and biogeography of Antarctic and sub-Antarctic mollusca. *Deep sea research Part II: Topical studies in oceanography*, *53*(8-10), 985-1008.

Lischka, S., Büdenbender, J., Boxhammer, T., & Riebesell, U. (2011). Impact of ocean acidification and elevated temperatures on early juveniles of the polar shelled pteropod Limacina helicina: mortality, shell degradation, and shell growth. *Biogeosciences (BG)*, *8*, 919-932.

Liu, J., & Curry, J. A. (2010). Accelerated warming of the Southern Ocean and its impacts on the hydrological cycle and sea ice. *Proceedings of the National Academy of Sciences*, *107*(34), 14987-14992.

Logan, D. L. (2011). A first course in the finite element method. Cengage Learning.

Lombardi, C., Gambi, M., Vasapollo, C., Taylor, P. & Cocito, S. (2011). Skeletal alterations and polymorphism in a Mediterranean bryozoan at natural CO2 vents. *Zoomorphology* 130, 135–145.

Longhurst, A. (1995). Seasonal cycles of pelagic production and consumption. *Progress in oceanography*, *36*(2), 77-167.

Ludbrook, N. H., & Moore, R. C. (1960). Scaphopoda. *Treatise on Invertebrate Paleontology, Part I (Mollusca 1)*.

Ludescher, J., Yuan, N., & Bunde, A. (2019). Detecting the statistical significance of the trends in the Antarctic sea ice extent: an indication for a turning point. *Climate dynamics*, *53*(1), 237-244.

Mabille, J., & Rochebrune, A. T. (1889). 1889. Mollusques. *Mission scientifique du Cap Horn*, *3*(6), 1-143.

Mackensen, A., & Douglas, R. G. (1989). Down-core distribution of live and dead deep-water benthic foraminifera in box cores from the Weddell Sea and the California continental borderland. *Deep Sea Research Part A. Oceanographic Research Papers*, *36*(6), 879-900.

Mackensen, A., Grobe, H., Kuhn, G., & Fu, D. K. (1990). Benthic foraminiferal assemblages from the eastern Weddell Sea between 68 and 73 S: distribution, ecology and fossilization potential. *Marine micropaleontology*, *16*(3-4), 241-283.

Mackenzie, C. L., Ormondroyd, G. A., Curling, S. F., Ball, R. J., Whiteley, N. M., & Malham, S. K. (2014). Ocean warming, more than acidification, reduces shell strength in a commercial shellfish species during food limitation. *PLoS One*, *9*(1).

Marcus, L. F. (1990, May). Traditional morphometrics. In *Proceedings of the Michigan morphometrics workshop* (Vol. 2, pp. 77-122). Ann Arbor^ eMichigan Michigan: The University of Michigan Museum of Zoology.

Marchitto, T. M., & Broecker, W. S. (2006). Deep water mass geometry in the glacial Atlantic Ocean: A review of constraints from the paleonutrient proxy Cd/Ca. *Geochemistry, Geophysics, Geosystems*, *7*(12).

Matoo, O. B., Ivanina, A. V., Ullstad, C., Beniash, E., & Sokolova, I. M. (2013). Interactive effects of elevated temperature and CO_2 levels on metabolism and oxidative stress in two common marine bivalves (Crassostrea virginica and Mercenaria mercenaria). *Comparative Biochemistry and Physiology Part A: Molecular & Integrative Physiology*, *164*(4), 545-553.

Markert, B., Wappelhorst, O., Weckert, V., Herpin, U., Siewers, U., Friese, K., & Breulmann, G. (1999). The use of bioindicators for monitoring the heavy-metal status of the environment. *Journal of Radioanalytical and Nuclear Chemistry*, *240*(2), 425-429.

Markulin, K., Peharda, M., Mertz-Kraus, R., Schöne, B. R., Uvanović, H., Kovač, Ž., & Janeković, I. (2019). Trace and minor element records in aragonitic bivalve shells as environmental proxies. *Chemical Geology*, *507*, 120-133.

Martens, E. V. (1878). Einige Conchylien aus den kälteren Meeresgegenden der südlichen Erdhälfte. *Sitzungsbericht der Gesellschaft naturforschender Freunde zu Berlin*, *1878*, 20-26.

Martinson, D. G., & McKee, D. C. (2012). Transport of warm Upper Circumpolar Deep Water onto the western Antarctic Peninsula continental shelf. *Ocean Science*, *8*(4), 433-442.

McNeil, B. I., & Matear, R. J. (2008). Southern Ocean acidification: A tipping point at 450-ppm atmospheric CO_2. *Proceedings of the National Academy of Sciences*, *105*(48), 18860-18864.

Meland, M. Y., Jansen, E., Elderfield, H., Dokken, T. M., Olsen, A., & Bellerby, R. G. (2006). Mg/Ca ratios in the planktonic foraminifer Neogloboquadrina pachyderma (sinistral) in the northern North Atlantic/Nordic Seas. *Geochemistry, Geophysics, Geosystems*, *7*(6).

Melatunan, S., Calosi, P., Rundle, S. D., Widdicombe, S., & Moody, A. J. (2013). Effects of ocean acidification and elevated temperature on shell plasticity and its energetic basis in an intertidal gastropod. *Marine Ecology Progress Series*, *472*, 155-168.

Melles, M., Kuhn, G., Fütterer, D., & Meischner, D. (1995). Processes of Modern Sedimentation in the Southern Weddell Sea, Antarctica-Evidence from Surface Sediments. *Polarforschung*, *64*(2), 45-74.

Melvill, J. C., & Standen, R. (1907). Notes on a collection of terrestrial and fluviatile Mollusca, made in north-eastern Rhodesia, during 1905, by Mr. Sheffield A. Neave, MA, B. Sc. *Memoirs of the Manchester Literary and Philosophical Society (Manchester Memoirs)*, *51*(4), 1-16.

Melvill, J. C., & Standen, R. (1914). XII.—Notes on Mollusca collected in the North-west Falklands by Mr. Rupert Vallentin, FLS, with descriptions of six new species. *Annals and Magazine of Natural History*, *13*(73), 110-136.

Melzner, F., Mark, F. C., Seibel, B. A., & Tomanek, L. (2019). Ocean Acidification and Coastal Marine Invertebrates: Tracking CO2 Effects from Seawater to the Cell. *Annual review of marine science*, *12*.

Melzner, F., Gutowska, M. A., Langenbuch, M., Dupont, S., Lucassen, M., Thorndyke, M. C., ... & Pörtner, H. O. (2009). Physiological basis for high CO2 tolerance in marine ectothermic animals: pre-adaptation through lifestyle and ontogeny?. *Biogeosciences (BG)*, *6*, 2313-2331.

Melzner, F., Stange, P., Trübenbach, K., Thomsen, J., Casties, I., Panknin, U., ... & Gutowska, M. A. (2011). Food supply and seawater p CO2 impact calcification and internal shell dissolution in the blue mussel Mytilus edulis. *PloS one*, *6*(9), e24223.

Meredith, M. P., Falk, U., Bers, A. V., Mackensen, A., Schloss, I. R., Ruiz Barlett, E., Jerosch, K., Silva Busso A. & Abele, D. (2018). Anatomy of a glacial meltwater discharge event in an Antarctic cove. *Philosophical Transactions of the Royal Society A: Mathematical, Physical and Engineering Sciences*, *376*(2122), 20170163.

Meredith, M., Sommerkorn, M., Cassotta, S., Derksen, C., Ekaykin, A., Hollowed, A., ... & Schuur, E. A. (2019). Polar Regions. Chapter 3, IPCC Special Report on the Ocean and Cryosphere in a Changing Climate.

Michaelidis, B., Ouzounis, C., Paleras, A., & Pörtner, H. O. (2005). Effects of long-term moderate hypercapnia on acid–base balance and growth rate in marine mussels Mytilus galloprovincialis. *Marine Ecology Progress Series*, *293*, 109-118.

Mitchell, B. G., & Holm-Hansen, O. (1991). Observations of modeling of the Antartic phytoplankton crop in relation to mixing depth. *Deep Sea Research Part A. Oceanographic Research Papers*, *38*(8-9), 981-1007.

Molinos, J. G., Halpern, B. S., Schoeman, D. S., Brown, C. J., Kiessling, W., Moore, P. J., ... & Burrows, M. T. (2016). Climate velocity and the future global redistribution of marine biodiversity. *Nature Climate Change*, *6*(1), 83-88.

Montes-Hugo, M., Doney, S. C., Ducklow, H. W., Fraser, W., Martinson, D., Stammerjohn, S. E., & Schofield, O. (2009). Recent changes in phytoplankton communities associated with rapid regional climate change along the western Antarctic Peninsula. *Science*, *323*(5920), 1470-1473.

Morley, S. A., Suckling, C. C., Clark, M. S., Cross, E. L., & Peck, L. S. (2016). Long-term effects of altered pH and temperature on the feeding energetics of the Antarctic Sea urchin, Sterechinus neumayeri. *Biodiversity*, *17*(1-2), 34-45.

Mouchi, V., De Rafélis, M., Lartaud, F., Fialin, M., & Verrecchia, E. (2013). Chemical labelling of oyster shells used for time-calibrated high-resolution Mg/Ca ratios: a tool for estimation of past seasonal temperature variations. *Palaeogeography, palaeoclimatology, palaeoecology*, *373*, 66-74.

Murphy, E. J., Watkins, J. L., Reid, K., Trathan, P. N., Everson, I., Croxall, J. P., ... & Hofmann, E. (1998). Interannual variability of the South Georgia marine ecosystem: biological and physical sources of variation in the abundance of krill. *Fisheries Oceanography*, *7*(3-4), 381-390.

Murphy, E. J., Watkins, J. L., Trathan, P. N., Reid, K., Meredith, M. P., Thorpe, S. E., ... & Forcada, J. (2007). Spatial and temporal operation of the Scotia Sea ecosystem: a review of large-scale links in a krill centred food web. *Philosophical Transactions of the Royal Society B: Biological Sciences*, *362*(1477), 113-148.

Murphy, E. J., Clarke, A., Abram, N. J., & Turner, J. (2014). Variability of sea-ice in the northern Weddell Sea during the 20th century. *Journal of Geophysical Research: Oceans*, *119*(7), 4549-4572.

Murray, J. W. (1991). Ecology and Palaeoecology of Benthic Foraminifera. New York, Longman Scientific & Technical, John Wily & Sons Inc.

Nehrke, G., Poigner, H., Wilhelms-Dick, D., Brey, T., & Abele, D. (2012). Coexistence of three calcium carbonate polymorphs in the shell of the Antarctic clam Laternula elliptica. *Geochemistry, Geophysics, Geosystems*, *13*(5).

Nelson, D. M., & Smith Jr, W. 0. (1991). Sverdrup revisited: Critical depths, maximum chlorophyll levels, and the control of Southern Ocean productivity by the irradiance-mixing regime. *Limnology and Oceanography*, *36*(8), 1650-1661.

Nicholls, K. W., Østerhus, S., Makinson, K., Gammelsrød, T., & Fahrbach, E. (2009). Ice-ocean processes over the continental shelf of the southern Weddell Sea, Antarctica: A review. *Reviews of Geophysics*, *47*(3).

Nicol, D. (1966). Descriptions, ecology, and geographic distribution of some Antarctic pelecypods. *Bull, Amer. Paleont.*, *51*, 1-102.

Nienhuis, S., Palmer, A. R., & Harley, C. D. (2010). Elevated CO_2 affects shell dissolution rate but not calcification rate in a marine snail. *Proceedings of the Royal Society B: Biological Sciences*, *277*(1693), 2553-2558.

Nolan CP & Clarke A. (1993). Growth in the bivalve Yoldia eightsi at Signy Island, Antarctica, determined from internal shell increments and calcium-45 incorporation. *Marine Biology* 117: 243–250.

Oehlmann, J., & Schulte-Oehlmann, U. (2003). Molluscs as bioindicators. In *Trace Metals and other Contaminants in the Environment* (Vol. 6, pp. 577-635). Elsevier.

Olsen, A., Lange, N., Key, R., Tanhua, T., Álvarez, M., Becker, S., ... & Van Heuven, S. (2019). GLODAPv2. 2019-an update of GLODAPv2.

Orr, J. C., Fabry, V. J., Aumont, O., Bopp, L., Doney, S. C., Feely, R. A., Gnanadesikan A., Gruber N., Ishida A., Joos F., & Key, R. M. (2005). Anthropogenic ocean acidification over the twenty-first century and its impact on calcifying organisms. *Nature*, *437*(7059), 681-686.

Orsi, A. H., & Whitworth, T. (2005). *Hydrographic Atlas of the World Ocean Circulation Experiment (WOCE): Volume 1: Southern Ocean*. Southampton, UK: WOCE International Project Office.

Palacios, R., Orensanz, J. M., & Armstrong, D. A. (1994). Seasonal and life-long variation of Sr/Ca ratio in shells of Mya arenaria from Grays Harbor (Washington)—an ancillary criterion in demographic studies. *Estuarine, Coastal and Shelf Science*, *39*(4), 313-327.

Parker, L. M., Ross, P. M., O'Connor, W. A., Pörtner, H. O., Scanes, E., & Wright, J. M. (2013). Predicting the response of molluscs to the impact of ocean acidification. *Biology*, *2*(2), 651-692.

Parkinson, C. L., Rind, D., Healy, R. J., & Martinson, D. G. (2001). The impact of sea ice concentration accuracies on climate model simulations with the GISS GCM. *Journal of Climate*, *14*(12), 2606-2623.

Parkinson, C. L., & Cavalieri, D. J. (2012). Antarctic sea ice variability and trends, 1979-2010.

Palmer (1979). "Scaphopoda" in The Encyclopedia of Paleontology R.W. Fairbridge & D. Jablonski (eds). pp. 738-744. Dowden, Hutchinson & Ross, Inc., Stroudsburg, PA.

Peck, L. S., Brockington, S., & Brey, T. (1997). Growth and metabolism in the Antarctic brachiopod Liothyrella uva. *Philosophical Transactions of the Royal Society of London. Series B: Biological Sciences*, *352*(1355), 851-858.

Peck, L. S., & Conway, L. Z. (2000). The myth of metabolic cold adaptation: oxygen consumption in stenothermal Antarctic bivalves. *Geological Society, London, Special Publications*, *177*(1), 441-450.

Peck, L. S., Webb, K. E., & Bailey, D. M. (2004). Extreme sensitivity of biological function to temperature in Antarctic marine species. *Functional Ecology*, *18*(5), 625-630.

Peck, L. S. (2005). Prospects for survival in the Southern Ocean: vulnerability of benthic species to temperature change. *Antarctic Science*, *17*(4), 497-507.

Peck, L. S. (2011). Organisms and responses to environmental change. *Marine genomics*, *4*(4), 237-243.

Peck, L. S., Morley, S. A., Richard, J., & Clark, M. S. (2014). Acclimation and thermal tolerance in Antarctic marine ectotherms. *Journal of Experimental Biology*, *217*(1), 16-22.

Peck, L. S. (2018). Antarctic marine biodiversity: adaptations, environments and responses to change. In: Hawkins, S.J.; Evans, A.J.; Dale, A.C.; Firth, L.B.; Smith, I.P., (eds.) *Oceanography and Marine Biology: An Annual Review, Volume 56.* Taylor and Francis, 105-236.

Pennington, B. J., & Currey, J. D. (1984). A mathematical model for the mechanical properties of scallop shells. *Journal of Zoology*, *202*(2), 239-263.

Peterson, R. G. (1992). The boundary currents in the western Argentine Basin. *Deep Sea Research Part A. Oceanographic Research Papers*, *39*(3-4), 623-644.

Pfister, C. A., Roy, K., Wootton, J. T., McCoy, S. J., Paine, R. T., Suchanek, T. H., & Sanford, E. (2016). Historical baselines and the future of shell calcification for a foundation species in a changing ocean. *Proceedings of the Royal Society B: Biological Sciences*, *283*(1832), 20160392.

Poloczanska, E. S., Brown, C. J., Sydeman, W. J., Kiessling, W., Schoeman, D. S., Moore, P. J., ... & Duarte, C. M. (2013). Global imprint of climate change on marine life. *Nature Climate Change*, *3*(10), 919-925.

Ponis, E., Robert, R., & Parisi, G. (2003). Nutritional value of fresh and concentrated algal diets for larval and juvenile Pacific oysters (Crassostrea gigas). *Aquaculture*, *221*(1-4), 491-505.

Pörtner, H. O., Hardewig, I., Sartoris, F. J., & Van Dijk, P. L. M. (1998). Energetic aspects of cold adaptation: critical temperatures in metabolic, ionic and acid-base regulation. *Cold ocean physiology*, *66*, 88-120.

Pörtner, H. O., Peck, L., Zielinski, S., & Conway, L. Z. (1999). Intracellular pH and energy metabolism in the highly stenothermal Antarctic bivalve Limopsis marionensis as a function of ambient temperature. *Polar biology*, *22*(1), 17-30.

Pörtner, H. O., & Knust, R. (2007). Climate change affects marine fishes through the oxygen limitation of thermal tolerance. *science*, *315*(5808), 95-97.

Pörtner, H. O., & Farrell, A. P. (2008). Physiology and climate change. Science, 690-692.

Pörtner, H. O., Karl, D. M., Boyd, P. W., Cheung, W., Lluch-Cota, S. E., Nojiri, Y., Schmidt, D.N., Zavialov, P.O., Alheit, J., Aristegui J, & Armstrong, C. (2014). Ocean systems. In *Climate change 2014: impacts,*

adaptation, and vulnerability. Part A: global and sectoral aspects. contribution of working group II to the fifth assessment report of the intergovernmental panel on climate change (pp. 411-484). Cambridge University Press.

Poulain, C., Gillikin, D. P., Thébault, J., Munaron, J. M., Bohn, M., Robert, R., ... & Lorrain, A. (2015). An evaluation of Mg/Ca, Sr/Ca, and Ba/Ca ratios as environmental proxies in aragonite bivalve shells. *Chemical geology*, *396*, 42-50.

Poulton, S. W., & Raiswell, R. (2005). Chemical and physical characteristics of iron oxides in riverine and glacial meltwater sediments. *Chemical Geology*, *218*(3-4), 203-221.

Prazeres, M., & Pandolfi, J. M. (2016). Effects of elevated temperature on the shell density of the large benthic Foraminifera Amphistegina lobifera. *Journal of Eukaryotic Microbiology*, *63*(6), 786-793.

Prézelin, B. B., Hofmann, E. E., Mengelt, C., & Klinck, J. M. (2000). The linkage between Upper Circumpolar Deep Water (UCDW) and phytoplankton assemblages on the west Antarctic Peninsula continental shelf. *Journal of Marine Research*, *58*(2), 165-202.

Purchon, R. D. (1968). The biology of the Mollusca, International series of monographs in pure and applied biology. *Pergamon Press*, *40*, 561.

Purroy, A., Milano, S., Schöne, B. R., Thébault, J., & Peharda, M. (2018). Drivers of shell growth of the bivalve, Callista chione (L. 1758)–Combined environmental and biological factors. *Marine environmental research*, *134*, 138-149.

R Core Team (2017). R: A language and environment for statistical computing. Vienna, Austria. URL https://www.R-project.org/.

Rahman, I. A. (2017). Computational fluid dynamics as a tool for testing functional and ecological hypotheses in fossil taxa. *Palaeontology*, *60*(4), 451-459.

Ragazzola, F., Foster, L. C., Jones, C. J., Scott, T. B., Fietzke, J., Kilburn, M. R., & Schmidt, D. N. (2016). Impact of high CO 2 on the geochemistry of the coralline algae Lithothamnion glaciale. *Scientific reports*, *6*(1), 1-9.

Ragazzola, F., Foster, L. C., Form, A. U., Büscher, J., Hansteen, T. H., & Fietzke, J. (2013). Phenotypic plasticity of coralline algae in a high CO 2 world. *Ecology and Evolution*, *3*(10), 3436-3446.

Rasband, W. S. (2011). 1997–2011. ImageJ. *Bethesda, MD: National Institutes of Health*.

Rayfield, E. J. (2007). Finite element analysis and understanding the biomechanics and evolution of living and fossil organisms. *Annu. Rev. Earth Planet. Sci.*, *35*, 541-576.

Reed, A. J., Thatje, S., & Linse, K. (2012). Shifting baselines in Antarctic ecosystems; ecophysiological response to warming in Lissarca miliaris at Signy Island, Antarctica. *PloS one*, *7*(12).

Reed, A. J., Morris, J. P., Linse, K., & Thatje, S. (2013). Plasticity in shell morphology and growth among deep-sea protobranch bivalves of the genus Yoldiella (Yoldiidae) from contrasting Southern Ocean regions. *Deep Sea Research Part I: Oceanographic Research Papers*, *81*, 14-24.

Reimer, O., & Tedengren, M. (1996). Phenotypical improvement of morphological defences in the mussel Mytilus edulis induced by exposure to the predator Asterias rubens. *Oikos*, 383-390.

Rex, M. A., & Etter, R. J. (1998). Bathymetric patterns of body size: implications for deep-sea biodiversity. *Deep-Sea Research (Part II, Topical Studies in Oceanography)*, *45*(1), 103-127.

Reynolds, P. D. (1997). The phylogeny and classification of Scaphopoda (Mollusca): an assessment of current resolution and cladistic reanalysis. *Zoologica Scripta*, *26*(1), 13-21.

Reynolds, P.D. & Okusu, A. (1999). Phylogenetic relationships among families of the Scaphopoda (Mollusca). *Zoological Journal of Linnean Society*, 126:131-154.

Reynolds, P. D. (2002). The scaphopoda. *Advances in marine biology*, *42*, 137-236.

Reynolds, P. D. (2006). Scaphopoda: The tusk shells. *The Mollusks: A Guide to Their Study, Collection, and Preservation*, 229-237.

Reynolds P.D. & Steiner G. (2008). Scaphopoda. In: Phylogeny and Evolution of the Mollusca. Ponder W.F. & Lindberg D.R., (eds)., pp. 143–161. University of California Press, Berkeley.

Riccardi, N., Froufe, E., Lopes-Lima, M., & Mazzoli, C. (2016). When and how? Freshwater mussel recolonization in Lake Orta. *Journal of Limnology*, *75*.

Richardson, C. A., Collis, S. A., Ekaratne, K., Dare, P., & Key, D. (1993). The age determination and growth rate of the European flat oyster, Ostrea edulis, in British waters determined from acetate peels of umbo growth lines. *ICES Journal of Marine Science*, *50*(4), 493-500.

Ries, J. B., Cohen, A. L., & McCorkle, D. C. (2009). Marine calcifiers exhibit mixed responses to CO2-induced ocean acidification. *Geology*, *37*(12), 1131-1134.

Rintoul, S. R., Chown, S. L., DeConto, R. M., England, M. H., Fricker, H. A., Masson-Delmotte, V., ... & Xavier, J. C. (2018). Choosing the future of Antarctica. *Nature*, *558*(7709), 233-241.

Ritman, E. L. (2004). Micro-computed tomography—current status and developments. *Annu. Rev. Biomed. Eng.*, *6*, 185-208.

Robinson, L., & Waller, R. (2011). Historic perspectives on climate and biogeography from deep-sea corals in the Drake Passage. *Cruise report RVIB Nathaniel B Palmer Cruise*, 11-03.

Rodriguez-Romero, A., Jimenez-Tenorio, N., Basallote, M. D., Orte, M. R. D., Blasco, J., & Riba, I. (2014). Predicting the impacts of CO2 leakage from subseabed storage: effects of metal accumulation and toxicity on the model benthic organism Ruditapes philippinarum. *Environmental science & technology*, *48*(20), 12292-12301.

Roemmich, D., Church, J., Gilson, J., Monselesan, D., Sutton, P., & Wijffels, S. (2015). Unabated planetary warming and its ocean structure since 2006. *Nature climate change*, *5*(3), 240.

Roger, L., George, A., Shaw, J., Hart, R., Roberts, M., Becker, T., ... & Evans, N. (2017). Geochemical and microstructural characterisation of two species of cool-water bivalves (Fulvia tenuicostata and Soletellina biradiata) from Western Australia. *Biogeosciences*, *14*(6), 1721-1737.

Rogers, A. D., Yesson, C., & Gravestock, P. (2015). A biophysical and economic profile of South Georgia and the South Sandwich Islands as potential large-scale Antarctic protected areas. In *Advances in marine biology* (Vol. 70, pp. 1-286). Academic Press.

Rogers, A. D., Frinault, B. A. V., Barnes, D. K. A., Bindoff, N. L., Downie, R., Ducklow, H. W., ... & Wright, R. M. (2020). Antarctic futures: an assessment of climate-driven changes in ecosystem structure, function, and service provisioning in the Southern Ocean. *Annual Review of Marine Science*, *12*, 87-120.

Román-González, A., Scourse, J. D., Butler, P. G., Reynolds, D. J., Richardson, C. A., Peck, L. S., Brey, T., & Hall, I. R. (2017). Analysis of ontogenetic growth trends in two marine Antarctic bivalves Yoldia eightsi and

Laternula elliptica: Implications for sclerochronology. *Palaeogeography, Palaeoclimatology, Palaeoecology*, *465*, 300-306.

Rozema, P. D., Venables, H. J., Van De Poll, W. H., Clarke, A., Meredith, M. P., & Buma, A. G. J. (2017). Interannual variability in phytoplankton biomass and species composition in northern Marguerite Bay (West Antarctic Peninsula) is governed by both winter sea ice cover and summer stratification. *Limnology and Oceanography*, *62*(1), 235-252.

Rucker, J. B., & Valentine, J. W. (1961). Salinity response of trace element concentration in Crassostrea virginica. Nature, 190(4781), 1099-1100.

Ruddy, G. M., Feng, S. Y., & Campbell, G. S. (1975). The effect of prolonged exposure to elevated temperatures on the biochemical constituents, gonadal development and shell deposition of the American oyster, Crassostrea virginica. *Comparative Biochemistry and Physiology Part B: Comparative Biochemistry*, *51*(2), 157-164.

Santhiya, N., Sanjeevi, S. B., Gayathri, M., & Dhanalakshmi, M. (2013). Economic importance of marine molluscs. *Research in Environment and Life Sciences*, *6*(4), 129-132.

Saucède, T., Griffiths, H., Moreau, C., Jackson, J. A., Sands, C., Downey, R., Reed A., Mackenzie M., Geissler P., & Linse, K. (2015). East Weddell Sea echinoids from the JR275 expedition. *ZooKeys*, (504), 1.

Seed, R. (1968). Factors influencing shell shape in the mussel Mytilus edulis. *Journal of the Marine Biological Association of the United Kingdom*, *48*(3), 561-584.

Schmiedl, G., Mackensen, A., & Müller, P. J. (1997). Recent benthic foraminifera from the eastern South Atlantic Ocean: dependence on food supply and water masses. *Marine micropaleontology*, *32*(3-4), 249-287.

Schmidt, D. N., Rayfield, E. J., Cocking, A., & Marone, F. (2013). Linking evolution and development: Synchrotron Radiation X-ray tomographic microscopy of planktic foraminifers. *Palaeontology*, *56*(4), 741-749.

Schmidtko, S., Heywood, K. J., Thompson, A. F., & Aoki, S. (2014). Multidecadal warming of Antarctic waters. *Science*, *346*(6214), 1227-1231.

Schneider, S., Fürsich, F. T., Schulz-Mirbach, T., & Werner, W. (2010). Ecophenotypic plasticity versus evolutionary trends—morphological variability in Upper Jurassic bivalve shells from Portugal. *Acta Palaeontologica Polonica*, *55*(4), 701-732.

Schofield, O., Saba, G., Coleman, K., Carvalho, F., Couto, N., Ducklow, H., ... & Montes-Hugo, M. (2017). Decadal variability in coastal phytoplankton community composition in a changing West Antarctic Peninsula. *Deep Sea Research Part I: Oceanographic Research Papers*, *124*, 42-54.

Schöne, B. R., Fiebig, J., Pfeiffer, M., Gleβ, R., Hickson, J., Johnson, A. L., Dreyer, W. & Oschmann, W. (2005). Climate records from a bivalved Methuselah (Arctica islandica, Mollusca; Iceland). *Palaeogeography, Palaeoclimatology, Palaeoecology*, *228*(1-2), 130-148.

Schöne, B. R., Zhang, Z., Jacob, D., Gillikin, D. P., Tütken, T., Garbe-Schönberg, D., ... & Soldati, A. (2010). Effect of organic matrices on the determination of the trace element chemistry (Mg, Sr, Mg/Ca, Sr/Ca) of aragonitic bivalve shells (Arctica islandica)—Comparison of ICP-OES and LA-ICP-MS data. *Geochemical journal*, *44*(1), 23-37.

Schöne, B. R., & Gillikin, D. P. (2012). Unraveling environmental histories from skeletal diaries—advances in sclerochronology.

Schöne, B. R., Radermacher, P., Zhang, Z., & Jacob, D. E. (2013). Crystal fabrics and element impurities (Sr/Ca, Mg/Ca, and Ba/Ca) in shells of Arctica islandica—implications for paleoclimate reconstructions. *Palaeogeography, palaeoclimatology, palaeoecology*, *373*, 50-59.

Shadwick, E. H., Trull, T. W., Thomas, H., & Gibson, J. A. E. (2013). Vulnerability of polar oceans to anthropogenic acidification: comparison of Arctic and Antarctic seasonal cycles. *Scientific reports*, *3*, 2339.

Sheridan, J. A., & Bickford, D. (2011). Shrinking body size as an ecological response to climate change. *Nature climate change*, *1*(8), 401-406.

Shimek, R. I. (1989). Shell Morphometrics and Systematics: A Revision. *Veliger*, *32*(3), 233-246.

Shirai, K., Kawashima, T., Sowa, K., Watanabe, T., Nakamori, T., Takahata, N., ... & Sano, Y. (2008). Minor and trace element incorporation into branching coral Acropora nobilis skeleton. *Geochimica et Cosmochimica Acta*, *72*(22), 5386-5400.

Shirayama, Y., & Thornton, H. (2005). Effect of increased atmospheric CO2 on shallow water marine benthos. *Journal of Geophysical Research: Oceans*, *110*(C9).

Sigwart, J., & Sumner-Rooney, L. (2015). Mollusca: Caudofoveata, Monoplacophora, Polyplacophora, Scaphopoda and Solenogastres. *Structure and evolution of invertebrate nervous systems*, 172-189.

Smith, B. N. (1972). Natural abundance of the stable isotopes of carbon in biological ystems. *BioScience*, *22*(4), 226-231.

Smith, R. C., & Stammerjohn, S. E. (2001). Variations of surface air temperature and sea-ice extent in the western Antarctic Peninsula region. *Annals of Glaciology*, *33*, 493-500.

Smith, R. C., Martinson, D. G., Stammerjohn, S. E., Iannuzzi, R. A., & Ireson, K. (2008). Bellingshausen and western Antarctic Peninsula region: Pigment biomass and sea-ice spatial/temporal distributions and interannual variabilty. *Deep Sea Research Part II: Topical Studies in Oceanography*, *55*(18-19), 1949-1963.

Smith, A. M., & Spencer, H. G. (2016). Skeletal mineralogy of scaphopods: an unusual uniformity. *Journal of Molluscan Studies*, *82*(2), 344-348.

Sokolova, I. M., Bock, C., & Pörtner, H. O. (2000). Resistance to freshwater exposure in White Sea Littorina spp. II: Acid-base regulation. *Journal of Comparative Physiology B*, *170*(2), 105-115.

Spooner, D. E., & Vaughn, C. C. (2006). Context-dependent effects of freshwater mussels on stream benthic communities. *Freshwater Biology*, *51*(6), 1016-1024.

Stammerjohn, S., Massom, R., Rind, D., & Martinson, D. (2012). Regions of rapid sea ice change: An inter-hemispheric seasonal comparison. *Geophysical Research Letters*, *39*(6).

Stanley, S. M. (1977). Coadaptation in the Trigoniidae, a remarkable family of burrowing bivalves. *Palaeontology.* 20:869-899.

Stanley, S. M. (1981). Infaunal survival: alternative functions of shell ornamentation in the Bivalvia (Mollusca). *Paleobiology*, 384-393.

Stecher III, H. A., Krantz, D. E., Lord III, C. J., Luther III, G. W., & Bock, K. W. (1996). Profiles of strontium and barium in Mercenaria mercenaria and Spisula solidissima shells. *Geochimica et Cosmochimica Acta*, *60*(18), 3445-3456.

Steffani, C. N., & Branch, G. M. (2003). Growth rate, condition, and shell shape of Mytilus galloprovincialis: responses to wave exposure. *Marine Ecology Progress Series*, *246*, 197-209.

STEINER, G. (1992). Phylogeny and classification of Scaphopoda. *Journal of Molluscan Studies*, *58*(4), 385-400.

Steiner, G., & Linse, K. A. T. R. I. N. (2000). Systematics and distribution of the Scaphopoda (Mollusca) in the Beagle Channel (Chile). *Mitteilungen aus dem Hamburgischen Zoologischen Museum und Institut*, *96*, 13-30.

Steiner, G., & Dreyer, H. (2003). Molecular phylogeny of Scaphopoda (Mollusca) inferred from 18S rDNA sequences: support for a Scaphopoda–Cephalopoda clade. *Zoologica Scripta*, *32*(4), 343-356.

Stumpp, M., Wren, J., Melzner, F., Thorndyke, M. C., & Dupont, S. T. (2011). CO2 induced seawater acidification impacts sea urchin larval development I: elevated metabolic rates decrease scope for growth and induce developmental delay. *Comparative Biochemistry and Physiology Part A: Molecular & Integrative Physiology*, *160*(3), 331-340.

Stumpp, M., Hu, M. Y., Melzner, F., Gutowska, M. A., Dorey, N., Himmerkus, N., Holtmann, W.C., Dupont, S.T., Thorndyke, M.C., & Bleich, M. (2012). Acidified seawater impacts sea urchin larvae pH regulatory systems relevant for calcification. *Proceedings of the National Academy of Sciences*, *109*(44), 18192-18197.

Suckling, C. C., Clark, M. S., Richard, J., Morley, S. A., Thorne, M. A., Harper, E. M., & Peck, L. S. (2015). Adult acclimation to combined temperature and p H stressors significantly enhances reproductive outcomes compared to short-term exposures. *Journal of Animal Ecology*, *84*(3), 773-784.

Swan, E. F. (1956). The meaning of strontium-calcium ratios. *Deep-Sea Res.*, *4*, 71.

Swart, N. C., Gille, S. T., Fyfe, J. C., & Gillett, N. P. (2018). Recent Southern Ocean warming, and freshening driven by greenhouse gas emissions and ozone depletion. *Nature Geoscience*, *11*(11), 836-841.

Talmage, S. C., & Gobler, C. J. (2012). Effects of CO2 and the harmful alga Aureococcus anophagefferens on growth and survival of oyster and scallop larvae. *Marine Ecology Progress Series*, *464*, 121-134.

Thiel, H., 1975. The size structure of the deep-sea benthos. Internationale Revue der Gesampten *Hydrobiologie* 60, 575-606.

Thomsen, J., Casties, I., Pansch, C., Körtzinger, A., & Melzner, F. (2013). Food availability outweighs ocean acidification effects in juvenile M ytilus edulis: laboratory and field experiments. *Global change biology*, *19*(4), 1017-1027.

Trathan, P. N., Collins, M. A., Grant, S. M., Belchier, M., Barnes, D. K., Brown, J., & Staniland, I. J. (2014). The South Georgia and the South Sandwich Islands MPA: protecting a biodiverse oceanic island chain situated in the flow of the Antarctic Circumpolar Current. In *Advances in marine biology* (Vol. 69, pp. 15-78). Academic Press.

Trimborn, S., Brenneis, T., Sweet, E., & Rost, B. (2013). Sensitivity of Antarctic phytoplankton species to ocean acidification: Growth, carbon acquisition, and species interaction. *Limnology and Oceanography*, *58*(3), 997-1007.

Troncoso, J. S., Aldea, C., Arnaud, P., Ramos, A., & García, F. (2007). Quantitative analysis of soft-bottom molluscs in the Bellingshausen Sea and around Peter I Island. *Polar Research*, *26*(2), 126-134.

Trueman, E. R. (1968). The burrowing process of Dentalium (Scaphopoda). *Journal of Zoology*, *154*(1), 19-27.

Tunnicliffe, V., Davies, K. T., Butterfield, D. A., Embley, R. W., Rose, J. M., & Chadwick Jr, W. W. (2009). Survival of mussels in extremely acidic waters on a submarine volcano. *Nature Geoscience*, *2*(5), 344-348.

Turner, J., Colwell, S. R., Marshall, G. J., Lachlan-Cope, T. A., Carleton, A. M., Jones, P. D., ... & Iagovkina, S. (2005). Antarctic climate change during the last 50 years. *International journal of Climatology*, *25*(3), 279-294.

Turner, J., Barrand, N. E., Bracegirdle, T. J., Convey, P., Hodgson, D. A., Jarvis, M., Jenkins, A., Marshall, G., Meredith, M.P., Roscoe, H., & Shanklin, J. (2014). Antarctic climate change and the environment: an update. *Polar Record*, *50*(3), 237-259.

Turner, J., Lu, H., White, I., King, J. C., Phillips, T., Hosking, J. S., Bracegirdle, T.J., Marshall, G.J., Mulvaney, R. & Deb, P. (2016). Absence of 21st century warming on Antarctic Peninsula consistent with natural variability. *Nature*, *535*(7612), 411-415.

Tynan, E., Clarke, J. S., Humphreys, M. P., Ribas-Ribas, M., Esposito, M., Rérolle, V. M., ... & Achterberg, E. P. (2016). Physical and biogeochemical controls on the variability in surface pH and calcium carbonate saturation states in the Atlantic sectors of the Arctic and Southern Oceans. *Deep Sea Research Part II: Topical Studies in Oceanography*, *127*, 7-27.

Tyrrell, M., & Hornbach, D. J. (1998). Selective predation by muskrats on freshwater mussels in 2 Minnesota rivers. *Journal of the North American Benthological Society*, *17*(3), 301-310.

Urey, H. C., Lowenstam, H. A., Epstein, S., & McKinney, C. R. (1951). Measurement of paleotemperatures and temperatures of the Upper Cretaceous of England, Denmark, and the southeastern United States. *Geological Society of America Bulletin*, *62*(4), 399-416.

van Caspel, M. R. (2016). *The importance of the western Weddell Sea to Weddell Sea Deep Water formation* (Doctoral dissertation, Universität Bremen).

Vaughan, D. G., Marshall, G. J., Connolley, W. M., Parkinson, C., Mulvaney, R., Hodgson, D. A., ... & Turner, J. (2003). Recent rapid regional climate warming on the Antarctic Peninsula. *Climatic change*, *60*(3), 243-274.

Vekhova, E. E. (2013). Growth and shell morphology of three mytilidae (Bivalvia) species from the Sea of Japan. *Biology Bulletin*, *40*(9), 728-737.

Vermeij, G. J., & Covich, A. P. (1978). Coevolution of freshwater gastropods and their predators. *The American Naturalist*, *112*(987), 833-843.

Vernet, M., Geibert, W., Hoppema, M., Brown, P. J., Haas, C., Hellmer, H. H., ... & Brearley, J. A. (2019). The Weddell Gyre, Southern Ocean: present knowledge and future challenges. *Reviews of Geophysics*, *57*(3), 623-708.

Wanamaker, A. D., Butler, P. G., Scourse, J. D., Heinemeier, J., Eiríksson, J., Knudsen, K. L., & Richardson, C. A. (2012). Surface changes in the North Atlantic meridional overturning circulation during the last millennium. *Nature Communications*, *3*(1), 1-7.

Wanamaker Jr, A. D., & Gillikin, D. P. (2019). Strontium, magnesium, and barium incorporation in aragonitic shells of juvenile Arctica islandica: Insights from temperature controlled experiments. *Chemical Geology*, *526*, 117-129.

Watson, S. A., Peck, L. S., Tyler, P. A., Southgate, P. C., Tan, K. S., Day, R. W., & Morley, S. A. (2012). Marine invertebrate skeleton size varies with latitude, temperature and carbonate saturation: implications for global change and ocean acidification. *Global Change Biology*, *18*(10), 3026-3038.

Watson, S. A., Morley, S. A., & Peck, L. S. (2017). Latitudinal trends in shell production cost from the tropics to the poles. *Science advances*, *3*(9), e1701362.

Weber, J. N., & Woodhead, P. M. (1970). Carbon and oxygen isotope fractionation in the skeletal carbonate of reef-building corals. *Chemical Geology*, *6*, 93-117.

Weeber, A., Swart, S., & Monteiro, P. M. S. (2015). Seasonality of sea ice controls interannual variability of summertime Ω A at the ice shelf in the Eastern Weddell Sea--an ocean acidification sensitivity study. *Biogeosciences Discussions*, *12*(2).

Weiner, S., & Dove, P. M. (2003). An overview of biomineralization processes and the problem of the vital effect. *Reviews in mineralogy and geochemistry*, *54*(1), 1-29.

Wheeler, A. P. (1992). Mechanisms of molluscan shell formation. *Calcification in biological systems*, 179-216.

Whitehouse, M. J., Korb, R. E., Atkinson, A., Thorpe, S. E., & Gordon, M. (2008). Formation, transport and decay of an intense phytoplankton bloom within the High-Nutrient Low-Chlorophyll belt of the Southern Ocean. *Journal of Marine Systems*, *70*(1-2), 150-167.

Whitman, D. W., & Agrawal, A. A. (2009). What is phenotypic plasticity and why is it important. *Phenotypic plasticity of insects: Mechanisms and consequences*, 1-63.

Whitworth III, T., & Nowlin Jr, W. D. (1987). Water masses and currents of the Southern Ocean at the Greenwich Meridian. *Journal of Geophysical Research: Oceans*, *92*(C6), 6462-6476

Widdicombe, S., Spicer, J. I., & Kitidis, V. (2011). Effects of ocean acidification on sediment fauna. *Ocean acidification*, *16*.

Willi, Y., Van Buskirk, J., & Hoffmann, A. A. (2006). Limits to the adaptive potential of small populations. *Annu. Rev. Ecol. Evol. Syst.*, *37*, 433-458.

Winter, J. E. (1978). A review on the knowledge of suspension-feeding in lamellibranchiate bivalves, with special reference to artificial aquaculture systems. *Aquaculture*, *13*(1), 1-33.

Woltereck, R. (1909). Weitere experimentelle Unter-suchungen uber Artveranderung, speziell uber das Wesen quantitativer Artunterschiede bei Daphniden. *Verh. D. Tsch. Zool. Ges.*, *1909*, 110-172.

Wootton, J. T., Pfister, C. A., & Forester, J. D. (2008). Dynamic patterns and ecological impacts of declining ocean pH in a high-resolution multi-year dataset. *Proceedings of the National Academy of Sciences*, *105*(48), 18848-18853.

Yan, H., Chen, J., & Xiao, J. (2014). A review on bivalve shell, a tool for reconstruction of paleo-climate and paleo-environment. *Chinese Journal of Geochemistry*, *33*(3), 310-315.

Yan, L., Schöne, B. R., Li, S., & Yan, Y. (2014). Shells of Paphia undulata (Bivalvia) from the South China Sea as potential proxy archives of the East Asian summer monsoon: a sclerochronological calibration study. *Journal of oceanography*, *70*(1), 35-44.

Yochelson, E. L. (2004). The record of the early Scaphopoda (? Mollusca) reevaluated. *Annalen des Naturhistorischen Museums in Wien. Serie A für Mineralogie und Petrographie, Geologie und Paläontologie, Anthropologie und Prähistorie*, 13-31.

Yu, J. and H. Elderfield (2008). "Mg/Ca in the benthic foraminifera Cibicidoides wuellerstorfi and Cibicidoides mundulus: Temperature versus carbonate ion saturation." *Earth and Planetary Science Letters* 276(1-2): 129-139.

Zajac, K. (2014). Size-dependent predation by the Otter Lutra lutra on Swan mussels Anodonta cygnea (Linnaeus 1758)—observations and radiotelemetry experiment. *Journal of Conchology*, *41*, 559-564.

Zając, K., Zając, T., & Ćmiel, A. (2018). What can we infer from the shell dimensions of the thick-shelled river mussel Unio crassus?. *Hydrobiologia*, *810*(1), 415-431.

Zelditch, M. L., Swiderski, D. L., & Sheets, H. D. (2012). *Geometric morphometrics for biologists: a primer*. Academic Press.

Zienkiewicz, O. C., Taylor, R. L., & Zhu, J. Z. (2005). *The finite element method: its basis and fundamentals*. Elsevier.

Ziveri, P., Stoll, H., Probert, I., Klaas, C., Geisen, M., Ganssen, G., & Young, J. (2003). Stable isotope 'vital effects' in coccolith calcite. *Earth and planetary science letters*, *210*(1-2), 137-149.